

Semi-analytical Modeling Approach for Flow Boiling Heat Transfer in Uniformly Heated
Horizontal Micro-Channels

Amen Mansour Amer Younes

A Thesis

in

The Department

of

Mechanical and Industrial Engineering

Presented in Partial Fulfillment of the Requirements

For the Degree of Doctor of Philosophy

Concordia University

Montréal, Québec, Canada

Mar. 2016

©Amen Mansour Amer Younes, 2016

**CONCORDIA UNIVERSITY
SCHOOL OF GRADUATE STUDIES**

This is to certify that the thesis prepared

By: Amen Mansour Amer Younes

Entitled: Semi-analytical Modeling Approach for Flow Boiling Heat Transfer in
Uniformly Heated Horizontal Micro-Channels

and submitted in partial fulfillment of the requirements for the degree of

DOCTOR OF PHILOSOPHY (Mechanical Engineering)

complies with the regulations of the University and meets the accepted standards with respect to originality and quality.

Signed by the final examining committee:

| | |
|------------------------|----------------------|
| <u>Dr. J. Bentahar</u> | Chair |
| <u>Dr. J. Cotton</u> | External Examiner |
| <u>Dr. R. Paknys</u> | External to Program |
| <u>Dr. G. Vatistas</u> | Examiner |
| <u>Dr. N. Esmail</u> | Examiner |
| <u>Dr. I. Hassan</u> | Thesis Co-Supervisor |
| <u>Dr. L. Kadem</u> | Thesis Co-Supervisor |

Approved by

Dr. A. Dolatabadi
Chair of Department or Graduate Program Director

Mar. 10th, 2016

Dr. A. Asif
Dean of Faculty

Abstract

Semi-analytical Modeling Approach for Flow Boiling Heat Transfer in Uniformly Heated Horizontal Micro-channels

Amen Mansour Youns, Ph.D.

Concordia University, 2016

Two-phase flow boiling in mini/micro-channels is an essential topic for studying and developing miniature cooling systems which have a wide range of industrial, automotive, nuclear, and aerospace applications, since they insure providing higher heat dissipation and ability to work at surface temperature higher than those provided by conventional channel sizes. Therefore, it has gained much more attention recently and several extensive studies have been carried out for predicting the essential design parameters such as heat transfer coefficient, pressure drop, void fraction, and critical heat flux. However, most of the available predictive methods are mainly empirical correlations and few analytical models. Moreover, several essential and fundamental flow boiling phenomena, such as heat transfer mechanisms, liquid film dry-out, and bubble dynamics, are still unclear and need to be investigated and clarified.

The main objective of the present thesis is to investigate the characteristics of two basic flow patterns, namely, annular flow and slug flow for flow boiling in a single horizontal mini/micro-channel under uniform distribution of heat flux. A one-dimensional semi-analytical model has been developed based on the principle of the separated flow model. It predicts heat transfer coefficient, pressure drop, void fraction, and critical heat flux in the annular flow regime, which is usually observed at medium and high vapor qualities. The basic model equations are derived by applying the mass, momentum, and energy equations for each phase. The obtained equations are initial value differential equations, which are solved numerically by Runge-Kutta methods. Furthermore, the influences of interfacial parameters on the main dependent variables have been addressed. Liquid film, trapped between the vapor core and tube inner surface in the annular flow regime, is an essential parameter since the evaporation of liquid film is the

dominant heat transfer mechanism in this regime and the critical heat flux (CHF) is identified based on the dry-out of the liquid film. Therefore, the liquid film was fairly predicted, to estimate heat transfer coefficient and CHF in annular flow regime. Moreover, a semi-analytical model for slug flow has been developed based on the principle of drift flux model to investigate the characteristics of slug flow pattern such as bubble velocity, bubble length, liquid slug velocity, liquid slug length, and bubble frequency.

The effects of working fluid properties, mass flux, heat flux, and channel size on the modeled parameters have been taken into account. As a result, it has been found that in the annular flow regime, the CHF increases with the mass flux and channel size, while it is inversely proportional to the critical vapor quality. Furthermore, the results of two-phase flow boiling heat transfer coefficient showed that heat transfer coefficient increases with mass flux and vapor quality, while it decreases when the channel size increases. Regarding the pressure drop results, it has been observed that the pressure drop is inversely proportional to the channel size, and increases with the mass flux and vapor quality. Additionally, it has been shown that void fraction increases with vapor quality and decreases with channel size. Also, the bubble frequency in slug flow regime has been predicted, and it is shown that the bubble frequency increases with vapor quality and mass flux. Furthermore, it has been noticed that the peak of the bubble frequency increases with mass flux.

The proposed flow boiling models have been validated against extensive two-phase experimental data in literature for the critical heat flux CHF , heat transfer coefficient h_{tp} , pressure drop Δp_{tp} , and void fraction α , respectively, for different working fluids (Water, CO₂, LN₂, FC72, R134a, R1234ze, R245f2, R236fa, R410a, and R113) in horizontal micro-channels with a range of hydraulic diameters of $0.244 \leq D_h \leq 3.1 \text{ mm}$, and a range of the Reynolds numbers of $1,900 \leq Re_{eq} \leq 48,000$. The annular flow model predicted the tested experimental data of the CHF , h_{tp} , Δp_{tp} , and α , with mean absolute error of 20%, 18%, 23%, and 3%, respectively. Furthermore, a good agreement with the experimental data of bubble lengths and bubble frequency has been obtained with MAE of 27.83% and 29.55 %, respectively.

Acknowledgements

First of all, I Praise Allah for giving me the strengths and blessing to accomplishing my thesis. My special gratitude goes to my supervisor professor Ibrahim G. Hassan for his continuing support, encouragement, and giving guidance to me throughout my Ph.D. program. A special appreciation goes to my co-supervisor Dr. Lyes Kadem for his support and valuable advices. Special thanks to my friends and colleagues, Dr. Dino, Dr. Othman, Dr. Carol, Dr. Fan, Ling, Tina, Qian, Yingjie, and Haoming for their friendship, the good times we worked together, and shared our experiences.

I am very grateful and indebted to my beloved parents, for their love, encouragement, supports, and everything they provided to me. I would like to thank my darling wife, who provided me the support, encouragement, and motivation for accomplishing this work. I am really indebted to her for her patience throughout the hard times we have faced during my Ph.D. program. Last, I would like to thank all my brothers, sisters, and all friends, for their encouragement and support.

Table of Contents

| | |
|--|-----|
| List of Figures | x |
| List of Tables | xv |
| Nomenclature | xvi |
| 1. Introduction..... | 1 |
| 1.1. Motivation | 2 |
| 1.2. Objectives and Organization | 5 |
| 2. Literature Review | 6 |
| 2.1. Two-Phase Flow and Associated Dimensionless Groups | 6 |
| 2.2. Channel Classification Criteria | 7 |
| 2.3. Dominant Forces and Scale Size Effect | 10 |
| 2.4. Flow Patterns and Flow Pattern Maps..... | 12 |
| 2.5. Heat Transfer Mechanisms..... | 22 |
| 2.6. Bubble Dynamics | 26 |
| 2.7. Liquid Film in Slug and Annular Flow Regimes | 29 |
| 2.8. Critical Heat Flux (CHF)..... | 33 |
| 2.9. Two-Phase Heat Transfer Coefficient | 40 |
| 2.10. Two-Phase Pressure Drop..... | 54 |
| 2.11. Summary and Objectives | 62 |
| 2.11.1. Summary..... | 62 |
| 2.11.2. Objectives | 63 |
| 3. Modeling of Dry-out Incipience for Flow Boiling in a Circular Micro-channel at a Uniform Heat Flux..... | 65 |
| 3.1. Abstract | 66 |

| | | |
|--------|--|-----|
| 3.2. | Introduction | 67 |
| 3.3. | Model Analysis | 75 |
| 3.3.1. | Mass Conservation Equations..... | 77 |
| 3.3.2. | Momentum Conservation Equations | 78 |
| 3.3.3. | Energy Conservation Equations | 79 |
| 3.4. | Initial and Boundary Values of the Model..... | 84 |
| 3.5. | Results and Discussion..... | 85 |
| 3.6. | Conclusions | 99 |
| 4. | A Semi-Analytical Model of Heat Transfer and Pressure Drop in Annular Flow Regime for Flow Boiling in a Micro-Tube at Uniform Heat Flux..... | 100 |
| 4.1. | Abstract | 101 |
| 4.2. | Introduction | 102 |
| 4.3. | Modeling Methodology..... | 106 |
| 4.3.1. | Basic Assumptions: | 107 |
| 4.3.2. | Equations of Mass Conservation | 108 |
| 4.3.3. | Equations of Momentum Conservation | 109 |
| 4.3.4. | Equations of Energy Conservation | 111 |
| 4.3.5. | Estimation of Interfacial Parameters | 112 |
| 4.3.6. | Wall Shear Stress and Friction Factor: | 114 |
| 4.3.7. | Main Form of the Present Model:..... | 115 |
| 4.3.8. | Equivalent Reynolds Number:..... | 117 |
| 4.4. | Initial Values of the Model Variables | 117 |
| 4.4.1. | Initial Value of Void Fraction..... | 117 |
| 4.4.2. | Initial Values of Liquid Film and Vapor Velocities | 119 |
| 4.5. | Solution Procedure | 120 |

| | | |
|----------|---|-----|
| 4.6. | Results and Discussion..... | 121 |
| 4.6.1. | Two Phase Heat Transfer Coefficient..... | 121 |
| 4.6.2. | Two Phase Pressure Drop..... | 129 |
| 4.6.3. | Void Fraction..... | 136 |
| 4.6.4. | Vapor and Liquid Film Velocities..... | 140 |
| 4.6.5. | Liquid Film Thickness..... | 141 |
| 4.7. | Sensitivity Analysis of the Model..... | 143 |
| 4.8. | Conclusions..... | 144 |
| 5. | Investigation of Bubble Frequency in Slug Flow Regime for Flow Boiling in a Single Round Uniformly Heated Horizontal Micro-Channel..... | 145 |
| 5.1. | Abstract..... | 146 |
| 5.2. | Introduction..... | 147 |
| 5.3. | Analysis of the Two Phase Slug Flow Model..... | 150 |
| 5.3.1. | Basic Assumptions..... | 150 |
| 5.3.2. | Derivation of the Equations of Motion..... | 151 |
| 5.3.2.1. | Mass Conservation Equations..... | 152 |
| 5.3.2.2. | Momentum Conservation Equations..... | 153 |
| 5.3.2.3. | Energy Conservation Equations..... | 155 |
| 5.3.3. | Constitutive Relationships of the Model..... | 157 |
| 5.3.4. | Evaluation the Variation of Bubble/Liquid Slug Lengths..... | 161 |
| 5.4. | Calculation Procedure..... | 163 |
| 5.5. | Results and Discussion..... | 164 |
| 5.6. | Conclusions..... | 174 |
| 6. | Conclusions and Future Work..... | 176 |
| 6.1. | Conclusions..... | 176 |

| | |
|--|-----|
| 6.2. Future Work | 178 |
| 6.2.1. Investigation of the Non-Uniform Heat Flux Effects on the Characteristics of Flow Boiling Micro-Channels:..... | 178 |
| 6.2.2. Investigation of Bubble Dynamics and Heat Transfer in Coalescing Bubble Zone for Flow Boiling in a Single Horizontal Mini/Micro-Channel:..... | 179 |
| 6.2.3. Future Flow Pattern Maps | 180 |
| References | 181 |
| Appendix A..... | 198 |

List of Figures

Figure 2-1: Shows the effects of tube size on different forces for flow boiling of water at $G=200 \text{ kg/m}^2 \cdot \text{s}$ and $q_w'' = 1000 \text{ kW/m}^2$, (Kandlikar [13]) ----- 11

Figure 2-2: Flow pattern map developed by Thome & El Hajal [100] for evaporation in horizontal tubes considering the effect of working fluid. ----- 15

Figure 2-3: Flow patterns for R134a flowing with $G=500 \text{ kg/m}^2 \cdot \text{s}$ in a 0.79 mm channel has an average heat length $L=70 \text{ mm}$ at $T_{\text{sat}}=30 \text{ }^\circ\text{C}$ and $\Delta T_{\text{sub}}=30 \text{ }^\circ\text{C}$, observed by Revellin [90]. ----- 17

Figure 2-4: A new diabatic coalescing bubble map for evaporating flow in circular uniformly heated microchannels: R-134a, $D = 0.5 \text{ mm}$, $L = 70 \text{ mm}$, $T_{\text{sat}} = 30 \text{ }^\circ\text{C}$, $q_w'' = 50 \text{ kW/m}^2$, Revellin and Thome [75]. ----- 18

Figure 2-5: Variation of heat transfer coefficient with vapor quality for R12 in 2.46 mm channel at different values of heat flux Dupont et al. [152]. ----- 48

Figure 2-6: Variation of heat transfer coefficient with vapor quality for different fluids, Comparison the experimental data with those predicted by the model Consolini and Thome [145]. ----- 51

Figure 3-1: (a) schematic diagram of an annular flow pattern. (b) a symmetric sketch of the chosen control volume for applying mass balance. (c) a symmetric sketch shows the forces applied on the control volume. ----- 75

Figure 3-2: Flow chart shows the procedure of calculations for the present model ----- 86

Figure 3-3: Comparison of the Present CHF model with CHF data obtained by Qu and Mudawar [43] for flow boiling of Water in multiple channels heat sink. ----- 88

Figure 3-4: Comparison of the Present CHF model with CHF data obtained by Roday and Jensen [138] for flow boiling of Water in a single micro-tube with diameter of 0.427 mm. ----- 89

Figure 3-5: Comparison of the Present CHF model with CHF data of Wojtan et al. [45] for flow boiling of R134a in a single micro-tube for internal diameters 0.50 mm and 0.80 mm. ----- 90

Figure 3-6: Comparison of the Present CHF model with CHF data of Ong & Thome [139] for flow boiling of R134a in a single micro-tube for internal diameters 1.03, 2.20, and 3.04 mm. -- 91

Figure 3-7: Comparison of the Present CHF model with CHF data of Fan & Hassan [6] for flow boiling of FC-72 in a single micro-tube with an internal diameter of 0.889 mm. ----- 92

| | |
|--|-----|
| Figure 3-8: Comparison of the Present CHF model with CHF data of Qi et al. [46] for flow boiling of LN2 in mini and micro-tubes with internal diameters 0.531, 0.834, 1.042, and 1.931 mm. ----- | 93 |
| Figure 3-9: Comparison of experimental CHF data for flow boiling of R134a, LN2, FC72, and water in mini and micro-channels with that predicted by the present CHF model. ----- | 94 |
| Figure 3-10: Comparison of experimental CHF data for flow boiling of R134a, LN2, FC72, and water in mini and micro-channels with that predicted the CHF correlation of Wojtan et al. [45]. ----- | 95 |
| Figure 3-11: Comparison of experimental CHF data for flow boiling of R134a, LN2, FC72, and water in mini and micro-channels with that predicted by Ong & Thome [139] Correlation. ----- | 96 |
| Figure 3-12: Comparison of experimental CHF data for flow boiling of R134a, LN2, FC72, and water in mini and micro-channels with that predicted the CHF correlation of Qi et al. [46]. ----- | 97 |
| Figure 3-13: CHF versus critical vapor quality predicted by the present model for flow boiling of R134a through a 0.8mm inner diameter micro-tube, and compared with those measured by Wojtan et al. [45]. ----- | 98 |
| Figure 4-1: Sketch of an annular flow model in horizontal circular channel ----- | 106 |
| Figure 4-2: Symmetric sketch shows basic terms for deriving mass conservation equations for liquid film and vapor core phases. ----- | 109 |
| Figure 4-3: Symmetric sketch shows the forces acting on the control volume. ----- | 110 |
| Figure 4-4: Heat transfer coefficient for flow boiling of the refrigerant R134-a in 1.12 mm inner diameter micro-channel versus vapor quality for various mass fluxes, and comparison of the heat transfer data predicted by the present model with those of Saitoh et al. [226] at $T_{sat} = 10\text{ }^{\circ}\text{C}$ | 125 |
| Figure 4-5: Heat transfer coefficient for flow boiling of the refrigerant R134-a in 0.781mm inner diameter micro-channel versus vapor quality for various mass fluxes, and comparison of the heat transfer data predicted by the present model with those of Ali et al. [206] at $T_{sat} = 30\text{ }^{\circ}\text{C}$. -- | 125 |
| Figure 4-6: Heat transfer coefficient versus vapor quality for flow boiling of CO2 in 0.529 mm inner diameter micro-channel for various mass fluxes, and comparison of the present model with the data of Ducoulombier et al. [61] at $T_{sat} = 0\text{ }^{\circ}\text{C}$. ----- | 127 |
| Figure 4-7: Heat transfer coefficient versus vapor quality for flow boiling of the refrigerant CO2 in 1.5 mm inner diameter micro-tube for various mass fluxes, and compared with the experimental data of Choi et al. [144] at $T_{sat} = 10\text{ }^{\circ}\text{C}$.----- | 127 |

Figure 4-8: Using Bland-Altman Plot method for assessing the agreement between the average two-phase heat transfer coefficient predicted by the present model and those measured experimentally (602 data points) for various working fluids and flow conditions as shown in Table (4.1) for the annular flow regime ----- 128

Figure 4-9: Comparison of pressure drop predicted by the present model with that measured by Revellin and Thome [75] for flow boiling of R-134a at inlet saturation temperature of 30 °C through a micro-tube with an inner diameter of $D=0.509$ mm and heated length of 70.7 mm, for range of mass fluxes of 350 to 1500 $kg/m^2.s$. ----- 131

Figure 4-10: Comparison of pressure drop predicted by the present model with those measured by Hwang and Kim [166] for flow boiling of R-134a at inlet saturation pressure of 700 kPa through a circular micro-tube with an inner diameter $D=0.430$ mm. ----- 131

Figure 4-11: Comparison of pressure drop predicted by the present model with the experimental data of Ducoulombier et al. [227] for flow boiling of CO₂ at $T_{sat} = -5.0$ °C, through a circular micro-tube with $D=0.529$ mm, and heated length of 191 mm for mass fluxes range of 200 – 1000 $kgm^2.s$. ----- 134

Figure 4-12: Pressure drop predicted by the present model versus vapor quality and compared with experimental data of Wu et al. [177] for flow boiling of CO₂ at $T_{sat} = -10$ °C, through a circular micro-tube with $D=1.42$ mm, and heated length of 300 mm, for mass fluxes range 300 – 600 $kgm^2.s$.----- 134

Figure 4-13: Using Bland-Altman Plot method for assessing the agreement between the average two-phase pressure drop predicted by the present model and those measured experimentally (498 data points) for various working fluids and flow conditions as shown in Table (4.2) for annular flow regime. ----- 135

Figure 4-14: Void fraction versus vapor quality for flow boiling of R410a in 0.508 mm inner diameter tube at $T_{sat} = 44.0$ °C, and 600 $[kg/m^2.s]$ mass flux. ----- 136

Figure 4-15: vapor void fraction versus vapor quality for flow boiling of R410a in 1.19 mm inner diameter tube at $T_{sat} = 43.5$ °C, and 600 $[kg/m^2.s]$ mass flux. ----- 138

Figure 4-16: Void fraction versus vapor quality for flow boiling of R410a in 2.92 mm inner diameter tube at $T_{sat} = 50.0$ °C, and 600 $[kg/m^2.s]$ mass flux. ----- 138

| | |
|--|-----|
| Figure 4-17: Comparison of vapor void fraction predicted by the present model with those of Shedd [228] for flow boiling of R410a in 0.508, 1.19, and 2.92 mm inner diameter tubes at $T_{sat} = 44.0$ to 50.0 °C, and range of mass fluxes, 200 to 800 $[kg/m^2.s]$. ----- | 139 |
| Figure 4-18: Average vapor velocity versus vapor quality predicted by the present model for flow boiling of CO ₂ in 1.42 mm inner diameter tube at $T_{sat} = -10$ °C, and operating conditions similar to those of Wu et al. [177] as listed in Table (4.1). ----- | 140 |
| Figure 4-19: Liquid film velocity versus vapor quality predicted by the present model for flow boiling of CO ₂ in 1.42 mm inner diameter tube at $T_{sat} = -10$ °C, and operating conditions similar to those of Wu et al. [177] as listed in Table (4.1). ----- | 142 |
| Figure 4-20: Liquid film thickness versus vapor quality predicted by the present model for flow boiling of CO ₂ in 1.42 mm inner diameter tube and the working conditions of Wu et al. [177] presented in Table (4.1). ----- | 142 |
| Figure 4-21: Sensitivity analysis of the two-phase heat transfer coefficient predicted by the present model to the initial liquid film thickness. ----- | 143 |
| Figure 5-1: Sketch of fully developed slug flow unit for flow boiling in a horizontal micro-channel. ----- | 152 |
| Figure 5-2: A sketch of a control volume of a slug flow unit for deriving mass balance equation ----- | 153 |
| Figure 5-3: A sketch of control volume of a slug flow unit for deriving Momentum conservation equation. ----- | 154 |
| Figure 5-4: Shows the energy terms and works applied on the slug unit ----- | 156 |
| Figure 5-5: Bubble frequency predicted by the present model, and the one measured by Revellin et al. [91] versus vapor quality for R134a in 0.509 mm inner diameter micro-tube with a mass flux, 350 $kg/m^2.s$, at $T_{sat} = 30$ °C, and $\Delta T_{sub} = 3.0$. ----- | 166 |
| Figure 5-6: Bubble frequency predicted by the present model, and the one measured by Revellin et al. [91] versus vapor quality for R134a in 0.509 mm inner diameter micro-tube, 500 $kg/m^2.s$, at $T_{sat} = 30$ °C, and $\Delta T_{sub} = 3.0$. ----- | 167 |
| Figure 5-7: Bubble frequency predicted by the present model, and the one measured by Revellin et al. [91] versus vapor quality for R134a in 0.509 mm inner diameter micro-tube, 700 $kg/m^2.s$, at $T_{sat} = 30$ °C, and $\Delta T_{sat} = 3.0$. ----- | 168 |

Figure 5-8: Bubble frequency predicted by the present model, and the one measured by Revellin et al. [91] versus vapor quality for R134a in 0.509 mm inner diameter micro-tube, 1000 $kg/m^2.s$, at $T_{sat} = 30^\circ C$, and $\Delta T_{sub} = 3.0$. ----- 169

Figure 5-9: Bubble frequency versus vapor quality for flow boiling of R245fa in 3.0 mm inner diameter mini-tube at various mass fluxes. ----- 170

Figure 5-10 A comparison between bubble frequency data measured by Revellin et al. [91], and Charney et al. [108], and those predicted by the present model for a range of mass fluxes of 300 to 1000 [$kg/m^2.s$].----- 171

Figure 5-11: Bubble length versus vapor quality for flow boiling of R134a in a 0.509 mm inner diameter micro-tube. ----- 172

Figure 5-12: Bubble length data measured by Revellin et al. [91] versus those predicted by the present model for flow boiling of R134a in isolated bubble zone. ----- 172

Figure 5-13: Variation of bubble length, liquid slug length, and slug unit length versus vapor quality for flow boiling of R134a in a 0.509 mm inner diameter micro-tube with a mass flux 500 [$kg / (m^2.s)$] at an inlet saturation temperature $T_{sat}=30^\circ C$. ----- 174

List of Tables

Table)2-1): Shows different criteria used for channel classifications..... 8

Table (2-2): various trends of flow boiling heat transfer coefficient versus vapor quality in micro-channels, redrawn from Ribatski [180]..... 41

Table (3-1): CHF Correlations for flow boiling in mini and micro- channels..... 69

Table (3-2): Range of Confinement number of the data used to test the present model. 73

Table (3-3): Saturated CHF data of flow boiling in mini/micro- channels used to test the present model..... 87

Table (4-1): Test conditions of two-phase heat transfer data used for model validation 123

Table (4-2): Test conditions of two-phase pressure drop data points used for model validation 130

Table (4-3): Test conditions of vapor void fraction data of R410a measured by Shedd [283] and used here for model validation..... 139

Table (5-1): Experimental conditions of the data used for model validation 165

Table) A-1): Essential dimensionless groups for two-phase flow in horizontal mini/micro-channels..... 198

Table (A-2): Common predictive methods for evaluating heat transfer coefficient for two-phase flow in mini/micro-channels in mini/micro-channels..... 201

Table)A-3): Pressure drop correlations for two-phase flow in mini/micro-channels. 207

Nomenclature

| | | |
|------------|--|------------|
| A | <i>Cross section area.</i> | (m^2) |
| C_o | <i>Distribution parameter.</i> | $(-)$ |
| Bo | <i>Bond number.</i> | $(-)$ |
| Bl | <i>Boiling number.</i> | $(-)$ |
| Bl_{CHF} | <i>Boiling number at CHF.</i> | $(-)$ |
| Ca | <i>Capillary number.</i> | $(-)$ |
| Co | <i>Confinement number.</i> | $(-)$ |
| C_{pl} | <i>Specific heat capacity of the liquid</i> | $(J/kg.K)$ |
| CHF | <i>Critical Heat Flux.</i> | (W/m^2) |
| D | <i>Tube diameter.</i> | (m) |
| D_h | <i>Hydraulic diameter.</i> | (m) |
| D_f | <i>Liquid thermal diffusivity</i> | (m^2/s) |
| F | <i>Convective two phase multiplier factor.</i> | $(-)$ |
| f | <i>Friction factor.</i> | $(-)$ |
| Fa | <i>Fang number.</i> | $(-)$ |
| Fr | <i>Froude number.</i> | $(-)$ |
| F_s | <i>Surface tension term.</i> | (N) |

| | | |
|-----------|---|--------------------|
| G | <i>Mass flux.</i> | $(kg/m^2 \cdot s)$ |
| g | <i>Gravity constant.</i> | (m/s^2) |
| h_f | <i>Liquid specific enthalpy.</i> | (J/kg) |
| h_g | <i>Vapor specific enthalpy.</i> | (J/kg) |
| h_{fg} | <i>Latent heat of vaporization.</i> | (J/kg) |
| Ja | <i>Jacob number.</i> | $(-)$ |
| J | <i>Interfacial velocity.</i> | (m/s) |
| k_f | <i>Thermal conductivity of the working fluid.</i> | $(W/m \cdot K)$ |
| K_n | <i>Knudsen number.</i> | $(-)$ |
| L_h | <i>Heated length.</i> | (m) |
| L_b | <i>Bubble length.</i> | (m) |
| L_s | <i>Liquid slug length.</i> | (m) |
| L_u | <i>Length of a slug unit.</i> | (m) |
| MAE | <i>Mean absolute error.</i> | $(-)$ |
| M | <i>Molecular weight.</i> | (g/mol) |
| \dot{m} | <i>Mass flow rate.</i> | (kg/s) |
| N | <i>Number of data points</i> | $(-)$ |
| N_{pch} | <i>Phase change number.</i> | $(-)$ |
| Nu | <i>Nusselt number.</i> | $(-)$ |

| | | |
|---------|--|-------------|
| Pr | <i>Prandtl number.</i> | (—) |
| P_i | <i>Interfacial surface perimeter.</i> | (m) |
| p | <i>pressure</i> | (N/m^2) |
| p_r | <i>Reduced pressure</i> | (—) |
| P_w | <i>Tube inner perimeter</i> | (m) |
| p_g | <i>Pressure inside the bubble</i> | (N/m^2) |
| p_f | <i>Pressure in the liquid</i> | (N/m^2) |
| q_w'' | <i>heat flux</i> | (W/m^2) |
| q_c'' | <i>Critical heat flux.</i> | (W/m^2) |
| Re | <i>Reynolds number.</i> | (—) |
| R | <i>internal radius</i> | (m) |
| S | <i>Nucleate boiling suppression factor</i> | (—) |
| u_b | <i>bubble velocity</i> | (m/s) |
| u_f | <i>liquid film velocity</i> | (m/s) |
| u_s | <i>liquid slug velocity</i> | (m/s) |
| u_t | <i>Transitional velocity</i> | (m/s) |
| V_s | <i>Volume of spherical bubble</i> | (m^3) |
| V_b | <i>Volume of an elongated bubble</i> | (m^3) |
| We | <i>Weber number.</i> | (—) |

| | | |
|--------|---------------------------------------|-----|
| We_m | <i>Average Weber number.</i> | (–) |
| X | <i>Lockhart-Martinelli parameter.</i> | (–) |
| x | <i>Vapor quality.</i> | (–) |
| Z | <i>Flow direction.</i> | (–) |

Greek symbols

| | | |
|---------------|--|----------------------|
| α | <i>Void fraction.</i> | (–) |
| β | <i>Receding contact angle.</i> | (–) |
| Γ | <i>Mass flow rate.</i> | ($kg/m^2 \cdot s$) |
| Γ | <i>Ratio of bubble length to slug unit length.</i> | (–) |
| δ | <i>Liquid film thickness.</i> | (m) |
| ε | <i>Surface roughness.</i> | (μm) |
| Λ | <i>Wave length.</i> | (m) |
| μ | <i>Dynamic viscosity.</i> | ($N \cdot s/m^2$) |
| ρ | <i>Density.</i> | (kg/m^3) |
| σ | <i>Surface tension.</i> | (N/m) |
| τ | <i>Shear stress.</i> | (N/m^2) |
| ϕ^2 | <i>Two-phase multiplier.</i> | (–) |
| ψ | <i>Dimensionless mass flux.</i> | (–) |

Subscripts

| | | |
|-------------|---------------------------------------|-----|
| <i>A</i> | <i>Annular.</i> | (-) |
| <i>b</i> | <i>In terms of bubble.</i> | (-) |
| <i>c</i> | <i>Critical; or Vapor core.</i> | (-) |
| <i>CB</i> | <i>Coalescing bubble.</i> | (-) |
| <i>ch</i> | <i>Channel.</i> | (-) |
| <i>Conf</i> | <i>Confinement.</i> | (-) |
| <i>eff</i> | <i>Effective.</i> | (-) |
| <i>eq</i> | <i>Equivalent.</i> | (-) |
| <i>Exp</i> | <i>Experimental.</i> | (-) |
| <i>f</i> | <i>Liquid or liquid film.</i> | (-) |
| <i>g</i> | <i>Gas or vapor phase.</i> | (-) |
| <i>go</i> | <i>Only gas phase or vapor phase.</i> | (-) |
| <i>I</i> | <i>Intermittent.</i> | (-) |
| <i>IB</i> | <i>Isolated bubble.</i> | (-) |
| <i>l</i> | <i>Liquid phase.</i> | (-) |
| <i>lo</i> | <i>Only liquid phase.</i> | (-) |
| <i>mac</i> | <i>Macro.</i> | (-) |
| <i>mic</i> | <i>Micro.</i> | (-) |
| <i>nb</i> | <i>Nucleate boiling.</i> | (-) |

| | | |
|-------------|----------------------------|-----|
| <i>cb</i> | <i>Convective boiling.</i> | (-) |
| <i>o</i> | <i>Initial.</i> | (-) |
| <i>opt</i> | <i>Optimum.</i> | (-) |
| <i>Pred</i> | <i>Predicted.</i> | (-) |
| <i>sat</i> | <i>Saturated.</i> | (-) |
| <i>sub</i> | <i>Sub-cooling.</i> | (-) |
| <i>TP</i> | <i>Two phase.</i> | (-) |
| <i>w</i> | <i>Wall.</i> | (-) |

Chapter 1

1. Introduction

The demand of heat removing, from high heat flux devices, has led to a search for an alternative, attractive, and effective cooling system compared to those obtained from conventional ones, which is likely to be available in flow boiling mini/micro-channels. In other words, employing two-phase flow boiling micro-channels insures providing higher heat dissipation, higher heat transfer coefficient, and ability of the channel to be employed at surface temperature higher than those provided by single-phase micro-channels. Therefore, two-phase flow boiling in micro-channels has become a very significant and an essential topic for studying and developing miniature cooling systems which have a wide range of industrial, automotive, nuclear, and aerospace applications (e.g. cooling turbine blades, cooling concentrated photo voltaic cells (CPVs), automotive micro-channel heat exchangers, ... etc.).

By reviewing the available literature for flow boiling in micro-channels, it can be noted that three main important parameters of two-phase flow boiling have been focused on how to understand and clarify the essential flow boiling phenomena in micro-channels. These parameters are two-phase heat transfer coefficient, two-phase pressure drop, and critical heat flux (CHF). Knowing the heat transfer coefficient is very crucial to determine the thermal capacity of the micro-channel based on the required application. Moreover, knowing two-phase pressure drop is very important to calculate the pumping power and consequently to choose the proper pumping system. Regards to the predicting CHF, it is of importance in order to avoid the device overheating and damaging.

Two-phase flow in micro-channels can be classified based on several aspects into several branches. For instance, based on the number of channels: two-phase flow can be classified as:

single micro-channel, and multiple micro-channel. Moreover, in terms of flow orientation, the two-phase flow can be subdivided into vertical, horizontal, and inclined. According to the working conditions, two-phase flow can be classified as adiabatic two-phase flow and diabatic two-phase flow. Furthermore, it can be subdivided into subcooling and saturated two-phase flow based on the inlet conditions of the working fluid. Based on the distribution of applied heat flux, the two-phase flow boiling micro-channels can be subdivided into two-phase flow boiling with uniform and non-uniform heat flux. In the present research, the work is focused on saturated two-phase flow boiling in a single horizontal circular micro-channel subjected to a uniform heat flux.

Although several extensive studies have been carried out on two phase flow in mini/micro-channels either experimentally (e.g., Tran et al. [1]; Zhang et al. [2]; Revellin and Thome [3]; Zhao and Bansal [4]; Fan and Hassan [5, 6] ; Lim et al. [7]) , or analytically (e.g., Moriyama et al. [8]; Kandlikar [9]; Elazhary and Soliman [10]; Kim and Mudawar [11]; Megahed and Hassan [12]), many essential flow boiling phenomena (e.g. dominant heat transfer mechanism, onset of dry-out, bubble confinement and coalescence, liquid film behaviour, etc ...) are still unclear and need to be investigated and clarified. Additionally, one of the challenges that have been encountered in such area of research is getting a reliable predictive method either for heat transfer flow boiling, pressure drop, CHF, or void fraction that can accurately predict the flow boiling heat transfer characteristics under different working conditions.

1.1. Motivation

Microelectronic chips have many applications (e.g., Micro-Electro-Mechanical Systems MEMS, and very large scale integration circuits, VLSI... etc.). In recent years, there has been a tremendous increase in using microelectronics either in aerospace or industrial applications. Achieving high performance is a key factor for employing microelectronics, and to achieve this, the generated heat flux through the chips needs to be dissipated. As a result, a proper cooling system is required. By reviewing the literature, one can see that there have been a few cooling systems that may be used for cooling microelectronics (e.g., air-cooled systems, liquid-cooled systems, two-phase cooling systems ... etc.). Additionally, it has been known that these various cooling systems have different cooling performances and limits. For instance, air-cooling micro-

channels can dissipate high heat flux up to 80 W/cm^2 as addressed by Kandlikar [13]. On the other hand, in 1981, Tuckerman and Pease [14] proved that a very compact water-cooled heat sink was able to dissipate around 790 W/cm^2 with a maximum substrate temperature of 70 C . Colgan et al. [15] indicated that a single-phase micro-channel heat sink is able to dissipate heat fluxes up to 400 W/cm^2 . Kandlikar [13] revealed that flow boiling in micro-channel would be anticipated in much higher thermal performance than single phase micro-channel heat sinks.

Among the available cooling methods, it has been promised that two-phase micro-channel heat sinks, effectively and efficiently dissipate the generated heat from micro-electronics (e.g., Tran et al. [16]; Kandlikar and Grande [17]; Kandlikar [13]). Consequently, many experimental investigations for studying two-phase flow in micro-channels have been carried out in the last three decades for pool boiling (e.g., Kandlikar [9]; Cooke and Kandlikar [18]; Zhao [19]; Piasecka [20]), for mini/micro-channels, and for flow boiling in mini/micro-channels (e.g., Bao et al. [21]; Lee and Lee [22]; Liu and Garimella [23]; Huh et al. [24]; Bertsch et al. [25]; Bortolin et al. [26]; Yang et al. [27]). On the other hand, the analytical work conducted in this topic, particularly for flow boiling in micro-channels, is very limited and inadequate to explore the characteristics of two-phase flow boiling in micro-channel.

It has been reported that most of conventional two-phase correlations (e.g. Sani [28]; Eckels and Pate [29]; Hambraeus [30]; Zurcher et al. [31]; Oh et al. [32]; Lima et al. [33]) are not applicable to two-phase flow boiling in micro-channels, due to the size effect on the flow pattern and flow boiling characteristics. Furthermore, even those correlations performed for mini/micro-channels (e.g. Tran et al. [1]; Zhang et al. [34]; Revellin and Thome [3]; Zhao and Bansal [4]; Fan and Hassan [5, 6]; Lim et al. [7]) are limited for specific working conditions. Furthermore, vapor quality is one of the most important parameters which has been employed extensively for investigating two-phase flow boiling. The evidence from the available literature shows that the two-phase flow boiling heat transfer coefficient is influenced significantly by the vapor quality with a discrepant tendency. The reason for this discrepancy is related to the adopted heat transfer mechanism which is affected by the flow pattern regime, or the chosen correlations which may not be applicable for the real conditions. Thus, more investigations for flow boiling in micro-channels would help for developing a reliable general flow boiling heat transfer model that is

applicable to different flow pattern regimes and wider range of operating conditions and working fluids.

Liquid film plays a significant role for developing flow boiling heat transfer models for slug and annular flow regimes. In other words, for flow boiling in mini/micro-channels, predicting the liquid film variation and employing the critical liquid film thickness concept are key parameters for predicting local two-phase heat transfer coefficient and critical heat flux (CHF) respectively. Although several relevant investigations have been conducted for measuring and predicting liquid film thickness (e.g. Irandoust and Andersson [35]; Fukano and Kariyasaki [36]; Saitoh et al. [37]; Revellin et al. [38]; Ong and Thome [39]; Han et al. [40, 41]), the applicability of proposed correlations is either limited to a specific working fluid or certain channel geometry and working conditions. Consequently, further analytical and experimental studies would allow for better understanding of liquid film evaporation behavior and are strongly recommended to be carried out for a wide range of operating conditions and working fluids.

Studying the CHF analytically may help avoid the tremendous cost of CHF experimental test, particularly those related to the nuclear reactors. For instance, according to Piro et al. [42] (1999), the cost of CHF experimental tests for nuclear reactors for the period 1980-1999 only in Canada was about \$30.0 million. Furthermore, prediction of CHF is a crucial criterion for estimating the thermal capacity of the mini/micro-channel heat sinks, and an essential design parameter that helps avoiding the damage of the mini/micro-channel heat sinks. Consequently, several experimental investigations for CHF have been performed recently for flow boiling in mini/micro-channels (e.g. Piro et al. [42]; Qu and Mudawar [43]; Zhang et al. [44]; Wojtan et al. [45]; Qi et al. [46]; Kosar et al. [47]; Basu et al. [48]; Hsieh and Lin [49]; Tibirica et al. [50]; Kaya et al. [51]), and as a result, many experimental data sets and empirical correlations are collected and proposed for specific working conditions. On the other hand, only few semi-analytical saturated CHF models for flow boiling in micro-channels have been developed (e.g. Kandlikar [9]; Revellin and Thome [52]; Du et al. [53]). Since it is of importance to have a reliable CHF prediction model that can be applicable to a wide range of operating conditions and cover wider design parameters, extra efforts in analytical modeling for saturated CHF for flow boiling in micro-channels are needed.

1.2. Objectives and Organization

The main objective of this thesis is to investigate the characteristics of two-phase flow boiling in annular and slug flow regimes, and to provide a reliable predictive method for predicting the critical heat flux, heat transfer coefficient, pressure drop, and void fraction in horizontal micro-tubes under uniform heat flux. This has been done through achieving the following consecutive sub-objectives:

1. Developing a semi-analytical model for predicting the liquid film thickness in annular flow regime during two-phase flow boiling in a horizontal micro-tube. This stage was essential to study the incipience of the dry-out phenomenon and to predict the critical heat flux.
2. Developing a model to predict the two-phase heat transfer coefficient, pressure drop, and void fraction in annular flow regime. Effects of phasic enthalpies, viscous force, inertial force, and liquid film evaporation were considered in modeling. Following, the influence of the main operating conditions, working fluid properties, and channel size on the model results, were investigated.
3. Developing a semi-analytical model to study the bubble dynamics, bubble length, and bubble frequency in the slug flow regime based on the drift flux model, for a better understanding of flow boiling phenomena in mini/micro-channels. Extensive experimental data available in literature was used for validation of the developed models.

The thesis has been written in the format of manuscript-based-thesis and consists of six chapters. A detailed literature review has been provided in chapter 2 for two-phase flow in single horizontal mini/micro-channel for both adiabatic and diabatic conditions. The main objectives of the present work have been listed above for reader convenience, and repeated at the end of chapter 2. Investigation of critical heat flux (CHF) for flow boiling in a single horizontal mini/micro-tube subjected to a uniform heat flux is presented in chapter 3. Predictions of heat transfer coefficient, pressure drop, and void fraction have been studied and presented in chapter 4. The main characteristics of slug flow have been investigated and presented in chapter 5. The summary of this work and recommendations for further researches needed for flow boiling in mini/micro-channels have been provided in chapter 6.

Chapter 2

2. Literature Review

The aim of this chapter is to review the literature on two-phase flow boiling in mini/micro-channels, and address the essential aspects that should be focused on for better realizing and understanding of flow boiling phenomena in mini/micro-channels (e.g., micro-scale channel, basic flow patterns, flow pattern maps, two-phase heat transfer coefficient, two-phase pressure drop, critical heat flux, ... etc.).

2.1. Two-Phase Flow and Associated Dimensionless Groups

In order to study flow boiling in micro-channels, a simple way is used for describing the level of influence of the various essential parameters either if they are force terms or energy terms. Thus, it is crucial to identify some most common dimensionless group, used for two-phase flow boiling in micro-channels. Table (A-1) shows the essential dimensionless groups for two-phase flow in horizontal mini/micro-channels which are presented in the literature (e.g. Irandoust and Andersson [35]; Chen [54]; Akers et al. [55]; Rohsenow [56]; Wu et al. [57]; Ozawa et al. [58]; Li et al. [59]; Kandlikar [60]; Ducoulombier et al. [61]; Baba et al. [62]; Bretherton [63]; Shedd and Newell [64]; Han and Shikazono [65]; Harirchian and Garimella [66]).

2.2. Channel Classification Criteria

In the literature on two phase micro-channel, the relative importance of the criterion used to define the word “micro” has been a subject of considerable discussion. Furthermore, the size effect is one of the challenges faced in studying two-phase flow boiling. Additionally, it has been revealed in previous studies that two-phase flow boiling correlations and models developed for conventional-scale channels may not be applicable for micro-scale channels. Therefore, several studies have been carried out for clarifying the criteria that identify scale transition (e.g. Ong and Thome [39]; Kew and Cornwell [67]; Harirchian and Garimella [66]; Suo and Griffith [68]; Brauner and Maron [69]; Triplett et al. [70]; Mehendale et al. [71]; Kandlikar [72]; Cheng and Wu [73]; Li and Wu [74]; Revellin and Thome [75]). Table 2-1) shows different criteria which have been reported in the literature for channel classifications.

Table 2-1): Shows different criteria used for channel classifications.

| Author(s) | Criterion | Classification | Notes |
|------------------------|--|---|---|
| Suo and Griffith [68] | $\Omega = \rho_f g D^2 / 4\sigma$ | Capillary slug flow: $\Omega < 0.22$ | The authors suggested the gravity effect is neglected and the flow is as capillary slug flow at this critical value. |
| Brauner and Maron [69] | $\frac{(2\pi)^2 \sigma}{g(\rho_f - \rho_g) D^2}$ | Small pipe: $\frac{(2\pi)^2 \sigma}{g(\rho_f - \rho_g) D^2} > 1$ | They reported that the stratified flow pattern disappeared when surface tension overcomes the gravity and the bubble confined in the pipe. A pipe with a diameter less than critical bubble radius can be considered as a small pipe. |
| Kew and Cornwell [67] | Co | Small pipe: $Co \geq 0.5$ | They revealed that confinement phenomenon plays significant role for boiling in small hydraulic channels when confinement number $Co \geq 0.5$. |
| Triplett et al. [70] | Co | Micro-scale size: $Co \geq 1.0$ | They addressed two-phase flow patterns in capillary tubes. They defined micro-channel size as those channels that have Confinement number greater than one $Co \geq 1.0$. |
| Mehendale et al. [71] | D_h | Micro-scale size: $1 \mu m \leq D_h \leq 100 \mu m$ Miso scale size: $100 \mu m < D_h < 1 mm$ Compact scale size: $1 mm < D_h \leq 6 mm$ Conventional scale size: $6 mm < D_h$ | They studied two-phase heat transfer in micro/meso-channels and classified heat exchangers into four main categories. |

| | | | |
|-------------------------------|-------------|------------------------------------|--|
| Kandlikar [72] | D_h | Micro-scale size: | He considered $200 \mu m$ is the critical size in two-phase flow, and presented channel classification criteria based on gas flow consideration. |
| | | $10 \mu m \leq D_h \leq 200 \mu m$ | |
| | | Mini-scale size: | |
| | | $200 \mu m < D_h \leq 3 mm$ | |
| | | Conventional-scale size: | |
| | | $D_h > 3 mm$ | |
| Cheng and Wu [73] | Bo | Micro-scale size: | They discussed basic phase change heat transfer phenomena and classified the channels based on the ratio between buoyancy and surface tension forces. |
| | | $Bo < 0.05$ | |
| | | Meso/Mini-scale size: | |
| | | $0.05 < Bo < 3.0$ | |
| | | Macro-scale size: | |
| | | $Bo > 3.0$ | |
| Li and Wu [74] | $N_{conf.}$ | Micro/Mini-scale size: | They introduced a new criterion to distinguish between two-phase flow in conventional scale and micro-mini-scale channels taking into account the influences of four basic forces, gravitational, surface tension, viscous, and inertial forces. |
| | | $Bo.Re_l^{0.5} \leq 200$ | |
| | | Conventional-scale size: | |
| | | $Bo.Re_l^{0.5} > 200$ | |
| Harirchian and Garimella [66] | $N_{conf.}$ | Micro-scale size: | A new transition criterion for distinguishing between macro and micro-channels for flow boiling in multiple micro-channel in terms of “convective confinement number”, |
| | | $Bo.Re_l^{0.5} < 160$ | |

2.3. Dominant Forces and Scale Size Effect

There is evidence that the channel size and orientation affect the domination of various basic forces for two-phase flow boiling in mini/micro-channels. Moreover, some previous two-phase flow studies have reported that hydraulic diameter, and basic forces in flow boiling such as surface tension, viscous, inertia, and momentum change of evaporation have significant effects on both flow patterns and heat transfer characteristics in micro-channels, Kandlikar [72, 60].

Soliman [76] studied the effects of transition from mist to annular flow regime on heat transfer coefficient for condensation in horizontal tubes. He classified the forces acting on the two-phase flow into dominant destructive forces which are represented by the inertia force of the vapor phase, and stabilizing forces which are represented by the surface tension and liquid viscous forces. Moreover, he proposed a transition criterion for defining the transition from mist to annular flow in terms of a modified Weber number based on the force balance between the above mentioned forces.

Kandlikar [9] developed a theoretical CHF model for pool boiling on the upward-facing surface based on the force balance of a departure bubble. It has been reported that at the onset of the CHF, the force of the momentum due to evaporation is larger than the effects of buoyancy force together with the surface tension force. Moreover, Kandlikar [13] performed a scale analysis to investigate the effects of various forces, to estimate flow pattern transitions, and flow stability for flow boiling of water and FC72. It has been revealed that five main forces, namely, surface tension, viscous shear, inertia, evaporation momentum, and gravity forces play significant role for flow boiling in mini/micro-channels. Additionally, it has been pointed out that momentum change of evaporation and surface tension forces are dominant and significantly influence flow boiling characteristics, mainly for small channel size as shown in Figure 2-1.

Furthermore, buoyant and drag forces play essential roles for vertical flow boiling, particularly for studying bubble dynamics and its effects on heat transfer and pressure drop. Lee and Mudawar [77] developed a mechanistic model for predicting critical heat flux (CHF) for turbulent flow boiling in vertical mini/small tubes. They predicted the elongated bubble velocity and liquid film thickness trapped between the elongated bubble and the wall based on the force

balance between buoyancy and drag forces, and considering the influence of the lateral force which was created due to the bubble rotation.

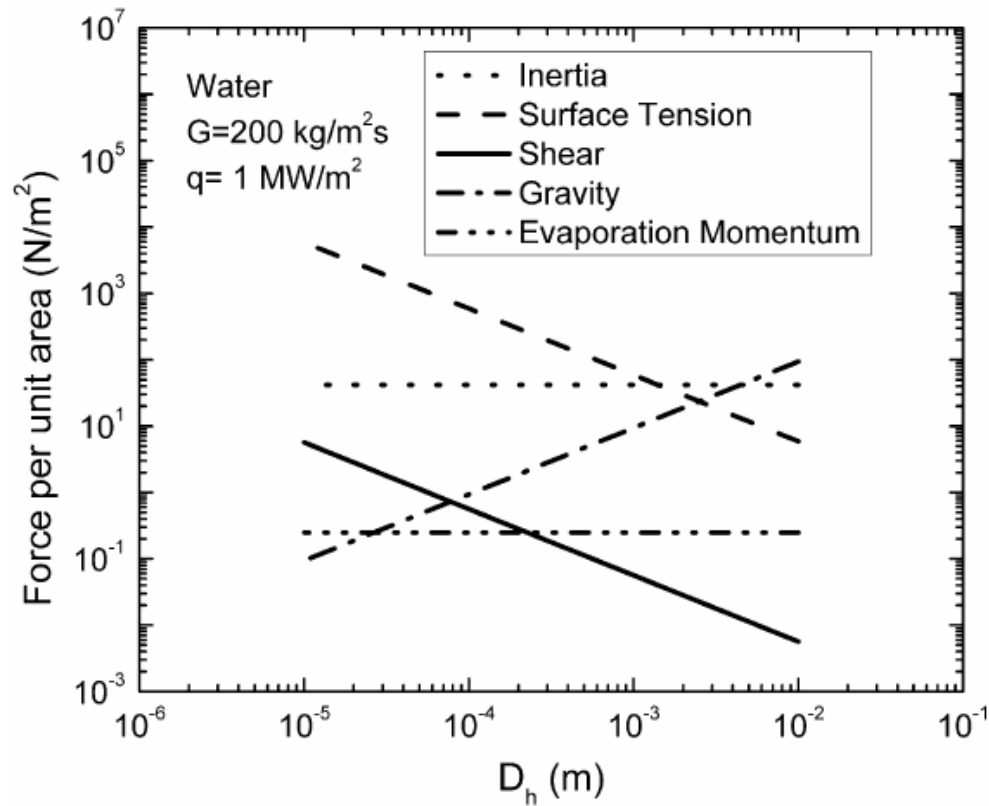


Figure 2-1 : Shows the effects of tube size on different forces for flow boiling of water at $G=200$ $[kg/m^2.s]$ and $q_w = 1000 kW/m^2$, (Kandlikar [13])

Kandlikar [72] revealed that as the channel size decreases, some parameters become more significant. For instance, the change of momentum of evaporation, which affects the bubble departure and growth diameter and consequently the confinement phenomenon and flow patterns, becomes more important in small channels. Moreover, the significant effect of inner wall roughness related to pressure drop estimation becomes very crucial as the channel size decreases. Furthermore, Kandlikar [60] analyzed the basic forces influencing the flow boiling features for flow boiling in micro-channels and proposed two dimensionless groups, K_1 and K_2 . K_1 is defined as the ratio between the momentum evaporation and inertia forces, while K_2 is defined as the ratio between the momentum evaporation and surface tension forces. It has been reported that higher values of K_1 indicates the dominance of momentum evaporation force which

influences the interface movements, while K_2 controls the movement of the interphase at the contact line, yet the contact angle was not included in the definition of the dimensionless group K_2 . Overall, the proposed two dimensionless groups were introduced to be implanted in predicting CHF.

Shikazono and Han [78] investigated the liquid film thickness for flow boiling in annular flow regime considering the effects of viscous, surface tension, and inertial forces, as well as the channel size and geometry in micro-scale two-phase flow. It has been found that in flow boiling micro-scale, in addition to viscous and surface tension forces, inertial force has a significant effect on liquid film thickness even at laminar flow, and should be considered for future developed two-phase flow liquid film correlations. Based on the flow visualization and measurement of the liquid film thickness for flow boiling of R134a, R236fa, and R245fa, in horizontal mini-tubes with a range of inner diameter of $0.50 \leq D_h \leq 3.04 \text{ mm}$, Ong and Thome [39] revealed that the effects of gravity force are insignificant, while the surface tension and shear forces are dominant for $Co \cong 1.0$. In other words, the gravity force effects decrease by decreasing the channel diameter. Moreover, in terms of void fraction, it has been reported that as the void fraction increases, the effects of surface tension and gravity forces decrease while the effects of shear forces become more significant and dominant. Additionally, the effect of gravity force is still significant for $Co \leq 0.34$.

2.4. Flow Patterns and Flow Pattern Maps

Identifying the flow pattern and developing a reliable flow pattern map is very significant for predicting transition boundaries of the flow patterns. Therefore, several studies have been done for investigating flow pattern and flow pattern maps in mini/micro-channels (e.g. Kandlikar [72]; Garimella et al. [79]; Revellin and Thome [75]; Saisorn and Wongwises [80]; Karayiannis et al. [81]; Alexeyev et al. [82]; Kattan et al. [83]; Coleman and Garimella [84]; Yang and Shieh [85]), for different working fluids, channel sizes, channel orientation, and working conditions.

An excellent analysis and experimental investigation of two-phase capillary flow in horizontal mini/micro tubes were performed by Suo and Griffith [68]. They investigated two-phase flow of various working fluids, (Water-air, Water-N₂, N-Heptane-N₂, N-Heptane-He, and

N-Octane-N₂), through 0.514, and 0.795 mm inner diameter single horizontal mini/micro-tubes. Three main flow patterns have been observed, namely, slug flow, bubbly-slug (where the bubble tail is broken up into smaller bubbles), and annular flow patterns. The transition lines of the observed flow patterns were determined based on both the measured data and the conducted analytical work. It has been revealed that the slug flow pattern can be observed at the following restrictions: $(\rho_f/\rho_g) \gg 1$, $(\mu_f/\mu_g) > 25$, and $(\rho_f g R_o^2/\sigma) < 0.22$.

Alexeyev et al. [82] investigated experimentally flow patterns for two-phase flow of Helium in horizontal mini-channels with 1 mm gap size of rectangular and round slots. They developed flow pattern maps for two-phase Helium flow in terms of liquid and vapor superficial velocities based on the obtained and previous data. Moreover, five basic flow patterns were identified which are bubbly, stratified, intermittent, annular-dispersed and dispersed, and mist flow patterns. Surprisingly, slug flow pattern was not observed in their experiments, and it was attributed to the influence of either a geometrical factor such as the slot shape or a hydrodynamic factor such as the liquid-vapor interface instability. Furthermore, the authors revealed that the transition lines of the two-phase Helium flow patterns were different compared to other fluids due to the effects of the physical properties of the Helium which are influenced by the operating pressure.

To better understand flow pattern and transition boundaries for flow boiling conditions, it would be essential to consider the influence of applied heat flux on flow patterns. Therefore, Kattan et al. [83] developed a flow pattern map for two phase flow boiling in horizontal tubes, which is applicable to both adiabatic and diabatic conditions, based on the experimental database of five working fluids, (R134a, R123, R404a, R404a, and R502) in 12 mm inner diameter horizontal tube. Five main flow patterns were included in their flow pattern map: intermittent flow (I), annular flow (A), mist flow (M), stratified flow (S), and stratified wavy flow (SW). The flow pattern map was coordinated in terms of mass flux and exit vapor quality. Furthermore, the onset of partial dry-out that occurs at the top of the test section has been predicted based on the maximum heat transfer coefficient in the annular flow regime. The transition line from intermittent to annular flow is represented by,

$$X_{I/A} = \left[0.34^{(1/0.875)} (\rho_g / \rho_f)^{-(1/1.75)} (\mu_f / \mu_g)^{-(1/7)} + 1 \right]^{-1} \quad (2.1)$$

Coleman and Garimella [84] studied the effects of tube size, and geometrical shape on the flow pattern of air-water two-phase flow in circular and rectangular horizontal small channels. They presented flow regime maps of air-water two-phase flow and identified the boundaries of flow patterns in terms of liquid and gas superficial velocities. It has been concluded that for adiabatic two-phase flow in small tubes, say less than 10 mm, the tube size, and the surface tension force have significant effects on the observed flow patterns and their transition boundaries, where the stratified flow pattern was suppressed and the range of intermittent flow is expanded.

Yang and Shieh [85] investigated the effects of working fluid and tube size on flow pattern characteristics in small horizontal tubes. They studied the flow pattern of air/water, and R134a in small horizontal tubes, $1.0 \leq D_h \leq 3.0 \text{ mm}$, where six different flow patterns were observed which are bubbly, slug, plug, wavy stratified, dispersed, and annular flow patterns. The authors used superficial velocities of gas and liquid phases for identifying the boundaries of observed flow patterns. A significant effect of the surface tension on the transition boundaries of the flow patterns in small channels was reported. Moreover, it was revealed that for the same tube size, and working conditions, the transition from plug flow to bubbly flow for the air-water flow occurs earlier than that for R134a due to the high surface tension of water. Additionally, none of the flow pattern maps available at that time was able to predict flow patterns of both tested working fluids.

Triplett et al. [70] investigated two-phase flow patterns of air-water flow in 1.1, and 1.45 mm inner diameter circular mini-tubes, and 1.09, and 1.49 mm hydraulic diameter of triangular cross section mini-tubes. Five various flow patterns were observed which are bubbly; churn; slug; slug-annular; and annular flow patterns. A flow pattern map coordinated in terms of liquid and gas superficial velocities was presented, and compared with some available flow pattern maps which did not give a good agreement with the measured data. In a follow up study, Thome and El Hajal [86] developed a flow pattern map for evaporation in small horizontal tubes by modifying the flow pattern map of Kattan et al. [83] and involving the Rouhani-Axelsson drift

flux model [87] which was developed for predicting void fraction. The proposed flow pattern map is presented in Figure 2-2, and valid for adiabatic and diabatic flow conditions in small horizontal tubes, but it was not validated to be applicable for macro/micro-tubes. The transition line between intermittent flow and annular flow is determined by the correlation proposed by Kattan et al. [83] for fixed Loackhart-Martinelli parameter $X_{tt} = 0.34$.

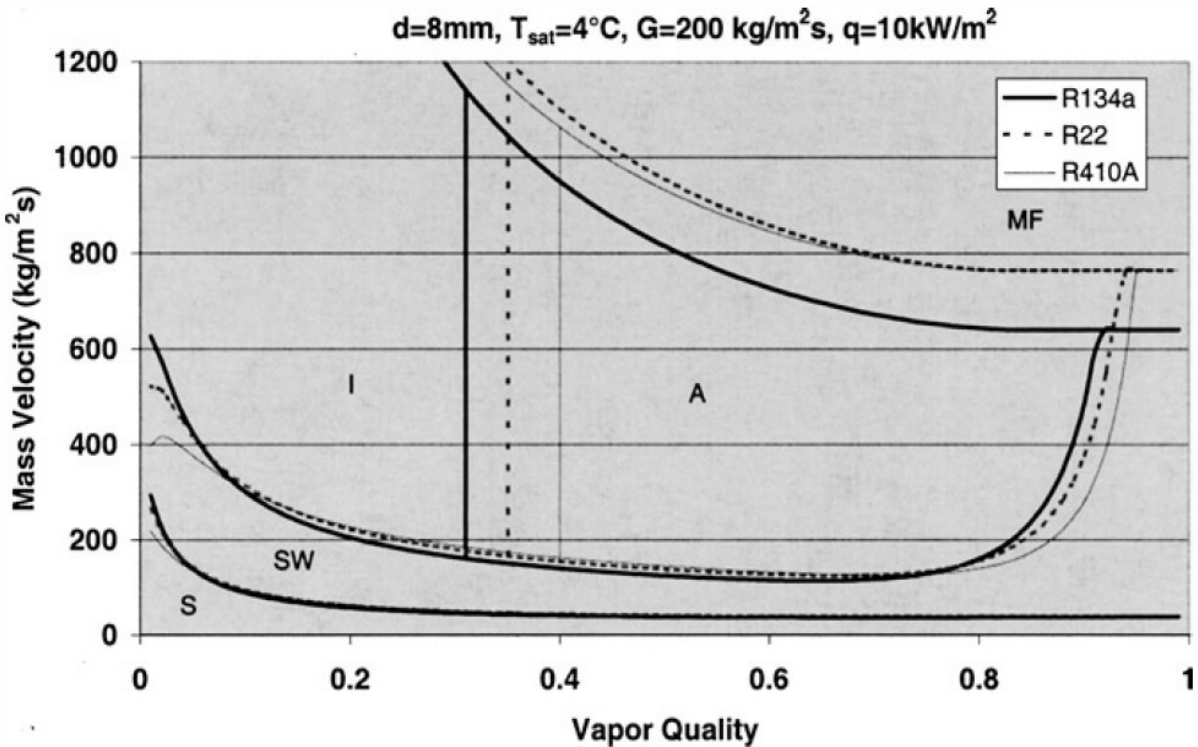


Figure 2-2: Flow pattern map developed by Thome and El Hajal [86] for evaporation in horizontal tubes considering the effect of working fluid.

In 2005, Hassan et al. [88] developed two universal flow pattern maps for two-phase flow in vertical and horizontal micro-channels in terms of liquid and gas superficial velocities. Four basic flow patterns were defined, bubbly flow, intermittent flow, churn flow, and annular flow pattern. It has been revealed that the effect of surface tension in two-phase micro-channel is very significant and influences the flow patterns as well as the transition lines. Based on the force-type dominance, the authors divided flow patterns into two main types. The first zone is that mainly controlled by the surface tension and this includes bubbly, slug, and confined flow patterns. The second zone is mainly influenced by the inertia force, and this includes dispersed

and annular flow patterns. Based on the experimental database from their and previous studies for two-phase flow in macro/micro-channels with a range of hydraulic diameter of $0.1 \leq D_h \leq 1.0 \text{ mm}$, the authors proposed two flow pattern maps for vertical and horizontal flow in micro-channels. The authors reported that a lack in two-phase micro-channel experimental database still exists and more experimental work particularly for channels with $D_h \leq 0.5 \text{ mm}$ is needed. Furthermore, in order to implement the proposed flow pattern maps, the phasic superficial velocities are needed which make it a quite hard to identify the transition line correctly. Additionally, the effects of applied heat flux on the flow patterns and their transition boundaries is very significant and should be considered for determining flow pattern boundaries.

Recently many researchers have studied the relation between heat transfer and flow pattern maps. Cheng et al. [89] analyzed flow boiling heat transfer and flow pattern maps for flow boiling of CO₂ in horizontal tube. Based on the observed variation in heat transfer tendency, the authors proposed criteria for predicting flow patterns transition lines from intermittent flow to annular flow, and from annular flow to dry-out flow which are given by,

$$X_{I/A} = \left[1.8^{(1/0.875)} (\mu_f / \mu_g)^{-(1/7)} (\rho_g / \rho_f)^{-(1/1.75)} + 1 \right]^{-1} \quad (2.2)$$

$$X_{A/D} = 0.58 \exp \left[0.52 - 0.67 We^{0.17} Fr_g^{0.348} (\rho_g / \rho_f)^{0.25} (q_w'' / q_{CHF}'')^{0.7} \right] \quad (2.3)$$

In a major flow pattern study, Revellin [90] investigated the flow patterns of R134a and R245fa for flow boiling in 0.790 mm and 0.509 mm inner diameter round single micro-tubes. He revealed that seven flow patterns were recognized and identified as bubbly flow, bubbly/slug flow, slug flow, slug/semi-annular flow, semi-annular flow, wavy annular flow and smooth annular flow. Figure 2-3 shows the flow pattern obtained for R134a. In general, it has been found that the basic flow patterns that have been observed for flow boiling in horizontal micro-channels, may be classified into three basic flow patterns, namely as bubbly flow, slug flow, and annular flow.

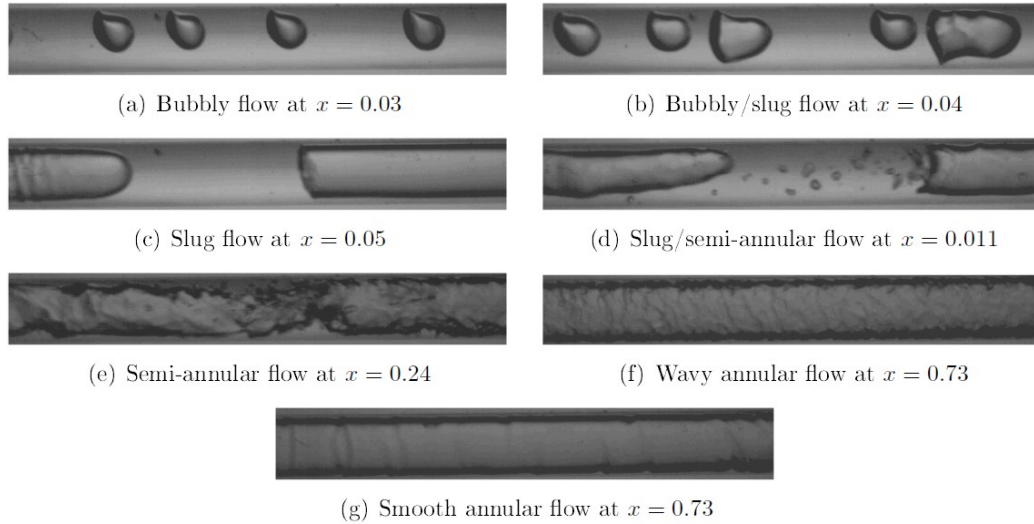


Figure 2-3: Flow patterns for R134a flowing with $G=500$ [$\text{kg}/\text{m}^2 \cdot \text{s}$] in a 0.79 mm channel has an average heat length $L=70$ mm at $T_{\text{sat}}=30$ °C and $\Delta T_{\text{sub}}=30$ °C, observed by Revellin [90].

Revellin et al. [91] carried out diabatic two-phase experimental work for investigating the main bubble characteristics and flow patterns of flow boiling of R134a in a 0.5 mm inner diameter horizontal micro-tube by developing an optical measurement technique. It has been revealed that the bubble coalescence phenomenon and mass flux affect flow pattern boundaries. Moreover, the authors developed a new diabatic flow pattern map, as shown in Figure 2-4, for evaporation in horizontal micro-channels based on visualization data of flow boiling of R134a, and R245fa in 0.509 , and 0.790 mm inner diameter single micro-tubes. Four main flow regimes were observed namely, isolated bubble regime, (IB) coalescing bubbly regime, (CB), annular flow regime, (A), and post dry-out regime, (PD). The IB regime was identified as the zone where the bubble generation rate dominates the bubble coalescing rate and this includes the bubbly flow and the slug flow regime. The CB regime was identified as the zone where the bubble coalescing rate dominates the bubble generation rate. The transition lines from IB to CB and from CB to A flow regimes are represented by the Eq. (2.22) and Eq. (2.23) respectively. Furthermore, the authors recommended including the influence of flow instability on flow pattern transition boundaries for future work in order to extend the ability of the model to predict the incipience of back flow in two-phase flow boiling micro-channels.

$$x_{IB/CB} = 0.763 \left(\frac{Re_{lo} Bo}{We_{go}} \right)^{0.41} \quad (2.4)$$

$$x_{CB/A} = 0.00014 Re_{lo}^{1.47} We_{lo}^{-1.23} \quad (2.5)$$

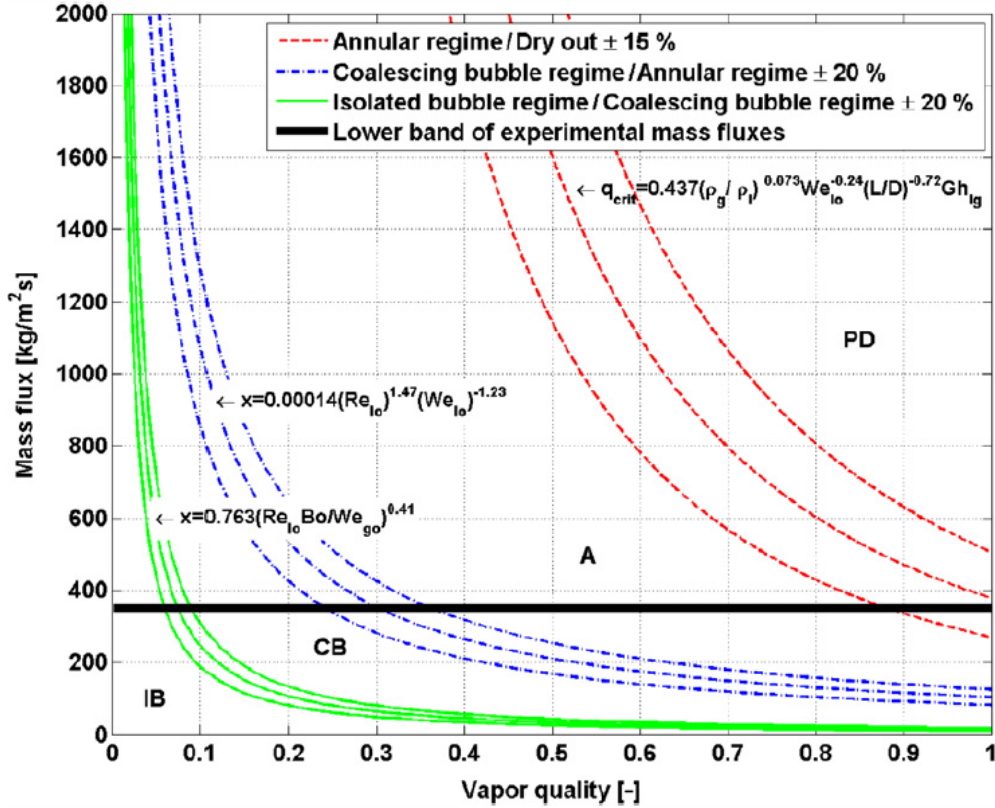


Figure 2-4: A new diabatic coalescing bubble map for evaporating flow in circular uniformly heated microchannels: R-134a, $D = 0.5$ mm, $L = 70$ mm, $T_{sat} = 30$ °C, $q''_w = 50$ [kW/m²], Revellin and Thome [75].

In a follow up study, Zhang and Fu [92] investigated the effects of tube size on flow patterns and transition boundaries of liquid nitrogen in 0.531, and 1.042 mm inner diameter vertical micro-tubes. Four basic flow patterns have been observed which are bubbly, slug, churn, and annular flow. For the micro-tube size, they have observed confined bubble flow pattern, which is characterized by the axial expansion of the bubble that has hemispherical shapes at both ends of the bubble. Furthermore, mist flow pattern has been reported due to the existence of small droplets in the vapor core, and dry-out of the liquid film. The authors have pointed out that

even in vertical flow boiling micro-channels; the gravity force effect is insignificant compared to inertial and surface tension forces. They compared their experimental data with some available models for predicting flow pattern transition boundaries, and concluded that none of the existing models was able to predict micro-channel flow pattern boundaries. Additionally, they measured heat transfer coefficient and void fraction, and reported that in vertical micro-channels, heat transfer enhancement was observed in annular flow regime.

Rashid et al. [93] studied the flow boiling of R134a in a 0.781 mm inner diameter of horizontal micro-tube subjected to uniform heat fluxes within the range of $5 \leq q_w'' \leq 45 [kW/m^2]$, and mass fluxes ($100 \leq G \leq 400 [kg/m^2.s]$). They reported that main observed flow patterns are isolated bubbly, confined bubble, elongated bubble, slug flow, semi-annular, and annular flow patterns. Furthermore, they predicted the main bubble features, such as bubble length, velocity, and frequency considering the effects of main operating parameters. It has been revealed that bubble frequency increases by increasing mass, and heat fluxes, which significantly affects the flow patterns transition lines. They recommended conducting extra flow visualization of flow boiling in micro-channels for a better understanding of two-phase boiling in micro-channels.

Arcanjo et al. [94] conducted experimental work for studying bubble characteristics and flow patterns of flow boiling of R134a, and R245fa in a 2.32 mm inner diameter horizontal mini-tube using a high speed video camera with mass flux range, $50 \leq G \leq 600 [kg/m^2.s]$, taking into account the effect of inlet saturation temperature. Four main flow patterns were observed which are bubbly, elongated bubbles, churn, and annular flow patterns. The authors presented flow regime map of the obtained results in terms of mass flux and vapor quality, and compared the transition lines of the observed flow patterns with those proposed by Barnea et al. [95], Felcar et al. [96], Revellin and Thome [75], and Ong and Thome [97] at saturation temperatures 22, 31, and 41 °C. Their experimental data gave good agreement with those developed by Felcar et al. [96], and Ong and Thome [97]. Based on flow visualization, the authors measured bubble velocity, length, and frequency. It has been concluded that bubble velocity increases by increasing the mass flux and vapor quality, while it decreases by increasing the inlet saturation temperature.

Celata et al. [98] carried out two-phase flow experiments for studying the flow patterns of flow boiling of FC-72 in a 0.48 mm inner diameter horizontal micro-tube. Basically, four main flow patterns have been observed namely, bubbly, slug, annular and dry-out flow patterns. However, two mixed flow patterns were observed without clear flow pattern boundaries namely bubbly/slug and slug/annular flow patterns. The churn flow pattern was not observed in such small size of the micro-tube. It has been pointed out that the flow boiling instability has been observed due to the backward and forward expansion of the elongated bubble in axial direction. The authors identified the observed flow patterns in terms of mass flux and exit vapor quality, and compared them with the flow regime maps of larger tube sizes ($2.0 \leq D_h \leq 6.0 \text{ mm}$) developed by Mishima and Ishii [99], McQuillan and Whalley [100], and Ong and Thome [39]. It has been revealed that none of the used flow pattern maps was able to predict the transition line from bubbly flow to slug flow of the 0.48 mm micro-tube data. The authors attributed this to the shift movement of the bubbly flow toward the sub-cooled region due to decreasing the tube size. Furthermore, they noted that the flow pattern map of McQuillan and Whalley [100] was not able to predict the transition line from slug to annular flow for mass flux ($G \leq 1250 \text{ [kg/m}^2 \cdot \text{s]}$) since it was originally developed for large tubes at adiabatic working conditions, which is not the case for micro-tubes at diabatic conditions. On the other hand, both flow pattern maps of McQuillan and Whalley [100], and Ong and Thome [39] were able to fairly predict the transition line from slug flow to annular flow regime of the FC-72. Overall, the authors reported a need for developing a method able to quantitatively describe flow pattern boundaries and covering the sub-cooled and saturated regions in micro-tubes.

One of the crucial parameters affecting the flow pattern in micro-channels is the reduced pressure. Therefore, Mastrullo et al. [101] investigated the effects of reduced pressure on flow pattern transition boundaries of flow boiling of CO₂ and R410A in a 6.0 mm inner diameter horizontal small tube. They performed their experiments for the range of mass fluxes ($150 \leq G \leq 500 \text{ [kg/m}^2 \cdot \text{s]}$), and heat fluxes ($5 \leq q_w'' \leq 20 \text{ [kW/m}^2 \cdot \text{s]}$) for reduced pressure range of $0.57 \leq p_r \leq 0.64$. Additionally, they compared their observed flow pattern transition boundaries from intermittent to annular, which is denoted as (I/A), and from annular to dry-out flow regime, which is denoted as (A/D), with the flow regime maps of Wojtan et al. [102], Cheng et al. [103], Barbieri et al. [104], and Canière et al. [105]. It has been noted that none of the tested flow

pattern maps was able to predict the flow pattern transition lines fairly, except the annular to dry-out flow transition line (A/D) which was well predicted by the flow pattern map proposed by Wojtan et al. [102]. Consequently, based on the performed comparison and 1420 data points, the authors developed correlations for predicting the flow pattern transition boundaries for slug, intermittent, annular, and dry-out flow patterns by predicting the vapor quality at which the transition occurs. The proposed correlations predicted the transition lines with reasonable MAE.

Ali et al. [106] investigated the characteristics of flow boiling of R134a in a 0.781 mm inner diameter horizontal micro-tube subjected to a uniform heat flux ranging from 5 to 45 [kW/m^2] with low mass flux, 100 to 400 [$kg/m^2 \cdot s$]. Five main flow patterns were presented as follows: bubbly flow (isolated bubble flow and confined bubble); slug flow (elongated bubble, and slug flow); semi annular flow (slug annular, and wavy annular flow); annular flow; and mist flow pattern. Considering the effects of working conditions, it has been revealed that wavy annular flow can be obtained at high mass flux, while mist flow pattern was observed at very low mass flux. Furthermore, it was reported that bubble frequency increases with mass flux, and increasing the pressure system leads to a shift of the transition boundaries toward lower superficial vapor velocity due to the sub-cooling effect.

It is of importance here to notice that Ali et al. [106] employed the experimental dataset of Martin-Callizo et al. [107] which was measured for flow boiling of R134a in a 1.33 mm inner diameter vertical mini-tube, to study the effect of tube size on flow pattern neglecting the influence of flow orientation. However, churn flow pattern was observed for vertical flow in the study of Martin-Callizo et al. [107], while it was not observed for horizontal flow. Furthermore, Ali et al. [106] reported that, due to the confinement effects, the transition lines from bubbly to slug flow are shifted to lower vapor quality for smaller tubes than those for large tubes. On the other hand, due to the significance of surface tension in small channels, they revealed that the transition line from slug to annular flow was shifted to higher vapor quality for small tubes than those observed for the large tubes.

Transition boundaries from intermittent to annular flow regime play a significant role for flow boiling in micro-channels. Charnay et al. [108] investigated the characteristics of flow patterns of flow boiling of R245fa in a 3.0 mm inner diameter horizontal small tube considering

a wide range of mass, $100 \leq G \leq 1500 [kg/m^2.s]$, and heat fluxes of $10 \leq q_w'' \leq 90 [kW/m^2]$ using high speed video camera. Four basic flow patterns have been observed, which are bubbly flow, bubbly-slug flow, slug flow, and annular flow. It has been found that (I/A) transition line is dependent of applied heat flux. Furthermore, the authors measured bubble characteristics and demonstrated that at the peak of bubble frequency, the flow pattern changes. Additionally, they linked the (I/A) transition line to the dominant heat transfer mechanism, where they observed that transition boundary from intermittent to annular flow corresponded to the transition from nucleate boiling to convective boiling heat transfer mechanism.

Recently, Tibirica and Ribatski [109] conducted an experimental work for studying flow patterns and bubble behavior for flow boiling of R134a, and R245fa in a 0.38 mm inner diameter stainless steel horizontal micro-tube with a heated length of 200 mm. The authors performed their experiments employing a high speed camera ($10^5 fps$), for a wide range of mass fluxes, ($100 \leq G \leq 900 [kg/m^2.s]$), and high heat flux reaches to $q_w'' \leq 226 [kW/m^2]$. Four basic flow patterns have been observed namely as bubbly flow, slug flow, annular flow, and dry-out flow patterns. The authors analyzed bubble characteristics and proposed new correlations for predicting the bubble departure diameter and bubble departure frequency for flow boiling in micro-channels. They found that bubble departure frequency increases with mass flux. Furthermore, the authors highlighted the main interfacial waves that affect the observed flow patterns and result in interfacial instability. They reported that the interfacial waves can result from five main sources: 1. they can be created due to the dominant of drift vapor velocity; 2. Oscillation of liquid slug; 3. Bubble coalescing phenomenon; 4. Bubble nucleation in trapped liquid film; 5. Non-uniformity of applied heat flux. Additionally, liquid entrainment droplets were observed in the vapor core for 0.4 mm micro-tube due to two different sources of interfacial instability which are caused by liquid slug instability, and bubble coalescing phenomenon.

2.5. Heat Transfer Mechanisms

Flow boiling in micro-channels has a complex nature from the point view of the heat transfer mechanism. This is still a debated question that needs to be well clarified. Furthermore, it is very crucial to adopt the real heat transfer mechanism that goes with the corresponding flow pattern for more a realistic flow boiling model. In other words, knowing the heat transfer

mechanism is a fundamental issue for modeling two-phase flow boiling flow, particularly, in mini/micro-channels. Some previous studies reported that the dominant heat transfer mechanism for boiling in mini/micro-channels is nucleate boiling based on the relation between the heat transfer coefficient and the applied heat flux (e.g., Lazarek and Black [110]; Wambsganss et al. [111]; Bao et al. [21] ; Yen et al. [112]; Kandlikar and Balasubramanian [113]; and Kandlikar [60]). On the other hand, some other researchers, (e.g., Lee & Lee [22]; Jacobi and Thome [114]; Qu & Mudawar [115]) revealed that the convective boiling including liquid film evaporation is the dominant heat transfer mechanism in mini/micro-channels.

Chen [54] reported that the heat transfer mechanism varies by varying the flow regime, and it is of importance to correctly define the flow regime and check the applicability of any developed correlation or model used for that specific flow regime. To better understand the heat transfer mechanism for two-phase flow boiling, Chen [54] , proposed a heat transfer correlation based on an additive method principle, taking into account the contribution of both macro-convective and micro-convective heat transfer mechanisms. The macro-convective heat transfer term is related to the flowing of working fluid, while the micro-convective term is related to the bubble nucleation and bubble growth rate. The correlation was developed for saturated two-phase vertical flow boiling conditions at a heat flux lower than the CHF, in the absence of slug flow regime. The correlation was tested for 600 data points of water and organic working fluids, and gave a good agreement with a deviation of ∓ 12 %. The two-phase heat transfer coefficient was represented as

$$h = h_{mac} + h_{mic} \quad (2.6)$$

Where h_{mac} is the macro-convective heat transfer coefficient, which is a function of Reynolds number factor F , and h_{mic} is the micro-convective heat transfer coefficient which is a function of the suppression factor S that is described in terms of the ratio of effective superheat to the total superheat of the channel wall.

Lazarek and Black [110] investigated saturated heat transfer flow boiling of R113 in a 3.15 mm inner diameter vertical tube. They measured pressure drop, predicted heat transfer coefficient, and CHF. They pointed out that the heat transfer coefficient is significantly influenced by the applied heat flux and not affected by the vapor quality. Therefore, they

revealed that nucleate boiling is the dominant heat transfer mechanism. Wambsganss et al. [111] conducted an experimental investigation for heat transfer flow boiling of R113 in a 2.92 mm inner diameter horizontal tube. They observed that the flow boiling heat transfer coefficient is strongly affected by the applied heat flux, and slightly influenced by mass flux and vapor quality. Therefore, similar to Lazarek and Black [110], they concluded that nucleate boiling dominates the heat transfer mechanism due to the high boiling number. Bao et al. [21] performed similar experimental investigation, but for flow boiling of R11, and HCFC123 working fluids in a 1.95 mm inner diameter horizontal tube. Their results showed that the applied heat flux has a significant effect on the heat transfer coefficient, while is independent of mass flux and vapor quality. As a result, they reported that nucleate boiling dominates heat transfer mechanism for flow boiling in small channels.

Overall, the dominant heat transfer mechanism is flow pattern dependent. According to a study for boiling heat transfer in small channels presented by Kew and Cornwell [67], heat transfer mechanisms for boiling in small-diameter channels; $1.39 \leq D_h \leq 3.69$ mm; can be classified as nucleate boiling, confined bubble boiling, convective boiling, and partial dry-out heat transfer mechanisms corresponding to four different observed flow regimes defined as: isolated bubble, confined bubble, slug/annular, and partial dry-out flow. However, more than one mechanism may be dominant in a flow pattern. For instance, in the confined bubble flow regime, the heat transfer can occur through both thin film evaporation and conduction. Thome and Consolini [116] reported that in bubbly flow the nucleate boiling controls the heat transfer mechanism, whereas in slug and annular flow regimes the liquid film evaporation is the dominant heat transfer mechanism. Kandlikar and Balasubramanian [113] proposed a heat transfer correlation that shows the trend of heat transfer coefficient in terms of vapor quality, and they concluded that nucleate boiling dominates heat transfer for flow boiling in mini/micro-channels for low Reynolds number ($Re_{Lo} < 100$).

Some forces, such as surface tension, viscous shear, inertial, and momentum of evaporation, acting at the vapor-liquid interface, are essential for analyzing heat transfer characteristics of flow boiling in micro-channels. Kandlikar [60] derived two dimensionless groups by considering these forces namely K1 and K2. The first dimensionless group, K1, is defined as the ratio of the force of evaporation momentum to the inertia force, and represented in

terms of Boiling number and liquid to vapor density ratio. The second dimensionless group, K2, is defined as the ratio of the force of the evaporation momentum to surface tension. The author plotted the two derived dimensionless groups against a wide range of hydraulic diameter. On the question of dominant heat transfer mechanism, Kandlikar found that higher end values of K1 for the data sets indicated the dominance of nucleate boiling mechanism, while lower end values of K1 indicates the dominance of convective boiling mechanism. Additionally, the maximum values of K2 indicate the onset of CHF. K1 and K2 are expressed as follows

$$K_1 = Bo^2(\rho_f/\rho_g) \quad (2.7)$$

$$K_2 = Bo^2\left(\frac{D}{\rho_g\sigma}\right) \quad (2.8)$$

Where Bo is Boiling number.

Lee and Mudawar [117] investigated the two-phase heat transfer characteristics for flow boiling of R134a in micro-channel heat sinks at uniform high heat flux. They revealed that the dominant heat transfer mechanism of flow boiling in micro-channels is dependent on the flow pattern regime. The flow pattern was a major factor in their study to distinguish the dominant heat transfer mechanism. Therefore, they pointed out three different ranges of vapor qualities. The very low vapor quality regime (bubbly flow regime), ($x < 0.05$), is observed at low heat flux, where the nucleate boiling is dominant, while the intermediate vapor quality regime, bubbly/slug flow regime, ($0.05 < x < 0.55$), and high vapor quality regime $x > 0.55$, the convective boiling is the dominant heat transfer mechanism.

It has been concluded that the nucleate boiling is the dominant heat transfer mechanism in the bubbly flow regime where the vapor quality is low, while the convective mechanism is dominant at intermediate and high vapor quality ranges for the slug and annular flow regimes respectively for flow boiling in micro-channels. Further, it has been recommended, for future research, to generalize a flow pattern map for heat transfer prediction of flow boiling in micro-channels that covers all flow regimes for wide operating conditions and channel sizes considering the surface roughness effects at the meantime.

2.6. Bubble Dynamics

It has been known that the bubble dynamics is an essential aspect for studying pool boiling and flow boiling phenomena, particularly, in mini/micro-channels whether for vertical or horizontal conditions. Therefore, several previous studies for bubble nucleation, growth rate, departure diameter, and departure frequency have been carried out (e.g. Lee et al. [118], Fu et al. [119], Arcanjo et al. [94]).

Lee et al. [118] investigated experimentally the bubble characteristics for flow boiling of de-ionized water in a $41.3 \mu\text{m}$ inner hydraulic diameter trapezoidal micro-channel. They observed that bubble growth rate in single micro-channels falls in the range 0.13 to $7.08 \mu\text{m}/\text{ms}$. Moreover, the bubble growth is influenced by various factors based on the growth stage. In the first stage of the bubble growth, the bubble growth is mainly controlled by the inertial forces, while in the latter stages of the bubble growth, the bubble growth rate is basically, controlled by the thermal diffusion through the latent heat of evaporation. Investigating bubble growth rate raised a question, which is "is the evaporation rate at the bubble interface uniform or not?", Lee et al. [118], stated that the evaporation rate at the bubble interface is non-uniform, where it is higher at the heated wall and low at the bubble tip. Additionally, they concluded that the bubble growth rate is governed by the inertial force, while the bubble departure diameter is controlled by the surface tension. Regards to the bubble frequency, they revealed that the bubble frequency in the micro-channel is equivalent to that of conventional size channels.

Lie and Lin [120] conducted an experimental work for investigating the influence of the channel size and operating conditions on bubble characteristics and heat transfer coefficient of saturated flow boiling of R134a in 1.0, and 2.0 mm gap-size annular ducts. The influence of channel size has long been a question of a great interest in heat transfer flow boiling. In their study, it has been observed that decreasing the duct size was found to increase the saturated heat transfer coefficient, the bubble departure diameter, and the mean bubble departure frequency. Furthermore, the authors revealed that the mean bubble frequency increases with the mass flux, and inlet saturation temperature. Moreover, it has been reported that increasing the mass flux causes a slight decrease in bubble departure diameter, and lower the density of nucleation sites. Based on their experimental data, the authors proposed correlations for predicting bubble

departure diameter, frequency, and the density of nucleation site in terms of Reynolds number, Boiling number, Prandtl number, confinement number, and fluid properties. The proposed correlations gave a good agreement with the tested data. The developed correlation for predicting the mean bubble departure frequency, f , is given as follows.

$$\frac{f \cdot D_d}{\mu_f / (\rho_f D_h)} = 3.7 Re_f^{1.33} \cdot Pr_f^2 \cdot Bo^{0.725} \cdot N_{conf}^{0.59} \quad (2.9)$$

where the mean bubble departure diameter, D_d , is correlated as.

$$\frac{D_d}{\sqrt{\sigma / g \cdot \Delta \rho}} = 0.353 \left(\frac{\rho_f}{\rho_g} \right)^{0.5} \cdot Re_f^{-0.2} \cdot Bo^{0.2} \cdot N_{conf}^{0.19} \quad (2.10)$$

The correlation of the density of the nucleation site is given by,

$$N_{ac} D_d^2 = -0.029 + 4.82 Bo^{0.409} Re_f^{-0.15} \quad (2.11)$$

Situ et al. [121] have studied experimentally, the bubble departure frequency for forced convective sub-cooled boiling flow of water in upward vertical channel. They investigated the applicability of existing models and correlations for predicting bubble departure frequency. It has been revealed that the correlations developed for pool boiling do not predicted well the bubble departure frequency for forced convective sub-cooled boiling flow. Moreover, the available models are applicable for narrow limited conditions. Therefore, they provided a new correlation based on their experimental data and those available in the literature for predicting the bubble departure frequency considering the influence of applied heat flux on the bubble departure frequency. The proposed correlation gave a good agreement with the tested data measured at operating conditions with low wall superheat temperatures.

Agostini et al. [122] investigated the relationship between the elongated bubble and bubble length for flow boiling of R134a in micro-channels at diabatic conditions considering the influence of a wide range mass flux, 200 to 1500 $kg/m^2 \cdot s$, and tube diameter, 0.509, and 0.790 mm. A strong relation between the bubble relative velocity and the one calculated based on the homogenous model, and the bubble length has been reported. The authors found that the relative bubble velocity increases with the bubble length, the mass flux, and the channel inner diameter.

Furthermore, the authors developed an analytical model for describing the relation between the relative velocity and the corresponding bubble length. The proposed model which predicted 90 % of the experimental data with a deviation error band of ± 20 % is expressed as follows,

$$U_g = \frac{D \cdot \gamma}{1 + \frac{C}{Co}} \frac{1 - \exp\left(\frac{-2f_i L_g}{D}\right)}{2f_i} + U_h \quad (2.12)$$

where, C , is a coefficient, $C = -0.58$, and Co is denoted for confinement number, U_h , is the homogenous velocity, and γ , is defined by

$$\gamma = \frac{4q}{D \cdot h_{fg} \cdot \rho_g} \quad (2.13)$$

In a study of bubble collision, Revellin et al. [123] have conducted experimental work for investigating the characteristics of bubble collision for flowing of R134a in 0.5, and 0.7 mm inner diameter micro-tubes at both diabatic and adiabatic conditions, collecting about 412 data points, including the measurements of bubble length. It has been observed that due to the variation of bubble sizes, the bubble collision occurs. The model, predicted bubble length distribution, and bubble frequency in terms of exit vapor quality. Their results showed that the peak of bubble frequency was obtained at low vapor quality.

Fu et al. [119] have conducted vertical upward flow boiling experiments for investigating the bubble growth, departure, and related flow patterns for liquid nitrogen in mini-tubes with a range of 1.3 to 1.5 mm inner diameters. The authors focused on studying the bubble growth rates for two cases, when the bubble slides along the tube wall, and when the bubble attached the nucleating sites. The bubble coalescence phenomenon was not considered in their study. A similarity in bubble growth rates before and after bubble departure has been observed, and the authors attributed this to the dominance of inertial force effects on bubble growth rate. It has been revealed that liquid film evaporation is the dominant heat transfer mechanism for flow patterns observed beyond the bubble confinement. It has been observed that bubble departure mechanism is significantly influenced by mass and heat fluxes. The authors found that increasing the mass flux shorten the bubble period, and accelerated the bubble departure. On the other hand,

they found that increasing the heat flux delayed the bubble period. They attributed this to the dominance of the forces acting on the bubble growth during the period of bubble growth. Based on Situ et al.'s model of bubble lift-off diameter [124], the authors proposed a correlation for predicting bubble departure diameter as given by,

$$\frac{D_d}{D_i} = \frac{kJa^2 Pr_f^{-1}}{Re} \quad (2.14)$$

where D_d , is departure bubble diameter, D_i , is inner diameter of the tube, k , is an empirical parameter equals to 0.04, Pr_f , is Prandtl number for the fluid. The proposed correlation predicted their tested data with a deviation limits of $\pm 30\%$.

2.7. Liquid Film in Slug and Annular Flow Regimes

Liquid film thickness influences the liquid film gradient temperature and consequently, the rate of heat transferred to the channel. Therefore, it plays an important role in the investigation of flow boiling heat transfer in mini/micro-channels, Moriyama and Inoue [125]. Several investigations for predicting liquid film variation either in slug flow or annular flow have been done.

Irandoost and Andersson [35] investigated theoretically and experimentally the liquid film thickness for upward and downward Taylor's flow in capillaries. They solved Navier-Stokes equations and surface tension equations numerically for the theoretical part, and implemented a photometric technique for various working fluids named as air-ethanol, air-water and air-glycerol to measure liquid film thickness. They developed a correlation for liquid film thickness considering the capillarity effect, and the Capillary number is calculated based on bubble velocity. The analytical solution gave a good agreement with data of air-ethanol but underestimated those for air-water. The correlation of liquid film thickness is proposed as follows:

$$\delta_o/D = 0.18 [1 - \exp(-3.08Ca^{0.54})] \quad (2.15)$$

Fukano and Kariyasaki [36] investigated the characteristics of air-water flow in a capillary tube at an adiabatic condition taking into account the influences on flow direction and tube size on the flow pattern, pressure drop, bubble velocity, and liquid film. They concluded that for the two-phase flow in capillaries, neither the stratified flow pattern, nor the small bubbles in liquid slug or liquid film have been observed. Furthermore, the liquid film thickness decreases with the tube size and increasing the gas superficial velocity.

Moriyama and Inoue [125] measured the liquid film thickness formed due to the expansion of the bubble formed between two narrow horizontal plates. They assumed that the heat transferred from the plate surface is enough to evaporate the liquid film, and based on this assumption, the transient temperature variation of the plate surface was estimated. The influence of the acceleration of the bubble on the liquid film thickness was considered. It has been revealed that the liquid film thickness is affected by the Capillary number for large bubble acceleration where $Bo \leq 2.0$. On the other hand, it is noted that the liquid film thickness is mainly influenced by the viscous boundary layer for small bubble acceleration where $Bo > 2.0$. The proposed correlation is presented as,

$$(\delta/d) = \begin{cases} 0.10(\delta^*)^{0.84} & Bo > 2 \\ 0.07 Ca^{0.41} & Bo \leq 2 \end{cases} \quad (2.16)$$

The challenge in implementing this correlation is how to estimate the time required for the bubble nose to reach the measuring point from the bubble nucleation.

Hazuku et al. [126] have conducted experimental two-phase flow work for measuring liquid film thickness for flowing of water and nitrogen gas in 0.5-2.0 mm inner diameter mini/micro-tubes at adiabatic conditions by developing a laser focus displacement meter (LFD). They concluded that LFD technique with a transparent fluorocarbon tubes allows to measure the liquid film thickness thinner than 1 μm .

Steinbrenner et al. [127] measured liquid film thickness for adiabatic two-phase flow (stratified flow) of water and air injected in a micro-channel with size of $D_h \leq 500 \mu\text{m}$, using fluorescence imaging technique. Furthermore, they developed a separated flow model for predicting the liquid film thickness at adiabatic conditions. The model gave a good agreement with their experimental data and is useful to be applied for mixing micro-channels applications

such as fuel delivery cells. On the other hand, to be applicable for flow boiling micro-channel applications their model needs some extra essential considerations. For instance, the stratified flow pattern is promised not to be observed in flow boiling micro-channel. Furthermore, the influence of heat flux on the liquid film characteristics is very crucial and must be taken into account for more realistic two-phase flow boiling model.

Han and Shikazono [128] studied the liquid film thickness at steady conditions of two phase adiabatic flow for slug flow regime in micro-tubes. A correlation for predicting initial liquid film thickness was developed in terms of Re, We, and Ca numbers. It was presented as follows:

$$\left(\frac{\delta_o}{D}\right)_{\text{steady}} = \begin{cases} \frac{0.67 Ca^{2/3}}{1 + 3.13 Ca^{2/3} + 0.504 Ca^{0.672} Re^{0.589} - 0.352 We^{0.629}} & Re < 2000 \\ \frac{106 (\mu^2/\rho\sigma D)^{2/3}}{1 + 497.0(\mu^2/\rho\sigma D)^{2/3} + 7330(\mu^2/\rho\sigma D)^{2/3} - 5000(\mu^2/\rho\sigma D)^{2/3}} & Re \geq 2000 \end{cases} \quad (2.17)$$

In a follow up study, Han and Shikazono [129] have considered the influence of bubble acceleration on the viscous boundary layer which has a significant effect on the liquid film thickness in slug flow regime. They have employed (LFD) imaging technique for measuring liquid film thickness of flowing ethanol, water, and FC-40 in 0.5, 0.7, and 1.0 mm inner diameter micro-tubes. An empirical correlation for predicting the initial liquid film thickness in slug flow regime in terms of Bond number, Capillary number, and bubble acceleration was developed and presented as follows:

$$\left(\frac{\delta_o}{D}\right)_{\text{accel}} = \frac{0.968 Ca^{2/3} Bo_{\text{accel}}^{-0.414}}{1 + 4.838 Ca^{2/3} Bo_{\text{accel}}^{-0.414}} \quad (2.18)$$

Where, Bo is the Bond number based on the bubble acceleration. The initial liquid film thickness for a wide range of Capillary number is estimated based on the above two equations Eq. (2.17), and Eq. (2.18) as,

$$\left(\frac{\delta_o}{D}\right) = \min \left[\left(\frac{\delta_o}{D}\right)_{\text{steady}}, \left(\frac{\delta_o}{D}\right)_{\text{accel}} \right] \quad (2.19)$$

This correlation gave a good agreement with the data of the liquid film thickness.

Tibirica et al. [130] presented the methods and measurement techniques for estimating the two phase liquid film thickness in mini/micro-channels. They discussed the challenges that may be faced by the measurement techniques. They concluded that the LFD method is promised to be an accurate and the most proper optical technique for measuring liquid film thickness for flow boiling in micro-channels. Furthermore, it has been noted that the rate of the experiments conducted the liquid film measurement in annular flow regime is lower than those performed for the slug flow. Kanno et al. [131] measured the liquid film thickness for the two phase flow in the annular flow regime in micro tubes at adiabatic conditions employing water and FC-40 as working fluids. The obtained experimental data were compared with the analytical model of the critical liquid film thickness developed by Revellin et al. [38] for saturated flow boiling in micro-channels. The model over predicted the measured data and the authors attributed this to the influence of interface instability.

Ong and Thome [39] measured liquid film thickness for flow boiling of R134a, R236fa and R245fa on three different channel sizes, 1.03, 2.2 and 3.04 mm. they have used a MATLAB image processing code for image post-processing to detect the liquid-vapor interface and estimate the number of pixels. Then, the top and bottom liquid film thickness was estimated qualitatively considering each pixel equals 18 μm approximately. It has been noted that the gravity force still has a clear effect for flow boiling of R236fa in 1.03 mm channel diameter at lower vapor quality and $Co = 0.83$ where a difference in liquid film thickness between the top and bottom was observed.

Han et al. [40] studied the effects of liquid film evaporation on the heat transfer coefficient of flow boiling in a micro tube at boiling conditions. The liquid film thickness was measured in the slug flow regime using the LFD techniques. The obtained data were compared to those predicted by the correlations developed at adiabatic conditions. The heat transfer coefficient was evaluated by two different methods. The first method was based on the measured wall temperature, and the second one was based on the measured liquid film thickness, and both methods gave a good agreement at low vapor quality. It has been revealed that the initial liquid

film thickness at boiling conditions may fairly be estimated using the correlations developed at adiabatic conditions.

2.8. Critical Heat Flux (CHF)

CHF plays a significant role in developing and designing conventional and compact heat exchangers, particularly, mini/micro-channel heat sinks. Therefore, several CHF studies have been carried out since 1960s. Some authors investigated CHF for saturated flow boiling conditions (e.g. Wojtan et al. [45]; Revellin et al. [38]; Kim and Mudawar [132]), other researchers focused on CHF for sub-cooled conditions (e.g. Vandervort et al. [133]; Kandlikar [134]; Hsieh and Lin [135]).

Considering pool and forced convection boiling on submerged bodies in saturated liquids, Katto [136] analyzed the sub-cooled flow boiling CHF based on the principle of liquid sub-layer dry-out for various conditions of heated surface and fluid flow configurations. He developed a hydrodynamic model for predicting CHF based on the critical liquid film thickness, and reported two essential phenomena that play a key role in forming the liquid film and therefore influence the onset of CHF, which are the Kelvin-Helmholtz instability that appears at the liquid-vapor interface, and the liquid inflow rate that feeds the liquid film.

In an attempt to study the CHF at very high heat flux conditions in small mini-tubes, Vandervort et al. [133] carried out convective flow boiling experiments for water in mini-tubes with a range of inner diameter of $0.3 \leq D \leq 2.7 \text{ mm}$, subjected to a very high heat flux $q_w'' \geq 10^5 \text{ [kW/m}^2\text{]}$ and an extremely high range of mass fluxes, $5000 \leq G \leq 40000 \text{ [kg/m}^2\text{.s]}$, considering the effects of length-to-diameter ratio for the range of $2.0 \leq L/D \leq 50.0$, and the sub-cooling within a range of $40 \leq \Delta T_{sub} \leq 135 \text{ }^\circ\text{C}$. They revealed that the CHF increased nonlinearly with the sub-cooling, tube diameter, and the length-to-diameter ratios for $(L/D) \leq 10$. One of the interesting and significant findings in their results is that some test sections were damaged, where a premature test section failure has been observed at heat fluxes 20 % lower than the CHF for two test sections 1.8, and 2.4 mm inner diameter tubes. They attributed this premature failure to the influence of some thermal-hydrodynamic phenomena that can happen after the onset of boiling, and due to the spontaneous nucleation-type instability which is related

to the surface roughness of the inner wall of the test section that influences the nucleation sites. Furthermore, they proposed a new CHF correlation for high flux boiling region, which was defined as the zone where the tube surface is subjected to a heat flux as high as $10^4 \leq q_w'' \leq 2 \times 10^5 [kW/m^2]$. They have taken into account the influences of five main parameters, mass flux, pressure, exit sub-cooling, tube diameter, length-to-diameter ratio, on the CHF. The proposed correlation was developed based on 721 CHF data points measured only for tubes with inner diameter $D \leq 3.0$ mm.

Wojtan et al. [45] investigated experimentally CHF of saturated flow boiling of R134a, and R245fa in 0.5 mm, and 0.8 mm inner diameter single horizontal micro-tubes subjected to a uniform heat flux, considering the effects of saturated temperature, inlet sub-cooling, mass flux, tube diameter, and heated length. They performed their experiments for a heated length range $20 \leq L_h \leq 70$ mm, inlet saturation temperatures, 30, and 35 °C, with a range of mass fluxes of $400 \leq G \leq 1600 [kg/m^2.s]$, and inlet sub-cooling $2 \leq \Delta T_{sub} \leq 15$ °C. It has been reported that increasing the heated length decreases the CHF, while increasing the mass flux increases the CHF. Moreover, the CHF increases with the saturation temperature for mass fluxes higher than $G \geq 1000 [kg/m^2.s]$. On the other hand, no sub-cooling effect on the CHF has been observed for the tested conditions. Based on the Katto-Ohno correlation, and the measured CHF data points, they proposed a CHF correlation which is applicable for annular flow regime, and working conditions where $(\rho_g/\rho_f) < 0.15$ for a good predictive accuracy, and is given by,

$$q_c'' = 0.437 \left(\frac{\rho_g}{\rho_f} \right)^{0.073} We^{-0.24} \left(\frac{L_h}{D} \right)^{-0.72} Gh_{fg} \quad (2.20)$$

Qi et al. [46] performed a series of experiments for studying the heat transfer coefficient and CHF for flow boiling of liquid nitrogen in 0.531, 0.834, 1.042, and 1.931 mm inner diameter single micro-tubes subjected to a range of a uniform heat flux of $50.0 \leq q_w'' \leq 214 [kW/m^2]$, with a mass flux range of $440 \leq G \leq 3000 [kg/m^2.s]$, and at an inlet temperature range, $78.2 \leq T_{in} \leq 79.8$ K. They recognized the incipience of CHF based on the sudden jump in the wall temperature which is observed close to the exit of the micro tube combining with a steep drop in heat transfer coefficient. It has been noticed that the CHF increases with the mass flux, while the critical vapor quality decreases with the mass flux. Based on the Katto-Ohno

correlation of the CHF, the authors proposed a CHF correlation taking into account the effects of tube size by including the confinement number, which is given by,

$$\frac{q_c''}{Gh_{fg}} = (0.214 + 0.140 Co) \left(\frac{\rho_g}{\rho_f} \right)^{0.133} \left(\frac{1}{We} \right)^{0.333} \frac{1}{1 + 0.03 L/D} \quad (2.21)$$

The proposed correlation showed an inverse relation between the CHF and tube diameter. However, this is different from the results presented by the same authors, where it showed that at a constant mass flux, the CHF increases by increasing the tube size.

Revellin and Thome [52] developed a semi-analytical CHF model for flow boiling in a single horizontal uniformly heated micro-channel considering the influence of interfacial waves of the annular liquid film. They reported that CHF occurs in annular flow regime and can be recognized when a partial dry-out of the liquid film is experienced at a certain value of the liquid film thickness, (i.e. $\delta > 0$), where the vapor quality in this case is $x_{\text{exit}} < 1.0$. In other words, the CHF model was defined based on the dry-out of the liquid film and the height of the interfacial wave, and the critical film thickness was modeled based on Kelvin-Helmholtz critical wave length λ_c , at the channel outlet where the dry-out occurs. The correlation involved the effects of gravity and surface tension, which is given by,

$$\delta = CR \left(\frac{u_g}{u_f} \right)^{j_1} \left(\frac{(\rho_f - \rho_g)gR^2}{\sigma} \right)^{K_1} \quad (2.22)$$

Where R is the internal radius of the tube, C, j_1 , and K_1 are parameters estimated based on the CHF database. Furthermore, the authors assumed that the CHF occurs when the liquid film thickness reaches the minimum assumed values, which is defined here as, $\delta_{\text{min}} \cong 0.05D$. The model was tested with CHF experimental data points obtained for four different fluids at wide range of channel sizes $D_h = [0.215 \text{ to } 3.15 \text{ mm}]$, mass fluxes range of $[29 \text{ to } 1600 \text{ kg/m}^2 \cdot \text{s}]$, various heated length $[10 \text{ to } 126 \text{ mm}]$, and inlet sub-cooling range $[2 \text{ to } 77^\circ\text{C}]$. The model predicted 90 % of the tested data with the error band $\pm 20 \%$ and MAE of 9.3 %. The best values for the parameters C, j_1 and k_1 , proposed by the authors are 0.15, $-3/7$ and $-1/7$, respectively. CHF results showed that the CHF increases by increasing the mass flux, the channels size and the inlet sub-cooling ΔT_{sub} , while decreases by increasing the channels heated length.

Wu and Li [137], studied the effects of heated length to diameter ratio (L_h/d_h) on the saturated CHF in mini/micro channels. They found that the Boiling number at CHF, Bl_{CHF} , decreases greatly with (L_h/d_h) at low values of (L_h/d_h). A new criterion ($BoRe_l^{0.5} \leq 200.00$) was adopted to identify the macro-to-micro-scale region. The authors compiled 1672 saturated CHF database points for flow boiling of various refrigerants and water in mini and micro-channels. The threshold value of ($L_h/d_h = 150$) was reported as there is no significant effect of L_h/d_h on saturated CHF beyond this value. In general, the compiled database was divided into two main regions and a new CHF correlation was proposed for each region. For the region, which is characterized by ($BoRe_l^{0.5} \leq 200$), and ($L_h/d_h \leq 150$), the CHF correlation is given in terms of Boiling number at CHF as,

$$Bl_{CHF} = \left(\frac{q_{CHF}''}{Gh_{fg}} \right) = 0.62 \left(\frac{L_h}{d_h} \right)^{-1.19} \cdot x_e^{0.82} \quad (2.23)$$

Furthermore, the effects of inertia, viscous and surface tension forces were taken into account and represented by the non-dimensional group ($We_m Ca_l^{0.8}$) to represent the second region ($BoRe_l^{0.5} \leq 200$), and ($L_h/d_h > 150$). The CHF for this region is given by

$$Bl_{CHF} = 1.16 \times 10^{-3} (We_m Ca_l^{0.8})^{-0.16} \quad (2.24)$$

It is of importance to notice that Weber number is calculated in terms of average density, and the gravity force effect was not considered in the proposed CHF correlation. The authors tested the reliability of the proposed correlations in saturated CHF prediction compare to some selected CHF correlation, they found that their correlations captured 95.5 % of the non-aqueous CHF database with a $MAE = 12.6 \%$, while predicted 93.5 % of the Water CHF database with a $MAE = 18.6 \%$ within $\pm 30 \%$ error bands.

Basu et al. [48] investigated experimentally the effects of mass flux, inlet sub-cooling, saturation pressure, and channel size on the CHF of flow boiling of R134a in 0.5, 0.96, and 1.60 mm inner circular small tubes. The authors identified the CHF based on the sudden increase in the wall temperature measured close to the tube exit. It has been found that the CHF increases with mass flux, inlet sub-cooling, and tube diameter. On the other hand, it has been revealed that the CHF decreases with the saturation pressures. Based on two flow pattern maps developed by

Hassan et al. [88], and Revellin and Thome [75], the authors mapped their experimental data and revealed that the CHF occurs in the annular flow regime for 0.96 mm, and 1.6 mm inner diameter tubes, while it occurs in the slug flow regime for a 0.5 inner diameter tube. Using their CHF data of R134a, and those measured by Roday and Jensen [138] for R123, the authors proposed a CHF correlation that predicted the CHF with a MAE of 10 %. The proposed CHF correlation is given by,

$$\left(\frac{q_{CHF}''}{Gh_{fg}}\right) = 0.3784 \left(\frac{\rho_g}{\rho_f}\right)^{0.051} \left(\frac{L_h}{d_h}\right)^{-1.03} x^{0.8} \quad (2.25)$$

Ong and Thome [139] conducted similar series of experiments to study the effects of the main parameters of the working conditions on the heat transfer coefficient and CHF for flow boiling in mini/micro-channels, including the influence of confinement number. They performed their experiments for flow boiling of various working fluids, R134a, R236fa, and R245fa, in 1.03, 2.20, and 3.04 mm inner diameter tubes. The onset of CHF was identified based on the rapid increase in the wall temperature. It has been found that the CHF increases with the mass and heat fluxes. On the other hand, it was reported that the CHF increases by decreasing the tube diameter and saturation temperature, and no significant effect of the inlet sub-cooling was revealed. Regards to the effect of flow pattern on the CHF, it has been reported that all the CHF measured were fallen in the annular flow regime. The authors proposed a new CHF correlation based on the correlation of Wojtan et al. [45] considering the confinement effects, the proposed correlation is applicable for flow boiling of the tested working fluids in mini/micro-channels with a range of hydraulic diameter of $0.35 \text{ mm} \leq D \leq 3.04 \text{ mm}$, for mass fluxes $84 \leq G \leq 3736 \text{ [kg/m}^2\cdot\text{s]}$, heated length to diameter ratios, $22.7 \leq (L_h/D) \leq 178$, vapor to liquid density ratios $0.024 \leq (\rho_g/\rho_f) \leq 0.036$, liquid to vapor dynamic viscosity ratios, $14.4 \leq (\mu_f/\mu_g) \leq 53.1$, and heated-length-based liquid Weber number range of, $7 \leq We_f \leq 20 \times 10^4$, and is given by,

$$\left(\frac{q_{CHF}''}{Gh_{fg}}\right) = 0.12 \left(\frac{\mu_f}{\mu_g}\right)^{0.183} \left(\frac{\rho_g}{\rho_f}\right)^{0.062} \left(\frac{L_h}{d_h}\right)^{-0.7} \left(\frac{D}{D_{th}}\right)^{0.11} We_f^{-0.141} \quad (2.26)$$

Where D_{th} represents the threshold criterion for macro-to-microscale effects and can be written as follows,

$$D_{th} = \frac{1}{Co} \sqrt{\frac{\sigma}{g(\rho_f - \rho_g)}} \quad (2.27)$$

with a confinement number $Co=0.5$.

Del Col and Bortolin [140] investigated experimentally the CHF flow boiling of R134a, R32, and R245fa in a 0.96 mm inner diameter circular mini-tube subjected to a non-uniform heat flux. The method used for heating the test section was performed by supplying a hot water around the test section. The applied heat flux increased axially along the test section. The influence of the mass flux and reduced pressure on the CHF were considered for the range of $100 \leq G \leq 900 [kg/m^2.s]$ and $0.05 \leq p_r \leq 0.34$. Based on the rapid change in the standard deviation of the wall temperature, the CHF was identified. The authors compared the obtained CHF data with some CHF predicting methods, it has been indicated that the model of Revellin and Thome [52] gave a good agreement with their experimental data.

To better understand the effects of high mass flux on CHF in micro-channels, Kaya et al. [141] performed experiments for flow boiling of de-ionized water in micro-tubes with a range of inner diameter of $249 \leq D \leq 494 \mu m$ and for mass fluxes range of $20,511 \leq G \leq 38,111 [kg/m^2.s]$. It has been found that the CHF increased with mass flux, and decreasing tube diameter, and heated length to diameter ratio. They related the onset of CHF to the departure of nucleate boiling mechanism (DNB) due to the high mass flux and low vapor quality conditions. Moreover, they compared their CHF data points with the correlations developed for sub-cooled and low vapor quality flow, and proposed a new CHF correlation considering the data of Kosar et al. [47] as well. The proposed CHF correlation is applicable for flow boiling of water in micro-tubes with inner diameter range $0.1 \leq D \leq 0.5 mm$, and for a wide range of mass flux $1,200 \leq G \leq 50,000 [kg/m^2.s]$ and heated length to diameter ratios $7 \leq L_h/D \leq 400$ at low vapor quality conditions. Kaya et al. [141] correlation is given by,

$$q''_{CHF} = 0.8636 \times 10^{-4} \left(\frac{\mu_f h_{f,g}}{D^{1.32}} \right) Re^{1.06} \left(\frac{L_h}{D} \right)^{-0.72} \left(\frac{C_{p,e} \Delta T_{sub,i}}{h_{f,g,e}} \right)^{0.2} \quad (2.28)$$

In recent years, there has been an increasing in investigations of CHF for saturated flow boiling conditions. Tibirica et al. [50] investigated experimentally, the effects of working fluid, mass flux, saturation temperature, heated length, and inlet sub-cooling on the CHF for flow boiling of R134a, and R245fa in a 2.2 mm inner diameter macro-tube. They carried out their experiments for a range of mass flux of $100 \leq G \leq 1,500 [kg/m^2.s]$ and for exit saturated temperatures 25, 31, and 35 °C, and two different heated lengths, 154, and 361 mm. The onset of CHF mechanism was identified based on the steep growth in the wall superheating. It has been revealed that the CHF increases by increasing the mass flux and inlet sub-cooling, while decreases by increasing the saturation temperature, and heated length. They compared their CHF data with the CHF correlations of Katto and Ohno [142], Shah [143], Zhang [44], and Ong and Thome [139], and reported that Katto and Ohno [142] correlation gave the best agreement with their data followed by the correlation of Ong and Thome [139].

There is evidence that inlet sub-cooling plays an important role in occurrence of CHF in mini/micro-channels. Kim and Mudawar [132] pointed out that four various mechanisms that may initiate and be responsible for the onset of CHF for sub-cooled flow boiling in mini/micro-channels. These mechanisms are categorized as separation of boundary layer; dry-out of sub-layer; bubble crowding; and interfacial lift off. Moreover, they investigated the CHF and dry-out incipience vapor quality, x_{di} , for saturated flow boiling in mini/micro-channels. They attempted to develop a generalized correlation for predicting the dry-out vapor quality by collecting 997 dry-out data points from 26 sources covering flow boiling of 13 working fluids in mini/micro-channels with a range of hydraulic diameter $0.51 \leq D_h \leq 6.0 \text{ mm}$ and mass fluxes $29 \leq G \leq 2303 [kg/m^2.s]$, which corresponded to liquid Reynolds number ranges, $125 \leq Re_f \leq 53,770$, Boiling numbers, $0.31 \times 10^{-4} \leq Bl \leq 44.3 \times 10^{-4}$, and reduced pressures, $0.005 \leq p_r \leq 0.78$. The proposed correlation of dry-out incipience vapor quality is given by,

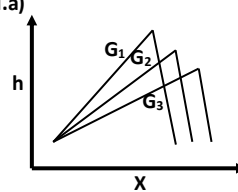
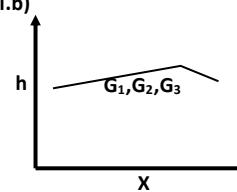
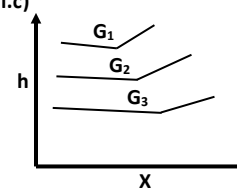
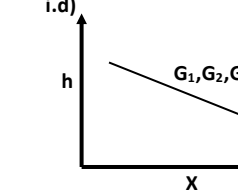
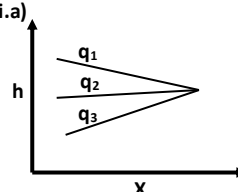
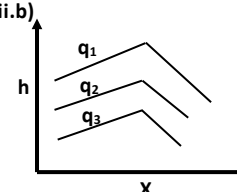
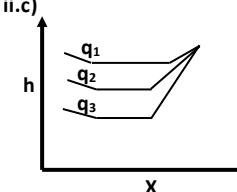
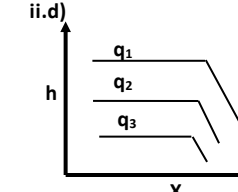
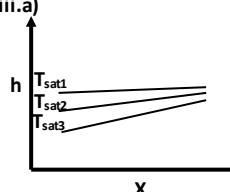
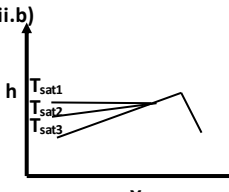
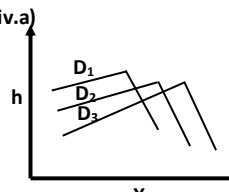
$$x_{di} = 1.4 We_f^{0.03} p_r^{0.08} - 15.0 \left(Bl \frac{P_H}{P_F} \right)^{0.15} \left(\frac{\rho_g}{\rho_f} \right)^{0.06} Ca^{0.35} \quad (2.29)$$

2.9. Two-Phase Heat Transfer Coefficient

Two-phase boiling heat transfer coefficient has been an object of research and interest for several decades, since it is one of the most significant parameters for investigating the characteristics of two-phase flow boiling, particularly, in mini/micro-channels. Therefore, a considerable amount of researches for investigating two-phase heat transfer have been performed in the last three decades. Some of these studies are experimental (e.g. Lie and Lin [120]; Choi et al. [144]; Ong and Thome [97]; Bortolin et al. [26]), and some others are semi-analytical, (e.g. Moriyama et al. [8]; Megahed and Hassan [12]; Consolini and Thome [145]). Consequently, several prediction methods of two-phase heat transfer coefficients have been proposed. Table (A-2) lists most of these methods which have been developed so far. Moreover, most of the results of two-phase heat transfer coefficient in the literature are presented versus vapor quality. Furthermore, a largely debated question in flow boiling in micro-channels is whether the heat transfer coefficient increases or decreases with vapor quality. In his review, for flow boiling in micro-scale channels, Ribatski [146] provided a table which describes the different trends of the two-phase heat transfer coefficient in terms of vapor quality taking into account the effects of main working conditions, mass flux, heat flux, and saturation temperature, as depicted in Table (2-2).

Moriyama and Inoue [147] investigated adiabatic flow patterns, pressure drop and heat transfer for two-phase boiling flow of R-113 in very narrow passages with size of 35 – 110 μm . They proposed a phenomenological model for two-phase heat transfer coefficient prediction for low vapor quality region (slug flow) and high vapor quality region (film flow). In the slug flow model, the authors neglected the interaction between elongated bubble and liquid slug while considered the drag force effect. Thus, the model underestimated the experimental data that were used for model validation. Moreover, according to their experimental results, a sharp rising in heat transfer coefficient was observed in the single-phase region at low quality range [0.0 – 0.1], while there was not a significant change in heat transfer coefficient in the two-phase region in terms of vapor quality. Additionally, the order of magnitude of the two-phase heat transfer coefficient was 2 to 20 times higher than that one of liquid single-phase flow.

Table (2-2): various trends of flow boiling heat transfer coefficient versus vapor quality in micro-channels, redrawn from Ribatski [146].

| | | | |
|--|--|--|---|
| <p>i.a)</p>  <p>$G_1 > G_2 > G_3$</p> | <p>i.b)</p>  <p>$G_1 > G_2 > G_3$</p> | <p>i.c)</p>  <p>$G_1 > G_2 > G_3$</p> | <p>i.d)</p>  <p>$G_1 > G_2 > G_3$</p> |
| <p>Heat transfer coefficient Increases and dryout occurs at lower vapor qualities with increasing mass velocity.</p> | <p>Heat transfer coefficient almost independent of mass velocity and vapor quality until dryout.</p> | <p>Heat transfer coefficient Increases with mass velocity, presents a plateau at lower vapor quality and increases with vapor quality at higher vapor qualities.</p> | <p>Heat transfer coefficient almost independent of mass velocity and its value decreases with increasing vapor or quality.</p> |
| <p>ii.a)</p>  <p>$q_1 > q_2 > q_3$</p> | <p>ii.b)</p>  <p>$q_1 > q_2 > q_3$</p> | <p>ii.c)</p>  <p>$q_1 > q_2 > q_3$</p> | <p>ii.d)</p>  <p>$q_1 > q_2 > q_3$</p> |
| <p>Heat transfer coefficient Increases with heat flux for low vapor quality conditions, and its value tends to converge at high vapor qualities.</p> | <p>Heat transfer coefficient Increases with increasing heat flux and vapor quality until dryout conditions.</p> | <p>Heat transfer coefficient Increases with increasing heat flux and presents a V shape with increasing vapor quality.</p> | <p>Heat transfer coefficient Increases with heat flux and almost independent of vapor quality until dryout.</p> |
| <p>iii.a)</p>  <p>$T_{sat1} < T_{sat2} < T_{sat3}$</p> | <p>iii.b)</p>  <p>$T_{sat1} < T_{sat2} < T_{sat3}$</p> | <p>iv.a)</p>  <p>$D_1 < D_2 < D_3$</p> | |
| <p>Heat transfer coefficient Increases with saturation temperature.</p> | <p>Heat transfer coefficient Increases with saturation temperature for low vapor qualities and its effect becomes negligible for high vapor qualities.</p> | <p>Heat transfer coefficient Increases with decreasing diameter until the dryout vapor quality.</p> | |

Regards to the liquid-film region, the authors assumed that the liquid film thickness at the upper and lower wall are equal, and the flow is laminar in the film region while it could be laminar or turbulent for the vapor core. Surface tension effect was taken into account and the heat transfer model was developed based on the liquid-film evaporation. Furthermore, the average liquid film velocity, interfacial velocity, interfacial shear stress, two-phase multiplier and two-phase pressure drop were derived and presented in terms of liquid film thickness to diameter ratio, (δ/d) for the film flow and elongated bubble regions. Their predicted values and the experimental data were in a good agreement. The interfacial shear stress τ_i was estimated using Blasius formula based on the vapor relative velocity u_G to the interfacial velocity u_i .

$$\tau_i = \frac{c\rho_G^{1-n}\mu_G^n(u_G - u_i)^{2-n}}{2^{n+1}(d - 2\delta)^n} \quad (2.30)$$

Where n is defined as

$$n = \begin{cases} 1, & c = 24 \quad \text{for } Re_G < 2042 \\ 0.25, & c = 0.079 \quad \text{for } Re_G \geq 2042 \end{cases} \quad (2.31)$$

Wambsganss et al. [111] carried out flow boiling experiments for measuring local convective boiling heat transfer coefficient of R113 in a 2.92 inner diameter horizontal tube. They evaluated heat transfer correlations available in the literature, including Lazarek and Black's correlation [110], by comparing them with their heat transfer data base. They revealed that the measured local two-phase heat transfer coefficient was independent of mass flux and vapor quality, while significantly affected by the applied heat flux. Moreover, they identified the slug flow boundaries based on the flow regime map proposed by Damianides and Westwater [148] for water-air mixture. It has been reported that slug flow is observed in small channel for a wider range than those in conventional size tubes, and the nucleate bubbles in liquid film are not suppressed. Thus, the nucleation boiling is the dominant heat transfer mechanism in small channels.

Tran et al. [1] investigated experimentally heat transfer coefficient for nucleate boiling flow in small compact heat exchangers considering three various working fluids (R113, R12, and R134a). They proposed a correlation for predicting local heat transfer coefficient in terms of

applied heat flux, properties of working fluid, Boiling number, Reynolds number, and confinement number. Their correlation is presented as follows,

$$Nu = \frac{hD}{k_l} = c_1 (Bl.Re_l.Co)^{c_2} \left(\frac{\rho_g}{\rho_l} \right)^{c_3} \quad (2.32)$$

the authors measured local two phase heat transfer data for rectangular, circular, and square small channels and correlated the empirical parameters c_1 , c_2 , and c_3 as 770, 0.62, and 0.297, respectively. They carried out their experiments for nucleate boiling region, where it was distinguished by high heat flux and a superheat wall $\Delta T_{sat} > 2.7$ °C. The proposed correlation predicted fairly the majority of the local heat transfer data within ± 15 %. The authors revealed that the convective heat region is characterized by low mass flux, and low wall superheat, as well as the high vapor quality. Furthermore, the effects of some essential parameters such as surface tension and applied heat flux have been considered in this correlation. Consequently, it can be used for nucleate boiling flow region in small compact heat exchangers. However, the nucleate boiling conditions need to be defined for proper application of the correlation.

Yan and Lin [149] investigated the effects of heat flux, mass flux, saturation temperature, and average vapor quality on heat transfer coefficient and pressure drop for flow boiling of R134a in a horizontal 2.0 mm inner diameter tube. It has been reported that in the low vapor quality regime, the evaporative heat transfer coefficient increased by increasing the heat flux. Additionally, at low heat flux, the heat transfer coefficient increased by increasing mass flux and saturation temperature. Moreover, the authors compared their heat transfer database with those measured for large tube size ($D_h \geq 8.0$ mm), and they reported that evaporative heat transfer coefficient for small tubes is about 30 to 80 % higher than that of large tubes. Furthermore, the authors proposed a heat transfer correlation and friction factor correlation based on the measured and collected database of the heat transfer and pressure drop.

Jacobi and Thome [114] proposed a heat transfer model of the elongated bubble in slug flow regime in micro channels. They considered the thin-film evaporation as a dominant heat transfer mechanism. The model predicts the local heat transfer coefficient for the elongated bubble/liquid slug pair in a circular micro channel. The authors assumed the thin liquid film is uniform in the slug pair at a certain time. The obtained model is dependent of two unknown empirical parameters that can not be estimated analytically; the initial liquid film thickness δ_0 ,

and the nucleation critical radius r_{crit} . The conduction-limited model of Plesset and Zwick [150] was used to estimate the time required for creating two bubble/slug pairs and consequently predicting the bubble frequency. In addition, the model was developed by applying the void fraction equation, mass and energy conservation equations on the bubble/liquid slug pair. The heat transfer to the laminar liquid slug was neglected compared to the elongated bubble. Thus, the model considered the significance of the heat transfer only in the elongated bubble zone. The model showed that the flow boiling heat transfer coefficient is dependent on the applied heat flux while is independent of mass flux and vapor quality. Moreover, the authors confronted their model to the experimental database of Bao et al. [21] obtained for R11, for initial liquid film thickness $\delta_o = 12.5 \mu\text{m}$ and effective superheat of $\Delta T_{eff} = 28 \text{ K}$ with the average relative error less than 10 %. Further, they correlated other experimental data points for R – 12 performed by Wambsganss et al. [111], the model predicted their data with average deviation less than 13% for $\Delta T_{eff} = 23 \text{ K}$ and $\delta_o = 20 \mu\text{m}$. In general, the model was able to predict the effects of saturation pressure p_{sat} , heat flux q , mass flux G and vapor quality x on the heat transfer coefficient in the elongated bubble zone with a reasonable agreement with the experimental data depending on the estimated values of ΔT_{eff} , and δ_o .

Qi et al. [46] proposed a correlation for predicting two-phase heat transfer coefficient in terms of Boiling number, Bl , confinement number, C_o , Weber number, We , pressure dimensionless parameter, K_p , and Lockhart-Martinelli parameter, X . Two major regions were classified based on the dominated heat transfer mechanism using the critical vapor quality, $x = 0.3$, as a criterion for defining the applicability of the proposed correlation. The dominant heat transfer mechanism was defined based on the measured heat transfer data, and the influence of mass flux, heat flux on the heat transfer coefficient. According to their measured heat transfer data, the authors reported that for the low vapor quality region, $x < 0.3$, the heat transfer coefficient is influenced by the applied heat flux, so the dominant heat transfer mechanism is nucleate boiling, and the proposed correlation is given by,

$$Nu_{TP} = 1059.83Bl^{0.454}We^{0.045}K_p^{0.106}X^{0.107}C_o^{-1.825} \quad (2.33)$$

On the other hand, for the intermediate and high vapor quality, $x \geq 0.3$, it has been noted that the heat transfer coefficient is influenced by mass flux. Consequently, the dominant heat transfer mechanism in this region is convection, and the heat transfer correlation is given by,

$$Nu_{TP} = 0.0042Bl^{-0.872}We^{-0.059}K_p^{0.293}X^{0.065}Co^{-1.704} \quad (2.34)$$

Where the pressure dimensionless parameter is expressed in terms of working fluid properties as given by,

$$K_p = p/[\sigma g(\rho_f - \rho_g)]^{0.5} \quad (2.35)$$

Surprisingly, in their results, it has been observed that two-phase heat transfer coefficient decreases by decreasing the tube size.

Thome et al. [151] proposed the three-zone flow boiling model for the elongated bubble regime in micro-channels. The three zones are identified as the vapor slug, the elongated bubble, and the liquid slug. The thin liquid film trapped between the elongated bubble and the channel wall was modeled. In addition, the time-average local heat transfer coefficient of flow boiling in slug flow regime was predicted by the model. The authors analyzed the heat transfer coefficient of each zone and calculated the time-averaged heat transfer coefficient for one period of pair generation τ . Originally, this time τ was predicted using the model of Plesset and Zwick [150] for bubble growth radius. Consequently, the slug pair frequency f is calculated as follows,

$$f = 1/\tau = \left[\frac{\rho_l c_{pl} \Delta T_{sat}}{\rho_v \Delta h_{lv} R} \right]^2 \frac{12\alpha_l}{\pi} \quad (2.36)$$

Where α_l is defined as the liquid film diffusivity. A correlation for initial liquid film δ_o prediction was developed based on the correlation of Moriyama and Inoue [125], by adding an empirical correction factor C_{δ_o} using R-113 database.

$$\frac{\delta_o}{d} = C_{\delta_o} \left(3 \sqrt{\frac{\nu_l}{U_p d}} \right)^{0.84} [(0.07Bo^{0.41})^{-8} + 0.1^{-8}]^{-1/8} \quad (2.37)$$

Where ν_l is the kinematic viscosity of the liquid, U_p is the pair velocity, and Bo is the Bond number. By applying the energy balance for the thin liquid film, the wall dry-out time t_{dry} , dry-

zone equivalent length L_{dry} , the residence time of liquid slug t_l and liquid film t_{film} were obtained. The partial dry-out was assumed to occur at the minimum thin liquid film δ_{min} . Thus, the local time-averaged heat transfer coefficient of the slug pair was identified as follows,

$$h(z) = \frac{t_1}{\tau} h_l(z) + \frac{t_{film}}{\tau} h_{film}(z) + \frac{t_{dry}}{\tau} h_v(z) \quad (2.38)$$

Where the heat transfer coefficient for the liquid film zone $h_{film}(z)$ is predicted as,

$$h_{film}(z) = \frac{1}{t_{film}} \int_0^{t_{film}} \frac{\lambda_l}{\delta(z,t)} dt = \frac{\lambda_l}{\delta_0 - \delta_{end}} \ln \left(\frac{\delta_0}{\delta_{end}} \right) \quad (2.39)$$

In general, the model contains three different empirical parameters which are difficult to be estimated theoretically. These parameters are the minimum reasonable liquid film thickness that is acceptable at dry-out δ_{min} , the initial value of the liquid film thickness δ_0 , and the bubble frequency f . The minimum liquid film thickness significantly affects the heat transfer coefficient in the liquid film zone. According to the above equation in the logarithmic term when $\delta_{end} \xrightarrow{yields} 0$ (i.e. the dry out occurs), then $h_{film} \xrightarrow{yields} \infty$.

Dupont et al. [152] extended the work of Thome et al. [151] where the three-zone model was compared with 1591 experimental points obtained for seven different fluids for circular tubes with a various size range of $0.7 \text{ mm} \leq D_h \leq 3.1 \text{ mm}$. The Least Squared Error method was used for obtaining new optimum values of the required three parameters δ_{min} , δ_0 and C_{δ_0} which employed and showed an improvement in the model where more than 70 % of the collected database were captured within $\pm 30\%$. It has been demonstrated that the optimum value of the pair frequency f_{opt} is mainly dependent of applied the heat flux and identified as $f_{opt} = (q/q_{ref})^{n_f}$ where the reference heat flux q_{ref} is dependent of the reduced pressure $q_{ref} = \alpha_q (p_{sat}/p_{crit})^{n_q}$. It has been recommended to use the following optimum values of the empirical parameters that give the best fit with above mentioned deviation and captured percentage: $f_{opt} = (q/q_{ref})^{1.74}$, $q_{ref} = 3328(p_{sat}/p_{crit})^{-0.5}$, $C_{\delta_0} = 0.29$, $\delta_{min} = 0.3 \mu\text{m}$. In addition to the previous parameter optimizations, the authors discussed the effect of vapor quality, saturated pressure, mass flux and heat flux on the heat transfer coefficient based on the proposed model and chosen experimental database. Moreover, the model showed a clear

influence of the of heat flux and vapor quality on the heat transfer. The vapor quality zone is categorized into three zones as ($x < 0.12$); ($0.12 < x < 0.38$) and ($x > 0.38$). It can be seen that the heat transfer coefficient increases in the first two zones where it reaches the peak at the end of second zone and the new trend observed here is the shifting peak toward the high vapor quality when the heat flux increases as shown in Figure 2-5 for flowing R12 in $d = 2.46 \text{ mm}$ channel. This was attributed to the effect of heat flux on the pair frequency, where the maximum residence time of thin liquid film t_{film} and vapor t_v affected by the heat flux variation. To conclude, the study showed the sensitivity of the predicted values of the minimum liquid film thickness to the predicted heat transfer coefficient for flow boiling. Thus, deriving a proper correlation that precisely describes bubble frequency and its effect on heat transfer coefficient is needed.

Ribatski et al. [153] studied the combined effect of elongated bubble frequency and flow pattern on the heat transfer coefficient for flow boiling in micro-scale passages. The work was performed based on two main previous studies. The first is the three-zone model for the micro-scale channels in elongated bubble/slug flow regime published by Thome et al. [151]. The second is the flow pattern map for convective evaporation inside the micro-scale channels proposed by Revellin [90]. The flow pattern map was utilized to separate experimental database of the Acetone of the elongated bubble regime and compared with that obtained by the three-zone model using the new proposed values of the empirical parameters previously suggested. Again, new values of the empirical parameters were optimized as follows, $C_{\delta_o} = 0.40$, $\delta_{min} = 0.1 \mu\text{m}$, $\alpha_q = 4653$, $n_f = 1.70$, $n_q = -0.5$. It has been found that, for the chosen experimental database, the three-zone model with the new proposed empirical parameters captured 90% of the flow boiling database of the acetone within $\pm 30\%$. However, The reason for the increase or decrease of the proposed empirical parameters is still unclear.

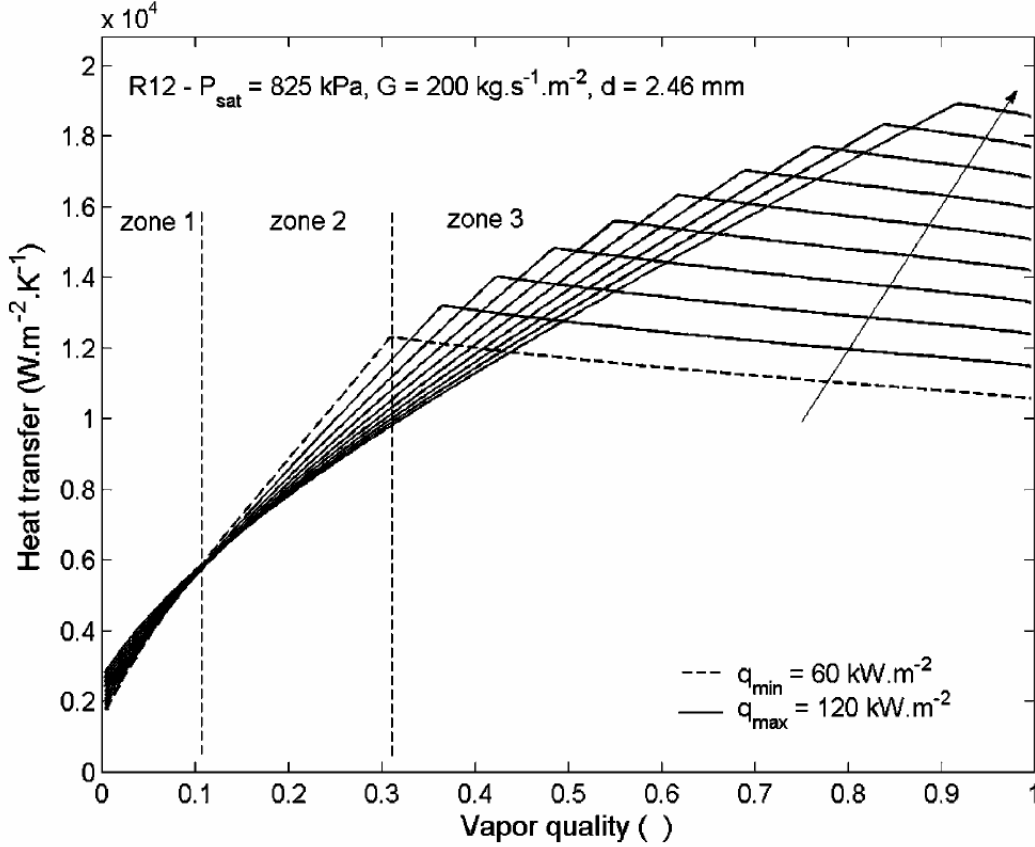


Figure 2-5: Variation of heat transfer coefficient with vapor quality for R12 in 2.46 mm channel at different values of heat flux Dupont et al. [152].

One of the major two-phase diabatic flow characteristics is bubble coalescence. A recent work by Consolini and Thome [145] involved developing a one dimensional analytical heat transfer model for coalescing bubbles flow in micro-channels subjected to a uniform heat flux. The effects of bubble coalescing dynamics and the liquid slug mass fraction placed to liquid film during the coalescence were taken into account. The interfacial shear stress was considered as a dominant parameter controlling the thin film movement. However, the pressure drop effect on liquid film thickness was not taken into account. The basic developed equation describes transient film thickness variations in terms of flow direction,

$$\delta(t, z) = \frac{\mu_l z}{\tau_i t} - \frac{q}{2\rho_l h_{lv}} t \quad (2.40)$$

Furthermore, two main relations describing the liquid film thickness variations at the tail and nose of the bubble were developed. The model is mainly dependent of the transition vapor quality boundaries ($x_c \leq x \leq x_a$). Where x_c represents the vapor quality transition from isolated to coalescence bubble flow regime, while x_a represents the vapor quality transition from coalescence bubble to annular flow regime. These boundaries were evaluated using the diabatic flow pattern map developed by Ong and Thome [97]. The conditions where the liquid film thickness is stable or unstable at the tail and the nose of the elongated bubble were analyzed and discussed based on the value of the non-dimensional mass flux parameter ψ_c . The averaged heat transfer coefficient model proposed is given by,

$$\bar{\alpha}(x) = \left(\frac{k_l}{D}\right) \frac{\left(\frac{\rho_l}{\rho_v}\right) \left[\left(\frac{x_a - x}{x_a - x_c}\right)^\beta\right]^{\gamma(x, x_c, x_a)} \ln\left(\frac{1 - \Theta_{1c}}{1 - \Theta_{2c}}\right)}{Bl(1 - \psi_c)} \quad (2.41)$$

Where Θ_{1c} , and Θ_{2c} are defined as follows:

$$\Theta_{1c} = \left(\frac{k_l}{D}\right) \frac{(1 - \psi_c) \ln^2\left(1 + \frac{\rho_l}{\rho_v} x_c\right)}{\Theta_{3c}} \quad (2.42)$$

$$\Theta_{2c} = \frac{(1 - \psi_c) \left[\ln\left(1 + \frac{\rho_l}{\rho_v} x_c\right) + 4Bl \left(\frac{x_a - x}{x_a - x_c}\right)^{-\beta} \right]^2}{\Theta_{3c}} \quad (2.43)$$

$$\Theta_{3c} = 8 \frac{\mu_l}{\tau_i} \frac{G}{\rho_v D} \frac{\rho_l}{\rho_v} x_c - \psi_c \ln^2\left(1 + \frac{\rho_l}{\rho_v} x_c\right) \quad (2.44)$$

The simulated diabatic flow pattern boundaries for R134a were estimated as,

The obtained model still includes some parameters that are estimated based on empirical correlations such as the interfacial shear stress τ_i , maximum bubble frequency f_{max} , liquid slug fraction placed to the liquid film ξ , frequency power exponent β , and dimensionless mass flux, ψ_c . The model was confronted to 980 database points for coalescence bubble regime for different refrigerants and fluids. The best results obtained by the model were for R134a data points, where 93 % of the database points were captured with $\pm 30\%$ error band. The obtained

trend for the averaged heat transfer coefficient in this mode showed a decrease in heat transfer coefficient in the neighborhood close to coalescence vapor quality x_c and then an increases when the vapor quality increases as shown in Figure 2-6. The authors presented an expression for bubble nose location with respect to time that can be extended for varying heat flux applications and recommended for future researches.

In another major heat transfer mechanisms study, Thome and Consolini [116] studied widely the heat transfer mechanisms and clarified the dominant heat transfer mechanism for flow boiling in micro-channels. Meanwhile, the dominant heat transfer mechanisms were demonstrated based on the flow pattern regime for flow boiling in micro-channels. It has been reported that in the bubbly flow regime, the dominant heat transfer mechanism is nucleate boiling and liquid convection, while in slug flow regime, the heat transfer mechanism may be occurring through liquid film evaporation and convection to the liquid and vapor slug. In the annular flow, the mechanism occurs by laminar or turbulent convective evaporation through the liquid film, while in mist flow regime, the dominant mechanism is vapor-phase heat transfer with droplet impingement. Moreover, several previous empirical heat transfer prediction methods, developed based on macro-scale correlations and nucleate boiling as a dominant heat transfer mechanism, have been reviewed.

It has been demonstrated that these correlations are not applicable for micro-scale channels because of the variation of heat transfer mechanism in micro-scale channels and Reynolds number in previous correlations was obtained based on tubular Reynolds number not on the liquid film. It has been reported that the surface roughness effects on the liquid film thickness controls the minimum liquid film thickness allowed at the elongated bubble tail where the dryness may occur. The authors used 1438 experimental data points for different fluids obtained by Agostini et al. [154] to test the three-zone model. The model captured 90% of the data within $\pm 30\%$ when they used measured surface roughness $0.17 \mu m$ instead of $0.3 \mu m$ for the silicon channel. While only 31 % of the database were captured within $\pm 30\%$ for surface roughness of $0.30 \mu m$.

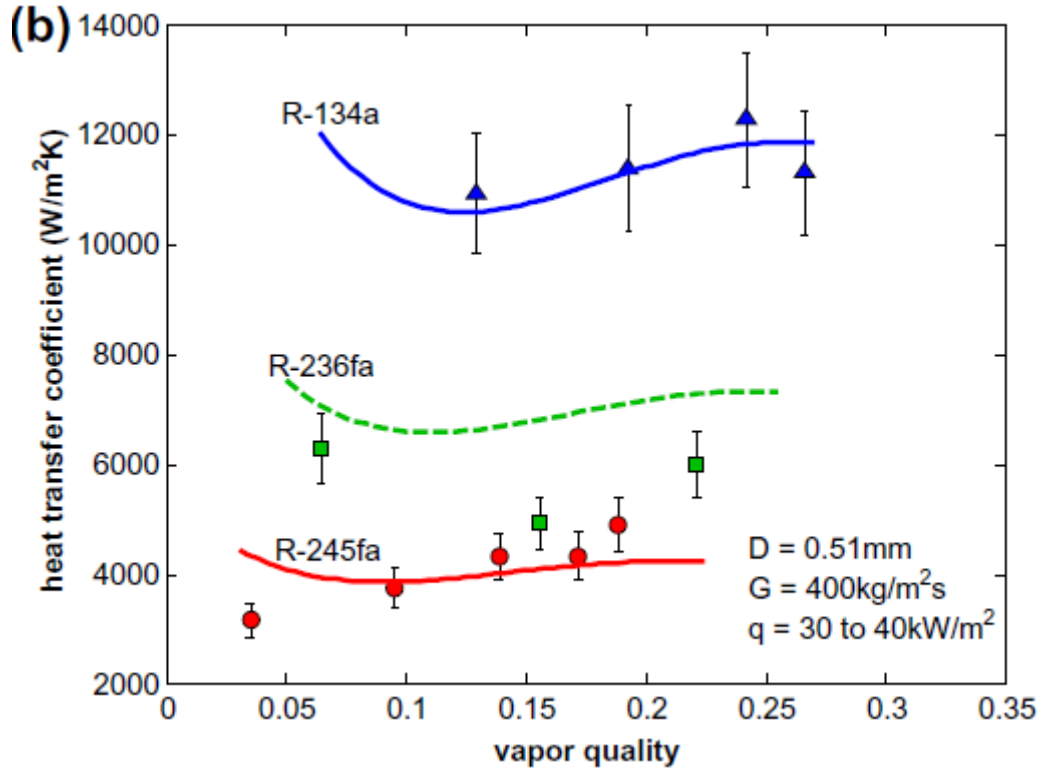


Figure 2-6: Variation of heat transfer coefficient with vapor quality for different fluids, Comparison the experimental data with those predicted by the model Consolini and Thome [145].

One of the essential parameters which may influence heat transfer characteristics for flow boiling in micro-channels is surface roughness. Thus, several studies have been recently performed considering the influence of surface roughness on the flow boiling heat transfer characteristics. One of them was carried out by Mahmoud et al. [155] for flow boiling of R134a in 1.1, and 1.16 mm inner diameter of various metallic vertical small tubes. The authors performed their experiments at a constant mass flux of $500 \text{ kg/m}^2 \cdot \text{s}$. A significant difference in heat transfer mechanisms has been observed between the various metallic tubes due to the inner surface effects. In the seamless cold drawn small tube, the authors concluded that the heat transfer coefficient is independent of mass flux, and vapor quality while increases by increasing the heat flux, thus, the dominant heat transfer mechanism is nucleate boiling. On the other hand, in the welded small tube, the heat transfer was dependent of the axial position and a non-uniform variation in heat transfer coefficient has been observed due to the manufacturing effects of the inner surface.

In a recent flow boiling experimental study, Oh et al. [156] investigated the effects of mass flux, heat flux, saturation temperature, working fluid properties, and hydraulic diameter on the flow boiling heat transfer coefficient in horizontal mini/micro-channels. They carried their experiments using five different working fluids, R134a, R22, R410a, C3H8, and CO₂, flowing in 0.5, 1.5, and 3.0 mm inner diameter horizontal tubes with various heated lengths. Based on 1588 heat transfer data points, the authors proposed a new nucleate suppression factor, S , and convective contribution factor, F , as a result, a new heat transfer correlation was introduced in the form of the superposition model which incorporates liquid heat transfer coefficient, h_f , and nucleate boiling heat transfer coefficient, h_{nbc} . The developed correlation for predicting two-phase heat transfer coefficient, h_{tp} , is listed in Table (A-2). It is of importance to note that Cooper's correlation is employed for predicting the contribution of nucleate boiling heat transfer coefficient h_{nbc} , while the liquid heat transfer coefficient was predicted based on the existing liquid phase heat transfer correlations. The new proposed correlation predicted the correlated data with a mean deviation of 15.28 %.

Basu et al. [157] carried out experimental investigation of flow boiling heat transfer of R134a in 0.5, 0.96, and 1.6 mm inner diameter horizontal mini/micro-tubes subjected to uniform heat flux, taking into account the effects of heat flux, mass flux, saturation pressure, tube size, and vapor quality on flow boiling heat transfer coefficient for flow conditions corresponding to a range for confinement number of $0.4 \leq Co \leq 3.3$. Moreover, seven heat transfer correlations were assessed and employed to predict the measured heat transfer data. It has been noted that two-phase heat transfer coefficient is linearly increasing with heat flux and saturation pressure, while insignificant effects of tube size and mass flux were reported. Regarding the influence of vapor quality, the authors pointed out that an unclear relation between the vapor quality and two-phase heat transfer coefficient can be concluded. Furthermore, due to an absence of flow visualization and reliable flow pattern map, the authors did not define the dominant heat transfer mechanism for the range of working conditions. Additionally, none of the seven assessed heat transfer correlations worked well with the measured heat transfer database of the R134a, thus, the authors modified the correlation proposed by Tran et al. [16] to make more reliable predictions with a MAE of 29 %.

One of the most recent attempts to develop a flow boiling heat transfer model for more than a flow pattern is the work conducted by Harirchian and Garimella [158]. They developed a flow regime-based model of heat transfer and pressure drop for flow boiling in micro-channels based on the comprehensive flow regime map proposed by Harirchian and Garimella [66] for a wide range of channel size and experimental operating conditions for FC77. The authors focused on providing flow-regime based models of heat transfer coefficients and pressure drops for the four common flow patterns. Firstly, for the bubbly flow, the authors presented Cooper's empirical correlation for pool boiling since it predicts the chosen experimental data very well with $MAE = 13.9\%$. Secondly, a physically analysis for local heat transfer coefficients was performed for the confined annular flow, and the model captured the chosen data with $MAE = 17.3\%$. Thirdly, the same model developed for confined annular flow was used for annular/wispy-annular flow regime but after obtaining optimized values of the correction factor for interfacial friction factor where the data base were captured with $MAE = 21.8\%$. Fourthly, the three-zone model of slug flow proposed by Thome et al. [151] was modified to be used for the slug flow regime with $MAE = 17.8\%$.

In a recent experimental work for flow boiling of deionized water in a 0.5 mm inner diameter horizontal micro-tube, Lim et al. [7] investigated the effects of working parameters on two-phase heat transfer coefficient for a low vapor quality range, $0.0 \leq x \leq 0.2$. It has been reported that the heat transfer coefficient is basically affected by heat flux rather than mass flux, and consequently the dominant heat transfer mechanism is nucleate boiling. Moreover, the authors revealed that none of the existing heat transfer correlations was able to predict, accurately, their experimental data considering the effects of vapor quality. Therefore, they proposed a heat transfer correlation, which predicted the measured data with a MAE of 7.2 %, in terms of Boiling number, Bo , Reynolds number, Re , and modified Froude number, C_{Fr} . The authors suggested that the transition to annular flow pattern occurs when modified Froude number is less than or equal to liquid Froude number $C_{Fr} \leq Fr_l$. In general, the applicability of this correlation, which listed in Table (A-2), is limited to $x \leq 0.2$.

2.10. Two-Phase Pressure Drop

Several researches for predicting two-phase pressure drop in horizontal mini/micro-channels have been done, and many predictive methods were proposed as listed in Table (A-3). Moreover, some of them were performed for adiabatic two-phase flow conditions, (e.g. Field and Hrnjak [159]; Revellin and Thome [3]; Kim et al. [160]; Li and Wu [74]), while some others were considered diabatic two-phase flow conditions, (e.g. Hashizume [161]; Lin et al. [162]; Hahne et al. [163]; Tran et al. [16, 164]; Yan and Lin [149]; Yun and Kim [165]; Hwang and Kim [166]; Park and Hrnjak [167]; Huh and Kim [168], Pamitran et al. [169]). Furthermore, some two-phase pressure drop investigations were carried out for specific flow pattern regimes, intermittent flow such as Garimella et al. [79], or adiabatic slug flow as that performed by Orell [170], or for various flow patterns as in Quiben and Thome [171]; and Cheng et al. [103], or for annular flow regime in Cioncolini et al. [172].

In 1991, Lin et al. [162] studied the frictional pressure drop for evaporation of R12 in capillary tubes taking into account the effects of vapor quality and surface roughness. It has been found that frictional pressure drop is higher than expansion pressure drop and the total pressure drop increased by increasing the vapor quality specifically close to the capillary exit. Moreover, the authors developed a correlation, as it is listed in Table (A-3), for predicting the total pressure drop which was able to predict their 238 data points with a standard relative error of 15.3 %. However, the proposed correlation is applicable for the low vapor quality regime which may not be valid for elongated bubble and annular flow regime.

Fukano and Kariyasaki [36] investigated the characteristics of air-water two-phase flow in capillary tubes considering the effects of pipe size (1.0, 2.4, 4.9 mm inner diameter), and orientation (vertical-upward, vertical-downward, and horizontal). They revealed that for two-phase flow in capillary size tubes, the flow orientation and gravity have insignificant effects on flow patterns, and the liquid film thickness is uniformly distributed. On the other hand, the authors reported the important influence of the sudden expansion of the liquid, which is observed at the end of the air-bubble, on the total pressure drop. Moreover, they proposed a correlation for predicting the pressure drop in capillary tubes taking into account the contribution of frictional and expansion effects which is given as follows,

$$\Delta p_t = \Delta p_f + \Delta p_e \quad (2.45)$$

Where Δp_f is the frictional pressure drop and evaluated in terms of superficial gas, j_g , and liquid, j_l , velocities and characteristics of intermittent flow as given by,

$$\Delta p_f = f \frac{L}{D} \frac{(j_g + j_l)^2 L_l}{(L_g + L_l)} \quad (2.46)$$

And Δp_e is the pressure drop due to liquid expansion, which is defined as,

$$\Delta p_e = \frac{w^2 L}{2(L_g + L_l)} \quad (2.47)$$

Where w is defined by,

$$w = \frac{(j_g + j_l) - [j_l - (j_g + j_l)(1 - \gamma)]}{\gamma(1 - \alpha_B)} \quad (2.48)$$

The area void fraction is denoted as α_B , and γ represents the ratio of bubble length to slug unit length, $\gamma = L_g / (L_g + L_l)$.

The above pressure drop correlation neglected the effects of working conditions and the properties of the working fluids as well as the phase change on the pressure drop evaluation. This limits its applicability to adiabatic air-water two-phase flow.

Mishima and Hibiki [173] studied the characteristics of adiabatic air-water two-phase flow in vertical round capillary tubes considering the influences of working conditions on flow pattern, void fraction, and frictional pressure drop. The authors correlated their experimental pressure data based on Chisholm's correlation, and proposed a new correlation for predicting two-phase frictional pressure drop which is applicable to adiabatic two-phase flow in horizontal and vertical flow with round and rectangular cross sections at the working conditions listed in Table (A-3).

Tran et al. [164] experimentally investigated the two-phase pressure drop of flow boiling of three various refrigerants, R-134a, R12, and R-113 in three different small channels, two are round tubes with inner diameters of 2.46, and 2.92 mm and one is a rectangular channel with

hydraulic diameter of 2.40 mm. The experiments were performed for range of mass fluxes from $G = 33$ to $833 \text{ kg/m}^2 \cdot \text{s}$ and heat fluxes from 2.2 to 129 kW/m^2 . The authors evaluated five correlations of two-phase frictional pressure drop prediction for large tubes, ($D_h \geq 8 \text{ mm}$), where none of these correlations predicted their data of small channels for mass flux $G > 150 \text{ kg/m}^2 \cdot \text{s}$ and vapor quality $x \geq 0.6$, where the annular flow pattern is usually experienced in small channels. They suggested that the transition from annular to mist flow regime occurs when $x \geq 0.85$. They reported that the two-phase pressure drop for flow boiling in small tubes is greatly affected by the dynamics of the confined bubbles and the surface tension of the liquid film trapped between the elongated bubble and the inner surface of the tube. Therefore, they developed a new two-phase frictional pressure drop, Δp_f , correlation based on Chisholm's B-coefficient method and considered the channel size effect by including the confinement number, Co , in this correlation. Their developed correlation is represented in Table (A-3), where Δp_{fLo} is the frictional pressure drop of the liquid, and Γ^2 is the ratio between the pressure gradient of the gas and that for the liquid.

Hwang and Kim [166] experimentally studied the two-phase pressure drop of R134a in 0.244, 0.43, and 0.792 mm inner diameter horizontal micro-tubes, taking into account the effects of mass flux, vapor quality, and tube size. It has been reported that two-phase frictional pressure drop increases by increasing mass flux and vapor quality, while decreased by increasing tube size. Furthermore, it has been found that the friction factor correlations of conventional size predicted well the friction factor for micro-tubes. Moreover, the authors proposed a new correlation for predicting two-phase pressure drop in micro-tubes in terms of Lockhart-Martinelli parameter, liquid phase Reynolds number, and confinement number. The proposed correlation, as is listed in Table (A-3), predicted the pressure drop experimental data of micro-tubes with an absolute deviation error of 8.1 %.

Revellin and Thome [3] measured the two-phase frictional pressure drop for flow boiling of the refrigerants R-134a and R-245fa in two micro-tubes with sizes of 0.509 mm and 0.790 mm. The authors plotted the two-phase friction versus two-phase Reynolds number and three different zones were observed, laminar ($Re_{TP} < 2000$), transition ($2000 \leq Re_{TP} < 8000$), and turbulent zone ($Re_{TP} \geq 8000$). Moreover, they proposed a new correlation for predicting the two-phase friction factor for each tested micro-tube for the turbulent zone based on the

homogenous model by modifying the two-phase friction factor. The two-phase friction factor, for each micro-tube tested, is expressed as follows:

$$f_{TP} = \begin{cases} 0.08Re_{TP}^{-1/5} & , D = 0.509 \text{ mm} \\ 6.0Re_{TP}^{-3/5} & , D = 0.790 \text{ mm} \end{cases} \quad (2.49)$$

The proposed correlation captured 85.7 % of their experimental data within ± 20 % error band and is limited for the tested conditions ($Re_{TP} \geq 8000$).

Cheng et al. [103] have recently developed a flow pattern map for flow boiling of CO₂ inside tubes and extended it to be applicable to a tube size range of $D_{eq} = 0.6 - 10.0 \text{ mm}$, mass fluxes, $G = 50 - 1500 \text{ kg/m}^2 \cdot \text{s}$, heat fluxes, $\dot{q} = 1.8 - 46.0 \text{ kW/m}^2$, and saturation temperature range of $T_{sat} = -28 \text{ to } +25 \text{ }^\circ\text{C}$. Based on their flow pattern map, they developed a phenomenological model for two-phase pressure drop prediction by correlating the friction factor coefficient for each flow regime. The authors correlated the two-phase pressure drop data, Δp_A , of the annular flow as follow:

$$\Delta p_A = 4f_A \frac{L}{D_{eq}} \frac{\rho_g u_g^2}{2} \quad (2.50)$$

Where D_{eq} is the equivalent diameter which is defined as $D_{eq} = \sqrt{4A/\pi}$, and f_A , is the friction factor coefficient of the annular flow which is expressed as:

$$f_A = 3.128Re_g^{-0.454} We_f^{-0.0308} \quad (2.51)$$

It is of importance here to mention the correlation used to predict the vapor quality, x_{IA} , at which the flow pattern changes from intermittent to annular flow, which is represented as:

$$x_{IA} = \left[1.8^{1/0.875} \left(\frac{\rho_g}{\rho_f} \right)^{-1/1.75} \left(\frac{\mu_f}{\mu_g} \right)^{-1/7} + 1 \right]^{-1} \quad (2.52)$$

The authors reported that their model predicts the experimental data of the two-phase pressure drop of the CO₂ better than the other methods. However, the proposed flow pattern map was

developed based on the available CO₂ data that was very limited due to the lack of experimental work conducted for CO₂.

Cioncolini et al. [172] collected an intensive set of two-phase pressure drop data, (3908 points), obtained for adiabatic flow in a wide channel size range from 0.517 mm to 31.7 mm inner diameter, using the criterion proposed by Kandlikar [174] for classifying macro and micro-channels and based on the flow pattern map developed by Hewitt and Roberts [175] for identifying the annular flow regime. The authors assessed 24 methods of two-phase pressure drop and thus, they proposed a new correlation for two-phase pressure drop prediction for adiabatic flow in macro and micro-channels based on the vapor core Weber number which is influenced by the annular liquid film estimation. The total two-phase pressure gradient was expressed as follows:

$$-\left(\frac{dp}{dz}\right)_{tpf-t} = 2f_{tp} \frac{G_c^2}{\rho_c d} + G^2 \frac{d}{dz} \left[\frac{x^2}{\rho_g \varepsilon} + \frac{e^2(1-x)^2}{\rho_l \gamma(1-\varepsilon)} + \frac{(1-e)^2(1-x)^2}{\rho_l(1-\gamma)(1-\varepsilon)} \right] + [\rho_l(1-\varepsilon) + \rho_g \varepsilon] g \sin(\theta) \quad (2.53)$$

Where ε , γ , and e are the void fraction, the liquid droplet hold-up, and the fraction of the liquid droplets in the vapor core, respectively. All these three parameters can be estimated using the proper methods available in the literature. While, the two-phase frictional factor f_{tp} , is predicted for both macro and micro-channels based on the vapor core Weber number as follow:

$$f_{tp} = \begin{cases} 0.172 We_c^{-0.372} & \text{for } Bo > 4.0 \\ 0.0196 We_c^{-0.372} Re_l^{0.318} & \text{for } Bo < 4.0 \end{cases} \quad (2.54)$$

Where, the vapor core Weber number is defined as:

$$We_c = \frac{G_c^2 D_c}{\rho_c \sigma} \quad (2.55)$$

In order to choose the proper correlation for predicting f_{tp} , the authors adopted the criterion proposed by Kew and Cornwell (1997) based on the Bond number, for defining the transition from Macro, ($Bo > 4.0$), to Micro-scale, ($Bo < 4.0$). The new correlation predicted 100 % of

the chosen data within a band error of $\mp 50.0\%$ and a MAE of 13.1% compare to the other tested correlations. Overall, the developed correlation depends strongly on the estimation of vapor core Weber number which is mainly dependent of the prediction of liquid film thickness.

Tibirica et al. [176] experimentally investigated flow boiling pressure drop for R-134a in a single horizontal micro-tube with inner diameter of 2.32 mm. They performed their experiments at diabatic conditions with a range of mass and heat fluxes, $100 - 600 (kg/m^2.s)$ and $10 - 55 (kW/m^2)$ respectively for inlet saturation conditions at $T_{sat} = 31\text{ }^\circ\text{C}$. The total pressure gradient was measured considering the lengths of the preheater and the test section, while the frictional two-phase pressure gradient was estimated by subtracting the single-phase pressure gradient from the total pressure gradient. They compared their experimental data to 13 two-phase pressure drop prediction methods and found that the method proposed by Cioncolini et al. [172] for two-phase pressure drop in the annular flow gives better predictions.

Wu et al. [177] have recently investigated the heat transfer and pressure drop for flow boiling of the CO₂ in a horizontal micro-tube with a diameter of 1.42 mm and a range of mass fluxes, $300 - 600 kg/m^2.s$, heat fluxes, $7.5 - 29.8 kw/m^2$, and a length to diameter ratio of $L/D \approx 211$. It is revealed that the nucleate boiling heat transfer is dominant at low vapor quality, ($x < 0.2$), where the two-phase pressure drop increases by increasing the heat flux. On the other hand, at a moderate vapor quality, it was observed that the annular flow is predominant and the nucleate boiling is suppressed by increasing the vapor quality. Furthermore, the maximum frictional two-phase pressure drop was observed at transition zone, from the annular flow zone to dry-out zone. The authors used the two-phase pressure drop correlation proposed by Cheng et al. [103] to predict their experimental data, but it over predicted the data at higher vapor quality ($x \geq 0.7$). Thus, they modified the correlation that predicts the friction factor coefficient for mist flow zone which is expressed as follows:

$$f_m = 2.214Re^{-0.521} \quad (2.56)$$

To better understand the effect of flow pattern on frictional two-phase pressure drop in micro-channels, Choi and Kim [178] carried out an experimental work for investigating two-phase frictional pressure drop of adiabatic flow of water-liquid/nitrogen-gas in a single horizontal rectangular micro-channel considering the flow visualization for the working

conditions listed in Table (A-3). The authors neglected the pressure drop due to the gravitational and acceleration effects and considered that the total two-phase pressure drop can be represented by frictional pressure drop. Thus, they measured the two-phase pressure drop for various observed flow patterns which were classified into three basic flow configurations. Firstly, bubbles flow zone (which covers the boundaries of bubbly, slug, and elongated bubble flows). Secondly, transition flow zone, that represents transition from intermittent flow to annular flow regime. Thirdly, liquid-ring flow zone which is observed in the annular flow regime. It has been found that the frictional two-phase pressure drop is significantly influenced by the dominant flow pattern. Consequently, the authors proposed pressure drop correlations for the observed flow patterns based on their experimental database and the assessment of previous correlations available in the literature. The proposed correlations can be classified into two-groups according to the considered two-phase model either homogeneous (HFM) or separated (SFM) flow model. In other words, the authors proposed correlations for predicting two-phase friction factor, f_{tp} , based on viscosity models which are developed according to HFM taking into account the effects of channel aspect ratio, AR. On the other hand, they proposed correlations for predicting Chisholm's parameter, C, based on SFM to calculate the two-phase frictional pressure drop multiplier as indicated in Table (A-3). Overall, the new flow pattern-based correlations are limited to predict adiabatic two-phase pressure drop in single rectangular micro-channels.

Maqbool et al. [179] have conducted flow boiling experiments for investigating two-phase pressure drop of Ammonia flow boiling in vertical small tubes. They performed the experiments considering the effects of tube size, ($D = 1.224 \text{ mm}, 1.70 \text{ mm}$), saturation temperature, ($T_{sat} = 23, 33, 43 \text{ }^\circ\text{C}$), mass flux, ($G = 100 - 500 \text{ kg/m}^2 \cdot \text{s}$), and heat flux, ($\dot{q} = 15 - 355 \text{ kW/m}^2$), on two-phase pressure drop in vertical flow channels. Similar to several previous studies, it has been shown that two-phase frictional pressure drop increases by increasing mass flux and vapor quality as well as the saturation temperature. Furthermore, the authors compared their experimental data points with some macro/micro two-phase pressure drop correlations and proposed a new form of Tran et al. [164] two-phase pressure drop correlation for mini/micro channels by modifying the term that contains the confinement number, C_o , to be $0.2C_o^{1.2}$ as shown in Table (A-3). Moreover, surface tension becomes significant when ($C_o \geq 1.0$) which was the case in their study. It has been reported that the

developed correlation predicts all of their ammonia data with a mean absolute deviation of $MAD = 16.0 \%$.

Lim et al. [180] carried out two-phase flow boiling experiments for investigating frictional two-phase pressure drop in a 0.5 mm hydraulic diameter horizontal rectangular mini/micro-channel. The authors performed their experiments for the working conditions listed in Table (2.3). Moreover, they assessed some previous correlations for predicting two-phase frictional pressure drop, which are Mishima and Hibiki [173]; Yu et al. [181]; Qu and Mudawar [182]; Lee and Mudawar [183]; Choi et al. [184]; and Lee and Garimella [185]. It has been found that the correlations of Lee and Garimella [185] and Choi et al. [184] are in good agreement with the tested experimental data of mini/micro-channel flow boiling compared to the other tested correlations. Moreover, they proposed a new correlation, in the form of Chisholm's constant, which was able to predict their experimental data with a MAE of 3.9 %. Overall, the proposed pressure drop correlation is limited to low vapor quality region which cover the range $0.0 \leq x \leq 0.2$.

In a recent study, Del Col et al. [186] have investigated the characteristics of two-phase flow of Propane (R290) in a 0.96 mm inner diameter single horizontal micro-channel. The authors investigated two-phase frictional pressure drop at adiabatic conditions and two-phase heat transfer flow boiling and condensation. They carried out their experiments for a range of mass flux, ($100 \leq G \leq 1000 [kg/m^2.s]$), and heat flux of, $10 \leq q_w'' \leq 315 [kW/m^2]$, which corresponds to a range of vapor quality, ($0.05 < x < 0.6$), and confinement number, ($1.27 \leq Co \leq 1.29$). It has been found that heat transfer coefficient of Propane is significantly influenced by the applied heat flux, while minor effects of mass flux and vapor quality have been noted. Furthermore, they compared their experimental pressure drop and heat transfer flow boiling and condensation data base with the existing prediction methods, and it has been shown that none of the existing flow boiling approaches was able to predict their R290 data points for two-phase flow in micro-channels.

2.11. Summary and Objectives

A detailed literature review for two-phase flow in horizontal mini/micro-channels under diabatic and adiabatic conditions has been provided. Three essential topics have been focused on, which are critical heat flux, two-phase heat transfer coefficient, and two-phase pressure drop for flow boiling in a single mini/micro-channel subjected to a uniform heat flux.

2.11.1. Summary

According to the literature review provided above, it appears that two-phase flow in mini/micro-channels is a hot topic with several industrial and medical applications. Moreover, it has essential features which need to be well investigated for a better understanding of two-phase flow phenomena in mini/micro-channels. The above literature review can be summarized as follows:

1. It has been proved that evaporative heat transfer coefficient of small channels is about 30 to 80 % higher than large channels.
2. Several criteria for identifying differences between conventional size and mini/micro-scale size have been addressed, and it has been found that the channel can be categorized as mini/micro-channel for confinement number $Co \geq 0.5$.
3. Critical heat flux, two-phase heat transfer coefficient, two-phase pressure drop, void fraction, and flow pattern maps are considered to be the main parameters required for studying and design flow boiling mini/micro-channel heat sinks.
4. Investigation of liquid film characteristics is the key parameter for predicting heat transfer coefficient, partial dry-out, and critical heat flux in slug and annular flow regimes.
5. Surface tension, viscous, inertial, and shear forces effects play a key role in horizontal mini/micro-scale channels, and have a significant effect on liquid film thickness. While gravity force can be neglected. Moreover, the dominant force is dependent on the specific flow pattern.
6. Several flow patterns for flow boiling in horizontal mini/micro-channels have been observed, but basic flow patterns can be identified which are bubbly flow, slug flow, and annular flow regime.

7. Available flow pattern maps for flow boiling in horizontal mini/micro-channels are very limited and a global flow pattern map is needed. Furthermore, prediction of transition boundaries of flow patterns is still challenging due to flow instability.
8. Two major heat transfer mechanisms are studied and reported, nucleate boiling and convective boiling heat transfer mechanism, which are dependent on the flow pattern. In other words, it has been reported that nucleate boiling dominates at low vapor quality region, while convective boiling dominates at intermediate and high vapor quality region.
9. Extensive and comprehensive investigations and researches have recently been performed for two-phase flow in mini/micro-channels. However, most of researches were performed experimentally rather than analytically, which limits the applicability of the proposed methods for predicting the essential parameters of flow boiling in mini/micro-channels. Therefore, developing an analytical flow boiling model is highly needed.
10. An obvious difference in heat transfer coefficient has been reported between conventional and small channels. Therefore, the prediction methods developed for two-phase conventional size channels are not applicable to two-phase mini/micro-channels. Moreover, discrepancies among mini/micro-scale predictive methods have been reported and still not fully clarified.
11. Very limited studies have taken into account some essential flow boiling phenomena, such as bubble confinement, bubble coalescence, and flow instability for investigating flow boiling characteristics in mini/micro-channels. Furthermore, there exist a lack in experimental data for flow boiling in horizontal mini/micro-channels with inner diameter $D < 0.5 \text{ mm}$, particularly for isolated bubble zone.

2.11.2. Objectives

The main objective of this thesis is to investigate the characteristics of two-phase flow boiling in annular and slug flow regimes, and to provide a reliable predictive method for predicting the critical heat flux, heat transfer coefficient, pressure drop, and void fraction in horizontal micro-tubes under uniform heat flux. This has been done through achieving the following consecutive sub-objectives:

1. Developing a semi-analytical model for predicting the liquid film thickness in annular flow regime during two-phase flow boiling in a horizontal micro-tube. This stage was essential to study the incipience of the dry-out phenomenon and to predict the critical heat flux.
2. Developing a model to predict the two-phase heat transfer coefficient, pressure drop, and void fraction in annular flow regime. Effects of phasic enthalpies, viscous force, inertial force, and liquid film evaporation were considered in modeling. Following, the influence of the main operating conditions, working fluid properties, and channel size on the model results, were investigated.
3. Developing a semi-analytical model to study the bubble dynamics, bubble length, and bubble frequency in the slug flow regime based on the drift flux model, for a better understanding of flow boiling phenomena in mini/micro-channels. Extensive experimental data available in literature was used for validation of the developed models.

Chapter 3

3. Modeling of Dry-out Incipience for Flow Boiling in a Circular Micro-channel at a Uniform Heat Flux

Amen Younes¹, Ibrahim Hassan^{1,2}

This paper was accepted & published in *J. of Heat Transfer* 137(2), 021502 (Feb 01, 2015)

¹Department of Mechanical and Industrial Engineering, Concordia University, 1455 de
Maisonneuve Blvd. W, Montreal, QC, Canada, H3G 1M8

² Mechanical Engineering Department, Texas A&M University at Qatar

P O Box 23874, Doha, Qatar

3.1. Abstract

Dry-out is an essential phenomenon that has been observed experimentally in both slug and annular flow regimes for flow boiling in mini and micro-channels. The dry-out leads to a drastic drop in heat transfer coefficient, reversible flow and may cause a serious damage to the micro-channel. Consequently, the study and prediction of this phenomenon is an essential objective for flow boiling in micro-channels. The aim of this work is to develop an analytical model to predict the critical heat flux (CHF) based on the prediction of liquid film variation in annular flow regime for flow boiling in a horizontal uniformly heated circular micro-tube. The model is developed by applying one-dimensional separated flow model for a control volume in annular flow regime for steady, and stable saturated flow boiling. The influence of interfacial shear and inertia force on the liquid film thickness is taken into account. The effects of operating conditions, channel sizes, and working fluids on the critical heat flux (CHF) have been investigated. The model was compared with 110 CHF data points for flow boiling of various working fluids, (Water, LN2, FC-72, and R134a) in single and multiple micro/mini-channels with diameter ranges of $(0.38 \leq D_h \leq 3.04 \text{ mm})$ and heated-length to diameter ratios in the range of $117.7 \leq L_h/D \leq 470$. Additionally, three CHF correlations developed for saturated flow boiling in a single micro-tube have been employed for the model validation. The model showed a good agreement with the experimental CHF data with MAE= 19.81 %.

Keywords: saturated flow boiling, liquid film, critical heat flux, annular flow regime.

3.2. Introduction

Dry-out is an important phenomenon which represents the critical heat flux (CHF) mechanism for flow boiling in micro-channels. It has been described early in the literature with various definitions as dry-out, burn-out, or critical heat flux as stated in Kandlikar [134]. It is very crucial to understand CHF phenomenon in order to study its effects on flow boiling heat transfer in mini/micro-channels. Furthermore, one of the most significant investigations of saturated CHF is to predict the maximum cooling capacity of the cooling devices that employ saturated flow boiling micro-channels. Several researches and investigations for studying CHF phenomenon in mini/micro-channels have been carried out, but the available CHF data and correlations are still not enough to provide thorough interpretation for CHF mechanism.

Katto [187], studied experimentally and analytically the relation between CHF and inlet sub-cooling liquid enthalpy ΔH_i for forced convection boiling in vertical uniformly heated round tubes. He attempted to develop a generalized correlation for CHF prediction by analyzing the CHF experimental data for seven different fluids. It has been revealed that four different CHF regimes exist and a CHF regime map was developed in terms of the dimensionless parameters $(\sigma\rho_l/G^2)$ and (l/d) . The CHF regimes are classified into four regimes called as L, H, N, and HP CHF regimes. The generalized CHF correlation has been revised later by Katto and Ohono [142] in order to be applicable for wider range of operating conditions. Considering inlet subcooling effects, exit vapor quality x_{exit} was defined in terms of CHF in Katto [187] as,

$$x_{exit} = \frac{4q_c L}{Gh_{fg} D} - \frac{\Delta h_i}{h_{fg}} \quad (3.1)$$

Qu and Mudawar [43] studied experimentally the CHF for flow boiling of the water in a micro-channel heat sink consists of 12 parallel rectangular micro-channels with cross section of $215 \times 821 \mu\text{m}^2$ for measuring new saturated CHF database and developing a new CHF correlation. Although the experiments were performed with upstream instability control throttle, a vapor backflow was observed when the heat flux reaches the CHF. Furthermore, the inlet temperature and mass flux effects were taken into account. A significant mass flux effect on the CHF has been reported. In fact, the CHF increased monotonically by increasing the mass flux

while the inlet temperature did not show any effect on the CHF. This may be attributed to the back flow that affects the inlet temperature effect. The proposed saturated CHF correlation was developed based on the CHF data of water and R-113 for rectangular and circular mini/micro-channel heat sinks respectively. A similar form of the CHF correlation proposed by Katto and Ohno [142] was adopted since it has been recommended for saturated CHF prediction for flow boiling in single circular mini-channels, but without considering the inlet sub-cooling effect. The new CHF correlation is listed in Table (3.1). This correlation was compared with 42 CHF data points collected for flow boiling of water and R-113 for channel sizes ranges of $380 \mu\text{m} \leq D_h \leq 2540 \mu\text{m}$, and gave a good agreement with the experimental data within a band error of $\pm 20 \%$ and $\text{MAE} = 4.0 \%$.

Understanding the mechanism of CHF is very crucial particularly, for micro-channel heat sinks designed based on saturated flow boiling. Moreover, a shortage in CHF data for stable conditions still exists. Bergles and Kandlikar [188] highlighted some CHF researches done for unstable conditions for flow boiling in micro-channels considering the instability effects on the CHF. It has been revealed that annular flow is the dominant flow pattern where the CHF may take place for flow boiling in micro-channels. Additionally, they recommended to consider the importance of flow and thermal conjugate effects for more reliable CHF database as well as to create a new saturated flow boiling CHF data for stable conditions. However, this is one of the CHF experimental difficulties in mini/micro-channels.

Further CHF investigations for flow boiling in micro-channels have been done recently considering various working fluids and heat transfer mechanisms. Qi et al. [46] studied experimentally the flow boiling heat transfer and CHF characteristics for liquid Nitrogen (LN_2) flowing in micro-tubes for four different sizes $D_h = 0.531, 0.864, 1.042, \text{ and } 1.931 \text{ mm}$. The CHF was predicted based on a sudden raise in inner wall temperature and a drastic drop in the local heat transfer coefficient which was observed at the end of the tested micro-tubes. The obtained new CHF data points were compared with the CHF correlations of Zhang et al. [44] and Katto [187]. Both correlations underestimated the CHF data thus, the authors developed a new CHF correlation as listed in Table (3.1), based on Katto [187] correlation, considering the tube size effect for better CHF prediction. The new CHF correlation predicted the CHF data for the liquid nitrogen with $\text{MAE} = 7.38 \%$ within an error band of $\pm 30 \%$.

Table (3-1): CHF Correlations for flow boiling in mini and micro-channels.

| Author | Correlation | Conditions |
|--------------------------|--|---|
| Qu and Mudawar [43] | $\left(\frac{q_c''}{Gh_{fg}}\right) = 33.43 \left(\frac{\rho_g}{\rho_f}\right)^{1.11} We^{-0.21} \left(\frac{L_h}{D}\right)^{-0.36}$ | 21 Rectangular micro-channels $215 \times 821 \mu m$, $0.38 \text{ mm} \leq D_h \leq 2.54 \text{ mm}$ CHF data for Water and R-113 in heat sinks are used |
| Wojtan et al. [45] | $\left(\frac{q_c''}{Gh_{fg}}\right) = 0.437 \left(\frac{\rho_g}{\rho_f}\right)^{0.073} We^{-0.24} \left(\frac{L_h}{D}\right)^{-0.72}$ | R134a, R245fa $0.5 \text{ mm} \leq D_h \leq 0.8 \text{ mm}$, $25 \leq L/D \leq 141$ $293 \leq We \leq 21,044$ |
| Qi et al. [46] | $\left(\frac{q_c''}{Gh_{fg}}\right) = (0.214 + 0.14 Co) \left(\frac{\rho_g}{\rho_f}\right)^{0.1333} We^{-0.333} \times \frac{1}{1+0.03(L/D)}$ | Based on the correlation of Katto [187] Weber number is calculated in terms of heated-length |
| Wu & Li [137] | $\left(\frac{q_c''}{G.h_{fg}}\right) = 0.62 \cdot \left(\frac{L_h}{d_{he}}\right)^{-1.19} x_e^{0.82}$ $\left(\frac{q_c''}{G.h_{fg}}\right) = 1.160 \times 10^{-3} (We_m Ca_l^{0.8})^{-0.16}$ | properties are estimated at the outlet of the channel. for $(L_h/d_{he} \leq 150)$ & $(BoRe_l^{0.5} \leq 200.00)$ for $(L_h/d_{he} > 150)$ & $(BoRe_l^{0.5} \leq 200.00)$ |
| Ong & Thome [139] | $\left(\frac{q_c''}{Gh_{fg}}\right) = 0.12 \left(\frac{\mu_f}{\mu_g}\right)^{0.183} \left(\frac{\rho_g}{\rho_f}\right)^{0.062} We^{-0.141} \left(\frac{L_h}{D}\right)^{-0.7} \left(\frac{D}{D_{th}}\right)^{0.11}$ | $D_{th} = \frac{1}{Co} \sqrt{\sigma/g(\rho_f - \rho_g)}$, $Co = 0.5$ |
| Chen and Garimella [189] | $\left(\frac{q_c''}{Gh_{fg}}\right) = 40.0 \left(\frac{\rho_g}{\rho_f}\right)^{1.12} We^{-0.24} \left(\frac{L_h}{D_e}\right)^{-0.34}$ | For flow boiling in micro-channel heat sinks |

Wojtan et al. [45], studied experimentally the effects of mass flux, inlet sub-cooling, heated length, working fluid and channel size on the saturated CHF in individual micro-channels. It has been demonstrated that all the previous parameters have significant effects on CHF except the inlet sub-cooling which did not show a clear effect on the CHF. The authors measured 34 new CHF data points for flow boiling of R134a in 0.5 mm and 0.8 mm heated uniformly micro-channels at quite wide experimental conditions. The CHF correlations of Qu and Mudawar [43] and Katto and Ohno [142] have been employed to predict the new CHF data. Katto and Ohno [142] correlation captured 40 % of the CHF data with a band error ± 15 % and MAE of 32 %. On the other hand, Qu and Mudawar [43] correlation overpredicted the new saturated CHF data, however it gives similar trend. Thus, the authors, proposed a new version of Katto and Ohno [142] correlation for saturated CHF prediction only for annular flow and for $(\rho_v/\rho_l) < 0.15$. The modified correlation which is listed in Table (3.1) captured 82.4 % of their CHF database with a band error of ± 15 % and MAE of 7.6 %. The critical vapor quality x_{crit} that represents the transition from annular to dry-out flow pattern is calculated based on saturated CHF and defined as follows,

$$x_{crit} = \frac{q_c}{G(h_{fg} + h_{sub})} \frac{4L_h}{D} \quad (3.2)$$

Turning to the analytical CHF models which have been developed for flow boiling in micro-channels, it can be seen that the investigations of CHF condition for flow boiling in micro-channels have been more experimental than analytical. Kandlikar [9] developed a theoretical CHF model for pool boiling in micro-channels by considering the effects of the surface-liquid interactions. The interfacial forces, which are parallel to heater surface and induced due to the evaporation of the liquid phase, have been taken into account for the CHF model. The author considered the effect of other forces, such as surface tension and gravitational forces, but recognized the CHF condition when the effect of the force of the momentum of the evaporation suppresses the effect of gravitational and surface tension forces. The model was applicable for prediction CHF conditions for saturated pool boiling of water, refrigerants, and cryogenic liquids for vertical and horizontal surfaces.

Kosar [190] has recently developed a simple analytical model for predicting CHF for flow boiling in mini and micro-channels. The approach used in developing the model was based

on the mass balance between the entrained liquid droplets in the vapor core and the liquid film in the annular flow regime. The model was compared with 151 CHF data points for low pressure refrigerants and water for mass fluxes range of 50 to 1600 $kg/m^2.s$. The comparison showed a good agreement with the CHF experimental data with (MAE=25.8%)

Kandlikar [191] developed a theoretical CHF model based on a scale analysis considering the effect of additional forces induced due to the evaporation and instability at the liquid-vapor interface. It has been revealed that the evaporation momentum force controls the CHF condition and as the channel size decreases, the gravity force decreases and the viscous force is dominant. . Moreover, the surface tension force becomes more significant for micro-tubes with hydraulic diameters $D_h \leq 200 \mu m$. The model predicted 75 % of CHF data obtained for flow boiling in tubes with a diameter range of (0.127- 3.36 mm) with (MAE=19.5 %).

Revellin and Thome [52] developed a theoretical CHF model for flow boiling in a single horizontal micro-channel uniformly heated. The model was developed based on conservation equations of the two-phase separated flow model considering the influence of interfacial waves of the annular liquid film. The CHF was defined based on the liquid film thickness and the interfacial wave height. In other words, the critical film thickness was modeled based on Kelvin-Helmholtz critical wave length λ_c , at the channel outlet where the dry-out occurs. The obtained correlation involved the effects of gravity and surface tension is identified as,

$$\delta = CR \left(\frac{u_g}{u_f} \right)^{j_1} \left(\frac{(\rho_f - \rho_g)gR^2}{\sigma} \right)^{K_1} \quad (3.3)$$

Where R is the internal radius of the tube, C, j_1 , and K_1 are parameters estimated based on the CHF database. It can be noted that the term in the right brackets represents the ratio between gravity and surface tension forces. However, in horizontal micro-channels the gravity effect does not have a significant role since the stratified flow is not a micro-channel flow pattern as has been proven in previous works by Triplett et al [70] and Serizawa et al [192]. The model was tested with CHF experimental data points obtained for four different fluids at wide range of channel sizes $D_h = [0.215 \text{ to } 3.15 \text{ mm}]$, mass fluxes range of $[29 \text{ to } 1600 \text{ kg/m}^2.s]$, various heated length $[10 \text{ to } 126 \text{ mm}]$, and inlet sub-cooling range $[2 \text{ to } 77^\circ\text{C}]$. The model predicted 90 % of the tested data with the error band $\pm 20 \%$ and MAE of 9.3 %. The best values for the

parameters C, j_1 and k_1 in Eq. (3.3), proposed by the authors are 0.15, $-3/7$ and $-1/7$, respectively. The CHF Results showed that the CHF increases by increasing the mass flux, the channels size and the inlet sub-cooling ΔT_{sub} , while decreases by increasing the channels heated length.

Wu and Li [137], studied the effects of heated length to heated equivalent diameter ratio (L_h/d_h) on the saturated CHF in mini/micro channels. They found that the Boiling number at CHF, Bl_{CHF} , decreases greatly by increasing (L_h/d_h) at low values of (L_h/d_h). A new criterion ($BoRe_l^{0.5} \leq 200.00$) was adopted to identify the macro-to-micro-scale region. The authors compiled 1672 saturated CHF database points for flow boiling of various refrigerants and water in mini and micro-channels. The threshold value of ($L_h/d_h = 150$) was reported as there is no significant effect of L_h/d_h on saturated CHF beyond this value. In general, the compiled database was divided into two main regions and a new CHF correlation was proposed for each region as presented in Table (3.1). Furthermore, the effects of inertia, viscous and surface tension forces were taken into account and represented by the non-dimensional groups ($We_m Ca_l^{0.8}$). The gravity force effect was not considered in the proposed CHF correlation, however many of correlated data corresponded to macro-scale region where the gravity effect has a significant influence. The authors tested the proposed correlations reliability in saturated CHF prediction compare to some selected CHF correlation, they found that their correlations captured 95.5 % of the non-aqueous CHF database within a ± 30 % error band and $MAE = 12.6$ %. While predicted 93.5 % of the Water CHF database within a ± 30 % error band and $MAE = 18.6$ %.

Ong and Thome [139] investigated the effects flow pattern, surface roughness, mass flux and fluid properties on flow boiling heat transfer coefficient and CHF in mini and micro-channels. They have developed a new CHF correlation which is able to predict the CHF in circular and rectangular single and multiple channels for the non-aqueous fluids R134a, R236fa, R245fa. Their CHF correlation and their experimental conditions are listed in Table (3.1). Moreover, the gravity force has a significant effect, but its influence decreases by decreasing the channel size. Ong & Thome [39] in another work, they investigated the channel confinement effect on the flow pattern for the flow boiling in micro-channels. They observed that when the confinement number, $Co \approx 1.0$, the gravity force effects are completely suppressed and shear

and surface tension become dominant. In this work the range of the confinement number of the data used to test the present model is $0.3 \leq Co \leq 6.3$, as shown in Table (3.2). It can be seen that majority of the data of all working fluids tested are for $Co \geq 0.8$.

There are many studies have been done for clarifying the dominant flow pattern for flow boiling in horizontal and vertical micro-channels, such as Qu and Mudawar [193], Revellin and Thome [75], Ong and Thome [39], and Kuznetsov et al [194]. Qu and Mudawar [193] verified that the annular flow is a dominant flow pattern in micro-channels at high heat flux conditions. According to the flow pattern map developed by Revellin and Thome [75] and improved later by Ong and Thome [39], it can be seen that the majority of data conditions which were used in testing the present model are fall in the annular flow regime.

Table (3-2): Range of Confinement number of the data used to test the present model.

| Working fluid | Hydraulic diameter, D_h, [mm] | Confinement Number, Co |
|----------------------|---|--|
| Water | 0.427 | 6.300 |
| R134a | 0.500 | 1.640 |
| | 0.800 | 1.025 |
| | 1.030 | 0.800 |
| | 2.200 | 0.373 |
| | 3.040 | 0.270 |
| LN2 | 0.531 | 1.950 |
| | 0.834 | 1.240. |
| | 1.040 | 0.990 |
| | 1.931 | 0.536 |
| FC-72 | 0.889 | 0.920 |

Chen and Garimella [189] conducted an experimental CHF work for flow boiling of FC-77 in a silicon test die. The test section has a size of $12.7 \text{ mm} \times 12.7 \text{ mm} \times 0.373 \text{ mm}$ and contains 60 parallel micro-channels, each has a size of $100 \mu\text{m} \times 387 \mu\text{m}$. The CHF was

measured for a mass flux range of 253.7 to 1015.0 kg/m².s. A new CHF correlation was proposed based on 49 CHF data points of five different experiments for three various working fluids, water, R-113 and FC-77. The new proposed CHF correlation predicted the selected CHF data points with the MAE = 7.67 %. It has been reported that the CHF affects the pressure drop trend in parallel multiple micro-channels where a decrease in pressure drop was observed when the CHF occurs. The authors attributed that to the abrupt decrease in flow rate through all of the micro-channels due to the accumulated bubbles which block the channel in the upstream.

It has been revealed in previous flow boiling studies that the annular flow is dominant in micro-channels. Jiang et al. [195] conducted an experimental work for flow boiling visualization in micro-channels and observed a stable annular flow with entrained liquid droplets at high heat flux. Zhang et al. [196] have also verified that the annular flow pattern is mostly dominant for flow boiling in micro-channels. Qu and Mudawar [193] investigated flow boiling of water in micro-channel heat sinks and they revealed that at high heat flux a stable annular flow was observed. However, the flow instability in the previous studies has been experienced and found to have a clear effect on the flow pattern. Recently many studies have been done for controlling the flow instability for flow boiling in micro-channels, such as Lee et al. [197]. They have investigated the effect of inlet restriction (orifice) on the flow instability in single and multiple micro-channels. It has been reported that the inlet orifice can reduce the flow instability and provide a stable flow pattern for flow boiling in micro-channels.

The annular flow is represented by the liquid film trapped between the vapor core and the inner surface of the channel. In the separated flow model, the conservation equations are applied for each phase separately. Among the two-phase flow models, it has been proven that the separated flow model can be applied properly to the annular flow in micro-channels (Moriyama and Inoue [147] and Ghiaasiaan [198]). Thus, in this paper, separated flow model principle is considered for modeling the two phase flow boiling in a horizontal micro-channel for annular flow regime. The liquid film variation is predicted in terms of applied operating conditions. The CHF is predicted based on the critical liquid film thickness value which is considered here to be equal to the roughness of the internal surface of the micro-tube. The model basic equations are solved numerically using Runge-Kutta method.

3.3. Model Analysis

The schematic of the annular flow pattern shown in Figure 3-1 is used to derive the equations of the present model. The main dependent variables considered in this model are the liquid film thickness δ , the liquid film velocity u_f , the core vapor velocity u_g , and the pressure p .

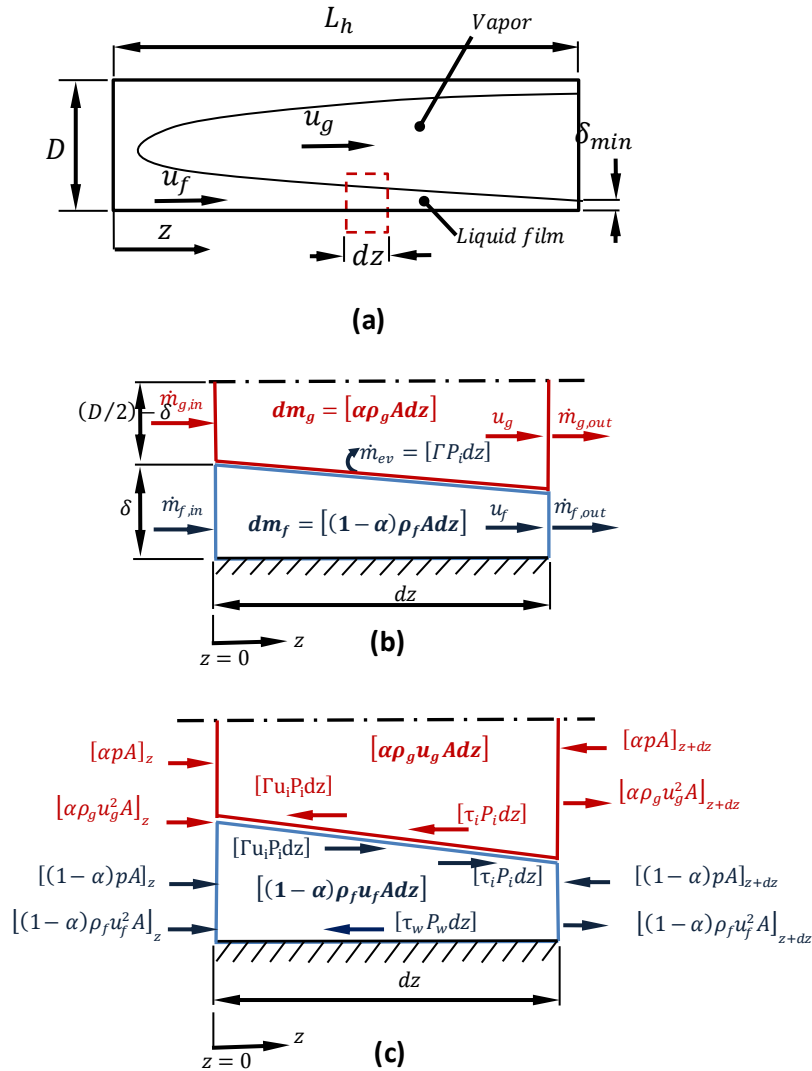


Figure 3-1: (a) schematic diagram of an annular flow pattern. (b) a symmetric sketch of the chosen control volume for applying mass balance. (c) a symmetric sketch shows the forces applied on the control volume.

By applying a uniform heat flux to external surface of the micro-tube, the heat transfers to the liquid film through the channel wall and the evaporation rate at the liquid/vapor interface increases till the liquid film reaches the critical value. Before deriving the model basic equations, the following set of assumptions have been considered:

1. The flow boiling is considered as a one dimensional steady state and fully developed flow. Thus, the dependent variables adopted vary only in axial flow direction.
2. The dominant flow pattern for flow boiling in micro-tubes is the annular flow.
3. The dominant heat transfer mechanism in the annular flow regime for flow boiling in micro-channels is the thin film evaporation.
4. The liquid film thickness is very small compare to the hydraulic diameter of the micro-tube.
5. The CHF is identified when the liquid film thickness reaches the critical value δ_c which is considered here to be equal to the internal surface roughness of the micro-tube.
6. The micro-tube is subjected to a circumferential and axial uniform heat flux.
7. As the channel size decreases, the gravity force effect decreases. Thus, in the present model and in the range of $D_h \leq 3\text{mm}$ tube diameter, the gravity force effect is neglected.
8. No entrained liquid droplets exist in the vapor core and no nucleate bubble exists in the liquid film in the annular flow regime for flow boiling in micro-channels.

It is of importance here to explain the base of adopting the assumption No. 5. A partial dry-out may occur even when the liquid film thickness is greater than the surface roughness, but not a complete dry-out. According to some previous flow boiling studies in micro-channels such as Hazuku et al. [126], Agostini et al. [154], and Ong and Thome [39], it has been justified that the CHF occurs when the liquid film thickness decreases lower than the surface roughness. Hazuku et al [126] justified that the minimum liquid film thickness is lower than $1\ \mu\text{m}$ in slug and annular flow regime. Considering the critical liquid film thickness to be equal to the inner surface roughness gave a good agreement with the experimental heat transfer data when the three-zone model was employed by Ong and Thome [39]. However, in the three-zone model, the critical liquid film thickness of the dry-out was suggested to be lower than the surface roughness $\approx 0.3\ \mu\text{m}$. Although this was applied to the elongated bubble zone, it would be more reasonable to be adopted in the annular flow regime.

It is known that the surface tension has a significant role which influences the evaporation process for flow boiling in micro-channels, but its effect becomes more important when considering the existence of nucleate bubbles in the liquid film in the annular flow. The reason for neglecting the surface tension force in the basic equations of the present model is for model simplification. Furthermore, no nucleate bubbles exist in the liquid film and the liquid film is considered to be driven by the effect of the shear force. The surface at the liquid-vapor interface is considered to be smooth. On the other hand, the effect of the surface tension on the prediction of the initial liquid film thickness is taken into account in the correlations employed in the present model.

In addition, two more pressure effects were not taken into account in the model analysis, the capillary and disjoining pressures. We believe that Capillary and disjoining pressures have more significance in the slug flow regime than the annular flow regime, where they affect the curvature of the liquid film and the meniscus. Moreover, the disjoining pressure effect becomes clear if a 2D model is developed. While only the axial pressure gradient is considered for both vapor and liquid phases in this model. Considering the above assumptions and applying the mass, momentum, and energy conservation equations for each phase to the differential element shown in Figure 3-1, six basic equations are derived as follows,

3.3.1. Mass Conservation Equations

The mass balance is applied for each phase in the chosen control volume as shown in Figure 3-1-b, in order to obtain the mass conservation equations.

$$\frac{d}{dz} [\rho_f u_f \delta (D - \delta)] = -\Gamma (D - 2\delta) \quad (3.4)$$

$$\frac{d}{dz} [\rho_g u_g (D - 2\delta)^2] = 4\Gamma (D - 2\delta) \quad (3.5)$$

Where Γ is the rate of evaporation of the liquid film at the liquid-vapor interface per unit surface area. Based on the vapor mass equation, Eq. (3.5), Γ can be identified in terms of liquid film thickness and vapor velocity gradients as follow,

$$\Gamma = -\rho_g u_g \frac{d\delta}{dz} + \frac{\rho_g}{4} (D - 2\delta) \frac{du_g}{dz} \quad (3.6)$$

Substituting Γ in Eq. (3.4) by Eq. (3.6) and rearranging the equation in terms of the gradient of the main dependent variables, the mass conservation equation of the whole mixture can be written as,

$$(\rho_g u_g - \rho_f u_f) \frac{d\delta}{dz} - \frac{1}{4} \rho_g (D - 2\delta) \frac{du_g}{dz} - \rho_f \frac{\delta(D - \delta)}{D - 2\delta} \frac{du_f}{dz} = 0 \quad (3.7)$$

3.3.2. Momentum Conservation Equations

The acting forces on the chosen control volume on both liquid film and vapor core phases are shown in Figure 3-1-c, two forces were neglected here, the body and virtual mass forces. The virtual mass force is a transient force that proportional with kinetic energy and acceleration of the isolated bubble, or the entrained liquid droplets, or in the two phase flow. A basic form of the virtual mass force has been addressed in many previous studies and one can refer to for more details as in Ghiaasiaan [198] and Ishii and Mishima [199]. The body force does not have a significant effect in micro-scale size, so it was neglected. Since, it was assumed that there is no entrained liquid droplets in the vapor core in the annular flow and according to a study performed by Ishii and Mashima [199], that shows the effect of virtual mass force is much less in the annular flow compare to its effect in slug flow, so it would reasonable to neglect the virtual mass force in the present model. Newton's Law is applied to each phase in the control volume for deriving the phasic momentum equations which can be written as,

$$\frac{d}{dz} [\rho_f u_f^2 \delta (D - \delta)] = -\frac{d}{dz} [p \delta (D - \delta)] - \tau_w D - \Gamma u_i (D - 2\delta) + \tau_i (D - 2\delta) \quad (3.8)$$

$$\frac{d}{dz} [\rho_g u_g^2 (D - 2\delta)^2] = -\frac{d}{dz} [p (D - 2\delta)^2] + 4\Gamma u_i (D - 2\delta) - 4\tau_i (D - 2\delta) \quad (3.9)$$

3.3.3. Energy Conservation Equations

By applying the first law of thermodynamic for each phase in the chosen control volume, the basic energy conservation equations for the liquid film and vapor phases are defined by Eq. (3.10) and Eq. (3.11) respectively.

$$\frac{d}{dz} \left[\rho_f u_f \delta (D - \delta) \left(h_f + \frac{u_f^2}{2} \right) \right] = q_w'' D - \Gamma h_f (D - 2\delta) + \tau_i u_i (D - 2\delta) \quad (3.10)$$

$$\frac{d}{dz} \left[\rho_g u_g (D - 2\delta)^2 \left(h_g + \frac{u_g^2}{2} \right) \right] = 4\Gamma h_g (D - 2\delta) - 4\tau_i u_i (D - 2\delta) \quad (3.11)$$

Substituting Γ in Eqs. (3.10),(3.11) by Eq. (3.6), the energy equations can be rearranged as,

$$\begin{aligned} \left[\rho_f u_f \left(h_f + \frac{u_f^2}{2} \right) - \rho_g u_g h_f \right] \frac{d\delta}{dz} + \rho_g h_f \frac{(D - 2\delta)}{4} \frac{du_g}{dz} \\ + \rho_f \left(h_f + \frac{3}{2} u_f^2 \right) \frac{\delta(D - \delta)}{D - 2\delta} \frac{du_f}{dz} = q_w'' D + \tau_i u_i \end{aligned} \quad (3.12)$$

$$(2\rho_g u_g^3) \frac{d\delta}{dz} + \frac{3}{2} \rho_g u_g^2 (D - 2\delta) \frac{du_g}{dz} = -4\tau_i u_i \quad (3.13)$$

According to Wallis [200], the liquid film thickness for the laminar annular flow is very thin compare to the channel hydraulic diameter. Thus, the shear stress variation in this boundary layer is very small and it would be reasonable to be $u_i = 2u_f$. In another approximation of the velocity at the interface, Ghiaasiaan [198] assumed that $u_i = (1/2)(u_f + u_g)$ is a reasonable assumption in stratified flow. Since the liquid film velocity is considered lower than the vapor core velocity and the tangential components of both velocities at the interface are considered to be the same, it

would be more reasonable to assume $u_i = (0.5u_g)$ for the present model simplification. Taking this assumption into account, the interfacial shear stress which has a significant effect on the liquid film thickness, can be derived from the energy equation of the vapor phase, Eq. (3.13), in terms of liquid film thickness, vapor velocity, and inertia force as follows:

$$\tau_i = \rho_g u_g^2 \frac{d\delta}{dz} - 3\rho_g u_g \frac{(D-2\delta)}{4} \frac{du_g}{dz} \quad (3.14)$$

The energy equation of the liquid film, Eq. (3.12), can be expanded more by inserting the equation of interfacial shear stress, Eq.(3.14), as follows,

$$\begin{aligned} & \left[\rho_f u_f \left(h_f + \frac{u_f^2}{2} \right) - \rho_g u_g \left(h_f + \frac{u_g^2}{2} \right) \right] \frac{d\delta}{dz} + \rho_g \left(h_f + \frac{u_f^2}{2} \right) \frac{(D-2\delta)}{4} \frac{du_g}{dz} \\ & + \left[\rho_f \frac{u_f^2}{2} + \rho_f \left(h_f + \frac{u_f^2}{2} \right) \frac{\delta(D-\delta)}{D-2\delta} \right] \frac{du_f}{dz} = q_w'' \frac{D}{D-2\delta} \end{aligned} \quad (3.15)$$

Now, considering the rate of phase change Γ , and the interfacial shear defined by Eq. (3.6), and Eq. (3.14) respectively, the momentum equations, Eqs. (3.8), (3.9), can be rearranged in the following form,

$$\begin{aligned} & \left(\rho_f u_f^2 + \frac{3}{2} \rho_g u_g^2 + p \right) \frac{d\delta}{dz} + \frac{7}{2} \rho_g u_g \frac{(D-2\delta)}{4} \frac{du_g}{dz} + 2\rho_f u_f \frac{\delta(D-\delta)}{D-2\delta} \frac{du_f}{dz} \\ & + \frac{\delta(D-\delta)}{D-2\delta} \frac{dp}{dz} = - \left(\frac{D}{D-2\delta} \right) \tau_w \end{aligned} \quad (3.16)$$

$$- \left(\frac{3}{2} \rho_g u_g^2 + p \right) \frac{d\delta}{dz} - \frac{3}{2} \rho_g u_g \frac{(D-2\delta)}{4} \frac{du_g}{dz} + \left(\frac{D-2\delta}{4} \right) \frac{dp}{dz} = 0 \quad (3.17)$$

Thus, the two-phase pressure gradient can be defined easily from the momentum equation of the vapor phase, Eq. (3.17), as,

$$\frac{dp}{dz} = \left(\frac{4}{D - 2\delta} \right) \left(\frac{3}{2} \rho_g u_g^2 + p \right) \frac{d\delta}{dz} + \frac{3}{2} \rho_g u_g \frac{du_g}{dz} \quad (3.18)$$

The wall shear stress τ_w , in the right side of the momentum equation of the liquid film, Eq. (3.16), can be represented in terms of liquid film velocity and the working fluid density as,

$$\tau_w = \frac{1}{2} \rho_f f_f u_f^2 \quad (3.19)$$

Since both laminar and turbulent flow are considered, the liquid film friction factor f_f is determined in terms of liquid film Reynolds number for better results as presented in Kim and Mudawar [201] as follows.

$$f_f = \begin{cases} (64/Re_f) & \text{for } Re_f \leq 2000 \\ 0.079 Re_f^{-0.25} & \text{for } 2000 < Re_f \leq 20,000 \\ 0.046 Re_f^{-0.20} & \text{for } 20,000 < Re_f \end{cases} \quad (3.20)$$

The friction factor estimation is mainly influenced by based-liquid film Reynolds number which is calculated in the present model using the predicted values of average liquid film thickness $\bar{\delta}$, and average liquid film velocity \bar{u}_f at every heat and mass fluxes applied as depicted in Eq. (3.21).

$$Re_f = \frac{\rho_f \bar{u}_f D_h}{\mu_f} = 4 \frac{\rho_f \bar{u}_f \bar{\delta} (D - 2\bar{\delta})}{\mu_f D} \quad (3.21)$$

In summary of the analytical part, four expanded equations represent the final form of the present model. These equations are the mass conservation equation of the whole mixture, Eq. (3.7), the energy conservation equation of the liquid film, Eq. (3.15), the momentum conservation equation of the liquid film, Eq. (3.16), and the momentum conservation equation of the vapor phase, Eq. (3.17). While the mass conservation equation, Eq. (3.5), and the energy conservation equation, Eq. (3.11), of the vapor phase are used to define the phase change rate, Γ ,

and the interfacial shear stress, τ_i , respectively . Thus, the final form of the present model equation is organized and formulated in a mass matrix form as follows:

$$AY = B \quad (3.22)$$

Where A is a square mass matrix which contains the coefficients of the dependent variables obtained by expanding the differential terms in the conservation equation. The gradient of main dependent variables is represented by the column vector Y , and the column vector B represents the non-homogeneous part of the present model. The main model equation can be rewritten in details as in Eq. (3.23).

$$\begin{bmatrix}
(\rho_g u_g - \rho_f u_f) & \left(-\frac{1}{4} \rho_g (D - 2\delta)\right) & \left(-\rho_f \frac{\delta(D - \delta)}{D - 2\delta}\right) & 0 \\
-\left(\frac{3}{2} \rho_g u_g^2 + p\right) & \left(-\frac{3}{2} \rho_g u_g \frac{D - 2\delta}{4}\right) & 0 & \left(\frac{D - 2\delta}{4}\right) \\
\left(\rho_f u_f \left(h_f + \frac{u_f^2}{2}\right) - \rho_g u_g \left(h_f - \frac{u_g^2}{2}\right)\right) & \left(\rho_g \left(h_f + \frac{u_f^2}{2}\right) \left(\frac{D - 2\delta}{4}\right)\right) & \left(\rho_f u_f^2 + \rho_f \left(h_f + \frac{3}{2} u_f^2\right) \left(\frac{\delta(D - \delta)}{D - 2\delta}\right)\right) & 0 \\
\left(p + \frac{3}{2} \rho_g u_g^2 + \rho_f u_f^2\right) & \left(\frac{7}{2} \rho_g u_g \left(\frac{D - 2\delta}{4}\right)\right) & \left(2\rho_f u_f \frac{\delta(D - \delta)}{D - 2\delta}\right) & \left(\frac{\delta(D - \delta)}{D - 2\delta}\right)
\end{bmatrix} \quad (3.23)$$

$$\times \begin{Bmatrix} \frac{d\delta}{dz} \\ \frac{du_g}{dz} \\ \frac{du_f}{dz} \\ \frac{dp}{dz} \end{Bmatrix} = \begin{bmatrix} 0 \\ 0 \\ -q_w \left(\frac{D}{D - 2\delta}\right) \\ -\tau_w \left(\frac{D}{D - 2\delta}\right) \end{bmatrix}$$

3.4. Initial and Boundary Values of the Model

In order to solve the main model equation, Eq. (3.23) the initial values of the dependent variables, δ_o , u_{go} , u_{fo} , and the inlet pressure p_o at the entrance of the micro-tube should be estimated properly. Furthermore, it should be noted that among these initial parameters, the most sensitive initial parameter that affects the obtained results is the initial liquid film thickness. There are many researchers who have investigated measuring liquid film thickness in micro-channels and revealed that, $\delta \ll D_h$, in the range of ($1.0 \leq D_h \leq 1.49$ mm) such as Hazuku et al. [126]. Based on the available literature, most of the correlations of liquid film prediction are developed based on Taylor's law (which is addressed in many two phase flow studies such as Aussilous and Quere [202]) and applicable for the flow regimes where the liquid film increases such in slug flow during the bubble coalescence or during the condensation in annular flow regime. However, two correlations for prediction of liquid film thickness, Eqs. (3.24) and (3.25) which were developed by Bretherton [63] and Irandoust and Andersson [35], may be applied properly in the annular flow regime for this model to predict the initial liquid film thickness. The Eq. (3.24) was developed analytically and its constants were obtained based on the numerical integration. On the other hand, the Eq. (3.25) was developed based on the experimental data of flow boiling in tubes with diameters ranging from 1.0 mm to 2.0 mm and length of 400 mm. Since, both of the equations were developed based on the assumption that (δ/d) is small, it would be very reasonable to be used either for the Taylor flow or the annular flow in the range of the mentioned diameters.

$$\delta_o/D = 0.67 Ca^{(2/3)} \quad (3.24)$$

$$\delta_o/D = 0.18 [1 - \exp(-3.08Ca^{0.54})] \quad (3.25)$$

Consequently, in the present model, the initial liquid film thickness is predicted using Eq. (3.24) and Eq. (3.25) for flow boiling of non-aqueous working fluids and water respectively. Furthermore, the initial vapor and film velocities at the onset of annular flow are calculated in terms of initial liquid film as follows:

$$u_{go} = (Gx_e/\rho_g)(D^2/(D - 2\delta_o)^2) \quad (3.26)$$

$$u_{fo} = (G(1 - x_e)/\rho_f)(D^2/(4\delta_o(D - \delta_o))) \quad (3.27)$$

Where x_e , is the vapor quality estimated at the exit of the micro-tube. In the present model it is calculated based on the energy balance of the micro-tube and represented as in Eq. (3.28) in terms of the heated length-to-diameter ratio for zero-inlet sub-cooling enthalpy (inlet saturated conditions).

$$x_e = 4 \frac{q_w}{Gh_{fg}} \frac{L_h}{D_h} \quad (3.28)$$

The initial value of the pressure at the inlet of the micro-tube is taken from the experimental conditions for each CHF database obtained.

3.5. Results and Discussion

The main differential equations represented in the mass matrix form by Eq. (3.23) are solved numerically. The procedure of the main calculations is explained by the flow chart shown in Figure 3-2. In order to test the model ability for CHF prediction, it was compared with various experimental CHF data points obtained previously from different resources for wide operating conditions for flow boiling in single and multi mini/micro-channels, as summarized in Table (3.3). For this validation, the mean absolute error (MAE) is defined as,

$$MAE = \frac{1}{N} \sum \frac{|q_{c_{exp}}'' - q_{c_{pred}}''|}{q_{c_{exp}}''} \times 100 \% \quad (3.29)$$

Where N is the number of the data points, $q_{c_{exp}}''$ is the measured value of the critical heat flux and $q_{c_{pred}}''$ is the predicted value of the critical heat flux.

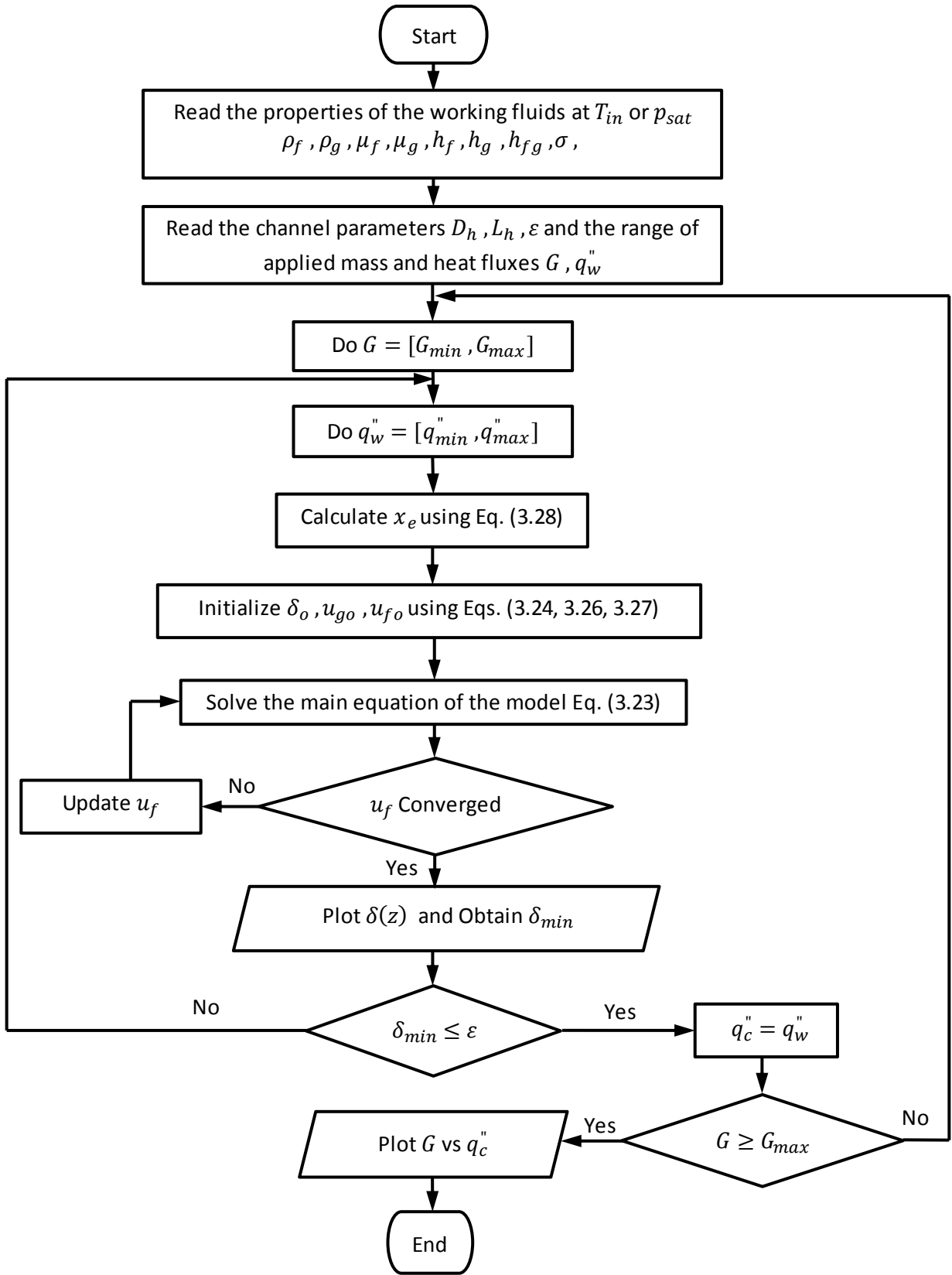


Figure 3-2: Flow chart shows the procedure of calculations for the present model

Table (3-3): Saturated CHF data of flow boiling in mini/micro- channels used to test the present model.

| Author | Geometry | Fluid & Operating conditions |
|------------------------|--|---|
| Qu and Mudawar [43] | 21 Rectangular micro-channels $215 \times 821 \mu\text{m}$, $D_h = 0.38 \text{ mm}$, $L/D = 117.7$ | Water, $p_{\text{out}} = 1.13 \text{ bar}$, $T_{\text{in}} = 60^\circ\text{C}$, $G = [86 - 368] \text{ kg/m}^2 \cdot \text{s}$, |
| Wojtan et al. [45] | single micro-tube, $D_h = [0.5 - 0.8] \text{ mm}$, $L_h = 70 \text{ mm}$ | R-134a, $T_{\text{sat}} = [30 - 35]^\circ\text{C}$, $G = [400 - 1600] \text{ kg/m}^2 \cdot \text{s}$, $q_w'' = [3.2 - 600] \text{ kW/m}^2$, |
| Qi et al. [46] | single micro-tube, $D_h = [0.531 - 0.834] \text{ mm}$, $L_h = 250 \text{ mm}$ | LN2, $T_{\text{in}} = [78.2 - 79.8] \text{ K}$, $G = [700 - 3000] \text{ kg/m}^2 \cdot \text{s}$, $q_w'' = [50.9 - 213.9] \text{ kW/m}^2$, |
| Roday and Jensen [138] | Single steel micro-tube, $D_h = [0.286 - 0.70] \text{ mm}$, $L_h = [21.66 - 96.0] \text{ mm}$ | Water, $\Delta T_{\text{sat}} = [40 - 60]^\circ\text{C}$ $p_{\text{out}} = [25.3 - 179] \text{ kPa}$, $G = [320 - 560] \text{ kg/m}^2 \cdot \text{s}$, |
| Ong & Thome [139] | $D_h = [1.03, 2.20, 3.04] \text{ mm}$ $L_h = [180, 396, 540] \text{ mm}$ | R134a , R236fa, R245fa $G = [100 - 1500] \text{ kg/m}^2 \cdot \text{s}$ |

Figure 3-3 shows a comparison of the CHF data for flow boiling of Water flowing in rectangular multiple micro-channels obtained by Qu and Mudawar [43] and those predicted by the present model. The present model predicted the whole CHF data of the water with a $MAE = 35.75 \%$. It can be seen that the model underestimated all the CHF data of Qu and Mudawar [43]. This underestimation is due to some reasons. Since the present model was developed based on dominant annular flow pattern in a single micro-tube, the major reason of the underestimation is

related to the difference in the flow characteristics and configuration between the single and multi-micro-channels. In addition, the deviation is partially attributed to the applicability of the correlation used to estimate the initial liquid film thickness of the water, Eq. (3.25), which was originally developed for boiling in a single tube with diameter range of (1.0 to 2.0 mm), while Qu and Mudawar [43] data were for flow boiling in multiple micro-channels. From Figure 3-3, it is seen that at low mass flux, $100 \leq G \leq 130 \text{ kg/m}^2.\text{s}$, the CHF predicted by the model does not show a clear influence by increasing the mass flux. At this low range of mass flux, it is seen that a little increase in the applied heat flux causes in decreasing in the liquid film thickness lower than the critical value, which is identified to be ($\delta_{\text{crit}} \leq 3\mu\text{m}$) in the present model. Furthermore, this can be considered as the lowest mass flux among the tested CHF data where the present model can predict the CHF data of flow boiling of the water in multiple micro-channels.

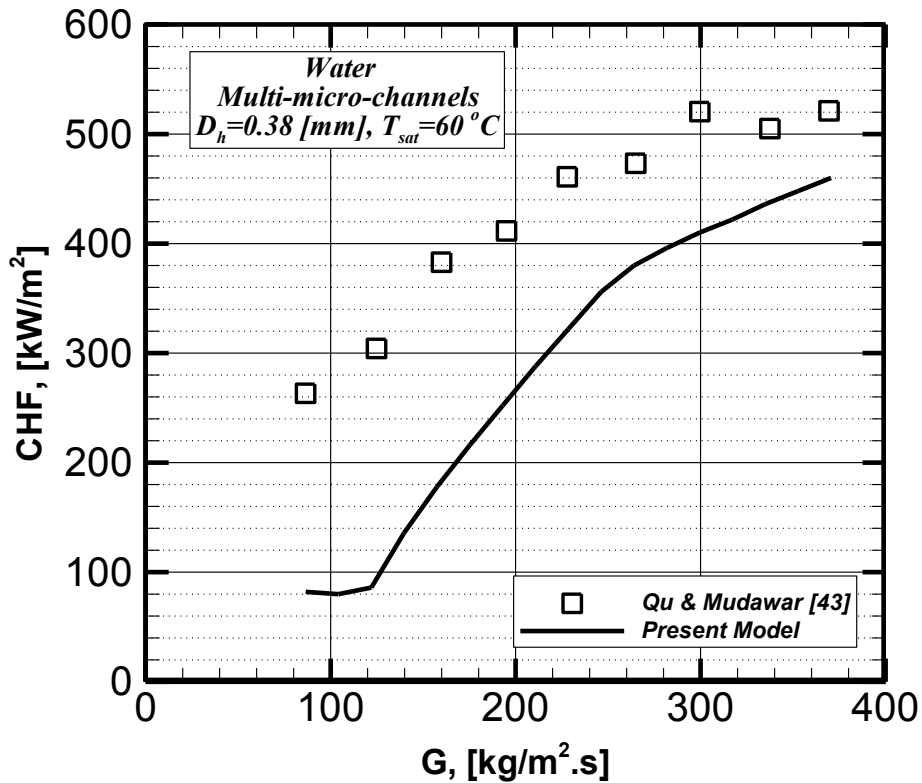


Figure 3-3: Comparison of the Present CHF model with CHF data obtained by Qu and Mudawar [43] for flow boiling of Water in multiple channels heat sink.

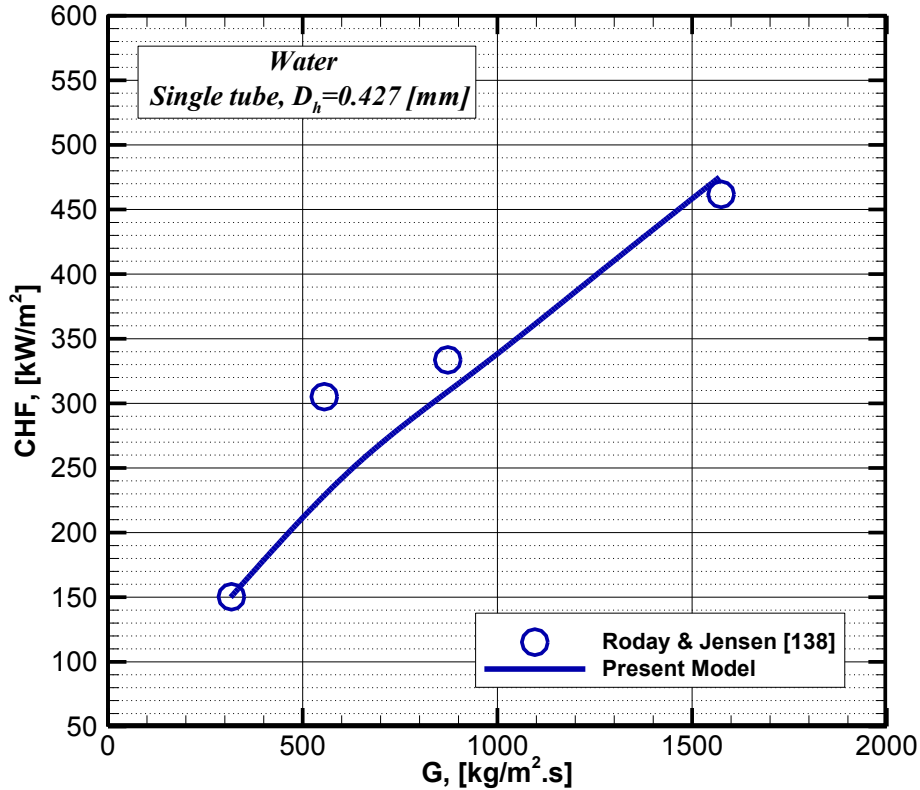


Figure 3-4: Comparison of the Present CHF model with CHF data obtained by Roday and Jensen [138] for flow boiling of Water in a single micro-tube with diameter of 0.427 mm.

For the same working fluid, water, but through a single micro-tube with internal diameter of 0.427 mm and at very high mass flux, the model was compared with the CHF data of Roday and Jensen [138] as depicted in Figure 3-4. A strong relationship between the CHF and mass flux can be seen here as well. It can be noted that the present model predicted well the CHF data a MAE = 8.76 %. Further parameters that affect the CHF have been considered for validating the present model, such as the working fluid and channel size effects. For instance, the model was compared with the experimental CHF data of Wojtan et. al. [45] for flow boiling of R134a through single micro-tubes with sizes of 0.5 mm and 0.8 mm as shown in Figure 3-5. The model fairly predicted the CHF data of diameter 0.5 mm with the MAE = 7.57%. Furthermore, the CHF data for R134a in the micro-tube of 0.8 mm were predicted properly as well with the MAE = 9.10%. Moreover, the influence of tube size can be noted clearly from this figure where the CHF increases by increasing the channel size.

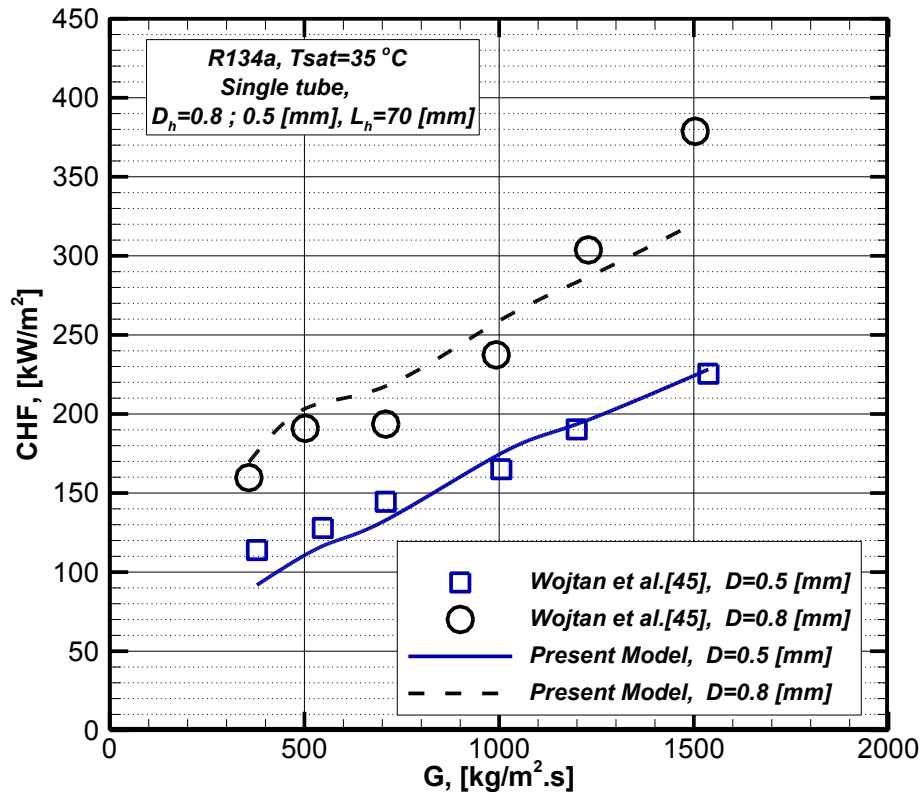


Figure 3-5: Comparison of the Present CHF model with CHF data of Wojtan et al. [45] for flow boiling of R134a in a single micro-tube for internal diameters 0.50 mm and 0.80 mm.

Additionally, in order to validate the present model for predicting the CHF for macro and conventional channels, it has been compared with the CHF experimental data of Ong & Thome [139] for saturated flow boiling of R134a in single tubes with sizes of 1.03mm, 2.02 mm, and 3.04 mm at low and high mass fluxes as shown in Figure 3-6. As can be seen the influence of mass flux and the channel size on the CHF is obvious in this graph. Although, for the mass fluxes $G \leq 500$ kg/m².s, the experimental data showed the independency of CHF of the channel size for all channel sizes, 1.03; 2.20; and 3.04 mm, while the present model showed a clear dependency on the channel size particularly for 2.02 mm and 3.04 mm tubes. In general, the model gives a very good agreement with these CHF data points for the three different tube sizes with MAE = 11.91%. According to the diabatic flow pattern map developed by Revellin and

Thome [75], it is seen that the experimental data of R134a in the range of mass fluxes ($320 \leq G \leq 560 \text{ kg/m}^2 \cdot \text{s}$) fall in the annular flow regime.

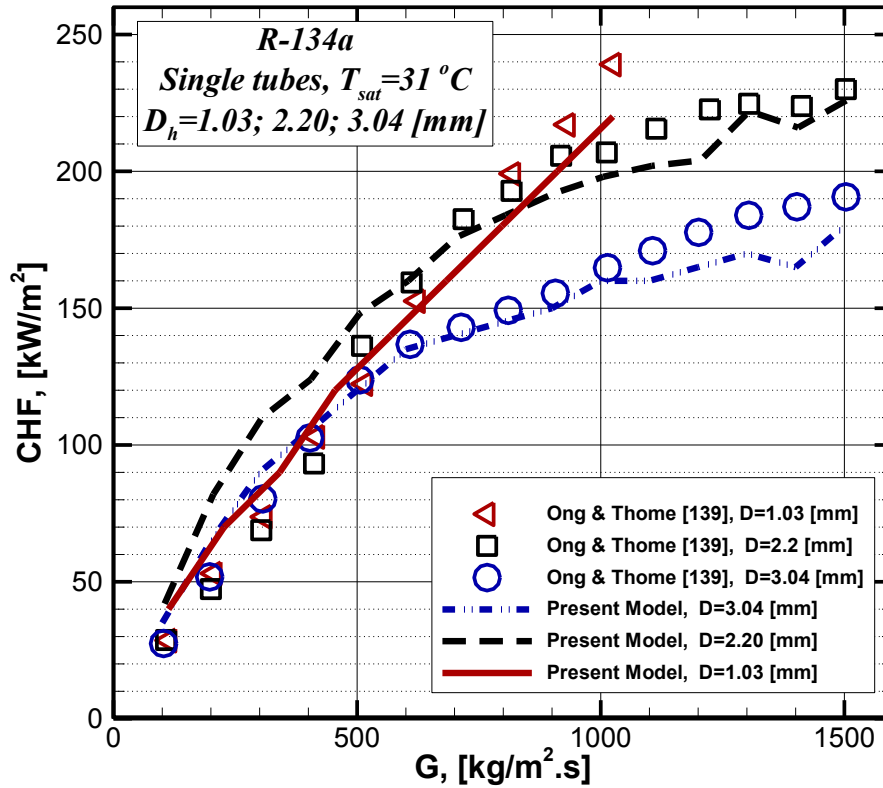


Figure 3-6: Comparison of the Present CHF model with CHF data of Ong & Thome [139] for flow boiling of R134a in a single micro-tube for internal diameters 1.03, 2.20, and 3.04 mm.

Figure 3-7, shows a comparison of the experimental CHF data of Fan and Hassan [6] for flow boiling of the dielectric fluid FC-72 in a single micro-tube of 0.889 mm with the present model. Notably, the CHF increases linearly by increasing the mass flux. Although, the CHF trend was predicted well, the model under predicted the experimental CHF data, and the MAE = 24.44%.

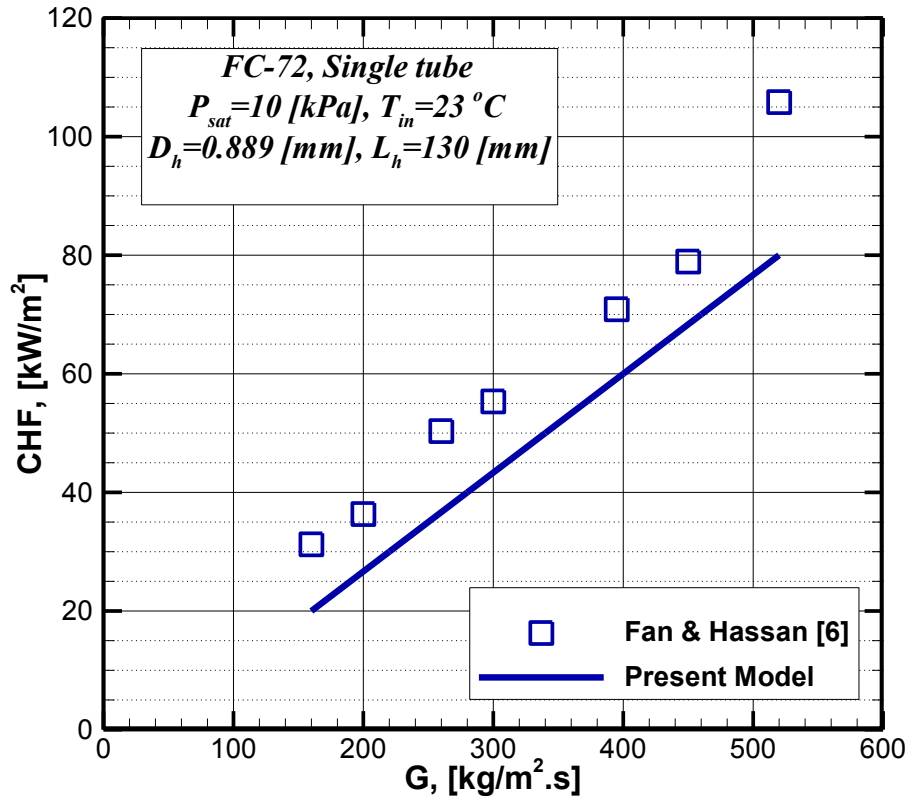


Figure 3-7: Comparison of the Present CHF model with CHF data of Fan & Hassan [6] for flow boiling of FC-72 in a single micro-tube with an internal diameter of 0.889 mm.

Further comparisons to the CHF experimental data have been performed. The present model was compared with the CHF data obtained by Qi et al. [46] for flow boiling of Liquid Nitrogen in single mini and micro-tubes with internal diameters of 0.531, 0.834, 1.042, and 1.931 mm as shown in Figure 3-8. It can be seen that the model underestimated the experimental data points at mass fluxes lower than $G \leq 1000$ [kg/m².s], particularly for those with diameters larger than 0.834 mm. This can be speculated to neglecting the gravity force effects in the basic model equations, where this force has a significant effect in conventional channels. One more reason for this deviation can be related to the flow boiling characteristics of the LN2 which are quite different of the low pressure refrigerants and water. In other words, the correlation used for predicting the initial liquid film was developed based on water-air experimental data and there is a much difference in the properties of the water and the LN2, particularly in the surface tension

and vapor density values. In general, the model predicted all CHF data points of LN2 with a MAE = 27.85%.

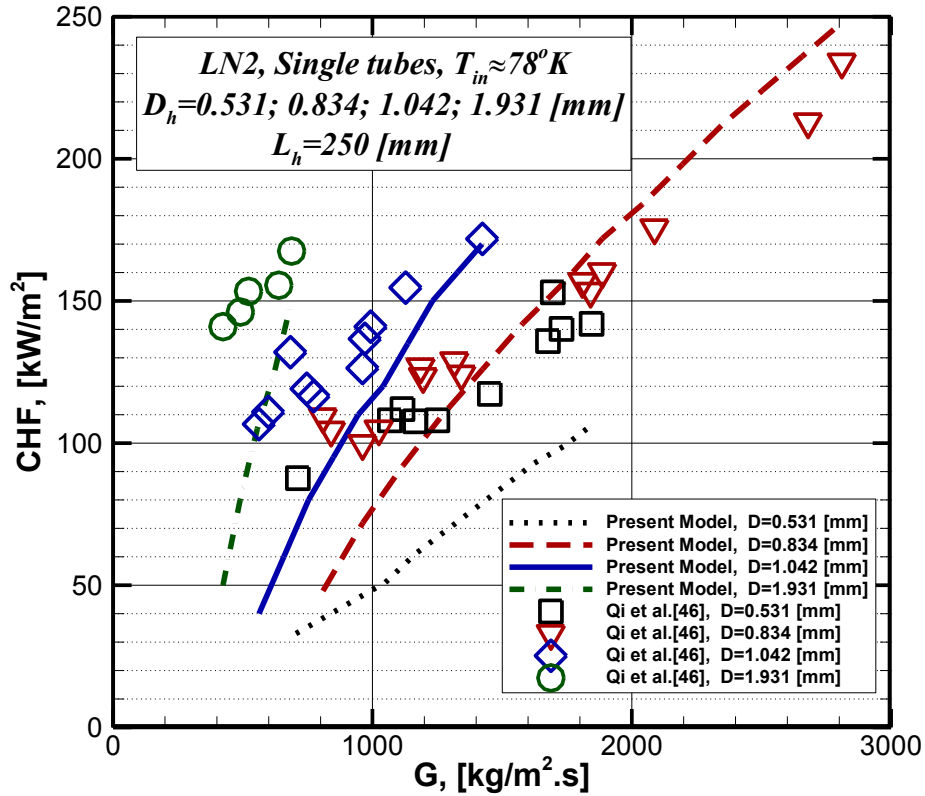


Figure 3-8: Comparison of the Present CHF model with CHF data of Qi et al. [46] for flow boiling of LN2 in mini and micro-tubes with internal diameters 0.531, 0.834, 1.042, and 1.931 mm.

In general, all CHF data points collected in this work including those for multiple mini and micro-channels were predicted successfully by the present model with MAE = 19.81% as shown in Figure 3-9. Furthermore, three saturated flow boiling CHF correlations, Wojtan et al. [45], Qi et al. [46], and Ong and Thome [139] were assessed to predict the same collected experimental CHF data base. The reason for choosing these three correlations is because they were developed originally for flow boiling in a single circular mini/micro channels and based on more than 80 % of the collected CHF data used in this work.

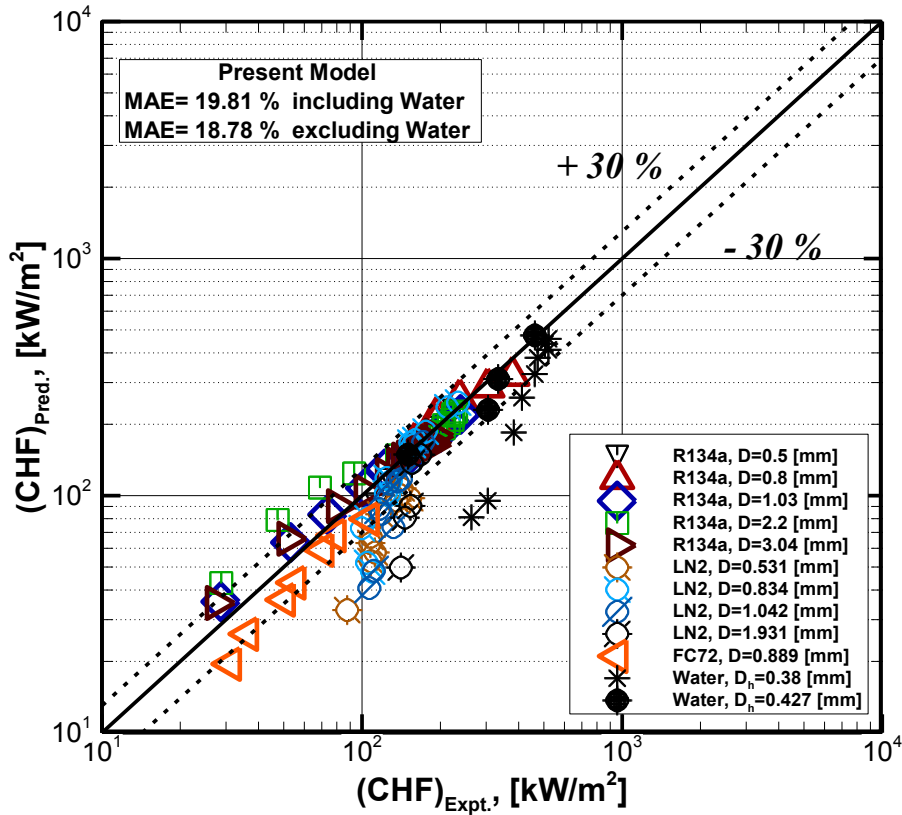


Figure 3-9: Comparison of experimental CHF data for flow boiling of R134a, LN2, FC72, and water in mini and micro-channels with that predicted by the present CHF model.

Figure 3-10 compares the saturated CHF data predicted by Wojtan et al. [45] correlation with those collected in this work for flow boiling of non-aqueous working fluids and water. The correlation predicted the all collected CHF data points with a MAE = 75.26% and only for non-aqueous working fluids with a MAE = 29.98%. The overestimation of CHF data of water may be speculated to the fact that this correlation was developed based on CHF data of non-aqueous working fluid.

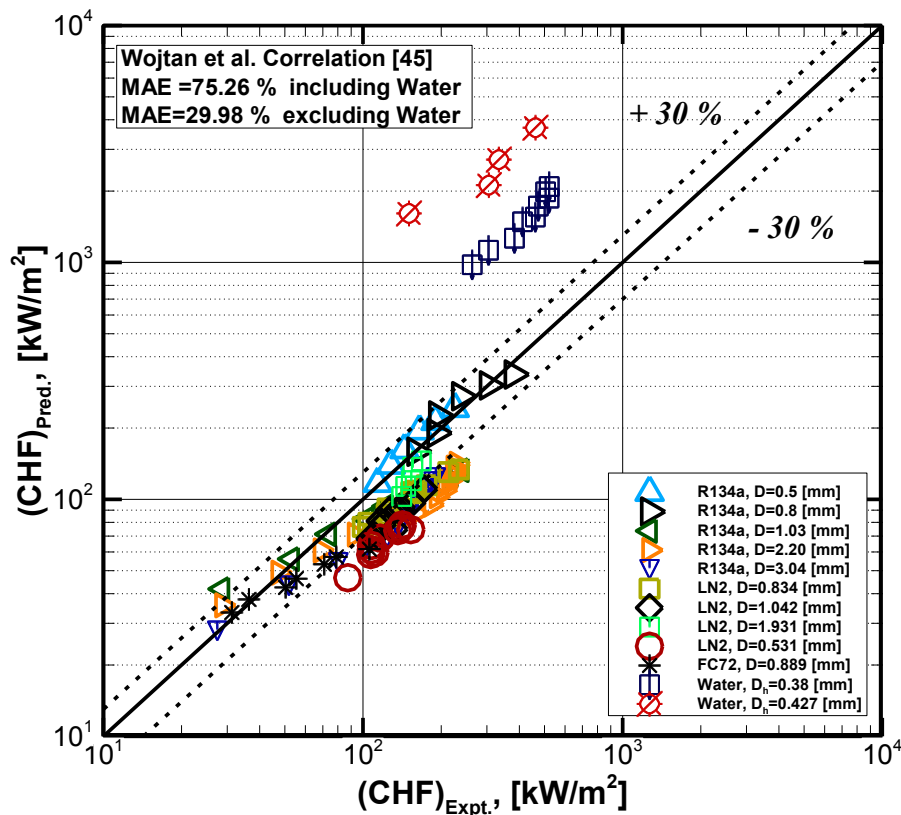


Figure 3-10: Comparison of experimental CHF data for flow boiling of R134a, LN2, FC72, and water in mini and micro-channels with that predicted the CHF correlation of Wojtan et al. [45].

The CHF correlation of Ong and Thome [139] was developed based the experimental data Wojtan et al. [45] for flow boiling of R-134a and R-245fa in single micro-tube with diameters (0.50 mm and 0.80 mm), and the data of Park and Thome [203] for flow boiling of low refrigerants (R134a, R236fa, R245fa) in multiple-micro-channels with the range of hydraulic diameter of (0.35mm to 0.88 mm), and their data for the flow boiling of the same refrigerant in single micro-tubes with diameters (1.03, 2.20, 3.04 mm). The ability of the CHF correlation proposed by Ong and Thome [139] to predict the collected saturated CHF data is shown in Figure 3-11. The correlation predicted the all CHF data with the MAE = 64.36%. It is seen that this correlation significantly over estimated the saturated CHF data of the Water and under estimated those for FC-72. The explanation for the large deviation of CHF data of the Water can be attributed to the CHF of the Water which is originally were obtained for two different

conditions as can be seen in Table (3.3) for both single and multiple mini and micro rectangular-channels. Although this correlation was developed considering the effect of working fluid on the CHF, but that was limited to non-aqueous fluids and only low pressure refrigerants. Thus, the big deviation obtained in predicting the Water CHF, can be related to the big difference between the properties of the water and the other refrigerants, particularly, the difference in surface tension and vapor densities. Furthermore, the inlet pressure of the CHF data of Qu and Mudawar [43] is lower than those of Ong and Thome [139], and according to Bao et al. [21], a strong effect of inlet pressure on the heat transfer characteristics of flow boiling in micro-channels has been observed. On the other hand, the correlation of Ong and Thome [139] predicted the CHF data for the non-aqueous working fluids with a good agreement with the saturated CHF experimental data with a MAE = 18.39%.

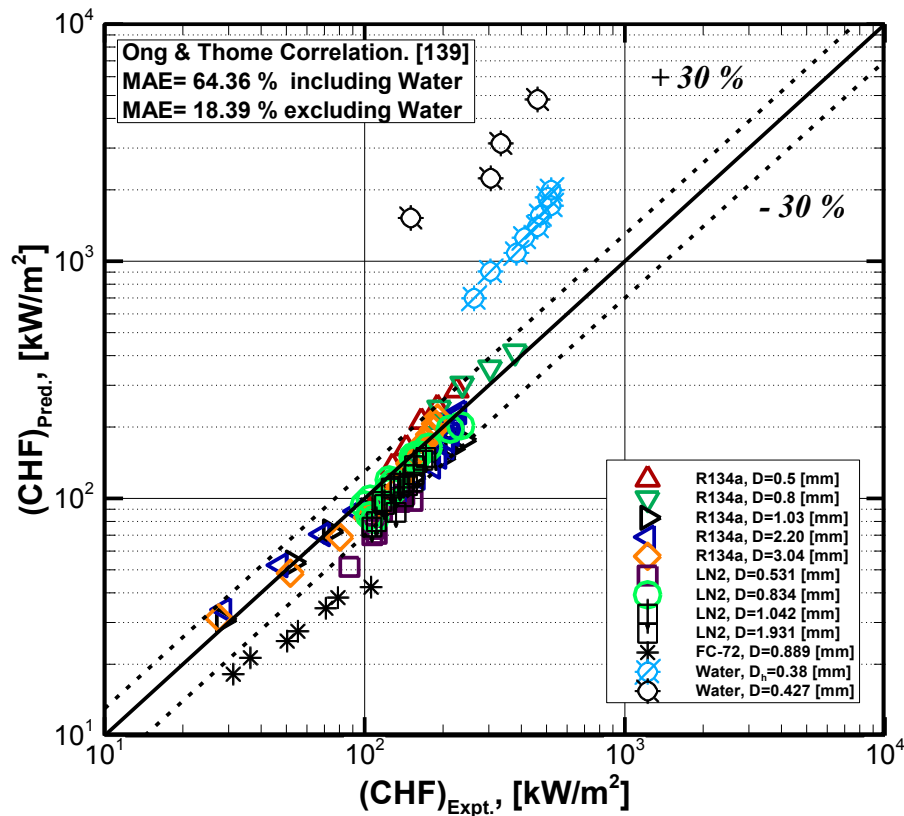


Figure 3-11: Comparison of experimental CHF data for flow boiling of R134a, LN2, FC72, and water in mini and micro-channels with that predicted by Ong & Thome [139] Correlation.

The last saturated CHF correlation was assessed is the correlation that was developed by Qi et al. [46] as shown in Figure 3-12. It can be seen that the correlation greatly over predicted the experimental CHF data of the Water and overestimated all of those obtained by Wojtan et al. [45] for flow boiling of R134a as well as most of those for FC-72. Generally, the correlation predicted the collected CHF data excluding those for the water with the MAE = 40.78 %.

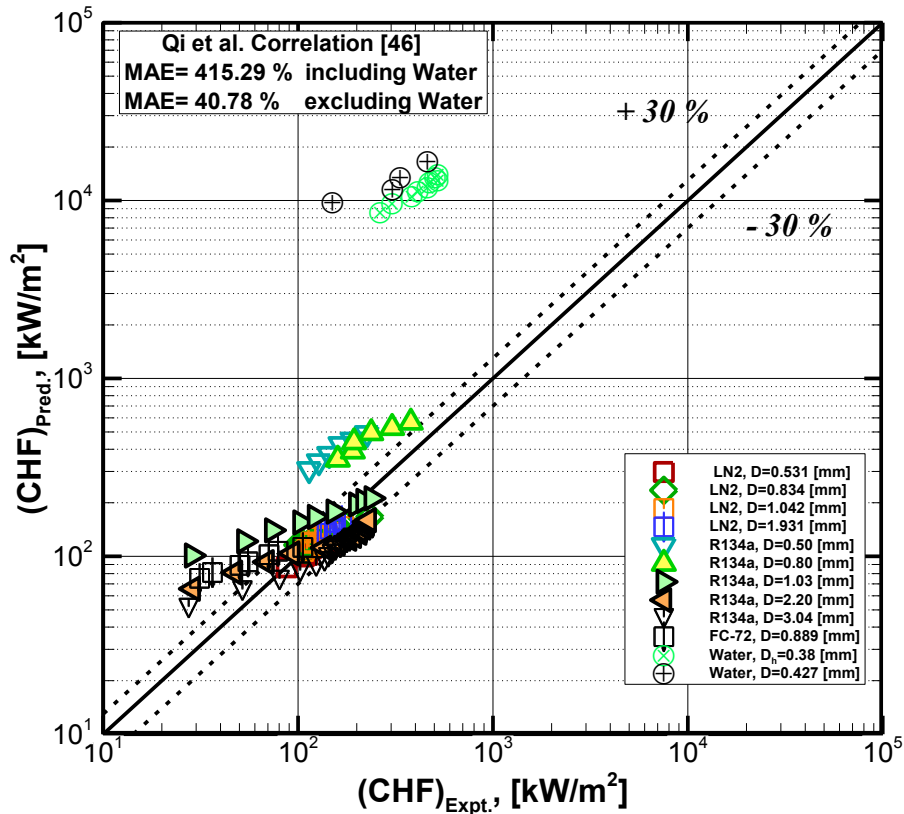


Figure 3-12: Comparison of experimental CHF data for flow boiling of R134a, LN2, FC72, and water in mini and micro-channels with that predicted the CHF correlation of Qi et al. [46].

Critical exit vapor quality is one of the interesting parameters which can be employed to present the current obtained results of the CHF in other form, and may be used in future work to investigate the CHF in micro-channels. It is defined as the vapor quality of the working fluid at the exit of the micro-tube when the CHF occurs. Figure 3-13, depicted the variation of the CHF data of Wojtan et al. [45] in terms of the critical exit vapor quality of the flow boiling of the working fluid, R134a, and showed the comparison with those predicted by the present model. It

is seen that the CHF decreases as the critical vapor quality increases. The present model predicted well the trend of the CHF in terms of critical vapor quality.

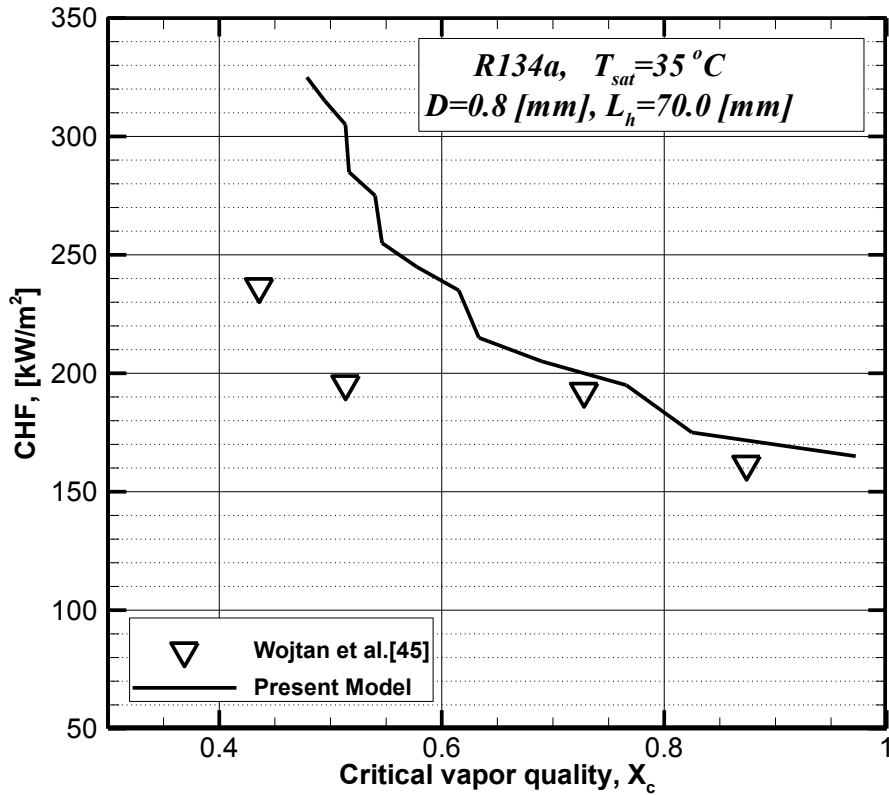


Figure 3-13: CHF versus critical vapor quality predicted by the present model for flow boiling of R134a through a 0.8mm inner diameter micro-tube, and compared with those measured by Wojtan et al. [45].

In summary, for the CHF data of non-aqueous working fluids, it can be seen that among the chosen saturated CHF correlations developed for flow boiling in single micro-channels, the correlation of Ong and Thome [139] predicts the collected CHF data of non-aqueous working fluids better than the other tested correlations in this work. However, when the CHF data of the Water is included, the present model has ability to predict the saturated CHF better than the other tested correlations.

3.6. Conclusions

An analytical heat transfer model of flow boiling in horizontal micro-channels for an annular flow subjected to uniform heat flux was developed in order to predict the saturated critical heat flux (CHF) based on the liquid film dry-out. The model was developed by applying the separated flow model for a control volume in annular flow regime. The main dependent variables of the present model are the liquid film thickness, the core vapor velocity, the liquid film velocity, and the pressure variation. The effects of operating conditions, channel sizes, and working fluid on the CHF have been investigated. The final form of the present model is represented in a mass matrix form. The model was compared with the saturated CHF data points collected for flow boiling of various working fluids, (Water, LN₂, FC-72, and R134a) in single and multiple mini and micro-channels with hydraulic diameter ranges of ($0.38 \leq D_h \leq 3.04$ mm) and heated-length to diameter ratios in the range of $117.7 \leq L_h/D \leq 470$. The model successfully predicted all experimental CHF data with the MAE= 19.81 %. Further validation of the present model has been done by assessing three saturated CHF correlations developed based on more than 80 % of the collected CHF data. Among the chosen CHF correlations, the correlation of Ong and Thome [139] showed a good ability to predict saturated CHF data for non-aqueous working fluids better than the other correlations. However, the chosen correlations significantly over predict the saturated CHF data of the water in single circular micro-channel and rectangular multiple channel heat sinks. On the other hand, the present model is able to fairly predicted saturated CHF data for flow boiling of aqueous and non-aqueous working fluids in single/multiple and mini/micro channels with a mean absolute error better than the tested correlations.

Chapter 4

4. A Semi-Analytical Model of Heat Transfer and Pressure Drop in Annular Flow Regime for Flow Boiling in a Micro-Tube at Uniform Heat Flux

Amen Younes¹, Ibrahim Hassan^{1,2}, Lyes Kadem¹

This paper was submitted to *J. of Heat Transfer*, and is still under review

¹Department of Mechanical and Industrial Engineering, Concordia University,

1455 de Maisonneuve Blvd. W, Montreal, QC, Canada, H3G 1M8

² Mechanical Engineering Department, Texas A&M University at Qatar

P O Box 23874, Doha, Qatar

4.1. Abstract

A semi-analytical model for predicting heat transfer and pressure drop in annular flow regime for saturated flow boiling in a horizontal micro-tube at a uniform heat flux has been developed based on one-dimensional separated flow model. The six main parameters considered are vapor velocity, liquid film velocity, vapor void fraction, local pressure, vapor enthalpy, and liquid enthalpy. Liquid film evaporation is considered as the dominant heat transfer mechanism in the annular flow regime. Based on Taylor's law, the initial value of the liquid film thickness at the onset of annular flow is estimated by employing the proper correlations available in literature. The main model equations obtained are non-homogeneous differential equations which have been solved numerically based on explicit Runge-Kutta method. More than 600 two-phase heat transfer, 498 two-phase pressure drop, and 153 void fraction experimental data points for annular flow regime have been collected from the literature for validating the present model. The collected data were recorded for various working fluids, R134a, R1234ze, R236fa, R410a, R113, and CO2 for round macro and micro single horizontal tubes with a range of inner diameter of $0.244 \text{ mm} \leq D_h \leq 3.1 \text{ mm}$, a heated length to diameter ratio of $90 \leq (L_h/D_h) \leq 2000$, a range of saturation temperature of $-10 \leq T_{sat} \leq +50 \text{ }^\circ\text{C}$, and liquid to vapor density ratios in the range $6.4 \leq (\rho_f/\rho_g) \leq 188$. The model was tested for laminar and turbulent flow boiling conditions corresponding to an equivalent Reynolds number, $1,900 \leq Re_{eq} \leq 48,000$, and a range of confinement number of $0.27 \leq C_{conf} \leq 3.4$. In the scope of annular flow regime, the present model predicted the collected data of the heat transfer, pressure drop, and void fraction with a mean absolute error (MAE) of 18.14 %, MAE of 23.02 %, MAE of 3.22 %, respectively.

Keywords: *saturated flow boiling heat transfer, two-phase frictional pressure drop, annular flow regime, flow pattern maps, liquid film thickness, equivalent Reynolds number, and Bland-Altman Plot.*

4.2. Introduction

Two-phase micro-channels are widely used and have many applications, extensively in heat sinks and compact heat exchangers. Typically, the main principle of micro-channel heat sinks is to dissipate a high heat flux at a lower mass flux. Additionally, predicting heat transfer coefficient and two phase pressure drop of flow boiling in micro-channels is one of the most important steps for designing micro-channel heat sinks. Furthermore, it has been reported in the literature that the channel size influences the applicability of the developed correlations or models. Therefore, the proposed correlations of two-phase frictional pressure drop prediction for large tubes are not applicable for small and mini-channel as has been proven in many previous studies (e.g. Tran et al [164]). There are several experimental investigations of two-phase heat transfer and pressure drop in micro-channels that have been reported recently for various working fluids and wide range of operating flow conditions. Some of them were performed for horizontal micro-channels at adiabatic flow conditions such as those presented by Cavallini et al. [204], Zhang et al. [34], Yun et al. [205], Basu et al. [157], Oh et al. [156], Ali et al. [206], Mahmoud and Karayiannis [207], and Ducoulombier et al. [61], and few experiments were performed at diabatic flow conditions, as those presented by Tibiriçá et al. [176], Yan and Lin [149] , and Wu et al. [177]. Furthermore, there are some experiments that were performed for vertical tubes such as the one reported by Maqbool et al. [179]. Some of the previous experimental investigations for predicting heat transfer and pressure drop of flow boiling in micro-channels have resulted in either predicting empirical parameters for developing/modifying some existing correlations or adding more experimental data points for flow boiling in mini-micro channels. However, most of the available correlations and approaches are either applicable only for a specific flow pattern or a limited range of working fluids and operating conditions, or are too poor in scope to predict the experimental data correctly.

On the other hand, a few analytical models of flow boiling heat transfer and pressure drop in micro-channels have been presented in the literature (e.g. Moriyama and Inoue [147] , LaClair and Mudawar [208], Na and Chung [209], Das et al. [210], Jacobi and Thome [114], Thome et al. [151]). The heat transfer model of an elongated bubble in slug flow regime in micro channels was proposed by Jacobi and Thome [114], and is reported to be good for predicting local heat

transfer coefficient for the elongated bubble/liquid slug pair regime in a circular micro channel. The three-zone flow boiling model that was developed by Thome et al. [151] contains three empirical parameters which are difficult to estimate theoretically. These parameters are minimum liquid film thickness that is acceptable at dry-out (δ_{\min}) initial value of the liquid film thickness (δ_o) and bubble frequency.

Heat transfer mechanisms for flow boiling in micro-channels play an important role in developing more realistic flow boiling models. Many researchers, (e.g. Kew and Cornwell [67], Bao et al. [21], Yen et al. [112], and Kandlikar [60]) have reported that dominant heat transfer mechanisms for boiling in small-and micro-channels are flow pattern dependent. Furthermore, the dominant heat transfer mechanism is affected by channel size as it has been studied by Park and Hrnjak [167]. Park and Hrnjak [167] found that nucleate boiling heat transfer is dominant in the conventional tube with 6.1 mm inner diameter, whereas convective boiling heat transfer becomes dominant as the tube diameter decreases. Moreover, it has been noted that due to the difference of the properties of the working fluids, channel size, as well as the operating conditions, different flow patterns can be observed. According to some other investigators (e.g. Lee and Lee [22], Qu and Mudawar [43], and Thome and Consolini [116]), it has been established that at intermediate and high vapor quality, where the annular flow pattern is usually observed (e.g. Tran et al. [164]), the evaporation of liquid film is the dominant heat transfer mechanism. Additionally, the forces acting at the liquid-vapor interface of the annular flow regime influence the heat transfer mechanism of flow boiling in micro-channels. Kandlikar [60] studied and analyzed the significance of various forces that are important during rapid evaporation at high heat flux conditions and also influence the liquid-vapor interface in micro-channels. Additionally, It has been well known that the surface tension σ effects are dominant in micro-channels of circular geometry but, the author has found that unexpectedly, rather viscous forces effects are more important here than surface tension for flow boiling in micro-channels.

Annular flow pattern is promised to be one of the main dominant flow patterns for flow boiling in micro-channels as it has been verified in many previous studies (e.g. Jiang et al. [195], Celata et al. [211], Thome [212], Revellin and Thome [75], Cioncolini and Thome [213]). Moreover, the ability to identify the flow pattern and its boundaries is an essential capability for developing a suitable heat transfer coefficient and pressure-drop prediction method.

Consequently, several researchers have developed flow pattern maps for flow boiling in micro-channels. More prominent reported works are: Kandlikar [72] , Garimella et al. [79], Wu and Cheng [214], Revellin and Thome [75] , Saisorn and Wongwises [80], Karayiannis et al. [81], and Harirchian and Garimella [66] [158]. Furthermore, having a comprehensive flow pattern map helps in developing a generalized flow boiling model for the basic flow patterns in micro-channels. For instance, Harirchian and Garimella [66] established a flow pattern map for a wide range of channel size and experimental operating conditions for FC – 77 and recently, Harirchian and Garimella [158] developed a flow regime-based model of heat transfer and pressure drop for flow boiling in micro-channels based on their comprehensive flow regime map.

However, several of these flow pattern maps were established for adiabatic flow database. Thome and El Hajal [86] have developed a two-phase flow pattern map, proposed by Zürcher et al. [31], which was able to predict fairly well the two-phase flow regimes of seven different refrigerants. Recently, Revellin and Thome [75] developed a new diabatic flow pattern map for flow boiling of R134a in single micro-tubes applicable for the range of tested working conditions. In 2008, Cheng et al. [103] developed a flow pattern map for flow boiling of CO₂ in small and mini-tubes which was proven to be applicable for a wide range of operating conditions. Thus, the two flow pattern maps presented by Revellin and Thome [75], and Cheng et al. [103] have been used in this work for predicting two-phase flow regimes of flow boiling of R134a and CO₂ respectively in macro/micro horizontal channels. In the meantime, a systematic process for determining the flow pattern transition criterion is still not clear and/or available. However, there are some correlations developed for predicting the transition line, $x_{CB/A}$ for transition from coalescence flow pattern to annular flow pattern, (the onset of annular flow), in single horizontal channels. For instance, those proposed by Thome and El Hajal [86], Revellin and Thome [75], and Ong and Thome [97]. Recently, Ong and Thome [97] modified the correlation of the transition line $x_{CB/A}$, presented by Revellin and Thome [75], so they can be made applicable to three working fluids (R134a, R236fa, and R245fa) and wider range of channel sizes and operating conditions. The correlation modified by Ong and Thome [97] that has been reported and are described as follows:

$$x_{CB/A} = \left(\frac{P_r}{P_{sat}(R134a)} \right)^{0.45} Re_{lo}^{1.47} We_{lo}^{-1.23} \quad (4.1)$$

Where P_r , and P_{sat} are the reduced and saturated pressures, respectively. Re_{l0} is the Reynolds number of the liquid phase, and We_{l0} is the Weber number of the liquid phase. Harirchian and Garimella [158] developed a flow regime map for flow boiling of FC-72 in multiple micro-channel heatsinks, and proposed a correlation for estimating the position of the transition from slug flow to annular flow along the micro-channels as follow:

$$L_{ao} = 96.65(Bo^{0.5}Re)^{-0.258} Bl^{-1} \frac{\rho_g}{\rho_f - \rho_g} D_{hH} \quad (4.2)$$

Where L_{ao} , is the onset of annular flow, Bo is the Bond number, Bl is the Boiling number, and D_{hH} is the hydraulic diameter based on the heated perimeter.

Two-phase frictional pressure drop for flow boiling in micro-channels has been investigated by many researchers. Revellin and Thome [3], and Cioncolini et al [172] proposed and developed new correlations for predicting the two-phase frictional pressure drop. According to some existing flow pattern maps, there are few phenomenological models that have been developed for two-phase pressure drop prediction in annular flow regime. For instance, the model proposed by Cheng et al. [103] based on the boundaries of annular flow regime. The two-phase pressure drop data, Δp_A , of the annular flow was correlated and given by Eq. (4.3) as follow,

$$\Delta p_A = 4f_A \frac{L}{D_{eq}} \frac{\rho_g u_g^2}{2} \quad (4.3)$$

Where D_{eq} is the equivalent diameter which is defined as $D_{eq} = \sqrt{4A/\pi}$, and f_A is the friction factor coefficient of annular flow which is expressed by Eq. (4.4) as follows:

$$f_A = 3.128 Re_g^{-0.454} We_f^{-0.0308} \quad (4.4)$$

Where Re_g is Reynolds number of the vapor phase, and We_f is Weber number of the liquid film.

In summary, the evidence from this review of previous works show that most of the investigations conducted for predicting two-phase heat transfer and pressure drop for flow boiling in micro-channels are experimental investigations that presented either empirical correlations, or semi-analytical models which are applicable for a specific working fluid, or a

certain flow pattern, or operating working condition. In contrast, only few analytical models for flow boiling in horizontal micro-channels have been developed. Furthermore, it has been known that developing an analytical model based on the physical phenomenon of the flow boiling feature is an effective and essential first step for designing flow boiling micro-channels. Therefore, development of analytical models for flow boiling in micro-channels, which can be applicable for wider range of operating conditions and fluids is needed. Consequently, the aim of this work is to develop a one dimensional semi-analytical model for predicting the saturated two-phase heat transfer coefficient, frictional pressure drop, and void fraction for the annular flow regime for saturated flow boiling in a horizontal micro-channel subjected to a uniform heat flux.

4.3. Modeling Methodology

A physical description of the two-phase annular flow model is shown in Figure 4-1. As can be seen, the annular flow consists of two continuous phases, the vapor core which flows with an average vapor velocity, u_g , and the liquid film phase, whose thickness is $\delta(z)$, which moves with an average liquid film velocity, u_f , in the axial direction, z , of the working fluid flow. The micro-tube is subjected to a uniform heat flux, q_w'' . Furthermore, the applied heat flux is transferred through the micro-tube wall to the liquid film. While, the evaporation of the liquid film is considered to be the dominant heat transfer mechanism in the annular flow regime.

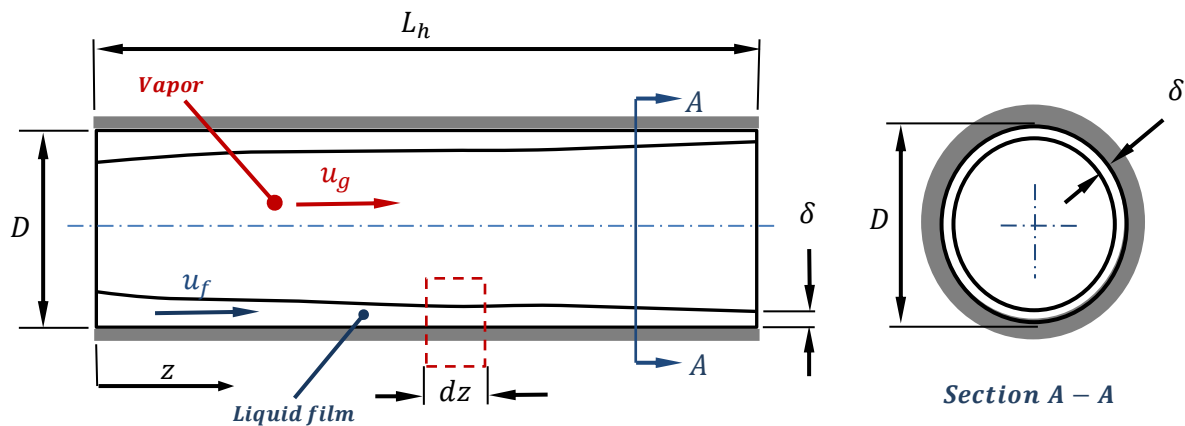


Figure 4-1: Sketch of an annular flow model in horizontal circular channel.

4.3.1. Basic Assumptions:

Two-phase annular flow is still a complex flow and has many challenges in modeling its real features. Thus, for model simplification, the following assumptions have been taken into account:

4. The flow boiling is considered as a one dimensional steady state and fully developed flow. Thus, the dependent variables adopted vary only in axial flow direction.
5. The dominant flow pattern for flow boiling in micro-tubes at intermediate and high vapor quality is the annular flow, and the dominant heat transfer mechanism in the annular flow regime is the evaporation of the thin film.
6. The micro-tube is subjected to a circumferential and axial uniform heat flux, and the working fluid enters the micro-tube at saturation conditions.
7. The liquid and vapor phases are considered to be at thermodynamic equilibrium.
8. As the channel size decreases, the gravity force effect decreases. Thus, in the present model the influence of gravity force is assumed to be negligible.
9. The pressure gradient in the radial direction is neglected, thus, the pressure of the liquid phase and vapor phase at the same radial cross section are equal.
10. No entrained liquid droplets exist in the vapor core and no nucleate bubbles exist in the liquid film trapped in the annular flow regime for flow boiling in micro-channels.
11. The conduction heat transfer in axial flow direction is neglected.
12. The liquid and vapor densities are constant at a given operating condition.
13. At the interface, the interfacial liquid enthalpy equals to liquid phase enthalpy, and the interfacial vapor enthalpy equals to vapor phase enthalpy. The specific enthalpy of each phase varies only in flow direction.

Taking the above assumptions into account, the basic equations of the model can be derived by applying the mass, momentum, and energy balances for each phase in the chosen control volume, as follows.

4.3.2. Equations of Mass Conservation

The mass balance has been applied for each phase, liquid film and vapor core phases, in the chosen control volume as shown in Figure 4-2. Consequently, the mass conservation equations of the liquid film phase and vapor phase for one dimensional and steady flow can be deduced and expressed by Eqs. (4.5) and (4.6), respectively.

$$\frac{d}{dz} [\rho_f \alpha_f u_f] = -\Gamma \frac{P_i}{A} \quad (4.5)$$

$$\frac{d}{dz} [\rho_g \alpha_g u_g] = \Gamma \frac{P_i}{A} \quad (4.6)$$

Where, u_f and u_g , are the liquid film and vapor mean velocities, respectively, and ρ_f and ρ_g , are the densities of the liquid phase and vapor phase respectively. α_f , and α_g are the liquid phase and vapor phase void fractions, where, $(\alpha_g = 1 - \alpha_f)$. The term Γ appearing on the right side of the above Eqs. (4.5) and (4.6) is defined as the rate of evaporation of the liquid film at the liquid-vapor interface per unit area of the interfacial surface, and it will be evaluated based on the gas kinetic theory. P_i is the interfacial perimeter at the liquid vapor interphase. By adding Eq. (4.5) to Eq. (4.6) and expanding the derivatives, the vapor mass equation and whole mixture mass equation can be as expressed by Eq. (4.7) and Eq. (4.8) respectively,

$$[\rho_g \alpha_g] \frac{du_g}{dz} + [\rho_g u_g] \frac{d\alpha_g}{dz} = \Gamma \frac{P_i}{A} \quad (4.7)$$

$$[\rho_f \alpha_f] \frac{du_f}{dz} + [\rho_g \alpha_g] \frac{du_g}{dz} + [\rho_g u_g - \rho_f \alpha_f] \frac{d\alpha_g}{dz} = 0 \quad (4.8)$$

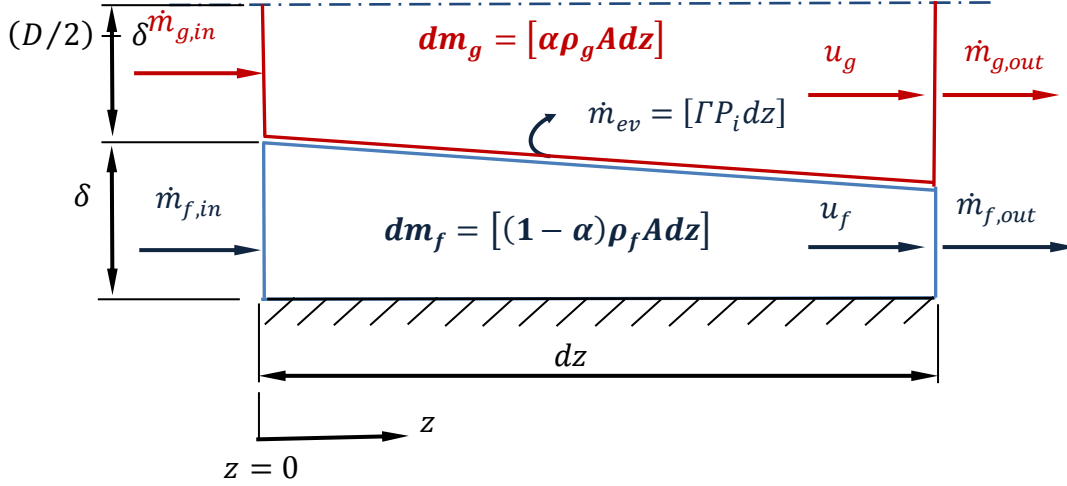


Figure 4-2: Symmetric sketch shows basic terms for deriving mass conservation equations for liquid film and vapor core phases.

4.3.3. Equations of Momentum Conservation

The acting forces on the chosen control volume in the two phases, liquid film and vapor core, are shown in Figure 4-3. The body and virtual mass forces were neglected here. For flow boiling in micro-channels, the effect of gravitational body force is small compared to viscous and inertial forces as it has been shown in several previous studies, (e.g. Kandlikar [60], Serizawa et al. [192]). The virtual mass force was neglected for model simplifications. Newton's Law can be applied to each phase in the control volume for deriving the liquid and vapor momentum equations respectively as follows,

$$\frac{d}{dz} [\rho_f \alpha_f u_f^2] = -\alpha_f \frac{dp}{dz} - \Gamma u_{fi} \frac{P_i}{A} - \tau_w \frac{P_w}{A} + \tau_{fi} \frac{P_i}{A} \quad (4.9)$$

$$\frac{d}{dz} [\rho_g \alpha_g u_g^2] = -\alpha_g \frac{dp}{dz} + \Gamma u_{gi} \frac{P_i}{A} - \tau_{gi} \frac{P_i}{A} \quad (4.10)$$

Where, τ_w is the wall shear stress, τ_{fi} and τ_{gi} are liquid and vapor phase interfacial shear stresses respectively. They are assumed here to be the same and denoted as ($\tau_{fi} = \tau_{gi} = \tau_i$). The interfacial phasic velocities of the liquid and vapor phase are assumed to be the same also ($u_{fi} = u_{gi} = u_i$), where u_i , is the interfacial velocity. P_w is the tube perimeter, and p is the system pressure. Adding Eq. (4.9) to Eq. (4.10), and expanding the derivatives, the momentum equations of the vapor phase, and the whole mixture are represented by Eq. (4.11), and Eq. (4.12), respectively as follows,

$$[2\rho_g u_g \alpha_g] \frac{du_g}{dz} + [\rho_g u_g^2] \frac{d\alpha_g}{dz} + \alpha_g \frac{dp}{dz} = \Gamma u_i \frac{P_i}{A} - \tau_i \frac{P_i}{A} \quad (4.11)$$

$$[2\rho_f u_f \alpha_f] \frac{du_f}{dz} + [2\rho_g u_g \alpha_g] \frac{du_g}{dz} + [\rho_g u_g^2 - \rho_f u_f^2] \frac{d\alpha_g}{dz} + \frac{dp}{dz} = \tau_w \frac{P_w}{A} \quad (4.12)$$

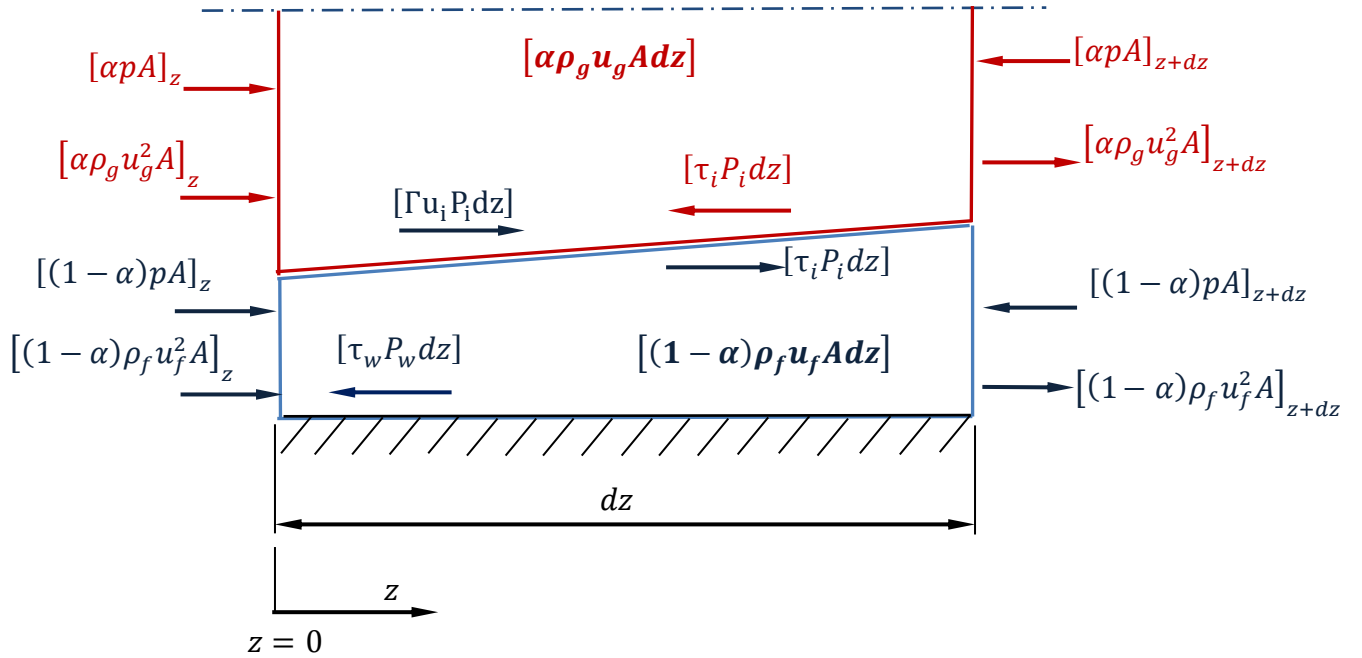


Figure 4-3: Symmetric sketch shows the forces acting on the control volume.

4.3.4. Equations of Energy Conservation

By applying the first law of thermodynamic for the liquid film and vapor core phases, the basic energy conservation equations of the liquid and vapor phases are expressed by Eq. (4.13), and Eq. (4.14) as follows,

$$\frac{d}{dz} \left[\rho_f \alpha_f u_f \left(h_f + \frac{u_f^2}{2} \right) \right] = q_w'' \frac{P_w}{A} - q_{fi}'' \frac{P_i}{A} - \Gamma \left(h_{fi} + \frac{u_{fi}^2}{2} \right) \frac{P_i}{A} + \tau_{fi} u_{fi} \frac{P_i}{A} \quad (4.13)$$

$$\frac{d}{dz} \left[\rho_g u_g \alpha_g \left(h_g + \frac{u_g^2}{2} \right) \right] = q_{gi}'' \frac{P_i}{A} + \Gamma \left(h_{gi} + \frac{u_{gi}^2}{2} \right) \frac{P_i}{A} - \tau_{gi} u_{gi} \frac{P_i}{A} \quad (4.14)$$

Where, q_w'' , is the uniform heat flux applied at the external surface of the micro-channel. For the evaporation conditions, the term q_{fi}'' is the heat flux transfers from the liquid phase to the interface, and q_{gi}'' is the heat flux transfers from the interface to the vapor core. h_f and h_g are the enthalpy of the liquid film and the vapor core respectively. h_{fi} and h_{gi} are the liquid and vapor interfacial enthalpies at the interphase which are assumed to be the same at thermodynamic equilibrium conditions. By expanding the derivatives, the energy equations of liquid and vapor phases, the energy equation of the vapor phase, and the whole mixture can be rearranged and represented by Eq. (4.15), and Eq. (4.16) as follows,

$$\begin{aligned} & \left[\rho_g \alpha_g \left(h_g + 3 \frac{u_g^2}{2} \right) \right] \frac{du_g}{dz} + \left[\rho_g u_g \left(h_g + \frac{u_g^2}{2} \right) \right] \frac{d\alpha_g}{dz} + [\rho_g u_g \alpha_g] \frac{dh_g}{dz} \\ & = q_{gi}'' \frac{P_i}{A} - \Gamma \left(h_{gi} + \frac{u_{gi}^2}{2} \right) \frac{P_i}{A} + \tau_i u_i \frac{P_i}{A} \end{aligned} \quad (4.15)$$

$$\begin{aligned}
& \left[\rho_f \alpha_f \left(h_f + 3 \frac{u_f^2}{2} \right) \right] \frac{du_f}{dz} + \left[\rho_g \alpha_g \left(h_g + 3 \frac{u_g^2}{2} \right) \right] \frac{du_g}{dz} \\
& + \left[\rho_g u_g \left(h_g + \frac{u_g^2}{2} \right) - \rho_f u_f \left(h_f + \frac{u_f^2}{2} \right) \right] \frac{d\alpha_g}{dz} + [\rho_g u_g \alpha_g] \frac{dh_g}{dz} \\
& + [\rho_f u_f \alpha_f] \frac{dh_f}{dz} = q_w'' \frac{P_w}{A}
\end{aligned} \tag{4.16}$$

4.3.5. Estimation of Interfacial Parameters

Considering the assumptions listed above in section 2.1., six main interfacial parameters at the liquid-vapor interphase, Γ , q_{gi}'' , q_{fi}'' , τ_i , u_i , and f_i , in the present work are still need to be evaluated for closing the model analysis. The mass flux of liquid film evaporation at the interface, Γ , is calculated based on the gas kinetic theory which has been discussed in many previous studies in the literature (e.g. Wayner et al. [215], Carey [216], Schonberg et al. [217], and Vij and Dunn [218]). Since, most of the proposed models for calculating mass flux at the interface are dependent of the thermo-physical properties of the phases, as well as the interfacial and vapor phase temperatures, it has been assumed in the present study, that the interfacial temperature equals to the vapor temperature which is evaluated here based on the modeled vapor enthalpy. On the other hand the liquid temperature is calculated based on the liquid enthalpy. Accordingly, the mass flux of evaporation at the interface can be expressed as follows,

$$\Gamma = p \left(\frac{M}{2\pi R} \right)^{1/2} \left(\frac{C_{pg}}{h_g} - \frac{C_{pf}}{h_f} \right)^{1/2} \tag{4.17}$$

Where p is the pressure, M is the molecular weight of the working fluid, R is the universal gas constant, C_{pg} is the vapor specific heat capacity, C_{pf} is the liquid specific heat capacity, h_g is the specific enthalpy of the vapor phase, and h_f is the specific enthalpy of the liquid film.

Regards to the energy transfers from the liquid at the interface, q_{fi}'' , one can assume that all the heat flux applied at external surface of the channel wall transfers by conduction through the channel wall into the liquid phase in the radial direction and no heat transfers in axial direction, consequently it will equal to the liquid heat flux at the interface, ($q_w'' = q_{fi}''$). Considering the

mass flux of liquid film evaporation, and the latent heat of evaporation, h_{fg} , the energy balance at the liquid-vapor interface can be represented as follows,

$$q_{gi}'' = q_w'' - \Gamma h_{fg} \quad (4.18)$$

The interfacial shear stress is one of the most important parameters in the annular flow regime, and has a significant effect on the liquid film thickness. In the present study, the interfacial shear stress was calculated based on the friction factor approach as follows,

$$\tau_i = \frac{1}{2} f_i \rho_g (u_g - u_f) |u_g - u_f| \quad (4.19)$$

For predicting the interfacial friction factor, several previous studies have discussed the correlations of interfacial friction factor (e.g. Chisholm [219], Wallis [200], Henstock & Hanratty [220], Brauner & Maron [69], Andritsos & Hanratty [221], Hartnett & Minkowycz [222], and Quiben & Thome [171]). The correlation of interfacial friction factor proposed by Quiben and Thome [171] for annular flow pattern is used in the present work and represented as follows,

$$(f_i)_{annular} = 0.67 \left(\frac{\delta}{D}\right)^{1.2} \left(\frac{(\rho_f - \rho_g)g\delta^2}{\sigma}\right)^{-0.4} \left(\frac{\mu_g}{\mu_f}\right)^{0.08} (We_f)^{-0.034} \quad (4.20)$$

Where D is the channel diameter, g is the gravity, μ_g is the vapor dynamic viscosity, μ_f is the liquid dynamic viscosity, ρ_g and ρ_f are the vapor and liquid densities respectively. δ is the liquid film thickness and can be defined in terms of vapor void fraction as follows,

$$\delta = \left(\frac{D}{2}\right) (1 - \alpha_g^{0.5}) \quad (4.21)$$

Liquid Weber number, We_f , is calculated as

$$We_f = \left(\frac{\rho_f u_f^2 D}{\sigma}\right) \quad (4.22)$$

The interfacial velocity at the interface plays a significant role for considering the influence of interfacial parameters in momentum and energy equations. In the present study, the interfacial

velocity is calculated in terms of working fluid properties and liquid film thickness using the relation proposed by Vij and Dunn [218], which is represented as follows,

$$u_i = 2 \left[\left(\frac{\mu_f}{\delta^2} \right) u_f - \left(\frac{\mu_g}{(D - 2\delta)^2} \right) u_g \right] / \left[\left(\frac{\mu_f}{\delta^2} \right) - \left(\frac{\mu_g}{(D - 2\delta)^2} \right) \right] \quad (4.23)$$

4.3.6. Wall Shear Stress and Friction Factor:

The wall shear stress τ_w , in the right side hand of the momentum equation of the whole mixture, Eq. (4.12), is given in terms of liquid film velocity and the working fluid density as,

$$\tau_w = \frac{1}{2} \rho_f f_f u_f^2 \quad (4.24)$$

For wide range of flow conditions which cover laminar transitional, and turbulent flow conditions, different correlations discussed in Li and Wu [74] for predicting friction factor have been employed including the correlation of Churchill [223] which takes into account surface roughness effect. The frictional correlation are expressed as follows,

$$f_f = \begin{cases} f_1 & \text{for } Re_f \leq 1600 \\ f_2 & \text{for } Re_f \geq 3,000 \\ f_3 & \text{for } 1600 > Re_f > 3,000 \end{cases} \quad (4.25)$$

Where

$$f_1 = 16/Re_f \quad (4.26)$$

$$f_2 = \left[\left(\frac{8}{Re} \right)^{12} + \frac{1}{(a+b)^{3/2}} \right]^{1/12} \quad (4.27)$$

$$a = \left[2.457 \ln \frac{1}{(7/Re) + 0.27(\epsilon/D)} \right]^{16}; \quad b = \left[\frac{37530}{Re_f} \right]^{16}$$

$$f_3 = f_1(1600) + \frac{Re - 1600}{1400} [f_2(3000) - f_1(1600)] \quad (4.28)$$

Where Re_f is the based-liquid film Reynolds number which is calculated in the present model using the predicted values of average liquid film thickness $\bar{\delta}$, and average liquid film velocity \bar{u}_f at every heat and mass fluxes applied as follows,

$$Re_f = \frac{\rho_f \bar{u}_f D_h}{\mu_f} \quad (4.29)$$

4.3.7. Main Form of the Present Model:

In summary of the analytical part, six expanded equations represent the final form of the present model. These equations are as follows: two equations from the mass balance which are the mass conservation equation of the vapor phase Eq. (4.7), and the mass conservation equation of the whole mixture, Eq. (4.8), and two momentum equations, which are the momentum conservation equation of the vapor phase, Eq. (4.11), and the momentum conservation equation of the whole mixture, Eq. (4.12), and the energy conservation equation of the vapor phase, Eq. (4.15), and the energy conservation equation of the whole mixture, Eq. (4.16). Consequently, the final form of the present model equation is organized and formulated in a mass matrix form as follows:

$$AY = B \quad (4.30)$$

Where A , is a square mass matrix which contains the coefficients of the dependent variables obtained by expanding the differential terms of the main equations. The gradient of the main dependent variables is represented by the column vector Y , and the column vector B represents the nonhomogeneous part of the present model. The main model equation can be rewritten in details as depicted in Eq. (4.31).

$$\begin{bmatrix}
\rho_g \alpha_g & 0 & \rho_g u_g & 0 & 0 & 0 \\
\rho_g \alpha_g & \rho_f u_f & (\rho_g u_g - \rho_f u_f) & 0 & 0 & 0 \\
2\rho_g \alpha_g u_g & 0 & \rho_g u_g^2 & \alpha_g & 0 & 0 \\
2\rho_g \alpha_g u_g & 2\rho_f \alpha_f u_f & (\rho_g u_g^2 - \rho_f u_f^2) & 1 & 0 & 0 \\
\rho_g \alpha_g \left(h_g + \frac{3}{2} u_g^2 \right) & 0 & \rho_g u_g \left(h_g + \frac{1}{2} u_g^2 \right) & 0 & \rho_g \alpha_g u_g & 0 \\
\rho_g \alpha_g \left(h_g + \frac{3}{2} u_g^2 \right) & \rho_f \alpha_f \left(h_f + \frac{3}{2} u_f^2 \right) & \rho_g u_g \left(h_g + \frac{1}{2} u_g^2 \right) - \rho_f u_f \left(h_f + \frac{1}{2} u_f^2 \right) & 0 & \rho_g \alpha_g u_g & \rho_f \alpha_f u_f
\end{bmatrix}
\begin{bmatrix}
\frac{du_g}{dz} \\
\frac{du_f}{dz} \\
\frac{d\alpha_g}{dz} \\
\frac{dp}{dz} \\
\frac{dh_g}{dz} \\
\frac{dh_f}{dz} \\
\frac{dz}{dz}
\end{bmatrix}
\quad (4.31)$$

$$= \begin{bmatrix}
\Gamma \frac{P_i}{A} \\
0 \\
(\Gamma u_i - \tau_i) \frac{P_i}{A} \\
\tau_w \frac{P_w}{A} \\
\left[q_{gi}'' + \Gamma \left(h_g + \frac{u_i^2}{2} \right) - \tau_i u_i \right] \frac{P_i}{A} \\
q_w'' \frac{P_w}{A}
\end{bmatrix}$$

4.3.8. Equivalent Reynolds Number:

It is very convenient and helpful in two-phase flow to use the equivalent Reynolds number (Re_{eq}) instead of liquid-phase and vapor-phase Reynolds numbers. The equivalent Reynolds number was defined in several previous studies (e.g. Akers et al. [55], Yan and Lin [149], and Laohalertdech and Wongwises [224]). In the present study, the equivalent Reynolds number is used to describe the range of database collected from the literature and employed for model validation as well as to describe the applicability of the present model. Re_{eq} is defined in terms of average vapor quality (x_m) and properties of the working fluid as developed by Akers et al. [55] and as given in Eq. (4.32),

$$Re_{eq} = \frac{GD_h}{\mu_f} \left[(1 - x_m) + x_m (\rho_f / \rho_g)^{0.5} \right] \quad (4.32)$$

4.4. Initial Values of the Model Variables

In order to solve the main model equation, Eq. (4.31), the initial values of the dependent variables, u_{go} , u_{fo} , α_{go} , p_o , h_{go} , and h_{fo} at the entrance of the micro-tube should be estimated properly. The initial values of the pressure, p_o , the vapor phase enthalpy, h_{go} , and the liquid phase enthalpy, h_{fo} , are evaluated based on the inlet saturation temperature. The initial values of the rest of the main parameters are evaluated as explained in the following sections.

4.4.1. Initial Value of Void Fraction

It should be noted that the initial vapor void fraction is mainly dependent on the initial liquid film thickness, which is an essential parameter for studying the annular flow regime. Furthermore, predicting its initial values properly is very significant. Thus, several investigations for predicting liquid film variation either in slug flow or annular flow have been done. It has been revealed by Moriyama and Inoue [125] that the liquid film thickness is influenced by the capillary number for large bubble acceleration, while mainly influenced by the viscous boundary layer for small bubble acceleration. Most of available correlations for liquid film thickness

prediction either for slug or annular flow regime were developed based on the experimental data measured at adiabatic flow conditions (e.g., Irandoust and Andersson [35], Han and Shikazono [225], [128], Kanno et al [131]). On the other hand, some other correlations of liquid film models developed based on boiling conditions, but overpredicted the experimental data due to the influence of interfacial instability as reported by Revellin et al. [38]. In general, it would be more realistic to employ a correlation for predicting the initial value of the liquid film thickness considering the above mentioned effects, (i.e., bubble acceleration, laminar, and turbulent flow). Additionally, the initial liquid film thickness at boiling conditions may be fairly estimated using the correlations developed at adiabatic conditions as it has been proven by Han et al. [40]. Consequently, in the present model, the initial liquid film thickness is predicted using the correlations developed by Han and Shikazono [128] as given by Eq. (4.33):

$$\left(\frac{\delta_o}{D}\right)_{steady} = \begin{cases} \frac{0.67 Ca^{2/3}}{1 + 3.13 Ca^{2/3} + 0.504 Ca^{0.672} Re^{0.589} - 0.352 We^{0.629}} & Re < 2000 \\ \frac{106 (\mu^2/\rho\sigma D)^{2/3}}{1 + 497.0(\mu^2/\rho\sigma D)^{2/3} + 7330(\mu^2/\rho\sigma D)^{2/3} - 5000(\mu^2/\rho\sigma D)^{2/3}} & Re \geq 2000 \end{cases} \quad (4.33)$$

The correlation developed by Han and Shikazono [128], Eq. (4.33), was able to predict the experimental data measured by the authors for various working fluids and micro-tube sizes with an accuracy of $\pm 15\%$. Furthermore, by considering the bubble acceleration effects, Han and Shikazono [129], expressed the initial liquid film thickness by Eq. (4.34).

$$\left(\frac{\delta_o}{D}\right)_{accel} = \frac{0.968 Ca^{2/3} Bo_{accel}^{-0.414}}{1 + 4.838 Ca^{2/3} Bo_{accel}^{-0.414}} \quad (4.34)$$

Where, Bo is the Bond number based on the bubble acceleration that is expressed as $Bo = (\rho_g a D_h^2 / \sigma)$. In the present model, the bubble acceleration is determined based on the mean vapor velocity, and heated length, $a = (\bar{u}_g^2 / 2L_h)$, instead of bubble velocity since the adopted flow pattern is the annular flow regime. Consequently, based on the two values obtained from Eqs. (4.33) and (4.34) of the ratio, (δ_o/D) , the initial liquid film thickness is given by the minimum value as reported by Han and Shikazono [128] [129], as expressed by Eq. (4.35),

$$\left(\frac{\delta_o}{D}\right) = \min \left[\left(\frac{\delta_o}{D}\right)_{steady}, \left(\frac{\delta_o}{D}\right)_{accel} \right] \quad (4.35)$$

The initial value of the vapor void fraction is calculated as follows,

$$\alpha_{go} = \left[\frac{(D - 2\delta_o)^2}{D^2} \right] \quad (4.36)$$

4.4.2. Initial Values of Liquid Film and Vapor Velocities

The initial values of vapor and liquid film velocities at the onset of annular flow are calculated in terms of initial liquid film thickness using Eq. (4.37) and Eq. (4.38):

$$u_{go} = (Gx_e/\rho_g)(D^2/(D - 2\delta_o)^2) \quad (4.37)$$

$$u_{fo} = (G(1 - x_e)/\rho_f)(D^2/(4\delta_o(D - \delta_o))) \quad (4.38)$$

Where, x_e is the vapor quality estimated at the exit of the micro-tube. In the present model, the exit vapor quality, x_e , is calculated based on the energy balance of a micro-tube subjected to a uniform heat flux, and it is given by Eq. (4.39) in terms of the heated length-to-diameter ratio for zero-inlet sub-cooling enthalpy (inlet saturated conditions), and the Boiling number.

$$x_e = 4Bl(L_h/D_h) \quad (4.39)$$

The Boiling number is calculated as expressed by Eq. (4.40) as follows,

$$Bl = (q_w''/Gh_{fg}) \quad (4.40)$$

The initial value of the pressure at the inlet of the micro-tube is evaluated based on inlet saturation conditions of the experimental data.

4.5. Solution Procedure

The main differential equations represented in the mass matrix form which are expressed by Eq. (4.31) are solved using a MATLAB code based on explicit Runge-Kutta method. The solution procedure can be described as follows:

1. Firstly, the operating conditions such as, inlet saturation temperature, mass flux, and heat flux, channel geometry, and heated length are defined, as well as the properties of the working fluid which are estimated at the inlet saturation temperature or pressure.
2. The domain of the micro-channel is divided based on the heated length into small segments with length Δz , and the local vapor quality is calculated using Eq. (4.39).
3. The non-dimensional numbers, Re , We , Bl , and Ca are calculated.
4. The initial liquid film thickness is calculated by Eq. (4.35), and consequently the vapor void fraction, α_{g0} , the initial values of vapor core velocity u_{g0} , liquid film velocity u_{f0} are estimated by Eqs. (4.36), (4.37), and (4.38), respectively.
5. The based-liquid film Reynolds number, Re_f , the liquid film friction factor f_f , and the wall shear stress τ_w , are calculated using Eqs. (4.29), (4.25), and (4.24), respectively.
6. The liquid Weber number, We_f , is calculated as defined by Eq. (4.22), while the mass flux of evaporation at the interface, Γ , and the vapor heat flux at the interface, q_{gi}'' are calculated by Eq. (4.17), and Eq. (4.18), respectively.
7. The interfacial velocity, u_i , the interfacial friction factor, f_i , and interfacial shear stress, τ_i , are calculated by Eqs. (4.23), (4.20), and (4.19), respectively.
8. Solving the set of equations of the present model represented by Eq. (4.31), considering the initial values as they have been estimated above.
9. Update the values of the main dependent parameters, u_g , u_f , α_g , p , h_g , and h_f , then repeat steps 3-7 for the next segment along the heated length. Consequently, the local values of the main parameters are determined.
10. The local and average heat transfer coefficients can be determined as explained in the following section by Eqs. (4.42), and (4.43), respectively.

4.6. Results and Discussion

Heat transfer coefficient, pressure drop, and void fraction have been predicted and discussed in the following sections. The experimental data collected from the literature which fall in the annular flow regime have been used for validating the present model. Furthermore, to ensure that the collected data from the literature can be classified as macro/micro scale data, the classification suggested by Ong and Thome [39] based on the confinement number, C_{conf} , has been addressed and added. According to Ong and Thome [39], the flow can be considered as a micro-scale flow when the confinement number reaches one, ($C_{conf} \approx 1$), where the surface tension effect is dominant. It is of interest to represent the confinement number here which is defined as,

$$C_{conf} = (1/D) \sqrt{\sigma/g(\rho_f - \rho_g)} \quad (4.41)$$

4.6.1. Two Phase Heat Transfer Coefficient

It has been revealed by many investigators that convective liquid film evaporation is promised to be the main dominant heat transfer mechanism for annular flow regime in horizontal micro-channels. Furthermore, there is a significant relation between the liquid film thickness and heat transfer coefficient in this regime. Based on the values of vapor void fraction predicted by the present model, and considering the relation between the vapor void fraction and liquid film thickness as represented by Eq. (4.21), the variation of liquid film thickness $\delta(z)$ in terms of heated length can be calculated. Assuming that the heat transferred by conduction through the channel wall equals to that transferred by convection through the liquid film. Thus, the local two-phase heat transfer coefficient $h_{tp}(z)$, under uniform heat flux conditions may be represented by Eq (4.42).

$$h_{tp}(z) = \frac{k_f}{\delta(z)} \quad (4.42)$$

Where k_f is the thermal conductivity of the liquid phase, which is always much larger than that of the vapor phase, of the working fluid estimated at the inlet saturation conditions.

By obtaining the local two-phase heat transfer coefficient along the heated length of the micro-channel, the average two-phase heat transfer coefficient can be calculated by the following expression, Eq. (4.43), for the exit vapor quality range that covers the annular flow regime:

$$\overline{h_{tp}} = \frac{1}{N} \int_0^{L_H} h_{tp}(z) dz \quad (4.43)$$

Two-phase heat transfer coefficient has been calculated by the present model and compared with various experimental heat transfer data for a wide range of operating conditions for flow boiling in single mini/micro-channels. The range of operating conditions of experimental heat transfer data points collected from the literature and used for heat transfer comparison are listed in Table (4.1).

Table (4-1): Test conditions of two-phase heat transfer data used for model validation.

| Author(s) | Geometry | Working fluid(s) | Hydraulic diameter D_h , [mm] | Heated length L_h , [mm] | Saturation Temperature T_{sat} , [°C] | Mass flux G , [kg/m ² .s] | Heat flux q_w'' , [kW/m ²] |
|-----------------------------|-------------|-------------------|------------------------------------|-------------------------------|--|---|---|
| Mahmoud & Karayiannis [207] | Circular | R134a | 0.52, 1.10 | 100, 450 | 22.0 | 300 | 56-78 |
| Tibirica [176] | Circular | R134a, R1234ze | 1.10 | 180 | 31 | 300-600 | 15-35 |
| Ali et al. [206] | Circular | R134a | 0.781 | 191 | 30.0 | 270-500 | 5.0-60.0 |
| Ong & Thome [97] | Circular | R134a, R236fa | 1.03 | 180 | 31.0 | 200-400 | 21.5-43.0 |
| Saitoh et al. [226] | Circular | R134a | 0.51, 1.12, 3.10 | 550, 935, 3235 | 5.0, 10.0 | 150-300 | 12.0-27.0 |
| Yan & Lin [149] | Circular | R134a | 2.0 | 200 | 31.0 | 100-200 | 5.0 |
| Ducoulombier et al. [61] | Circular | CO2 | 0.529 | 160 | -10.0 0.0 | 200-1200 200-600 | 10.0-30.0 |
| Wu et al. [177] | Circular | CO2 | 1.42 | 300 | -10.0 | 300-500 | 7.5-29.8 |
| Choi et al. [144] | Circular | CO2 | 1.50 | 2000 | +10.0 | 300-500 | 10.0 |
| Lee & Lee [22] | Rectangular | R113 | 0.784 | 300 | 50.0 | 104-208 | 5.0-15.0 |

Figure 4-4 shows the variation of two-phase heat transfer coefficient of saturated flow boiling of the refrigerant R-134a in terms of vapor quality as predicted by the present model for flow through a 1.12 mm inner diameter tube, and a ratio of heated length to inner diameter (L_h/D) = 835 at an inlet saturation temperature $T_{sat} = 10$ °C, corresponding to a confinement number $C_{conf} = 0.81$. It is apparent that by increasing the mass flux and the vapor quality, the heat transfer coefficient increases. Compared to the heat transfer data measured by Saitoh et al. [226], it can be seen that the model predicted well the heat transfer coefficient data at low mass flux, 150 [kg/m².s], in the range of vapor quality of ($0.38 \leq x_e \leq 0.70$) with a MAE of 5.90 %, and for mass flux 300 [kg/m².s], in the range of vapor quality of ($0.38 \leq x_e \leq 0.90$) with a MAE of 10.72 % . At low mass flux 150 [kg/m².s], the experimental data showed a decrease in heat transfer coefficient by increasing the vapor quality beyond the vapor quality line $x_e > 0.7$. A possible explanation for this is that this could be the effect of the transition from annular to dry-out flow regime at this vapor quality. On the other hand, the present model overpredicted the heat transfer data measured for 150 kg/m².s beyond the vapor quality line ($x_e > 0.7$), where it showed an increase in heat transfer coefficient by increasing the vapor quality. The corresponding equivalent Reynolds numbers for this range of mass fluxes are $3820 \leq Re_{eq} \leq 7370$. Additionally, the corresponding Re_{eq} for the mass flux 300 [kg/m².s] is $Re_{eq} = 7370$ where the present model provided a good agreement with experimental data even beyond the vapor quality $x_e > 0.7$, the liquid film evaporation dominance may explain the good match with experimental data in this regime.

For higher inlet saturation temperature $T_{sat} = 30$ °C, higher mass fluxes, $G = 270 - 500$ kg/m².s corresponding to ($3,175 \leq Re_{eq} \leq 6,077$), and smaller inner diameter tube, $D=0.781$ mm, and lower density ratio, $(\rho_f/\rho_g) = 31.64$, and $C_{conf} = 1.04$, the present model was compared with heat transfer data of Ali et al. [206] as shown in Figure 4-5. From this figure, the experimental data shows that the average two-phase heat transfer coefficient for the mentioned range of mass fluxes increases by increasing the mass flux and the vapor quality. The model predicted well the experimental data for mass fluxes 270, and 400 kg/m².s, with MAE of 6.87 %, and 11.51 % respectively. While for the mass flux, 500 kg/m².s, it can be seen that there is a slight underprediction of the data.

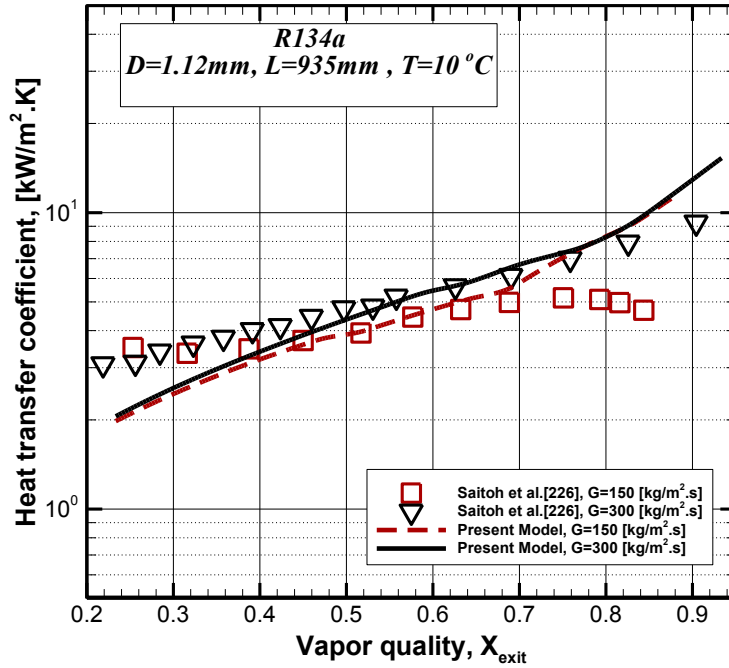


Figure 4-4: Heat transfer coefficient for flow boiling of the refrigerant R134-a in 1.12 mm inner diameter micro-channel versus vapor quality for various mass fluxes, and comparison of the heat transfer data predicted by the present model with those of Saitoh et al. [226] at $T_{sat} = 10\text{ °C}$

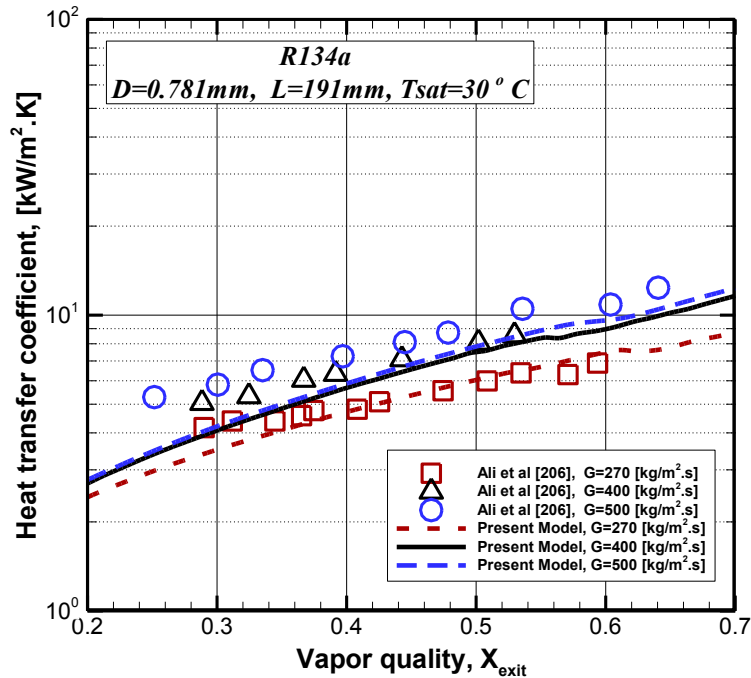


Figure 4-5: Heat transfer coefficient for flow boiling of the refrigerant R134-a in 0.781mm inner diameter micro-channel versus vapor quality for various mass fluxes, and comparison of the heat transfer data predicted by the present model with those of Ali et al. [206] at $T_{sat} = 30\text{ °C}$.

In order to investigate the influence of the working fluid on the heat transfer coefficient, the model was compared with the experimental heat transfer data available in the literature for flow boiling of CO₂ in 0.529 mm inner diameter horizontal smooth micro-tube, measured by Ducoulombier et al. [61] for low heated length to inner diameter ratio, $(L_h/D_h) = 302$, and low saturation temperature, $T_{sat} = 0^\circ\text{C}$, corresponding to $C_{conf} = 1.41$, and much lower density ratio, $(\rho_f/\rho_g) = 9.5$, as depicted in Figure 4-6. It is apparent that for the intermediate exit vapor quality, $0.25 \leq x_e \leq 0.75$, the model gave similar trend for the two-phase heat transfer coefficient for the tested mass fluxes, 200, 400, 600 kg/m².s, and corresponding equivalent Reynolds numbers, $2,170 \leq Re_{eq} \leq 7,320$. While beyond a certain value of vapor quality (e.g. $x_e > 0.72$ for mass flux 200 kg/m².s), the model showed a steep increase in heat transfer coefficient. This value of vapor quality increases by increasing the mass flux. Additionally, it has been noticed that the model slightly underpredicted the experimental heat transfer data for higher mass fluxes. The reason for this could be attributed to the significant effects of mass flux on the flow pattern and the boundary of annular flow regime as well as the onset of dry-out. Overall, for these flow conditions, the model predicted the tested heat transfer data of the annular regime with MAE = 10.98 %.

For a larger tube diameter, $D_h = 1.5$ mm, and same working fluid, CO₂, at higher saturation temperature, $T_{sat} = 10^\circ\text{C}$, corresponding to $C_{conf} = 0.41$, and much lower density ratio, $(\rho_f/\rho_g) = 6.37$, the model was compared to the data of Choi et al. [144], as depicted in Figure 4-7. According to the flow pattern map, updated by Cheng et al. [103] for CO₂, the boundaries of annular flow regime for mass fluxes 300, and 400 kg/m².s are $(0.23 \leq x \leq 0.72)$, and $(0.23 \leq x \leq 0.68)$, respectively. From the Figure 4-7, a good agreement with the tested data at an intermediate and a high vapor quality range, $(0.15 \leq x_{exit} \leq 0.75)$, can be clearly seen for mass fluxes 300, and 400 kg/m².s. However, for mass flux 500 kg/m².s, and vapor quality, $x \geq 0.45$, the model slightly underpredicted the experimental data. One reason of this underestimation is that the change of flow pattern of the tested data at this vapor quality. A second reason can be attributed to the flow instability where it is a quite hard to have a stable annular flow pattern. In general, for the tested range of equivalent Reynolds numbers, $8,700 \leq Re_{eq} \leq 12,060$, the model predicted the heat transfer data of the CO₂ with MAE = 10.67 %.

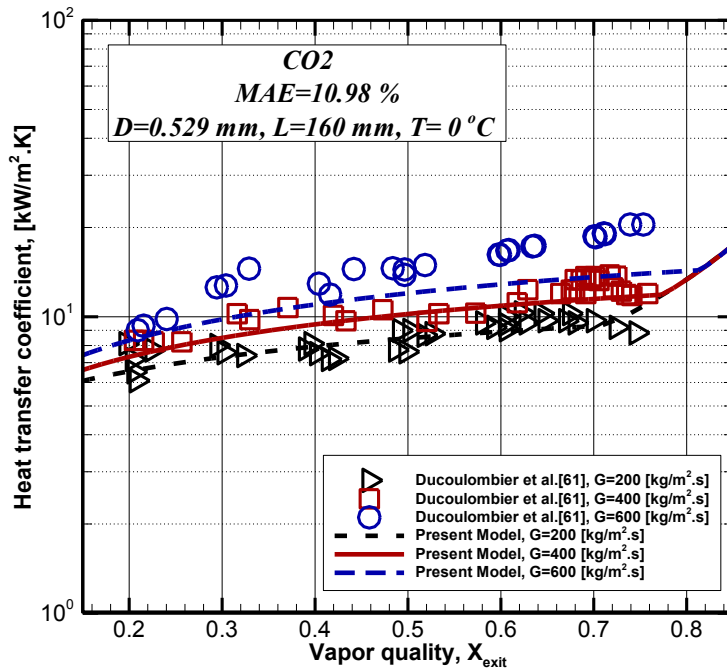


Figure 4-6: Heat transfer coefficient versus vapor quality for flow boiling of CO₂ in 0.529 mm inner diameter micro-channel for various mass fluxes, and comparison of the present model with the data of Ducoulombier et al. [61] at $T_{sat} = 0$ °C.

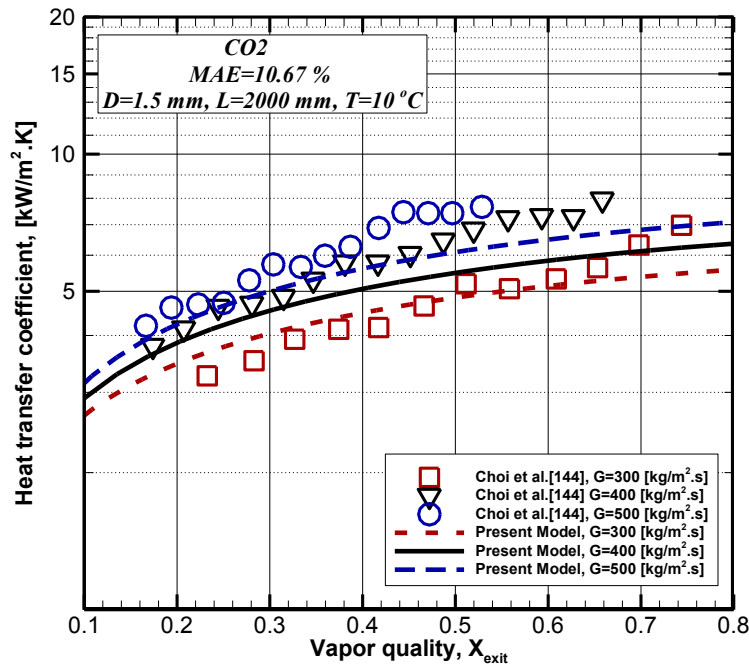


Figure 4-7: Heat transfer coefficient versus vapor quality for flow boiling of the refrigerant CO₂ in 1.5 mm inner diameter micro-tube for various mass fluxes, and compared with the experimental data of Choi et al. [144] at $T_{sat} = 10$ °C.

Overall, the present model has been compared with 602 two-phase heat transfer data points which have been collected from different resources for annular flow regime for various working fluids and operating flow conditions corresponding to a wide range of equivalent Reynolds number of $2,150 \leq Re_{eq} \leq 18,350$, as shown in Table (4.1). The model predicted the whole experimental heat transfer data of the annular flow regime with a MAE of 18.14 % as depicted in Figure 4-8. Bland-Altman plots have been employed here to analyze and assess the ability of the present model for predicting the heat transfer experimental data points. The upper limit of agreement (ULOA) is +9.85, while the lower limit of agreement (LLOA) is -6.14. As it can be seen, both of the data points predicted analytically and experimentally are uniformly scattered around the mean line of the difference, (Mean=1.85). However, as the average of the two results increases the difference increases and passes beyond the limits of the agreement. The results plotted over the upper limit of agreement (ULOA), are for the CO₂ flows with $Re_{eq} > 12,500$, where the model underestimated the experimental data points. Therefore, the range of model applicability is restricted to the limits of agreements (ULOA=+9.85, LLOA=-6.14).

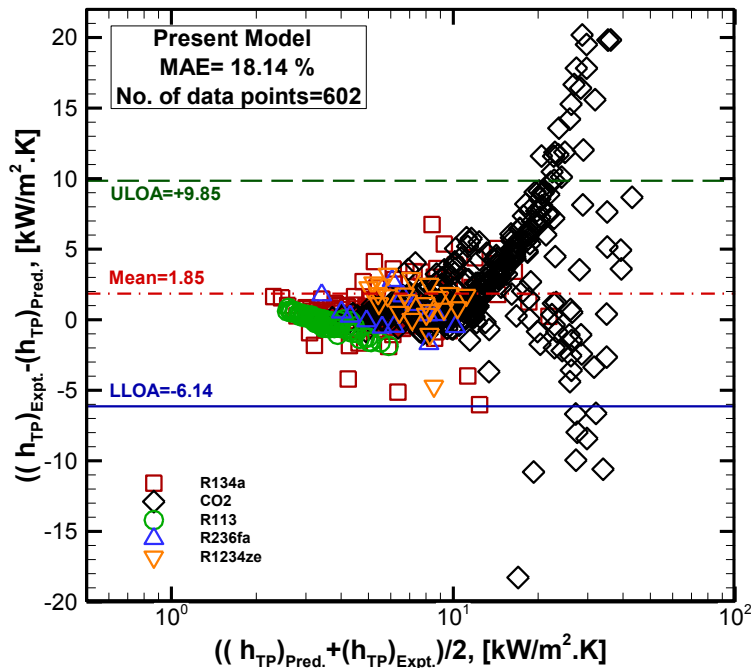


Figure 4-8: Using Bland-Altman Plot method for assessing the agreement between the average two-phase heat transfer coefficient predicted by the present model and those measured experimentally (602 data points) for various working fluids and flow conditions as shown in Table (4.1) for the annular flow regime

4.6.2. Two Phase Pressure Drop

Two-phase pressure drop for flow boiling in micro-channels have been predicted by the present model for the working fluids and operating flow conditions which are listed in Table (4.2). Figure 4-9 compares the two-phase pressure drop results obtained by the present model with those measured by Revellin and Thome [3] for flow boiling of the R134a through a micro-tube has an inner diameter of $D=0.509$ mm and a heated length to inner diameter ratio of $(L_h/D) = 138$, at an inlet saturation temperature $T_{sat} = 30$ °C, that matches a confinement number, $C_{conf} = 1.59$, for wide range of mass fluxes, 350 to 1500 $kg/m^2 \cdot s$, corresponding to a range of equivalent Reynolds number of $2,400 \leq Re_{eq} \leq 8,800$. According to the diabatic flow pattern map developed by Revellin and Thome [75] for flow boiling in micro-channels, for the same operating conditions, the transition lines from coalescing bubble to annular flow, and from annular to dry-out flow regimes vary by varying the mass flux. For instance, the boundaries of annular flow for mass fluxes 350, 700, and 1000 $kg/m^2 \cdot s$, are $(0.36 \leq x \leq 0.87)$, $(0.18 \leq x \leq 0.63)$, and $(0.13 \leq x \leq 0.54)$, respectively. It is of interest to notice that the boundaries of the annular flow regime become narrower as the mass flux increases. It can be seen from Figure 4-9 that the pressure drop increases as the mass flux and vapor quality increase. Additionally, for the annular flow regime, the present model predicted well the effect of mass flux and vapor quality on the pressure drop, and gave a good agreement with the experimental pressure drop data of Revellin and Thome [3], with a MAE of 23.24 %.

Table (4-2): Test conditions of two-phase pressure drop data points used for model validation

| Author(s) | Geometry | Working fluid(s) | Hydraulic diameter D_h , [mm] | Heated length L_h , [mm] | Saturation Temperature T_{sat} , [°C] | Mass flux G , [kg/m ² .s] | Heat flux q_w'' , [kW/m ²] |
|---------------------------|----------|------------------|------------------------------------|-------------------------------|--|---|---|
| Tran et al. [164] | Circular | R134a | 2.46 | 914 | 32.8 | 52 – 475 | 2.2-49.8 |
| Tibiriçá et al. [176] | Circular | R134a | 2.32 | 464 | 31.3 | 200 – 600 | 10-55 |
| Revellin & Thome [3] | Circular | R134a | 0.509, 0.790 | 70.7 | 30 | 350 – 1000 | 3.1-415 |
| Hwang & Kim [166] | Circular | R134a | 0.244, 0.430, 0.792 | 60, 180, 462 | 26.7 | 140 – 950 | - |
| Cavallini et al. [204] | Circular | R134a | 0.960 | 229 | 40 | 400, 600 | - |
| Ducoulombier et al. [227] | Circular | CO2 | 0.529 | 191 | -5, -10 | 200-1400 | - |
| Wu et al. [177] | Circular | CO2 | 1.42 | 300 | -10 | 300-600 | 7.5-29.8 |

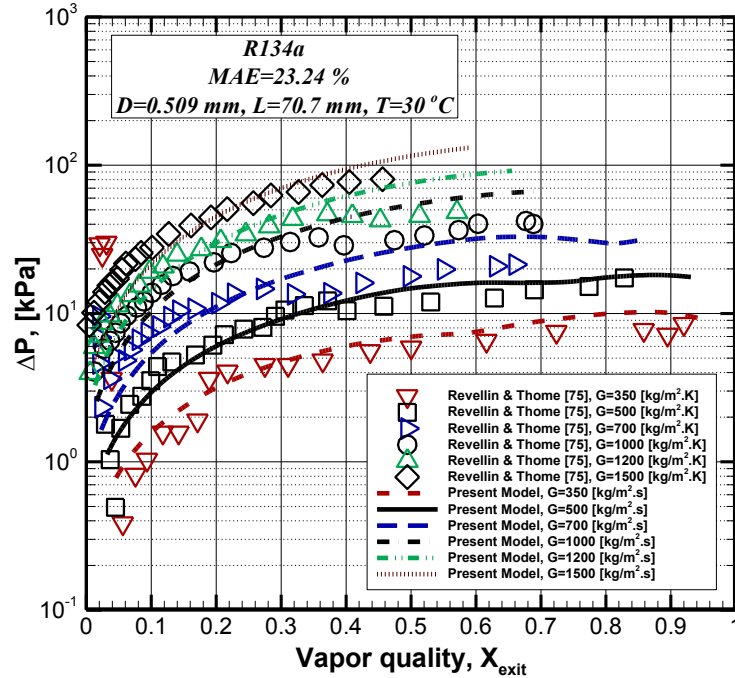


Figure 4-9: Comparison of pressure drop predicted by the present model with that measured by Revellin and Thome [75] for flow boiling of R-134a at inlet saturation temperature of 30 °C through a micro-tube with an inner diameter of $D=0.509$ mm and heated length of 70.7 mm, for range of mass fluxes of 350 to 1500 $[kg/m^2.s]$.

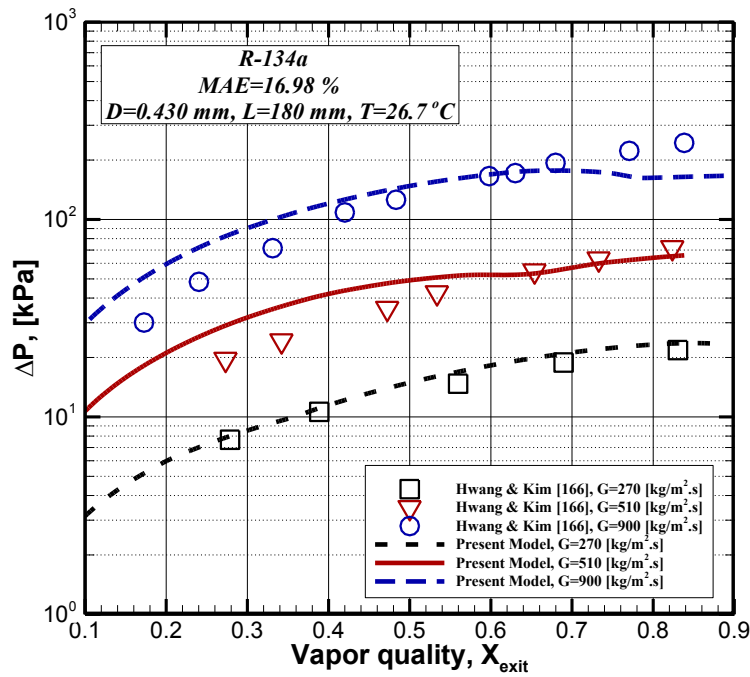


Figure 4-10: Comparison of pressure drop predicted by the present model with those measured by Hwang and Kim [166] for flow boiling of R-134a at inlet saturation pressure of 700 kPa through a circular micro-tube with an inner diameter $D=0.430$ mm.

Furthermore, Figure 4-10 compares the results of the pressure drop obtained by the present model with those measured by Hwang and Kim [166] for flow boiling of R-134a in a 0.486 mm inner diameter micro-tube at an inlet saturation temperature $T_{sat} = 26.7$ °C, matches a confinement number, $C_{conf} = 1.93$, and a ratio of heated length to inner diameter ($L_h/D = 415$) for a range of mass fluxes 270 to 900 $kg/m^2.s$, corresponding to a range of equivalent Reynolds number of ($2,113 \leq Re_{eq} \leq 7,611$). It has been seen that, for the mass flux 270 $kg/m^2.s$ which corresponds to an equivalent Reynolds numbers $Re_{eq} \cong 2,100$, the model showed a smooth and gradually increase in pressure drop by increasing the vapor quality in the range of vapor quality of ($0.28 \leq x \leq 0.84$) and predicted very well the experimental pressure drop data. On the other hand, for the mass flux 510 $kg/m^2.s$, and $Re_{eq} \cong 4,000$, the model, noticeably, overpredicted the pressure drop data at low and intermediate vapor quality, and a slight decline in the trend can be observed at the vapor quality $x \cong 0.60$, where beyond this vapor quality the model gives a good agreement with the pressure drop data. Regards, to the mass flux 900 $kg/m^2.s$, and $Re_{eq} \cong 7,600$, a very well agreement with pressure drop data can be noticed in the range of vapor quality of ($0.40 \leq x \leq 0.70$), while after this vapor quality a slight decrease in pressure drop was predicted by the model. The decline positions, observed in the line graphs for the mass fluxes 510 and 900 $kg/m^2.s$ may represent the transition lines from slug flow to annular flow, and from annular flow to dry-out flow regime, respectively. Overall, for the equivalent Reynolds numbers, $2,000 \leq Re_{eq} \leq 7,600$ the model gave a good agreement with the measured pressure drop data of Hwang and Kim [166] with MAE of 16.98 %.

Additionally, in order to investigate the influence of fluid properties on the two-phase pressure drop in micro-channels, the present model has been compared with the two-phase pressure drop data measured for CO₂. For instance, Figure 4-11 shows a comparison between two-phase pressure drop data predicted by the present model and those measured by Ducoulombier et al [227] for flow boiling of the CO₂ in a 0.529 mm inner diameter micro-tube at low inlet saturation temperature $T_{sat} = -5$ °C, and a confinement number, $C_{conf} = 1.52$, with a ratio of heated length to inner diameter (L_h/D) = 360, and a low liquid to vapor density ratio of ($\rho_f/\rho_g = 11.47$). Noticeably, the figure showed that a gradual increase in pressure drop by increasing the mass and vapor quality can be seen. Moreover, the model predicted well the pressure drop data for the range of mass fluxes, (200 to 800 $kg/m^2.s$), and equivalent Reynolds

number of ($2,260 \leq Re_{eq} \leq 9,025$). However, the model slightly, overpredicted the pressure drop data for the mass flux, $1000 \text{ kg/m}^2 \cdot \text{s}$ and ($Re_{eq} \cong 11,280$) for the vapor quality range ($0.40 \leq x \leq 0.80$). Again, a marked decline can be observed at different positions on the line graphs, which are varied by increasing the mass flux. A possible explanation for this is the influence of mass flux on the boundaries of flow pattern regimes. Moreover, a sharp decline in pressure drop can be seen for low mass flux, $200 \text{ kg/m}^2 \cdot \text{s}$ at very high vapor quality, $x > 0.96$, and this could be attributed to the dry-out of the liquid film thickness at this vapor quality. The results of this comparison showed that the model gave a fairly good prediction of the pressure drop data of Ducoulombier et al. [227] which fall in the range of equivalent Reynolds number ($2,260 \leq Re_{eq} \leq 11,280$), with a MAE of 10.18 %.

Figure 4-12 presents the pressure drop of flow boiling of CO₂ in a 1.42 mm inner diameter mini-tube predicted by the present model, and compared with pressure drop data of Wu et al. [177] measured at a much lower inlet saturation temperature ($T_{sat} = -10 \text{ }^\circ\text{C}$), and a confinement number, $C_{conf} = 0.6$, with a lower ratio of heated length to inner diameter ($L_h/D = 211$), and a low liquid to vapor density ratio ($\rho_f/\rho_g = 13.83$), for mass flux range of 300 to $600 \text{ kg/m}^2 \cdot \text{s}$, and ($9,300 \leq Re_{eq} \leq 38,500$). The figure showed that there has been a noticeable underestimation by the model of the pressure drop data. However, the model predicted the pressure drop data in the mentioned range of equivalent Reynolds number with a MAE of 18.97 %. The degree of underestimation increases as the mass flux increases, and this can be attributed to the effect of the flow mode on the smoothness of the interface, and consequently on the flow instability of the flow pattern regime. Another possible explanation, for this underestimation, is that for $C_{conf} = 0.6$, the gravity force still plays a significant role and influences the model accuracy since it was neglected.

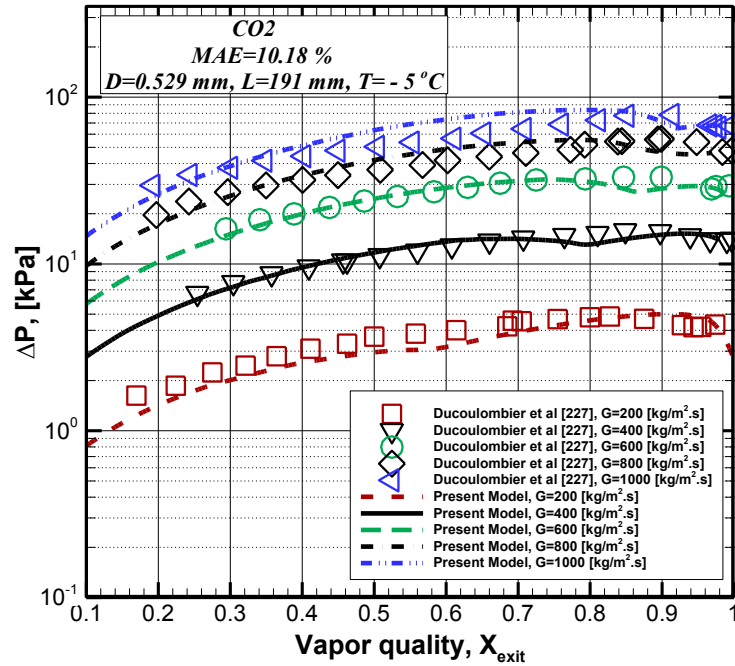


Figure 4-11: Comparison of pressure drop predicted by the present model with the experimental data of Ducoulombier et al. [227] for flow boiling of CO₂ at $T_{sat} = -5.0$ °C, through a circular micro-tube with $D=0.529$ mm, and heated length of 191 mm for mass fluxes range of 200 – 1000 $[kg/m^2.s]$.

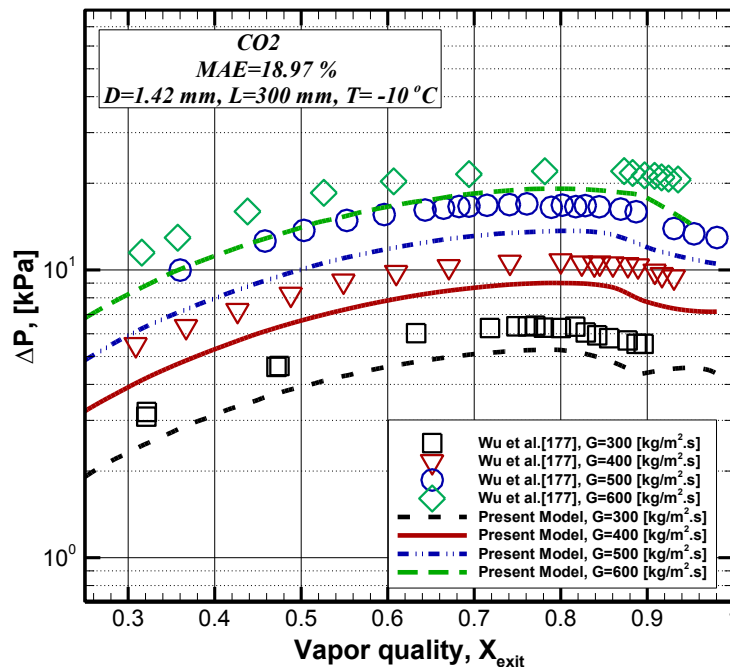


Figure 4-12: Pressure drop predicted by the present model versus vapor quality and compared with experimental data of Wu et al. [177] for flow boiling of CO₂ at $T_{sat} = -10$ °C, through a circular micro-tube with $D=1.42$ mm, and heated length of 300 mm, for mass fluxes range 300 – 600 $[kg/m^2.s]$.

In summary, the present model has been compared with 498 two-phase pressure drop data points of annular flow regime collected from the available literature for the working fluids and operating conditions shown in Table (4.2), corresponding to equivalent Reynolds numbers, $1,900 \leq Re_{eq} \leq 38,140$, heated length to inner diameter ratios, $90 \leq (L_h/D_h) \leq 580$, and saturation temperature range of, $-10^\circ\text{C} \leq T_{sat} \leq 40^\circ\text{C}$, that provide a wide range of liquid to vapor density ratio of $11.45 \leq (\rho_f/\rho_g) \leq 35.0$. The results predicted by the present model, along with collected experimental data have been plotted using Bland-Altman plot as shown in Figure 4-13. The calculated mean difference is Mean=-3.59, while the upper and lower limits of agreements are (ULOA=+18.75) and (LLOA=-25.95) respectively. As it can be seen, most of the data points (93.8 %) are fallen in the limits of the agreement. In general, the present model gave a good prediction for the two-phase pressure drop data points with a MAE of 23.02 %.

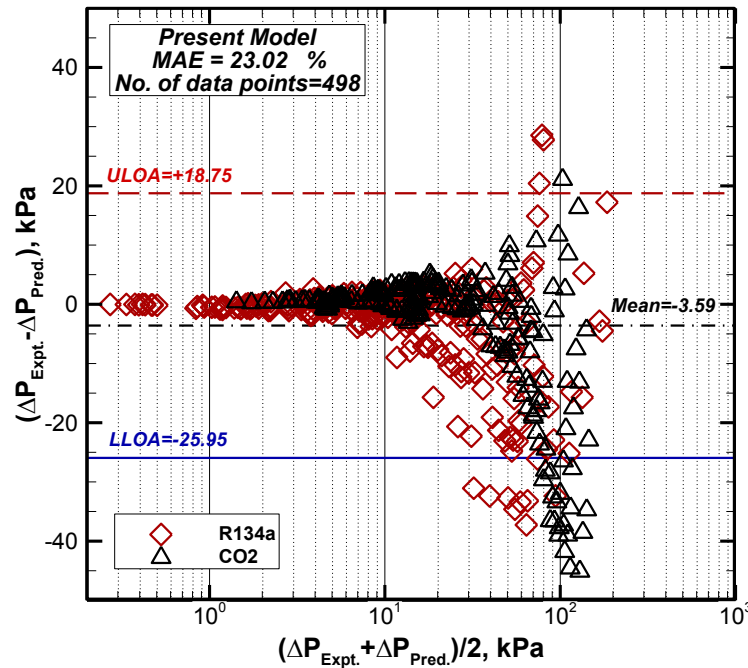


Figure 4-13: Using Bland-Altman Plot method for assessing the agreement between the average two-phase pressure drop predicted by the present model and those measured experimentally (498 data points) for various working fluids and flow conditions as shown in Table (4.2) for annular flow regime.

4.6.3. Void Fraction

Void vapor fraction for flow boiling in single micro-tubes has been calculated by the present model and compared with the experimental data measured by Shedd [228] for flow boiling of the refrigerant R410a in 0.508, 1.19, and 2.92 mm inner diameter single micro-tubes at inlet saturation temperature range from 43.5 to 50 °C and a range of mass flux from 200 to 800 [kg/m².s]. The results of vapor void fraction are presented as follows,

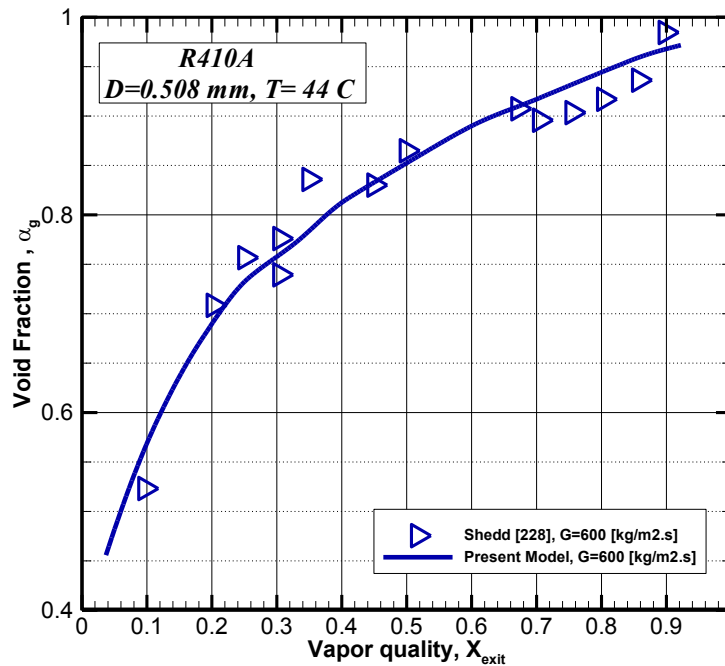


Figure 4-14: Void fraction versus vapor quality for flow boiling of R410a in 0.508 mm inner diameter tube at $T_{sat} = 44.0$ °C, and 600 [kg/m².s] mass flux.

Figure 4-14 shows the variation of vapor void fraction versus vapor quality predicted by the present model and those measured by Shedd [228] for flow boiling of R410a in 0.508 mm inner diameter tube at inlet saturation temperature 44 °C, and a confinement number, $C_{conf} = 1.14$, with mass flux of 600 [kg/m².s], which corresponds to an equivalent Reynolds number $Re_{eq} \cong 6,050$. It can be seen that the model predicted well the void fraction data in the range of vapor quality of $(0.10 \leq x \leq 0.90)$. However, a slight overprediction of the void fraction data can be observed beyond the vapor quality $x \geq 0.70$, which can be attributed to the transition

from annular flow to mist flow regime. For larger tube size, 1.19 mm, and the same mass flux, 600 [kg/m².s], and similar inlet saturation temperature, 43.5 °C, which matches a confinement number, $C_{conf} = 0.49$, and corresponds to a higher equivalent Reynolds number $Re_{eq} \cong 14,300$, the average vapor void fraction of the R410a, has been predicted and plotted together with the void fraction data of Shedd [228] as depicted in Figure 4-15. A steady increase in the void fraction predicted by the model can be observed for the void fraction fall in the vapor quality range of $(0.20 \leq x \leq 0.90)$, and a good agreement with the void fraction data points, which fall in the range of vapor quality of $(0.35 \leq x \leq 0.70)$, can be seen. Figure 4-16 presents the variation of vapor void fraction in terms of vapor quality predicted by the present model and those measured by Shedd [228] for flow boiling of R410a in a 2.92 mm inner diameter tube, with a higher inlet saturation temperature, 50 °C, and mass flux, 600 [kg/m².s], which matches an equivalent Reynolds number of $Re_{eq} \cong 35,400$, and confinement number, $C_{conf} = 0.27$. It has been seen that the model predicts the trend of void fraction in terms of vapor quality. Additionally, a good agreement with void fraction data can be seen for high vapor quality regime, $(0.65 \leq x \leq 0.90)$, which suggests the dominance of annular flow regime in this range of vapor quality. Furthermore, according to a flow pattern map developed by Shedd [228] for the flow of R410a in the same tube size and exact working conditions, the annular flow regime boundaries fall in the range of vapor quality of $(0.60 \leq x \leq 1.0)$. However, an obvious overprediction can be observed for the void fraction data fall in low and intermediate vapor qualities $(0.15 \leq x \leq 0.65)$. A possible explanation for this is that for the slug flow regime the void fraction is lower than that for the annular flow, and the present model was developed based on the annular flow. One more explanation is that the scale effect plays a significant role for $C_{conf} = 0.27$, where the gravity factor cannot be neglected anymore. Therefore, this result suggests the limit of the present model at this equivalent Reynolds number and tube size.

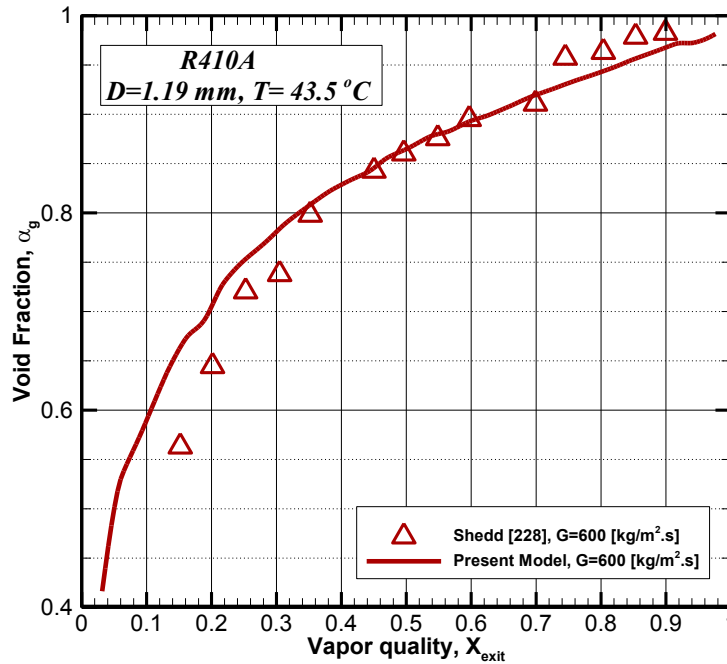


Figure 4-15: vapor void fraction versus vapor quality for flow boiling of R410a in 1.19 mm inner diameter tube at $T_{sat} = 43.5$ °C, and 600 [kg/m².s] mass flux.

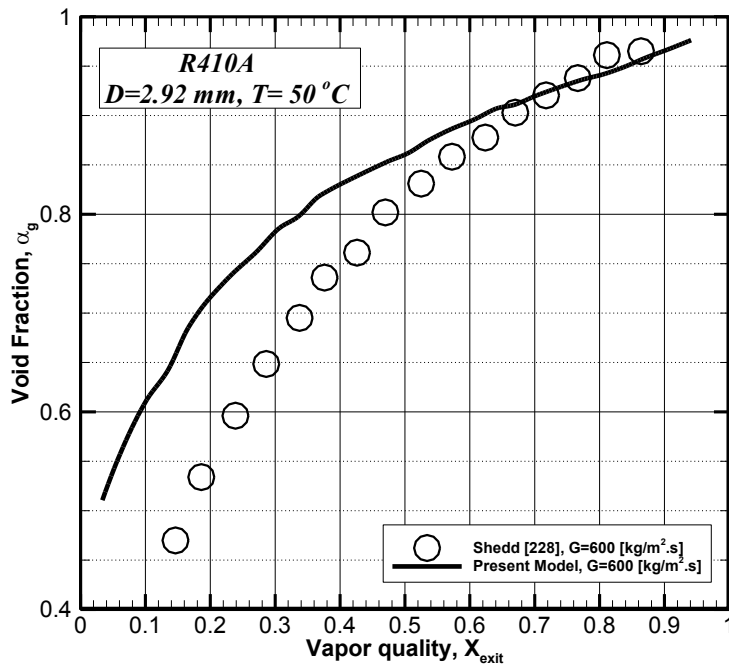


Figure 4-16: Void fraction versus vapor quality for flow boiling of R410a in 2.92 mm inner diameter tube at $T_{sat} = 50.0$ °C, and 600 [kg/m².s] mass flux.

Overall, the vapor void fraction of the flow boiling of the R410a has been calculated by the present model and compared with 153 void fraction data points measured by Shedd [228] for

the working conditions listed in Table (4.3), which correspond to a range of equivalent Reynolds number, $(2,160 \leq Re_{eq} \leq 48,000)$, and confinement number, $(0.27 \leq C_{conf} \leq 1.14)$. The results are shown in Figure 4-17, and a good agreement with void fraction data can be observed where the majority of the void fraction data points were predicted and fall in the limits of agreement, with a MAE of 3.22 %.

Table (4-3): Test conditions of vapor void fraction data of R410a measured by Shedd [228] and used here for model validation

| Hydraulic diameter | Saturation Temperature | Mass flux |
|--------------------|------------------------|-----------------------|
| $D_h, [mm]$ | $T_{sat}, [^{\circ}C]$ | $G, [kg/m^2 \cdot s]$ |
| 0.508 | 44.0 | 200, 400, 600, 800 |
| 1.19 | 44.0 | 200, 400, 600, 800 |
| 2.92 | 50.0 | 200, 400, 600, 800 |

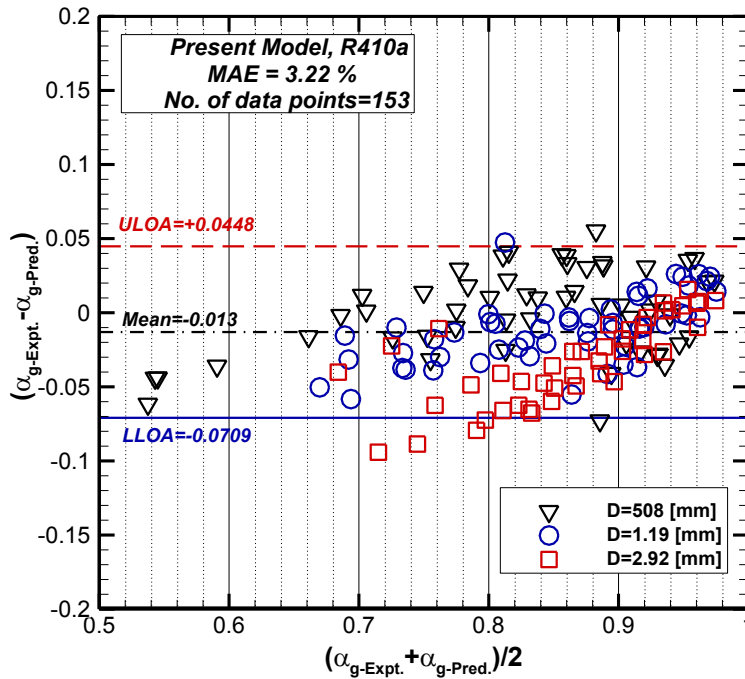


Figure 4-17: Comparison of vapor void fraction predicted by the present model with those of Shedd [228] for flow boiling of R410a in 0.508, 1.19, and 2.92 mm inner diameter tubes at $T_{sat} = 44.0$ to 50.0 °C, and range of mass fluxes, 200 to $800 [kg/m^2 \cdot s]$.

4.6.4. Vapor and Liquid Film Velocities

Vapor core, and liquid film velocities are modeled and calculated by the main model equation, Eq. (4.31). It is of interest to present a sample of calculated velocities here. Therefore, the vapor and liquid film velocities for flow boiling of CO₂ in 1.42 mm inner diameter tube were presented here. Figure 4-18 shows the variation of average vapor velocity versus the vapor quality predicted by the present model for flow boiling of CO₂ in 1.42 mm inner diameter tube with a ratio of heated length to inner diameter ($L_h/D \cong 210$), at a low inlet saturation temperature, -10 °C, for a range of mass fluxes, 300 to 500 [kg/m².s], which correspond to a range of equivalent Reynolds number, ($8,700 \leq Re_{eq} \leq 14,800$). The figure shows that there has been a steady increase in vapor velocity by increasing the vapor quality. Furthermore the model predicted the influence of mass flux on the vapor velocity, where it can be seen that the higher mass flux is, the higher vapor velocity predicted.

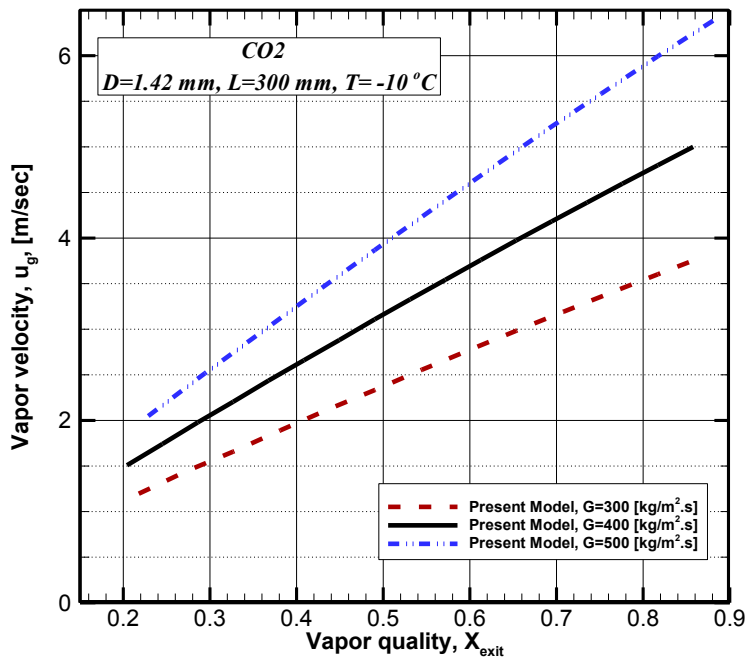


Figure 4-18: Average vapor velocity versus vapor quality predicted by the present model for flow boiling of CO₂ in 1.42 mm inner diameter tube at $T_{sat} = -10$ °C, and operating conditions similar to those of Wu et al. [177] as listed in Table (4.1).

For the same working conditions, the average liquid film velocity has been calculated by the present model, and plotted as shown in Figure 4-19. Looking to the figure, a similar trend of the liquid film velocity can be noticed at the three mass fluxes. For the mass flux 300 [kg/m².s], ($Re_{eq} \cong 8,700$), the liquid film velocity tends to slightly increase at the low vapor quality, ($x \leq 0.3$), and then it is likely to level off in the vapor quality range ($0.30 \leq x \leq 0.5$), after this, there has been a gradually decrease in liquid film velocity by increasing the vapor quality. According to the flow pattern map updated by Cheng et al. [103] for CO₂, the boundaries of annular flow regime corresponding to mass flux 300 [kg/m².s] are fallen in the vapor quality range, ($0.23 \leq x \leq 0.72$). It is of importance to mention here that these boundary values of vapor quality represent the center line of transition lines, since the transition from flow pattern to another does not occur instantly. With regards to the other two mass fluxes, 400, and 500 [kg/m².s], a slow decrease in liquid film velocity for ($0.4 \leq x \leq 0.68$), and ($0.45 \leq x \leq 0.62$), can be observed, and then a sharp decline in the liquid film velocity can be seen. The significance of this result in addition to showing the trend of liquid film velocity, is that it would be helpful to predict the transition line from annular flow to mist/dry-out flow regime. In other words, a slight fluctuation at $x=0.65$, and $x=0.67$ for the mass fluxes 400, and 500 respectively, has been observed, and these points are very close to those suggested by the flow pattern map updated by Cheng et al. [103] for CO₂.

4.6.5. Liquid Film Thickness

Liquid film thickness for various working fluids listed in Table (4.1), and Table (4.2) have been calculated by the present model, based on the relation between the modeled vapor void fraction and liquid film thickness which represented by Eq. (4.21). A sample of the obtained results for flow boiling of CO₂ in 1.42 mm inner diameter is presented and discussed in this section. Figure 4-20 shows the variation of liquid film thickness versus the vapor quality predicted by the present model for flow boiling of CO₂ in 1.42 mm inner diameter, with a mass flux, 300 [kg/m².s], which corresponds to, $Re_{eq} \cong 8,700$, at an inlet saturation temperature -10 °C . It can be noticed from the figure that the liquid film thickness decreases by increasing the vapor quality, and the mass flux. Moreover, the relationship between the liquid film thickness and vapor quality is nonlinear in the annular flow regime (i.e. for this case $0.2 \leq x \leq 0.8$), after

this, a sharp decrease in liquid film thickness can be observed, and this of course is due to the onset of dry-out phenomenon.

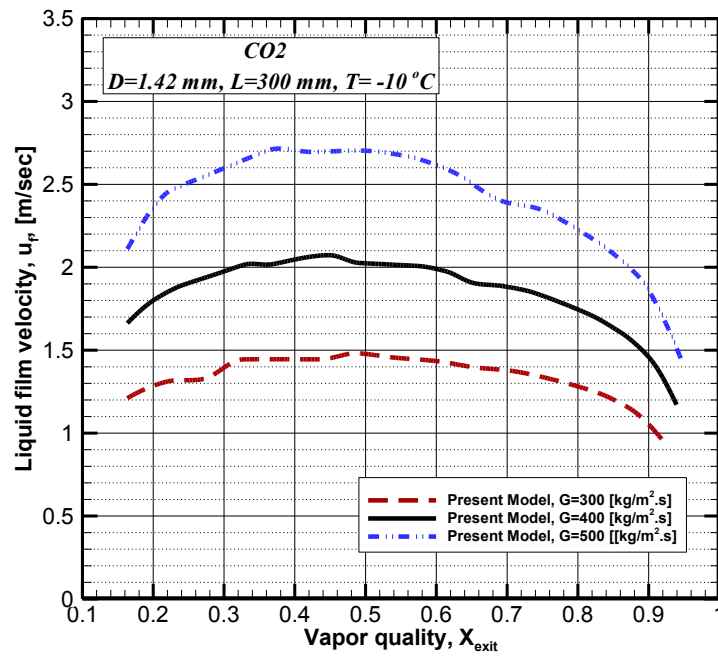


Figure 4-19: Liquid film velocity versus vapor quality predicted by the present model for flow boiling of CO₂ in 1.42 mm inner diameter tube at $T_{sat} = -10$ °C, and operating conditions similar to those of Wu et al. [177] as listed in Table (4.1).

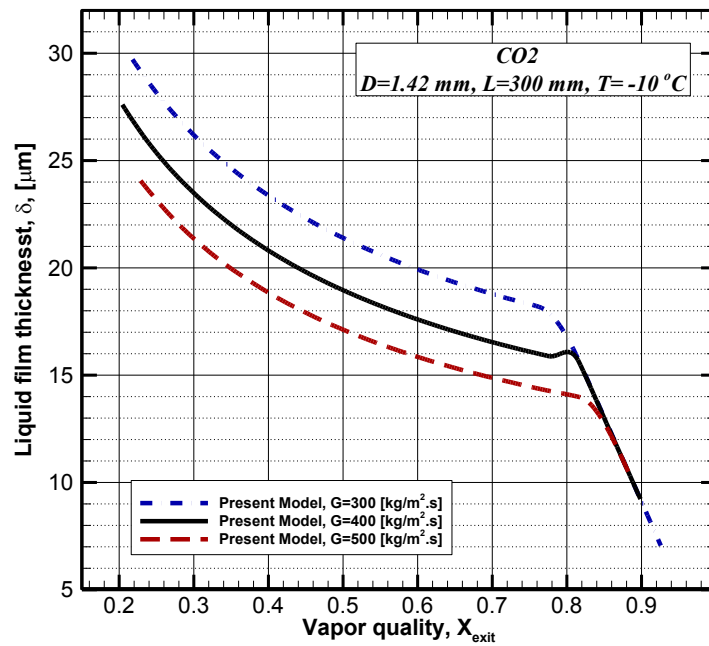


Figure 4-20: Liquid film thickness versus vapor quality predicted by the present model for flow boiling of CO₂ in 1.42 mm inner diameter tube and the working conditions of Wu et al. [177] presented in Table (4.1).

4.7. Sensitivity Analysis of the Model

The influence of the initial liquid film thickness which is calculated by Eq. (4.33), and Eq. (4.34) on the two phase heat transfer coefficient has been discussed by performing the sensitivity analysis of the model. The analysis was performed for results predicted by the present model for flow boiling of CO₂ in a 1.42 mm inner tube diameter for saturation conditions at -10 °C, with a mass flux, 300 [kg/m².s], and for a range of vapor quality of 0.3 ≤ x ≤ 0.8. Figure 4-21 shows the influence of initial liquid film thickness on the performance of the present model for predicting the two-phase heat transfer coefficient in annular flow regime.

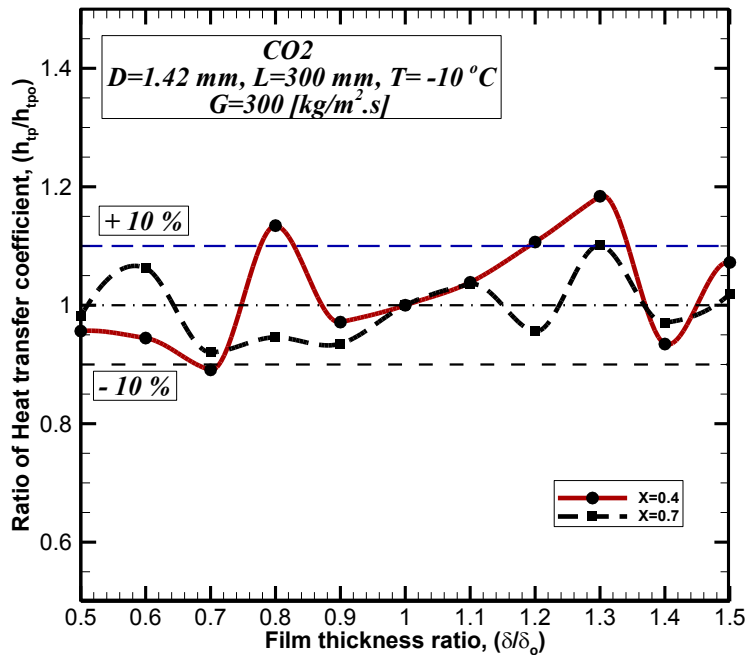


Figure 4-21: Sensitivity analysis of the two-phase heat transfer coefficient predicted by the present model to the initial liquid film thickness.

It can be seen that for the vapor quality, x=0.7, decreasing or increasing the initial liquid film thickness by ± 50 %, the deviation in the heat transfer coefficient does not exceed ± 10 %. On the other hand, for the vapor quality, x=0.4, it can be seen that the heat transfer model is more sensitive to the initial liquid film thickness. One possible explanation for this is that, at the vapor quality, x=0.4, the flow pattern could be slug flow pattern or coalescence bubble pattern which is close to the transition line, where the liquid film thickness fluctuates and becomes unsteady. As the vapor quality increases, the model is less sensitive to the initial liquid film

thickness. Therefore, in the range of annular flow regime, the sensitivity level of the model to the initial liquid film is reasonable, and acceptable.

4.8. Conclusions

A semi-analytical model to predict the two-phase heat transfer, pressure drop, and void fraction in annular flow regime for flow boiling in a horizontal micro-channel subjected to a uniform heat flux, has been developed based on the separated flow model. The influences of working fluid, channel size, and operating conditions on the two-phase heat transfer, pressure drop, and void fraction have been considered. It has been noticed that, in the annular flow regime, the two-phase heat transfer coefficient, pressure drop, and void fraction increase with mass flux and exit vapor quality. The model has been compared with 1,253 experimental data points, collected from the available literature, for model validation. The model was compared with 602 two-phase heat transfer data for flow boiling conditions that cover a range of equivalent Reynolds number $2,000 \leq Re_{eq} \leq 18,350$, and a range of confinement number, $0.3 \leq C_{conf} \leq 1.8$. The heat transfer data were predicted with model with a MAE of 18.14 %. Furthermore, the model was compared with 498 pressure drop data points, which fall in the range of equivalent Reynolds number $1,900 \leq Re_{eq} \leq 38,400$, and confinement number, $0.32 \leq C_{conf} \leq 3.4$, and showed a good agreement with the data with a MAE of 23.02 %. Regards to the void fraction, the model was compared with 153 void fraction data points corresponded to $2,150 \leq Re_{eq} \leq 48,000$, and $0.27 \leq C_{conf} \leq 1.14$, and predicted the data with a MAE of 3.22 %. The applicability of the present model can be limited in terms of equivalent Reynolds number and confinement number together. Overall, the present model is applicable for $1,900 \leq Re_{eq} \leq 18,000$, and $0.5 \leq C_{conf} \leq 3.4$. Moreover, two main applications of the present model can be addressed here. Firstly, estimating the cooling load of the micro-channel heat sink based on the operating condition. Secondly, predicting the two-phase pressure drop in the same flow regime, and hence, estimating the pumping power required for circulating the working fluid at the applied conditions. It is of interesting to point out here, that the present model may be extended for the future work by considering the surface tension effect, and force gravity to improve the model accuracy and expand its applicability range, and to be used for predicting the annular flow regime boundaries.

Chapter 5

5. Investigation of Bubble Frequency in Slug Flow Regime for Flow Boiling in a Single Round Uniformly Heated Horizontal Micro-Channel

Amen Younes¹, Ibrahim Hassan^{2*}, Lyes Kadem¹

This paper was submitted to *J. of Heat Transfer*, and is under review.

¹Department of Mechanical and Industrial Engineering, Concordia University,
1455 de Maisonneuve Blvd. W, Montreal, QC, Canada, H3G 1M

²Mechanical Engineering Department, Texas A&M University at Qatar
P O Box 23874, Doha, Qatar

5.1. Abstract

Slug flow is an essential flow pattern observed in micro-channels where its transition boundaries in micro-channels are characterized by two complex hydrodynamic phenomena, bubble confinement and bubble coalescence. Slug flow can be classified in terms of bubble size into two major zones, which are the isolated bubble zone and coalescence bubble zone. In this paper, a semi-analytical model for predicting the main characteristics of slug flow pattern (isolated bubble zone), including the bubble frequency, for flow boiling in a horizontal micro-channel is developed for diabatic flow conditions. The influences of surface tension, shear, and inertial forces are taken into account. The model is developed based on the principle of drift flux model, and a fully developed slug unit is chosen as a control volume for deriving the equations of motion. The effects of main operating conditions, mass and heat fluxes, on bubble length and bubble frequency have been investigated. The transition lines which represent the boundaries of slug flow regime have been estimated based on the most proper diabatic flow pattern map available in the literature for the chosen database. The model has been validated using the bubble length and frequency database available in the literature for flow boiling of two working fluids. The first one is R134a in a 0.509 mm inner diameter horizontal micro-tube for wide range of mass fluxes, ($300 \leq G \leq 1000 \text{ kg/m}^2 \cdot \text{s}$), which corresponded to liquid Reynolds numbers $970 \leq Re_l \leq 3,400$, and confinement number $C_{\text{conf}} \cong 1.6$. The second working fluid is R245fa flowing in a 3.0 mm inner diameter horizontal mini-tube for a range of mass fluxes ($300 \leq G \leq 700 \text{ kg/m}^2 \cdot \text{s}$), which corresponded to liquid Reynolds numbers, $3,390 \leq Re_l \leq 7,900$, and confinement number, $C_{\text{conf}} \cong 0.3$. This study has shown that the mass flux has a significant effect on the slug length and bubble frequency. The model gave a good agreement with the data of bubble length and bubble frequency with a mean absolute error of 27.83 % and 29.55 %, respectively.

KEY WORDS: flow boiling, horizontal mini/micro-channels, drift flux model, transitional velocity, slug flow pattern, bubble dynamics, bubble frequency, isolated bubble zone, pressure drop.

5.2. Introduction

Flow boiling micro-channels are widely used and have many applications, extensively in heat sinks and compact heat exchangers. Typically, the main principle of micro-channel heat sinks is to dissipate a high heat flux at a lower mass flux. Slug flow is promised to be one of the dominant flow patterns in flow boiling in micro-channels, and characterized by its complicated behaviour. Several experimental studies have been done for investigating slug flow characteristics in micro-channels (e.g., Triplett et al. [70]; Garimella et al. [79]; Lee et al. [118]; Revellin et al. [91]; Saisorn and Wongwises [80]; Fu et al. [119]; and Charnay et al [108]), and numerous numerical studies have attempted to simulate and study hydrodynamics of slug flow in micro-channels (e.g. Qian and Lawal [229]; He and Kasagi [230]; Zhuan and Wang [231]; and Magnini et al. [232]). On the other hand, only few attempts have been made to analytically predict slug flow characteristics in micro-channels (e.g. Moriyama et al. [8]; Abiev [233]; Consolini and Thome [145]).

Bubble growth rate is a key parameter for studying bubble dynamics particularly in bubbly flow regime where the onset of nucleate boiling is observed. A good attention for bubble nucleation, growth, and departure for two-phase flow has been paid in the past. Cooper [234] studied analytically the effect of micro-layer evaporation on the bubble growth rate in a liquid on a heated wall, and highlighted the significance of the micro-layer evaporation and surface tension on the bubble growth rate. Mikic et al. [235] have developed an analytical relation for predicting bubble growth rate, based on Rayleigh's equation, taking into account the influence of inertial force and thermal diffusion on the bubble growth rate in a uniformly superheated liquid. Lee et al. [118] experimentally investigated bubble dynamics for convective boiling in micro-channels and concluded that bubble growth rate is controlled by inertia force, while bubble departure is influenced by surface tension.

Liquid film is promised to dominate heat transfer mechanism in slug flow and annular flow regimes. In their analysis of modelling elongated bubble zone in micro-channels, Jacobi and Thome [114] confirmed that liquid film evaporation is a dominant heat transfer mechanism in this regime. Recently, Consolini and Thome [145] have developed a heat transfer model for predicting two-phase heat transfer coefficient for confined coalescing bubble flow which is

observed at an intermediate vapor quality. They considered the influence of liquid mass redistribution during bubble coalescing and predicted the coalescing bubble frequency where they found that it decreases with increasing the vapor quality. Additionally, they revealed that the liquid film evaporation dominates heat transfer mechanism in slug flow regime. Furthermore, the complex phenomenon of the slug flow is promised to enhance the heat transfer mechanism for flow boiling in micro-channels. Mehta and Khandekar [236] have recently investigated the effects of slug flow on the heat transfer coefficient by employing the Infrared Thermography techniques by creating a water/air intermittent flow in a $5\text{ mm} \times 5\text{ mm}$ square microchannel. It has been verified that slug flow provides a local time-averaged Nusselt number 1.2 to 2.0 higher than that obtained by liquid single phase at the same conditions. Similarly, in a study conducted by Patil and Kandlikar [237], for investigating the effects of micro-porous coating on heat transfer in pool boiling in open micro-channels, it has been found that departing bubbles enhanced heat transfer coefficient, and the porous coating of the chip-tops enhanced the critical heat flux (CHF).

Revellin et al. [91] experimentally investigated, using an optical technique, bubble coalescence and measured bubble velocity, bubble length, and bubble frequency for flow boiling of R134a in 0.509 mm inner diameter circular horizontal micro-tube at 30 °C inlet saturation temperature. In their study, they observed four main flow patterns and the transition lines, namely, bubbly, slug, semi-annular, and annular flow regimes. They highlighted the importance of bubble coalescing frequency in defining the transition line of the flow pattern. Moreover, they performed their experiments for a wide range of mass fluxes $350 \leq G \leq 2000$ [kg/m².s], and observed that the higher the mass flux is the narrower vapor quality range is for the bubble coalescence regime. Furthermore, at very high mass flux, the bubbly flow regime is hardly observed.

Recently, Tibirica and Ribatski [109] investigated bubble characteristics of flow boiling of R134a, and R245fa in a 0.4 mm inner diameter micro-tube for a range of mass flux of $100 \leq G \leq 900$ [kg/m².s], and at a uniform heat flux up to $q_w'' \leq 226$ [kW/m².s]. They performed flow visualization with a high speed optical technique (reaches to 10^5 fps) at diabatic conditions. They investigated the bubble departure diameter, bubble frequency, and liquid film characteristics. Furthermore, they assessed the available correlations of bubble departure

diameter and proposed new correlations for predicting bubble departure diameter and bubble frequency for flow boiling in horizontal small tubes. They assumed that inertial and drag forces dominate bubble departure mechanism, and therefore, bubble departure diameter is mainly influenced by the Reynolds number. It is somewhat surprising that the buoyancy effect is still observed for such a small tube size as well as the liquid entrainments in the vapour core, which have been related to the interface instability. Furthermore, contrary to the expectations, the authors pointed out that nucleation sites have been presented in all flow patterns including the annular flow regime for the test in the 0.4 mm inner diameter micro-tubes.

A study of the transient effects of bubbles in the slug regime in micro-channels has been recently carried out by Houshmand and Peles [238] based on the transient wall temperature measurement, and flow visualization. The micro-scale resistance temperature detectors technique (RTDs) was introduced as an effective method for measuring the transient wall temperature. The slug flow pattern was created by mixing the distilled water with an air injected with an average frequency of $f_b \cong 277 \text{ bubbles/sec}$. Three different zones were identified in the slug flow regimes, which are elongated bubble zone, the bubble wake zone, and the single phase liquid slug zone. It has been pointed out that the wall temperature increased in the elongated bubble zone due to the small thickness of the liquid film, while decreased in bubble wake zone due to the influence mixing caused by the small bubbles followed the wake of the elongated bubble.

To study slug behaviour and bubble characteristics of adiabatic flow, Yan et al. [239], performed flow visualization experiments on air/water flowing in a narrow rectangular duct, $D_h \cong 6.0 \text{ mm}$, considering the influence of inclination angle, gas, and liquid superficial velocities on the slug characteristics (slug velocity, length, and frequency). Based on the liquid Reynolds number, the authors defined two major regions of the flow, laminar flow region, which is defined as, $Re_l < 3000$, and turbulent flow region, which is defined as, $Re_l \geq 3000$. It has been revealed that the effect of the inclination angle on slug length and velocity was pronounced in the laminar flow region, while it did not show a remarked effect in the turbulent flow region. In other words, as the inclination angle decreases for laminar flow region, the slug length and velocity increase. On the other hand, it has been revealed that increasing the gas superficial velocity leads to increasing the slug length and decreasing the slug frequency. Since, these results have been obtained for adiabatic conditions, and the slug flow is created by mixing the air

with the injected water, it still does not show the influence of bubble nucleation, and applied heat flux on the bubble frequency and slug characteristics.

Overall the previous studies indicate that most of the methods available for modeling slug flow in micro channels have been developed basically for adiabatic conditions, and do not consider the contribution of the applied heat flux in the model basic equations. Thus, more analytical efforts for studying flow boiling slug flow in micro-channels are required. The aim of this work is to develop an analytical model for predicting the main slug flow parameters in the isolated bubble zone (i.e., from the onset of bubble confinement to the onset of bubble coalescence) for flow boiling in horizontal micro-channels. Therefore, a complete slug flow unit has been considered to be a control volume for deriving the three basic equations of motion for each phase, taking into account the principle of drift flux model and the influence of surface tension for more realistic slug flow conditions in micro-channels.

5.3. Analysis of the Two Phase Slug Flow Model

Slug flow is promised to be one of the main dominant flow patterns for flow boiling in micro-channels as it has been verified in many previous studies. It is characterized by its complex physical and periodic phenomenon. An ideal slug flow pattern of flow boiling in horizontal mini/micro-channels is represented by three main zones, which are the confined bubble, the liquid film thickness δ trapped between the confined bubble and the channel wall, and the liquid slug zone. In order to understand and simplify the analysis of this physical phenomenon, the present model consists of two main stages. Firstly, derive the equations of motion (mass, momentum, and energy equations) for a fully developed slug flow unit in order to predict the slug unit length, the liquid film velocity and the liquid slug velocity. Secondly, the mass balance of the whole mixture of the slug flow unit is derived to predict the variation of the liquid slug length, bubble length, and void fraction as a function of time.

5.3.1. Basic Assumptions

A set of assumptions has been considered here for simplifying the complexity of modelling slug flow. These assumptions are listed below,

1. All the thermo-physical properties are assumed to be constant at a certain saturation temperature.
2. The slug flow unit is fully developed and the two phases are in thermodynamic equilibrium.
3. The onset of slug flow is determined by the onset of bubble confinement in flow boiling micro-channels (i.e., when the bubble length is equal to channel diameter).
4. The applied heat flux is uniformly distributed circumferentially and axially along the channel length.
5. At the onset of bubble confinement, the volume change rate of the confined bubble is equal to the volume change rate of a spherical bubble growing in an infinite liquid on a uniformly heated surface.
6. The pressure in the elongated bubble is constant and the pressure drop through the slug unit is equal to the pressure difference between the pressure inside the bubble and the pressure of the liquid slug.
7. The dominant heat transfer mechanism in the elongated bubble zone is the convective liquid film evaporation, and the two-phase heat transfer is estimated based on the liquid film thickness for this zone, while in the liquid slug zone, the heat transfer coefficient is evaluated using an appropriate liquid single phase correlation.

5.3.2. Derivation of the Equations of Motion

Figure 5-1 shows an ideal fully developed slug flow unit with a length of L_u , which consists of a vapor bubble with a length of L_b and moves with a velocity u_b , the liquid film with a thickness δ and moves with a velocity u_f , and the liquid slug that moves with a velocity u_s and length of L_s . Choosing the control volume which considers the major physical parameters is very crucial for developing more realistic slug flow model, thus, a fully developed and complete slug unit has been chosen to represent the control volume required for deriving the equations of motion of the slug flow. Additionally, all the equations of motion will be derived relative to the translational velocity u_t of the slug unit. As it is assumed at a certain time, the features of the slug flow are regular and uniform along the micro-channel within the slug flow boundaries. Consequently, one can derive the governing equations for a fully developed slug flow as follows.

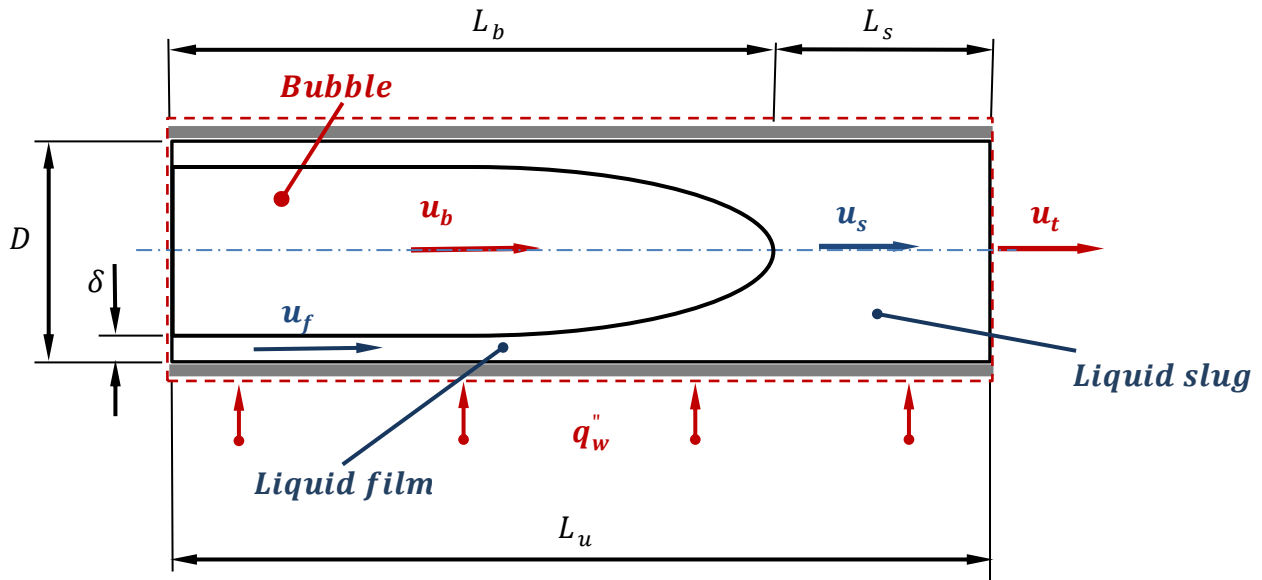


Figure 5-1: Sketch of fully developed slug flow unit for flow boiling in a horizontal micro-channel.

5.3.2.1. Mass Conservation Equations

The mass balance has been applied for each phase, liquid phase, which is represented by the liquid film and liquid slug zones, and vapor core phase, which is represented by an elongated bubble zone. The control volume has been chosen to contain an ideal and a complete slug flow unit as shown in Figure 5-1. Considering a one dimensional fully developed slug flow as depicted in Figure 5-2, the mass conservation equation for the liquid phase can be written as follow,

$$\rho_f(u_s - u_t) - \rho_f\alpha_f(u_f - u_t) = -\Gamma L_u \quad (5.1)$$

Where u_s is the phasic liquid slug velocity, and u_f is the phasic liquid film velocity, u_t is the translational velocity of the slug unit, L_u is the slug unit length, ρ_f the liquid phase density, Γ is the evaporation volumetric flow rate occurs at the liquid-vapor interface due to the phase change, and α_f is the void fraction of the liquid phase. The mass conservation of the vapor phase is expressed as follows:

$$-\rho_g \alpha_g (u_b - u_t) = \Gamma L_u \quad (5.2)$$

Where α_g is the void fraction of the vapor phase, u_b is the bubble velocity. Adding Eq. (5.1) to Eq. (5.2), the mass conservation equation for the whole mixture of the slug flow unit is written as follows:

$$\rho_f (u_s - u_t) - \rho_f \alpha_f (u_f - u_t) - \rho_g \alpha_g (u_b - u_t) = 0 \quad (5.3)$$

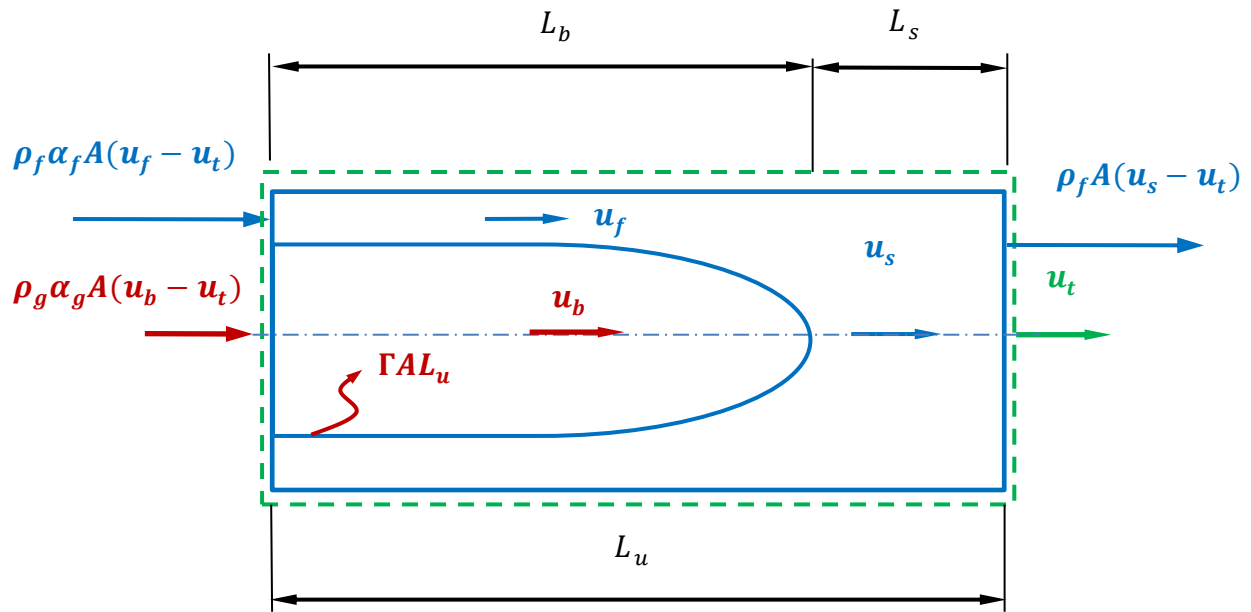


Figure 5-2: A sketch of a control volume of a slug flow unit for deriving mass balance equation.

5.3.2.2. Momentum Conservation Equations

Figure 5-3 shows the momentum terms and forces acting on the liquid phase. Considering the evaporation volumetric flow rate as defined in Eq. (5.2), the momentum conservation equation of the liquid phase for the slug unit can be derived as follows:

$$\begin{aligned} & \rho_f(u_s - u_t)^2 - \rho_f\alpha_f(u_f - u_t)^2 + \rho_g\alpha_g(u_b - u_t)u_i \\ & = \alpha_f p_1 - p_2 - \tau_w \frac{P_w L_u}{A} - \frac{F_{sw}}{A} - \tau_i \frac{P_i L_b}{A} - \frac{F_{si}}{A} \end{aligned} \quad (5.4)$$

Where u_i here is the liquid velocity at the interface, p_1 is the pressure applied at the left-hand side of the considered slug unit, p_2 is the pressure applied at the right-hand side of the slug unit, τ_w is the wall shear stress, τ_i is the shear stress at the interface, P_w is the micro-tube perimeter, P_i is the perimeter at the interface, F_{sw} is the force acting on the liquid phase at the wall due to the surface tension, F_{si} is the surface tension force acting from the other phase at the interface, and L_b is the bubble length.

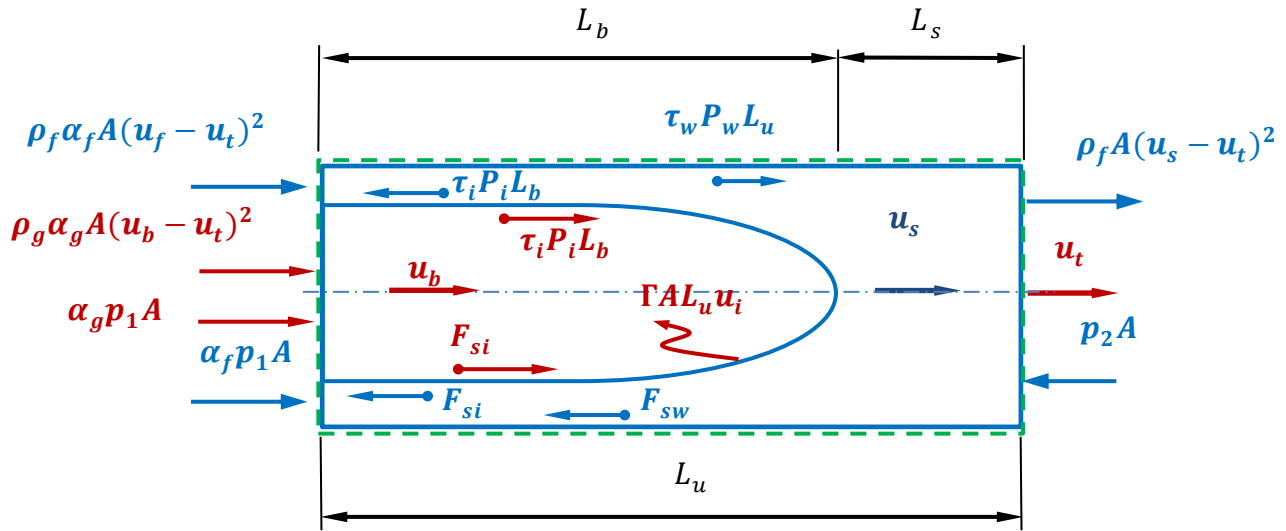


Figure 5-3: A sketch of control volume of a slug flow unit for deriving Momentum conservation equation.

Turning to the vapor phase, the main momentum terms and considered forces acting on the vapor phase are shown on the slug unit as depicted in Figure 5-3. The momentum conservation of the vapor phase for a steady-state and fully developed slug flow unit is written as follows:

$$-\rho_g \alpha_g (u_b - u_t)^2 - \rho_g \alpha_g (u_b - u_t) u_i = \alpha_g p_1 + \tau_i \frac{P_i L_b}{A} + \frac{F_{si}}{A} \quad (5.5)$$

By combining Eqs. (5.4), and (5.5), taking into account that, $(\alpha_g + \alpha_f = 1)$, the interfacial terms are terminated, and one can get the momentum conservation equation of the whole mixture of the slug unit as follows:

$$\rho_f (u_s - u_t)^2 - \rho_f \alpha_f (u_f - u_t)^2 - \rho_g \alpha_g (u_b - u_t)^2 = -(p_2 - p_1) - \tau_w \frac{P_w L_u}{A} - \frac{F_{sw}}{A} \quad (5.6)$$

5.3.2.3. Energy Conservation Equations

Energy conservation equations for the slug unit are derived for liquid and vapor phases based on the sketch shown in Figure 5-4. Consequently, the energy conservation equation of the liquid phase is expressed as follows:

$$\begin{aligned} \rho_f (u_s - u_t) h_{f-out} - \rho_f \alpha_f (u_f - u_t) h_{f-in} + \rho_g \alpha_g (u_b - u_t) h_{fi} \\ = q_w'' \frac{P_w L_u}{A} - \tau_i \frac{P_i L_b}{A} u_i - \frac{F_{si}}{A} u_i \end{aligned} \quad (5.7)$$

Where h_{f-out} is the specific enthalpy of the liquid phase at the right-hand side of the slug flow unit, h_{f-in} is the specific enthalpy of the liquid phase at the left-hand side of the slug flow unit, h_{fi} is the specific enthalpy of the liquid phase at the interface, and q_w'' is the heat flux applied at the micro-tube wall. The energy conservation equation of the vapor phase is written as follows:

$$-\rho_g \alpha_g (u_b - u_t) h_g - \rho_g \alpha_g (u_b - u_t) h_{gi} = \tau_i \frac{P_i L_b}{A} u_i + \frac{F_{si}}{A} u_i \quad (5.8)$$

Where h_g and h_{gi} are the specific enthalpies of the vapor phase at the left-hand side of the slug flow unit and at the interface, respectively. Adding Eq. (5.7), to Eq. (5.8), and assuming equal enthalpies of the two phases at the interface, (i.e. $h_{fi} = h_{gi}$), the conservation energy equation of the mixture can be written as follows:

$$\rho_f(u_s - u_t)h_{f-out} - \rho_f\alpha_f(u_f - u_t)h_{f-in} - \rho_g\alpha_g(u_b - u_t)h_g = q_w'' \frac{P_w L_u}{A} \quad (5.9)$$

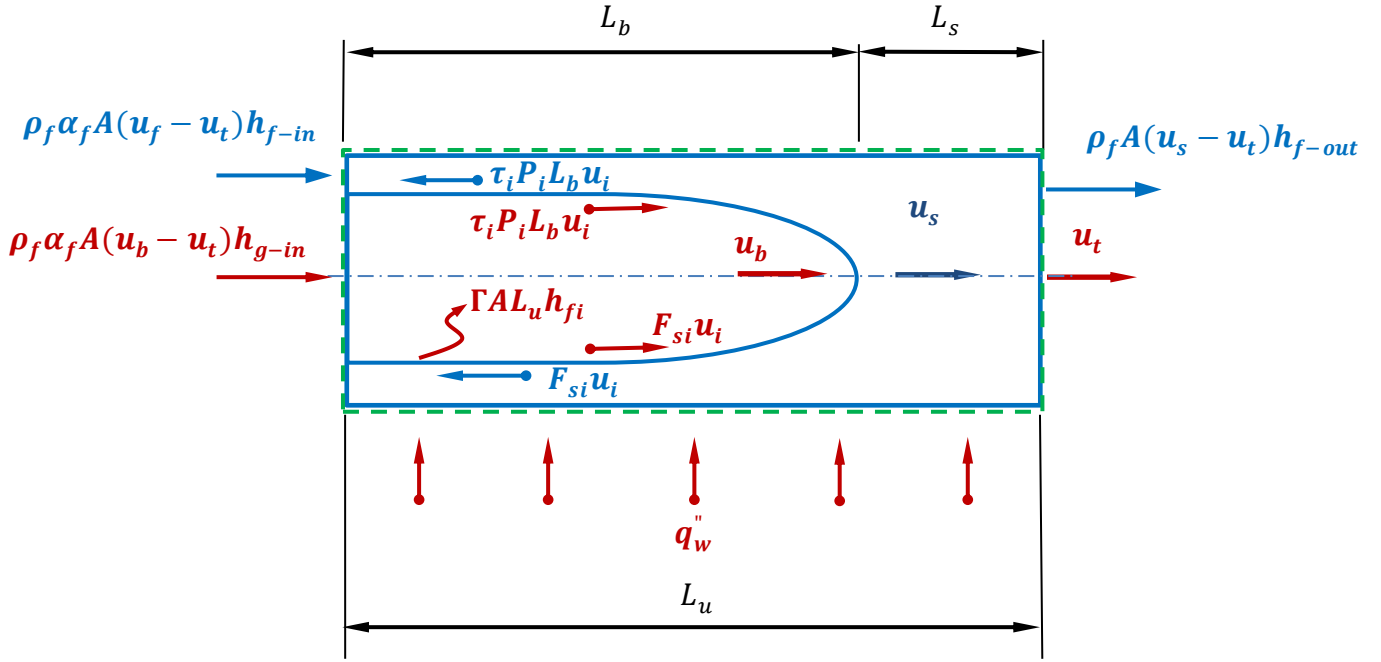


Figure 5-4: Shows the energy terms and works applied on the slug unit.

From the mass balance equation of the whole mixture Eq. (5.3), the relative liquid film velocity can be represented as follows:

$$(u_f - u_t) = \frac{1}{\alpha_f} (u_s - u_t) - \frac{\rho_g \alpha_g}{\rho_f \alpha_f} (u_b - u_t) \quad (5.10)$$

Substitute by relative liquid film velocity Eq. (5.10) in the energy equation of the whole mixture, Eq. (5.9), we get the relative liquid slug velocity as follow:

$$(u_s - u_t) = \left(\frac{\rho_g}{\rho_f}\right) \alpha_g (u_b - u_t) + \frac{1}{\rho_f} \left(\frac{4q_w''}{h_{fg}}\right) \left(\frac{L_u}{D}\right) \quad (5.11)$$

Now substitute by relative velocities of the liquid film and liquid slug, Eq. (5.10), and Eq. (5.11), respectively in the momentum equation of the whole mixture, Eq. (5.6), we obtain:

$$\begin{aligned} \rho_g \alpha_g \left(\frac{\rho_g}{\rho_f} \alpha_g - 1\right) (u_b - u_t)^2 - 2 \left(\frac{\rho_g}{\rho_f}\right) \alpha_g \left(\frac{4q_w''}{h_{fg}}\right) \left(\frac{L_u}{D}\right) (u_b - u_t) \\ - \left(\frac{1}{\rho_f}\right) \left(\frac{\alpha_g}{1 - \alpha_g}\right) \left(\frac{4q_w''}{h_{fg}}\right)^2 \left(\frac{L_u}{D}\right)^2 = -\Delta p - \tau_w \frac{P_w L_u}{A} + \frac{F_{sw}}{A} \end{aligned} \quad (5.12)$$

Now at this stage, we have seven parameters are still needed to be evaluated, vapor void fraction α_g , pressure drop Δp , surface tension force F_{sw} , wall shear stress τ_w , bubble velocity u_b , transitional velocity u_t , and the length of the slug unit L_u , which are explained and discussed in the following section.

5.3.3. Constitutive Relationships of the Model

There have been a few studies which modelled two-phase pressure drop for a segment of slug flow unit in terms of the slug flow characteristic lengths for two-phase flow in small and capillary tubes, (e.g. Bretherton [63], Fukanu et al. [240], Garimella et al. [79], Abiev [241]). Bretherton [63] gave a correlation for the estimation of the pressure drop through a single elongated bubble flowing in a capillary tube. Fukanu et al. [240] investigated experimentally, and analytically pressure drop of water-air flow in capillary tubes, and revealed that the expansion loss is dominant, and controls the pressure drop. Furthermore, it has been shown that the expansion loss increases by increasing the vapour velocity. In other words, as the bubble velocity increases due to the expansion, there is a liquid mass transfer, flowing from the liquid film into the liquid slug, and the bubble length increases while the liquid slug length decreases. Garemilla et al. [79] investigated the pressure drop for intermittent flow for flowing of R134a in small tubes, but for a condensation conditions. The pressure drop term in the present work will be evaluated based on Young-Laplace relation considering the influence of surface tension and fluid properties on pressure drop. In other words, it is reasonable to assume that for a fully

developed slug flow unit, the pressure drop through the slug flow unit equals to the pressure difference between the pressure inside the elongated bubble and the pressure in the liquid slug which can be defined using Young and Laplace relation as follow:

$$p_g - p_f = \sigma \left(\frac{1}{R_1} + \frac{1}{R_2} \right) \quad (5.13)$$

Where p_g , is the pressure inside the elongated bubble, p_f is the pressure in the liquid, R_1 and R_2 are the radii of the ends of the elongated bubble. We assume that the elongated bubble has a uniform and similar radii at the end, (i.e., $R_1 = R_2 = R_b$), R_b is denoted for bubble radius. Furthermore, considering the definition of cross sectional vapor void fraction as, ($\alpha_g = R_b^2/R^2$), the Eq. (5.13) is rewritten as follow,

$$\Delta p \cong - \frac{4\sigma}{\sqrt{\alpha}D} \quad (5.14)$$

It is known that the surface tension is dominant for flow boiling in micro-channels. Therefore, it is of importance to consider it here. Surface tension force is represented in terms of surface tension σ , contact line length L_c , and contact angle θ . For maximum value of surface tension force, the contact angle is assumed to be 180° , and the length of the contact line is the micro-tube perimeter πD . Consequently, the effects of surface tension force on a fully developed slug flow unit can be represented as follows,

$$F_{sw} \cong (\pi D)\sigma \quad (5.15)$$

Taking into account the pressure drop as represented by Eq. (5.14), and surface tension force as defined by Eq. (5.15), the momentum equation Eq. (5.12), can be recast as follows,

$$\begin{aligned} \rho_g \alpha_g \left(\frac{\rho_g}{\rho_f} \alpha_g - 1 \right) (u_b - u_t)^2 + \left(\frac{\rho_g}{\rho_f} \right) \alpha_g \left(\frac{8q_w''}{h_{fg}} \right) \left(\frac{L_u}{D} \right) (u_b - u_t) \\ - \left(\frac{1}{\rho_f} \right) \left(\frac{\alpha_g}{1 - \alpha_g} \right) \left(\frac{4q_w''}{h_{fg}} \right)^2 \left(\frac{L_u}{D} \right)^2 - \frac{4\sigma}{\sqrt{\alpha_g}D} + 4\tau_w \left(\frac{L_u}{D} \right) - 4 \frac{\sigma}{D} = 0 \end{aligned} \quad (5.16)$$

Now the wall shear stress τ_w , in the left side of Eq. (5.16), is estimated in terms of liquid film velocity and the working fluid density as given by,

$$\tau_w = \frac{1}{2} \rho_f f_f u_f^2 \quad (5.17)$$

For wide range of flow conditions which cover laminar transitional, and turbulent flow conditions, different correlations discussed in Li and Wu [74] for predicting friction factor have been employed including the correlation of Churchill [223] which takes into account the effect of the surface roughness. The frictional correlation are expressed as follows,

$$f_f = \begin{cases} f_1 & \text{for } Re_f \leq 1600 \\ f_2 & \text{for } Re_f \geq 3,000 \\ f_3 & \text{for } 1600 < Re_f < 3,000 \end{cases} \quad (5.18)$$

Where

$$f_1 = 16/Re_f \quad (5.19)$$

$$f_2 = \left[\left(\frac{8}{Re} \right)^{12} + \frac{1}{(a+b)^{3/2}} \right]^{1/12} \quad (5.20)$$

$$a = \left[2.457 \ln \frac{1}{(7/Re) + 0.27(\epsilon/D)} \right]^{16}; \quad b = \left[\frac{37530}{Re_f} \right]^{16}$$

$$f_3 = f_1(1600) + \frac{Re - 1600}{1400} [f_2(3000) - f_1(1600)] \quad (5.21)$$

Where Re_f is the based-liquid film Reynolds number which is calculated in the present model using the predicted values of average liquid film thickness $\bar{\delta}$, and average liquid film velocity \bar{u}_f at every heat and mass fluxes applied as follows,

$$Re_f = \frac{\rho_f \bar{u}_f D_h}{\mu_f} \quad (5.22)$$

The bubble velocity for slug flow in horizontal micro-channels has been correlated in some previous studies based on the drift-flux model, (e.g., Bretherton [63], Mishima and Hibiki [173], and Chen et al. [242]) and represented as follows:

$$u_b = C_o j \quad (5.23)$$

Where C_o is the distribution parameter for the bubbly and slug flow, which was correlated by Ishii [243] for horizontal slug flow in terms of vapor-to-liquid density ratio as follows,

$$C_o = 1.2 - 0.2 \sqrt{(\rho_g/\rho_f)} \quad (5.24)$$

And j is the superficial velocity which is defined as,

$$j = G \left(\frac{1-x}{\rho_f} + \frac{x}{\rho_g} \right) \quad (5.25)$$

To close the model for this stage, two closure relationships for cross sectional void fraction and translational velocity are needed. The translational velocity of the slug unit, u_t , is assumed to be equal to the two-phase superficial velocity (i.e., $u_t = j$).

The vapor quality in Eq. (5.25), is calculated based on the energy balance equation as,

$$x = 4 \frac{q_w'' L}{G h_{fg} D} \quad (5.26)$$

Thus the vapor cross sectional void fraction can be expressed as,

$$\alpha_g = \frac{Gx}{u_b \rho_g} \quad (5.27)$$

Finding a criterion for defining the bubble confinement is very crucial. In flow boiling micro-channel, the onset of slug flow is characterized by bubble confinement. Thus, the minimum bubble length considered in this model will be the inner diameter of the micro-channel, (i.e., $L_b \geq D$). Now, the length of the fully developed slug unit, L_u , can be calculated by solving Eq. (5.16). Regards to the liquid slug length, there have been some previous studies that investigated the relation between the bubble length and slug unit length or channel diameter or void fraction (e.g., Barnea and Brauner [244], Fukano et al. [240], Taitel et al. [245], and Abiev [241]). Overall, the liquid slug length is calculated in terms of bubble length, L_b , and liquid slug length, L_u , as

$$L_s = L_u - L_b \quad (5.28)$$

5.3.4. Evaluation the Variation of Bubble/Liquid Slug Lengths

At this stage of the present work, we consider the variation of the characteristics length of the slug unit in terms of time. Recalling the mass balance equation of the whole mixture of the slug unit one can write,

$$\frac{d}{dt}(\rho_f L_s + \rho_f \alpha_f L_b + \rho_g \alpha_g L_b) = -\rho_f(u_s - u_t) + \rho_f \alpha_f(u_f - u_t) + \rho_g \alpha_g(u_b - u_t) \quad (5.29)$$

Expanding the first derivation of the term on the left hand side, and taking into account that $(\alpha_g = \alpha)$, and $(\alpha_f = 1 - \alpha)$, the variation of the liquid slug length can be expressed as follows,

$$\begin{aligned} \frac{dL_s}{dt} = & \left(\frac{\rho_g}{\rho_f}\right) \alpha(u_b - u_t) + (1 - \alpha)(u_f - u_t) - (u_s - u_t) - \left[\left(\frac{\rho_g}{\rho_f} - 1\right) \alpha + 1\right] \frac{dL_b}{dt} \\ & - \left(\frac{\rho_g}{\rho_f} - 1\right) L_b \left(\frac{d\alpha}{dt}\right) \end{aligned} \quad (5.30)$$

The bubble in the slug unit elongates mainly in the flow direction, and the variation of bubble diameter in terms of time (dD_b/dt) comparing to bubble length variation (dL_b/dt) is very small. If we denote to the a volume of a confined elongated bubble as V_b , and the volume of spherical bubble grows in an infinite domain as V_s , then it would be reasonable to assume that the rate of change of the elongated bubble volume (dV_b/dt) in the slug unit is equal to that of a spherical bubble (dV_s/dt) growing on a surface and controlled by both thermal diffusion and inertial effects. Therefore, the relation developed by Mikic et al. [235] for predicting the rate of spherical bubble growth in a uniformly superheated liquid has been adopted here and modified to predict the variation of the elongated bubble length. The relation is given by

$$\frac{dR_s}{dt} = A_c [(t^+ + 1)^{(1/2)} - (t^+)^{(1/2)}] \quad (5.31)$$

Where R_s , is the radius of a spherical bubble grows in a uniformly superheated liquid, t^+ is a dimensionless time parameter which is defined as

$$t^+ = \left(\frac{A_c}{B_c}\right)^2 t \quad (5.32)$$

And A_c and B_c are defined as

$$A_c = \left[\frac{b\rho_g h_{fg} \Delta T}{\rho_f T_{sat}} \right]^{(1/2)} \quad (5.33)$$

$$B_c = \left[\frac{12}{\pi} Ja^2 D_f \right]^{(1/2)} \quad (5.34)$$

Where $b = (2/3)$ for a growing bubble in an infinite medium, and $b = (\pi/7)$ for a growing bubble on a surface, D_f is the liquid thermal diffusivity, and Ja is Jakob dimensionless number which is defined as,

$$Ja = \left[\frac{\rho_f C_{pl} \Delta T}{\rho_g h_{fg}} \right] \quad (5.35)$$

Now considering the above assumption, the rate of elongated bubble length can be expressed as follow,

$$\frac{dL_b}{dt} = 4A_c \left(\frac{R_s}{R_b}\right)^2 \frac{dR_s}{dt} \quad (5.36)$$

At the onset of bubble confinement (at time $t_o = D_b/u_b$), we assume the radii of the spherical bubble growing in an infinite medium and the bubble confined in the slug flow regime are the same. Thus the above equation can be simplified as,

$$\frac{dL_b}{dt} = 4A_c \left(\frac{R_s}{R_b}\right)^2 [(t^+ + 1)^{(1/2)} - (t^+)^{(1/2)}] \quad (5.37)$$

This equation can be applicable for the period of time ($t_o \leq t \leq t_c$), where t_o is the time where bubble confinement is observed, and t_c is the time where the bubble coalescence begins. Additionally, the term $(d\alpha/dt)$ in Eq. (5.30) may be simplified. Considering the energy balance principle only for the liquid film zone, and assuming that the heat transfers by conduction through the wall of the micro-tube leads to vaporize the liquid film, (as reported in some previous studies, either for the liquid film, Hetsroni et al. [246], or the micro-layer beneath a bubble grows on a surface, Cooper [234], one can write the variation of liquid film for evaporation conditions as follows.

$$\frac{d\delta}{dt} = -\frac{q_w''}{\rho_f h_{fg}} \quad (5.38)$$

Taking into account the relation between the liquid film and the area void fraction of the vapor phase, ($\alpha = (D - 2\delta)^2/D^2$), the variation of vapor void fraction can be expressed by,

$$\frac{d\alpha}{dt} = \frac{4q_w''}{\rho_f h_{fg} D} \alpha^{(1/2)} \quad (5.39)$$

By this relation, Eq. (5.38), the variation of liquid slug length can be calculated as represented in Eq. (5.30). Since we assumed that at the onset of bubble confinement, $R_s = R_c$, the time where the bubble confinement occurs, t_o , can be calculated based on the relation of bubble growth developed by Mikic et al. [235] which can be recast as follows,

$$D = \frac{4}{3} \frac{B_c^2}{A_c} \left[\left(\left(\frac{B_c}{A_c} \right)^2 t_o + 1 \right)^{(3/2)} - \left(\left(\frac{B_c}{A_c} \right)^2 t_o \right)^{(3/2)} - 1 \right] \quad (5.40)$$

5.4. Calculation Procedure

The model analysis preceded above is implemented for calculating the main slug flow parameters as follows:

1. Define the channel geometrical parameters, the hydraulic diameter, D_h , the heated length, L_h , and the material that the tube is made of, the relative roughness of the tube inner surface, (ϵ/D) .
2. Define the main operating conditions, such as the inlet saturation temperature, T_{sat} , or pressure, P_{sat} , the applied heat flux, q_w'' , the mass flux, G , and the super-heated temperature, ΔT_{sat} .
3. All the required properties of the tested working fluid are determined at the given inlet saturation temperature, T_{sat} , or pressure, P_{sat} as tabulated in [247] .
4. The transition lines are estimated using an appropriate flow pattern map. In this work, the flow pattern map developed by Revellin and Thome [75] for R134a has been employed.
5. The initial values of vapor quality, x_o , bubble velocity, u_{bo} , translational velocity, u_{to} , vapour void fraction, α_o , and the time of bubble confinement, t_o , are evaluated by Eqs.(5.26), (5.23), (5.25), (5.27), and (5.40) respectively, considering that the initial bubble length can be set as $(L_{bo} = D)$.
6. Slug unit length (L_u), liquid slug length (L_s), liquid slug velocity (u_s), and liquid film velocity (u_f) are calculated by Eqs. (5.16), (5.28), (5.11), and (5.10) respectively.
7. The bubble frequency for the slug flow, in isolated bubble zone, is defined as the ratio between the bubble velocity and the slug unit length ($f_b = u_b/L_u$).
8. Calculate the variation of void fraction ($\Delta\alpha$), bubble length (ΔL_b), and liquid slug length (ΔL_s), in a time step of (Δt) using Eqs. (5.39), (5.36), and (5.30) respectively.
9. Update the values of the parameters (L_b, L_s, x, α), and repeat the steps (5 to 7).

5.5. Results and Discussion

The main characteristic parameters of the slug flow unit, (liquid slug velocity, bubble length, liquid slug length, slug unit length, and bubble frequency), have been calculated by the present model for flow boiling of two different working fluids, (R134a, R245fa), and two sizes of circular channels (0.509 mm, and 3.0 mm inner diameter), respectively. Calculations were performed for wide range of mass fluxes ($300 \leq G \leq 1000 \text{ kg/m}^2 \cdot \text{s}$), which are similar to the

test conditions of the experiments performed by Revellin et al. [91], and Charnay et al. [108] as listed in Table (5.1). The results obtained are presented and discussed as following:

Table (5-1): Experimental conditions of the data used for model validation

| Author(s) | Working fluid | Tube ID, [mm] | L [mm] | G, [kg/m ² .s] | T _{sat} , [°C] | ΔT, [°C] |
|----------------------|---------------|---------------|--------|---------------------------|-------------------------|----------|
| Revellin et al. [91] | R134a | 0.5 | 70.7 | 350-1000 | 30 | 3.0 |
| Charnay et al. [108] | R245fa | 3.0 | 185.0 | 300-700 | 60 | - |

Figure 5-5 shows the bubble frequency measured by Revellin et al. [91], and the one predicted by the present model plotted versus the vapor quality for flow boiling of the working fluid, R134a, at a mass flux of, (G = 350 kg/m².s), in a 0.509 mm inner diameter micro-tub. A clear increase of bubble frequency by increasing the vapor quality can be observed until a certain vapor quality, ($x \cong 0.038$), for the experimental data, and $x \cong 0.04$ by frequency predicted by the present model, where the liquid slug length vanishes, and the first stage of bubble coalescence begins. Furthermore, close to the transition line from bubbly to bubbly/slug flow ($x \cong 0.018$), it can be seen that the model over-predicted the experimental data and this can be attributed to bubble size since the bubble confinement has not occurred yet. On the other hand, the model gives a good agreement with the experimental data which fall in the isolated bubble zone at this mass flux condition ($0.02 \leq x \leq 0.04$).

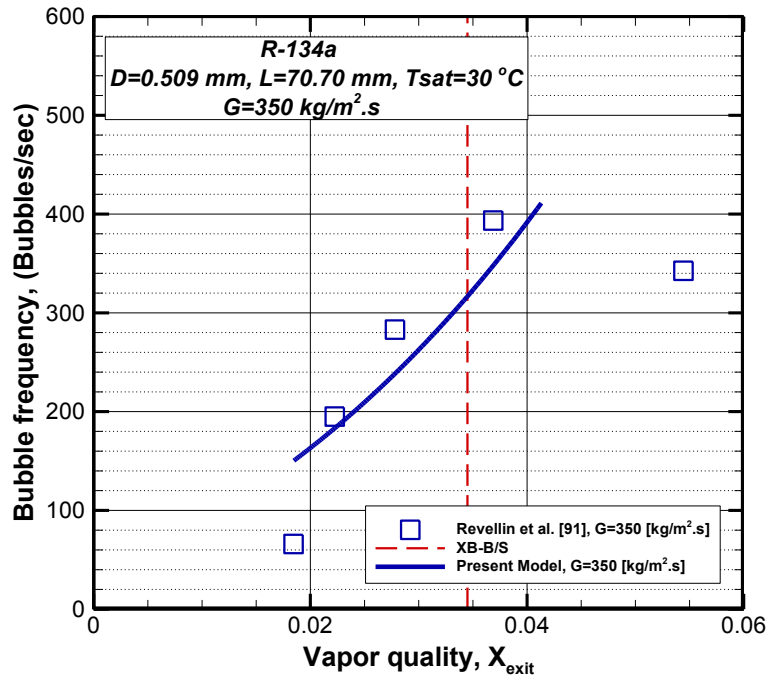


Figure 5-5: Bubble frequency predicted by the present model, and the one measured by Revellin et al. [91] versus vapor quality for R134a in 0.509 mm inner diameter micro-tube with a mass flux, $350 \text{ kg/m}^2 \cdot \text{s}$, at $T_{sat} = 30 \text{ }^\circ\text{C}$, and $\Delta T_{sub} = 3.0$.

Taking into account the influence of mass flux on the bubble frequency in the isolated bubble zone, Figure 5-6 Provides the results obtained by the present model for flow boiling of R134a in a 0.509 mm inner diameter micro-tube at a mass flux of $500 \text{ kg/m}^2 \cdot \text{s}$, that corresponds to a liquid Reynolds number $Re_l \cong 1,400$, and compared with those experimental data measured by Revellin et al. [91] at the same operating conditions. It is apparent from the figure that the model predicted, the trend of bubble frequency variation versus vapor quality, and gave a good agreement with the experimental data at low vapor quality, $x=0.02$. A possible explanation for this is that at this vapor quality and mass flux, the onset of bubble confinement would be expected, and therefore the assumption of that bubble length is equal to inner diameter is verified and works well at this condition. However, as the vapor quality increases, an under estimation of the data can be observed, and this can be attributed to several factors might be related to the uniformity of the flow pattern, the applicability of the correlation used for evaluating the wall friction factor, the flow instability which is expected to be experienced in this regime, and the influence of the flow pattern transition phenomenon, which may occur here for the vapor quality interval, as expressed by the small dashed-line in the figure. Additionally, as

the vapor quality increases, the bubble frequency is expected to increase, while the liquid slug length decreases, until it vanishes as shown in the Figure 5-6 as indicated by the dash-dot line at $x \cong 0.0382$, which represents the bubble frequency peak at this condition.

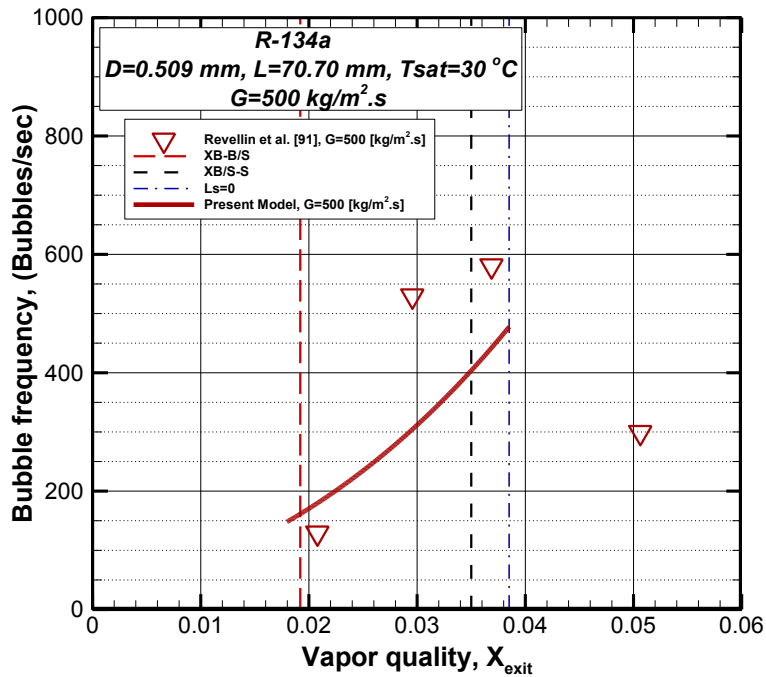


Figure 5-6: Bubble frequency predicted by the present model, and the one measured by Revellin et al. [91] versus vapor quality for R134a in 0.509 mm inner diameter micro-tube, $500 \text{ kg/m}^2 \cdot \text{s}$, at $T_{sat} = 30^\circ\text{C}$, and $\Delta T_{sub} = 3.0$.

Figure 5-7 presents the bubble frequency data of flow boiling of R134a measured by Revellin et al. [91] at higher mass flux, $700 \text{ kg/m}^2 \cdot \text{s}$, which corresponds to a liquid Reynolds number, $Re_l \cong 1,950$ compared with that predicted by the present model. Again, a steep increase in bubble frequency versus vapor quality can be observed from the figure. Interestingly, a better agreement can be seen with the measured data which fall in the range of vapor quality, $0.019 \leq x \leq 0.03$ than those where $x \leq 0.018$. This result may be explained by the fact that the bubble nucleation sites are not distributed uniformly on the inner surface which leads the nucleated bubbles to departure and grow with various bubble characteristics. Another explanation is that at the vapor quality range $0.019 \leq x \leq 0.03$, the elongated, isolated bubbles are expected to be more uniform and organized than at lower vapor quality at this mass flux.

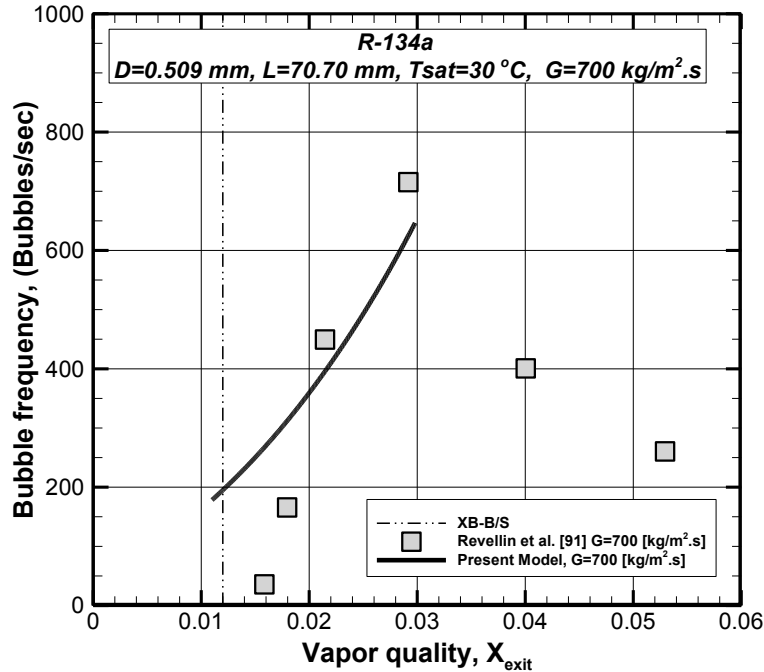


Figure 5-7: Bubble frequency predicted by the present model, and the one measured by Revellin et al. [91] versus vapor quality for R134a in 0.509 mm inner diameter micro-tube, 700 [kg/m².s], at $T_{sat} = 30\text{ }^{\circ}\text{C}$, and $\Delta T_{sat} = 3.0$.

Figure 5-8 presents the bubble frequency predicted by the present model versus the vapor quality, compared with those measured by Revellin et al. [91], for flow boiling of R134a in a 0.509 mm inner diameter horizontal micro-tube with a higher mass flux, 1000 kg/m².s, that corresponds to Reynolds number, $Re_l \cong 2,800$. According to the flow pattern map developed by Revellin and Thome [75] for flow boiling of R134a, the long-dashed line represents the transition line from the bubbly to bubbly-slug flow regime, the small-dashed line represents the transition line from bubbly-slug flow to slug flow regime. From the Figure 5-8, it can be observed that the present model, over-predicted the bubble frequency data in the isolated bubble zone. However, the model predicted well the bubble frequency trend, where the number of bubbles increases by increasing the vapor quality, until the bubble frequency peak is reached, where the liquid slug length is expected to vanished at this peak, which is predicted by the present model $L_s = 0$ at $x \cong 0.0201$, (represented by the dash-dot line). The observed over-prediction of the bubble frequency data may be influenced by the flow instability which can occur at the liquid vapor interface. Furthermore, the range of vapour quality for mass flux, 1000 kg/m².s, where the bubble frequency intends to increase, $0.012 \leq x \leq 0.02$, is narrower

than that obtained at mass flux , $350 \text{ kg/m}^2 \cdot \text{s}$, $0.019 \leq x \leq 0.04$, in Figure 5-5. In other words, the higher mass flux is the narrower isolated bubble zone is observed.

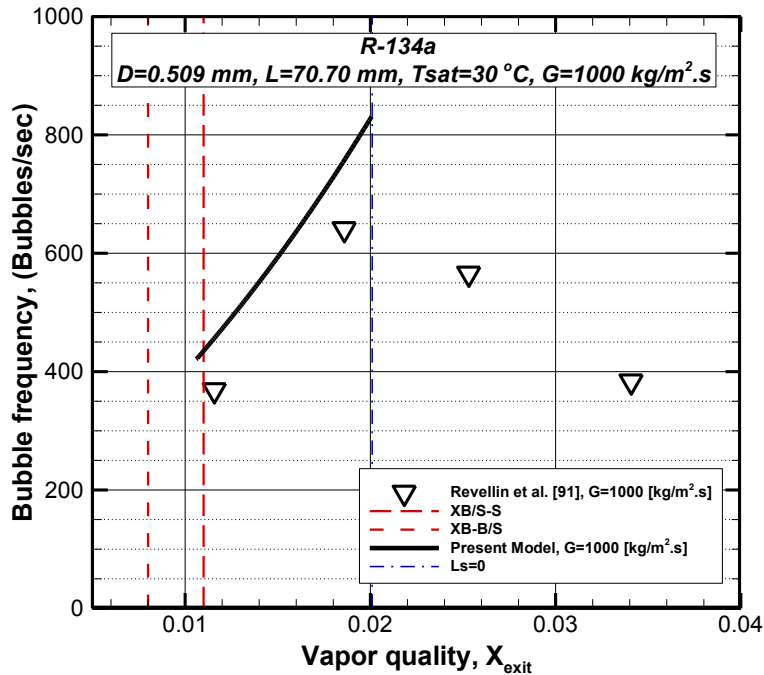


Figure 5-8: Bubble frequency predicted by the present model, and the one measured by Revellin et al. [91] versus vapor quality for R134a in 0.509 mm inner diameter micro-tube, $1000 \text{ [kg/m}^2 \cdot \text{s]}$, at $T_{sat} = 30^\circ\text{C}$, and $\Delta T_{sub} = 3.0$.

Taking into account the effect of working fluid, operating conditions, and the channel size, the present model has been implemented to predict the bubble frequency for flow boiling of R245fa in 3.0 mm inner diameter mini-tube at inlet saturation temperature of $60 \text{ }^\circ\text{C}$, and compared with bubble frequency data of Charnay et al. [108] for mass fluxes 300, 500, and $700 \text{ kg/m}^2 \cdot \text{s}$, which corresponded to liquid Reynolds numbers of 3,390 ; 5,650; and 7,900 respectively, as depicted in Figure 5-9. From this figure, we can see that, in the isolated bubble zone, the bubble frequency increases by increasing the vapor quality and mass flux. Furthermore, a significant effect of the mass flux on bubble frequency and flow pattern transition line (from isolated to bubble coalescence zone) can be observed. In other words, as the mass flux increases, the bubble frequency increases, and the bubble peak frequency increases. Additionally, bubble coalescence phenomenon is observed earlier at higher mass flux, where the liquid slug vanishes faster. It is of interest to note that the model well predicted the trend of bubble frequency versus the vapor quality for all tested mass fluxes. Besides, the bubble frequency peaks have been

quantitatively well predicted (where the liquid slug length is vanished). Under certain circumstances, the present model gave a slight shift for the bubble frequency peaks compared to the experimental data. Furthermore, with respect to the mass flux, $500 \text{ kg/m}^2 \cdot \text{s}$, and liquid-Reynolds number, $5,650$, a significant underprediction can be observed for the bubble frequency data points falling between the minimum bubble frequency and the peak. One explanation for this is that at these working conditions and channel size, which correspond to a confinement number, $C_{conf} = 0.3$, the gravity force significantly influenced the bubble characteristics and consequently, the obtained results.

Altogether, the experimental bubble frequency data predicted by the present model have been compared with those measured by Revellin et al. [91] for R134a, and Charnay et al. [108] for R245fa, in the isolated bubble zone, at the corresponding operating conditions for each set of data, and plotted in Figure 5-10. A good agreement is obtained with a mean absolute error of 29.55% .

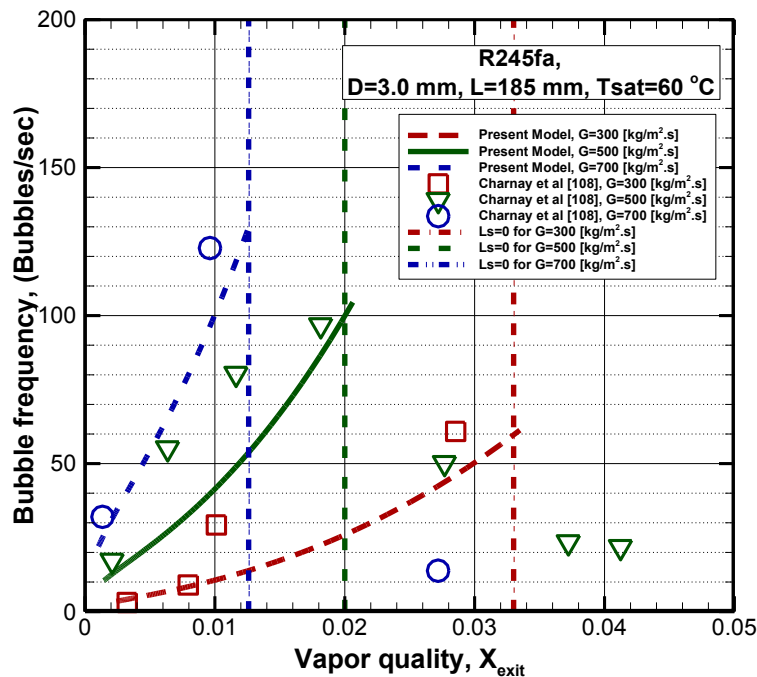


Figure 5-9: Bubble frequency versus vapor quality for flow boiling of R245fa in 3.0 mm inner diameter mini-tube at various mass fluxes.

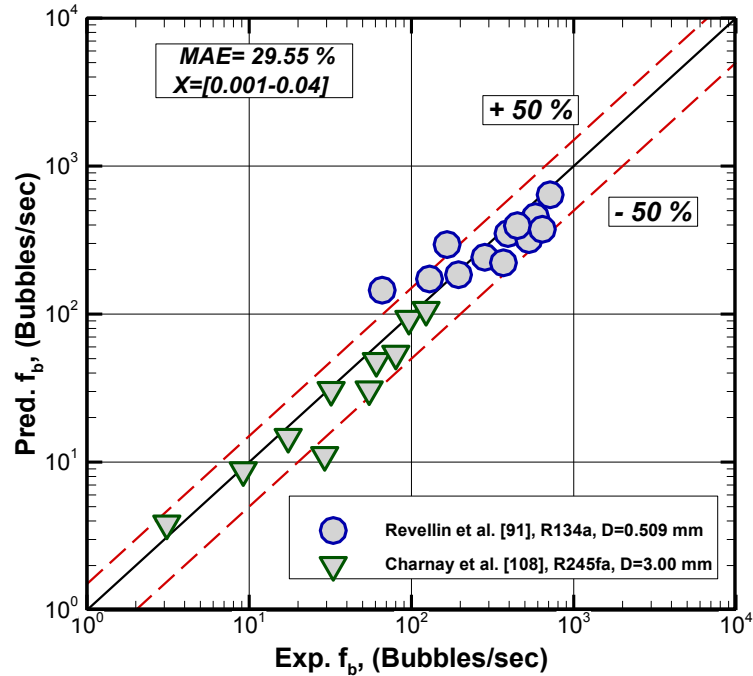


Figure 5-10 A comparison between bubble frequency data measured by Revellin et al. [91], and Charney et al. [108], and those predicted by the present model for a range of mass fluxes of 300 to 1000 $[kg/m^2.s]$.

Turning to the results of bubble lengths, Figure 5-11 shows the bubble length data measured by Revellin et al. [91] for flow boiling of R134a, and those predicted by the present model in the isolated bubble zone (beginning from the bubble confinement where it is assumed that the bubble length equals the channel diameter until the first stage of bubble coalescence). It has been noted that the bubble length increases with vapor quality. Additionally, the higher mass flux is the longer is the bubble length. The bubble length trend predicted by the present model matches those measured by Revellin et al. [91]. It can be seen that as the vapor quality increases, the model over-predicts the bubble length data in the isolated bubble zone. A possible explanation for this is that the effects of the thermal expansions and liquid film evaporation dominate the bubble elongation mechanism as the vapor quality increases. Furthermore, the superheat temperature has a significant effect on the rate of the liquid film evaporation which is measured to be 3 in the data of Revellin et al. [91] for all mass fluxes. In general, the present model predicted the bubble length data measured by Revellin et al. [91] for R134a in the isolated bubble zone and a good agreement is obtained with a mean absolute error of MAE=27.83 %, as can be seen in Figure 5-12.

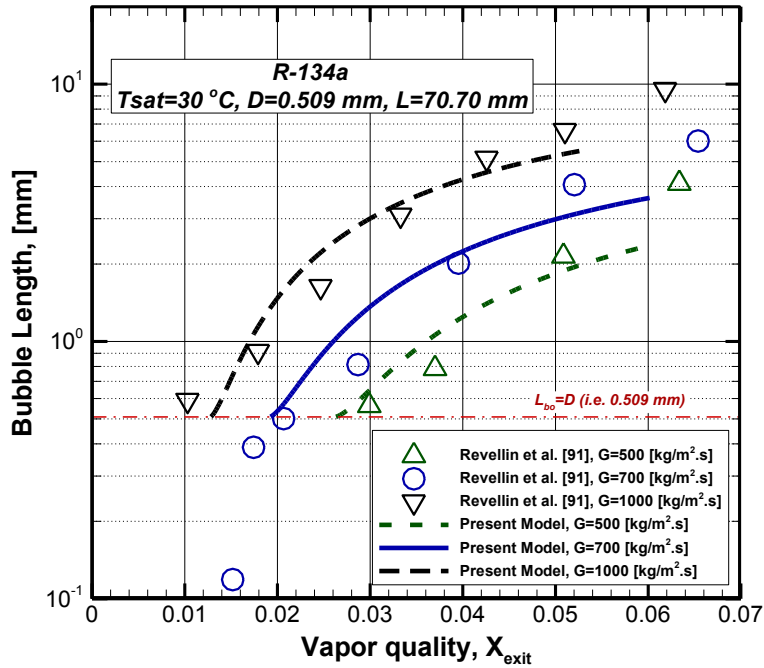


Figure 5-11: Bubble length versus vapor quality for flow boiling of R134a in a 0.509 mm inner diameter micro-tube.

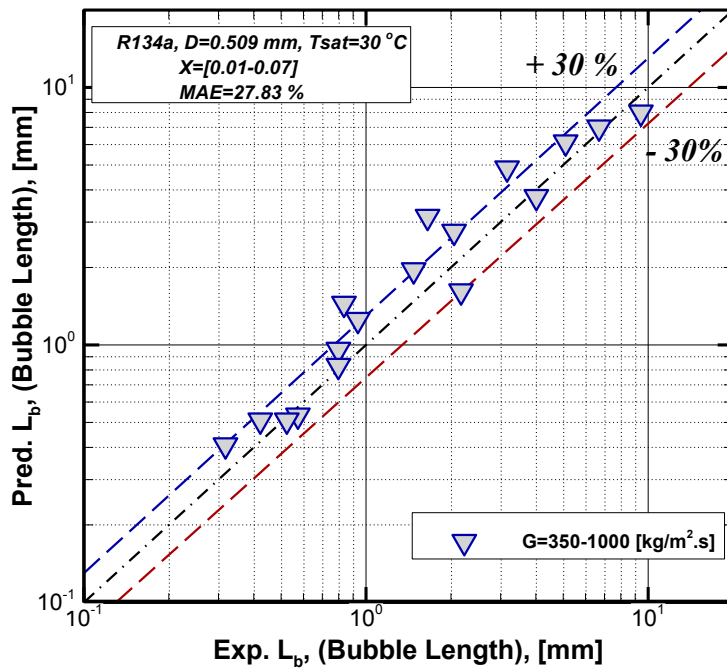


Figure 5-12: Bubble length data measured by Revellin et al. [91] versus those predicted by the present model for flow boiling of R134a in isolated bubble zone.

The slug unit length, L_u , the bubble length, L_b , and the liquid slug length, L_s , have been predicted by the present model at each vapor quality corresponds to the isolated bubble zone in the slug flow regime. A sample of the predicted lengths plotted versus the vapor quality is depicted in Figure 5-13 for flow boiling of R134a in a 0.509 mm inner diameter with mass flux, $500 [kg/m^2 \cdot s]$, at an inlet saturation temperature, which matches a liquid Reynolds number, $Re_l \cong 1,400$, and a confinement number, $C_{conf} \cong 1.6$. Furthermore, the figure shows the isolated bubble zone blundered by two vertical lines, the dotted line on the left side of the graph which represents the transition line from bubbly to bubbly-slug flow that corresponds to a vapor quality $x \cong 0.019$, and the dash-dot-dot line which represents the onset of bubble coalescence, where the liquid slug length vanishes, and corresponds to a vapor quality, $x \cong 0.039$. The minimum bubble length as assumed to be as same as the channel inner diameter at the onset of bubble confinement, as represented by the horizontal dash-dot line. Additionally it can be noticed that, in the isolated bubble zone, the slug unit length and liquid slug length decrease by increasing the vapor quality, while the bubble length increases. Moreover, a steep decrease in liquid slug length and a steady increase in bubble length versus vapor quality can be observed. A possible explanation for this is that both the thermodynamic and hydrodynamic effects influence the bubble and liquid slug zones due to the liquid film evaporation that causes the elongation of the bubble, and the inertial forces that affect the bubble nucleation and liquid slugs in this zone.

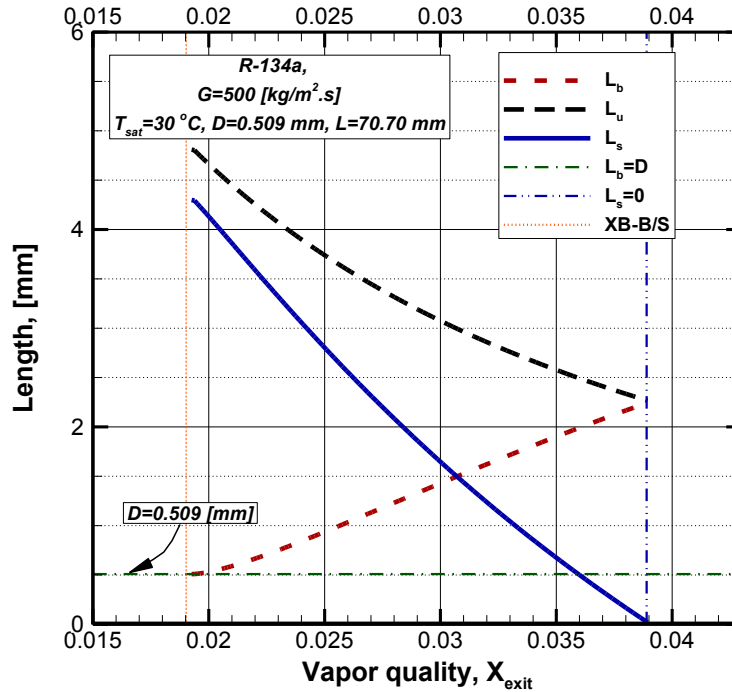


Figure 5-13: Variation of bubble length, liquid slug length, and slug unit length versus vapor quality for flow boiling of R134a in a 0.509 mm inner diameter micro-tube with a mass flux 500 [kg / (m².s)] at an inlet saturation temperature T_{sat}=30 °C.

5.6. Conclusions

The present study was designed to develop a semi-analytical model for predicting the main characteristics of slug flow for flow boiling in a single horizontal micro-channel for the isolated bubble zone at a uniform heat flux condition. The model was developed based on the mass, momentum, and energy equations of a fully developed slug unit, taking into account the influences of inertia, surface tension, and liquid film evaporation on the bubble behaviour. The pressure drop through the slug unit was evaluated based on the Young and Laplace relation, considering the effects of vapor void fraction. The main parameters, liquid slug velocity, liquid film velocity, liquid slug length, bubble length, slug unit length have been predicted, while bubble velocity was estimated based on the superficial flow velocity. Consequently, the bubble frequency has been predicted. This study has shown that the bubble frequency, increases by increasing vapor quality and mass flux. Furthermore, it has been noticed that the higher mass

flux is, the higher peak of the bubble frequency is predicted, the earlier bubble coalescence is observed, and the quicker liquid slug length decreases. One of the most interesting finding in the present study is that it is possible to predict the onset of bubble coalescence by predicting the liquid slug length. The bubble lengths and bubble frequency predicted by the present model have been compared against those measured by Revellin et al. [91] for flow boiling of R13a in 0.509 mm inner micro-tube for a wide range of mass fluxes ($350 \leq G \leq 1000 \text{ kg/m}^2 \cdot \text{s}$), corresponded to a range of liquid-Reynolds number, $970 \leq Re_l \leq 3,400$, and confinement number, $C_{\text{conf}} \cong 1.6$, and with those measured by Charnay et al. [108] for flow boiling of R245fa in a 3.0 mm inner diameter small tube with mass fluxes ($300 \leq G \leq 700 \text{ kg/m}^2 \cdot \text{s}$), corresponded to a range of liquid-Reynolds number, $3,390 \leq Re_l \leq 7,900$, and confinement number, $C_{\text{conf}} \cong 0.3$ in for the isolated bubble regime. A good agreement with the data of bubble lengths has been obtained with MAE of 27.83% and with the bubble frequency data with a MAE of 29.55 %, respectively. Neglecting the influence of the gravity and applying the model for conventional size channels results in decreasing the accuracy of the present model since the gravity force has a significant effect in conventional size channels. It is of importance to note that the major limitation of the present model is its applicability to the isolated bubble zone. However, for the future work, by considering the variation of bubble length during the bubble coalescence, the present model may be extended to be applicable for bubble coalescence regime. This study has showed that a shortage and lack of investigating bubble characteristics in the isolated bubble zone for flow boiling in mini/micro-channels still exists, and therefore, more experimental and theoretical investigations for the slug flow,(isolated bubble zone) is needed for clarifying and better understanding bubble dynamics in this zone. Additionally, since, the surface roughness influences bubble nucleation sites, it would be helpful to conduct further analytical work considering, the surface roughness effects on bubble characteristics in slug flow regime.

Chapter 6

6. Conclusions and Future Work

6.1. Conclusions

Two-phase flow boiling mini/micro-channels have several engineering applications. A detailed literature review for flow boiling in mini/micro-channels has been presented. It has been reported that the basic flow patterns for flow boiling in horizontal micro-channels are bubbly flow, slug flow, and annular flow regimes. The physical phenomena of flow boiling in mini/micro-channels, including the variation of liquid film thickness, partial dry-out of the liquid film either in slug flow or annular flow regimes, and their influence on the flow boiling heat transfer coefficient and pressure are still unclear and not fully understood. Moreover, a shortage in reliable and satisfactory predictive methods for predicting the main design parameters of the two-phase mini/micro-channel including two-phase heat transfer coefficient, two-phase pressure drop, critical heat flux, and void fraction still exist. The following conclusions can be drawn from the work done in this thesis:

1. A new semi-analytical model for predicting CHF, h_{tp} , Δp_{tp} , α was developed based on the mechanism of liquid film evaporation, and separated flow model in annular flow regime. Moreover, a semi-analytical model to determine slug characteristics in the isolated bubble zone was developed based on Drift-Flux Model.
2. The CHF data of both aqueous and non-aqueous working fluids were successfully predicted by the present model better than the tested CHF correlations with hydraulic diameter ranges of ($0.38 \leq D_h \leq 3.04$ mm) and heated-length to diameter ratios of $117.7 \leq L_h/D \leq 470$.

3. The tested data were collected from the literature for flow boiling in slug and annular flow regimes in single horizontal mini/micro-channels. Three recent developed flow pattern maps developed by Revellin and Thome [75] , Cheng et al. [103], and Charnay et al. [108], have been used, respectively, to define the boundaries of the slug and annular flow regimes for R134a, CO₂, and R-245fa.
4. The scope of the model is limited to slug and annular flow regimes in single mini/micro-channel. Therefore, it was validated against $\approx 1,250$ data points from literature for different working fluids (water, LN₂, FC-72, R134a, R1234ze, R236fa, R113 R410a, and CO₂), and is applicable for range of equivalent Reynolds number $2,000 \leq Re_{eq} \leq 48,000$, and confinement number $0.3 \leq Co \leq 3.4$.
5. Overall, the model predicted the parameters CHF, h_{tp} , Δp_{tp} , α , with MAEs of 19.81% , 18.14 %, 23.02 %, and 3.22 %. Furthermore, a good agreement with experimental data of bubble frequency, f_b , and bubble length, L_b , was obtained with MAE of 29.55%, and 27.83%, respectively.
6. The most obvious finding obtained from the heat transfer results is that flow boiling heat transfer coefficient in the annular flow increases with the vapor quality and mass flux, and mainly is affected by the liquid film thickness.
7. The pressure drop increases with mass flux and vapor quality, as well as by decreasing the tube size. Moreover, it is likely to decline after reaching the peak at high vapor quality which suggests that this peak point may be defined as a transition boundary from annular flow to dry-out flow regime.
8. The results obtained have shown that the bubble frequency increases with vapor quality and mass flux, and the peak of the bubble frequency shows the onset of bubble coalescence in terms of vapor quality.

6.2. Future Work

6.2.1. Investigation of the Non-Uniform Heat Flux Effects on the Characteristics of Flow Boiling Micro-Channels:

Most of electronic devices are characterized by hotspots that experienced on their chips such as electronic chips of CPUs. Consequently, a non-uniform heat flux distribution is experienced on the chip surface. It has been proven in several previous studies that flow boiling micro-channels heat sink is promised to be an effective cooling method for such electronic devices. However, the influences of non-uniform heating sources on the characteristics of flow boiling micro-channels have not been fully investigated and understood. Consequently, investigating the effects of non-uniformity of the heating source on flow boiling micro-channels should be performed analytically and experimentally as it is explained as follows:

Analytical Method:

In this part an analytical model will be developed for studying heat transfer flow boiling of a micro-tube subjected to a non-uniform heat flux conditions. The model will be developed for the basic three flow patterns of flow boiling in micro-tubes, namely, bubbly flow, slug flow, and annular flow. The model will be developed based on the two-phase flow equations of motions and constitutive relations available for each flow pattern. The main dependent variables considered in the model are two-phase heat transfer coefficient, pressure drop, bulk temperature, wall surface temperature, and total thermal resistance. Various non-uniform heat flux distributions will be considered including linearly axial increasing, decreasing, and mid-point peak shapes. The influence of these non-uniform heat fluxes on the dependent variables will be investigated and discussed considering various working fluids. The equations of the model will be solved numerically, and the available experimental flow boiling database for micro-channels will be used for model validation.

Experimental method:

It is of importance to investigate experimentally the influence of non-uniform heat flux conditions on the performance of flow boiling micro-channel heat sinks, taking into account the

design of micro-channel heat sink. In other words, different test sections with various geometries (rectangular and circular cross sections) including the locations of hotspots will be manufactured. The thermocouples and pressure transducers will be located in the proper positions based on the chosen test section. The uncertainties in measurements of temperature, pressure, and applied heat fluxes will be taken into account. The heat flux will be applied along the test section by applying various hotspots. Various working fluids (e.g. R134a, CO₂, and F72) will be employed. All data will be read using a computer based data acquisition system. A high speed camera will be used for visualization the flow boiling in the test section in order to define the boundaries of each observed flow pattern, to see the effect of hotspots location on the bubble nucleation, and to measure the liquid film thickness in slug and annular flow regime which will be used for calculating the total thermal resistance. Furthermore, this will help to predict the onset of dryness and study effect of non-uniform heat flux on the occurrence of critical heat flux. The effects of applied non-uniform heat flux on the wall temperature distribution, pressure drop, flow boiling instability, and micro-channel heat sink performance will be investigated. The experiments will be performed for wide range of operating conditions considering low and high mass fluxes.

6.2.2. Investigation of Bubble Dynamics and Heat Transfer in Coalescing Bubble Zone for Flow Boiling in a Single Horizontal Mini/Micro-Channel:

It has been reported that intermittent flow regime in horizontal flow boiling mini/micro-channels can be subdivided into two main zones, which are isolated bubble zone and coalescing bubble zone. Furthermore, a literature review indicates that a severe lack of knowledge on confined bubble coalescence exists and only few studies have been done for bubble coalescence zone for flow boiling in mini/micro-channels (e.g. Consolini and Thome [145]). Therefore, it is of importance to carry out more experimental works, and conduct more analytical studies related to this flow regime in order to fundamentally understand and clarify two-phase flow boiling in mini/micro-channels.

6.2.3. Future Flow Pattern Maps

The real application of two-phase flow boiling in micro-channels is related to micro-channel heat sinks which are subjected to non-uniform heat flux. Furthermore, no flow pattern maps, even those developed for diabatic flow are applicable for flow boiling in micro-channels under non-uniform heat flux. Therefore, for identifying the transition lines of each flow pattern, developing a flow pattern map for flow boiling in micro-channels at non-uniform heat flux will be very crucial and supports more understanding of the complex phenomenon of two-phase flow boiling in micro-channels.

References

- [1] Tran, T.N.; Wambsganss, M.W.; Chyu, M.C.; and France, D.M., "A Correlation for Nucleate Flow Boiling in Small Channel," in *Compact heat exchangers for the process industries conference 22-27 Jun 1997*, Snowbird, UT (United States), 1997.
- [2] Zhang, Hui ; Mudawar, Issam; and Hasan, Mohammad M., "Experimental assessment of the effects of body force, surface tension force, and inertia on flow boiling CHF," *International Journal of Heat and Mass Transfer*, vol. 45, no. 20, pp. 4079-4095, 2002.
- [3] Revellin, R., and Thome, J.R., "Adiabatic two-phase frictional pressure drops in microchannels," *Experimental Thermal and Fluid Science*, vol. 31, p. 673–685, 2007.
- [4] Zhao, X.; and Bansal, P., "Experimental investigation on flow boiling heat transfer of CO₂ at low temperatures," *Heat Transfer Engineering*, vol. 30, no. 1-2, pp. 2-11, 2009.
- [5] Fan, YF.; and Hassan, I., "Experimental investigation of flow boiling instability in a single horizontal microtube with and without inlet restriction," *Journal of Heat Transfer*, vol. 134, no. 8, pp. 1-11, 2012.
- [6] Fan, YF.; and Hassan, I., "Effect of inlet restriction on flow boiling heat transfer in a horizontal microtube," *Journal of Heat Transfer*, vol. 135, no. 2, pp. 1-9, 2013.
- [7] Lim, T.-W. ; You, S.-S.; Choi, J.-H.; and Kim, H.-S., "Experimental investigation of heat transfer in two-phase flow boiling," *Experimental Heat Transfer*, vol. 28, no. 1, pp. 23-36, 2015.
- [8] Moriyama, K. and Inoue, A.; and Ohira, H., "The thermo hydraulic characteristics of two-phase flow in extremely narrow channels," *J. Heat Transfer-Japanese Research*, vol. 21, no. 8, pp. 838-856, 1992.
- [9] S. Kandlikar, "A Theoretical Model to Predict Pool Boiling CHF Incorporating Effects of Contact Angle and Orientation," *Journal of Heat Transfer*, vol. 123, no. 6, pp. 1071-1079 , 2001.
- [10] Elazhary, A. ; and Soliman, H.M., "Analytical solutions of fluid flow and heat transfer in parallel-plate micro-channels at high zeta-potentials," *International Journal of Heat and Mass Transfer*, vol. 52, no. 19-20, p. 4449–4458, 2009.
- [11] Kim, S.M.; and Mudawar, I. , "Analytical heat diffusion models for heat sinks with circular micro-channels," *International Journal of Heat and Mass Transfer*, vol. 53, no. 21-22, p. 4552–4566, 2010.
- [12] Megahed, A.; and Hassan, I. , "Analytical Modeling of Annular Flow Boiling in microchannels," *Journal of Heat Transfer*, vol. 132, no. 4, pp. 1-11, 2010.
- [13] Kandlikar, S. "Scale effects on flow boiling heat transfer in microchannels A fundamental perspective," *International Journal of Thermal Sciences*, vol. 49, no. 7, pp. 1073-1085, 2010.
- [14] Tuckerman, D.B.; and Pease, R. F. W., "High-Performance Heat Sinking for VLSI," *IEEE Electron Device Letters*, vol. 2, no. 5, pp. 126-129, 1982.
- [15] Colgan, E.G.; Furman, B.; Gaynes, M.; Graham, W.S.; LaBianca, N.C.; Magerlein, J.H.; Polastre, R.J.; Rothwell, M.B.; Bezama, R.J.; Choudhary, R.; Marston, K.C.; Toy, H.;

- Wakil, J.; Zitz, J.A.; Schmidt, R.R., "A practical implementation of silicon microchannel Coolers for High Power Chips," *IEEE Transactions on Components & Packaging Technologies*, vol. 30, no. 2, pp. 218-225, 2007.
- [16] Tran, T.N. ; Wambsganss, M.W.; and France, D.M., "Small circular and rectangular channel boiling with two refrigerants," *International Journal of Multiphase Flow*, vol. 22, no. 3, pp. 485-498, 1996.
- [17] Kandlikar, S.G.; and Grande, W.J, "Evolution of micro-channel flow passages – thermohydraulic performance and fabrication technology," *Heat Transfer Engineering*, vol. 24, no. 1, pp. 3-17, 2003.
- [18] Cooke, D.; Kandlikar, S. G., "Pool Boiling Heat Transfer and Bubble Dynamics Over Plain and Enhanced Microchannels," *Journal of Heat Transfer*, vol. 133, no. 5, pp. 1-9, 2011.
- [19] Zhao, J-F., "Two-phase flow and pool boiling heat transfer in microgravity," *International Journal of Multiphase Flow*, vol. 36, no. 2, p. 135–143, 2010.
- [20] Piasecka, M., "Heat transfer research on enhanced heating surfaces in flow boiling in a minichannel and pool boiling," *Annals of Nuclear Energy*, vol. 73, pp. 282-293, 2014.
- [21] Bao, Z. Y., Fletcher, D. F., and Haynes, B. S., "Flow boiling heat transfer of Freon R11 and HCFC123 in narrow passages," *Int. J. of Heat and Mass Transfer*, vol. 43, pp. 3347-3358, 2000.
- [22] Lee, H. J., and Lee, S. Y., "Heat Transfer Correlation for Boiling Flows in Small Rectangular Horizontal Channels with Low Aspect Ratios," *Int. J. of Multiphase Flow*, vol. 27, pp. 2043-2062, 2001.
- [23] Liu, D.; and Garimella, S.V., "Flow boiling heat transfer in microchannels," *Journal of Heat Transfer*, vol. 129, no. 10, pp. 1321-1332, 2007.
- [24] Huh, C.; Kim, J.; and Kim, M. H. , "Flow pattern transition instability during flow boiling in a single microchannel," *International Journal of Heat and Mass Transfer*, vol. 50, no. 5-6, pp. 1049-1060, 2007.
- [25] Bertsch, S.; Groll, E. A.; and Garimella, S. V., "A composite heat transfer correlation for saturated flow boiling in small channels," *Int. J. of Heat and Mass Transfer*, vol. 52, no. 7-8, pp. 2110-2118, 2009.
- [26] Bortolin, S.; Del Col, D.; and Rossetto, L., "Flow Boiling of R245fa in a Single Circular Microchannel," *Heat Transfer Engineering*, vol. 32, no. 13-14, p. 1160–1172, 2011.
- [27] Yang, F.; Dai, X.; Peles, Y.; Cheng, P.; Khan, J.; and Li, C., "Flow boiling phenomena in a single annular flow regime in microchannels (I) Characterization of flow boiling heat transfer," *International Journal of Heat and Mass Transfer*, vol. 68, p. 703–715, 2014.
- [28] Sani, R., "Downflow boiling and non-boiling heat transfer in a uniformly heated tube," University of California, Berkeley, 1960.
- [29] Eckels, S.J. ; and Pate, M.B., "An experimental comparison of evaporation and condensation heat transfer coefficients for HFC-134a and CFC-12," *Int. J. Refrig.* 1991, vol. 14, pp. 70-77, 1991.
- [30] Hambreus, K., "Heat transfer coefficient during two-phase flow boiling of HFC-134a," *Int. J. Refrig.*, vol. 14, pp. 357-362, 1991.
- [31] Zürcher, O., Favrat, D., and Thome, J. R., "Development of a Diabatic Two-Phase Flow

- Pattern Map for Horizontal Flow Boiling," *Int. J. of Heat and Mass Transfer*, vol. 45, pp. 291-301, 2002.
- [32] Oh, H-K.; Ku, H-G.; Roh, G-S.; Son, C-H.; Park, S., "Flow boiling heat transfer characteristics of carbon dioxide in a horizontal tube," *Applied Thermal Engineering*, vol. 28, no. 8-9, pp. 1022-1030, 2008.
- [33] Lima, d-S. R.; Quibén, J. M.; and Thome, J. R., "Flow boiling in horizontal smooth tubes new heat transfer results for R-134a at three saturation temperatures," *Applied Thermal Engineering*, vol. 29, no. 7, p. 1289–1298, 2009.
- [34] Zhang, W. ; Hibiki, T.; and Mishima, K., "Correlation for flow boiling heat transfer in mini-channels," *Int. J. of Heat and Mass Transfer*, vol. 47, p. 5749–5763, 2004.
- [35] Irandoust, S., and Anersson, B., "Liquid film in Taylor flow through a capillary," *Ind. Eng. Chem.*, vol. 28, pp. 1684-1688, 1989.
- [36] Fukano, T. ; and Kariyasaki, A., "Characteristics of gas-liquid two-phase flow in a capillary tube," *Nuclear Engineering and Design*, vol. 141, no. 1-2, pp. 59-68, 1993.
- [37] Saitoh, S.; Daiguji, H.; and Hihara, E., "Correlation for boiling heat transfer of R-134a in horizontal tubes including effect of tube diameter," *International Journal of Heat and Mass Transfer*, vol. 50, no. 25-26, p. 5215–5225, 2007.
- [38] Revellin, R., Haberschill, P., Bonjour, J., and Thome, J.R., "Conditions of liquid film dryout during saturated flow boiling in microchannels," *Chem. Eng. Science*, vol. 63, pp. 5795-5801, 2008.
- [39] Ong, C.L.; and Thome, J.R., "Macro-to-microchannel transition in two-phase flow: Part 1 – Two-phase flow patterns and film thickness measurements," *Experimental Thermal and Fluid Science*, vol. 35, no. 1, pp. 37-47, 2011.
- [40] Han, Y., Shikazono, N., and Kasagi, N., "The effect of liquid film evaporation on flow boiling heat transfer in a micro tube," *Int. J. of Heat and Mass Transfer*, vol. 55, pp. 547-555, 2012.
- [41] Han, Y.; Kanno, H.; Ahn, Y-J.; and Shikazono, N. , "Measurement of liquid film thickness in micro tube annular flow," *International Journal of Multiphase Flow*, Vols. 264-274, pp. 264-274, 2015.
- [42] Piore, I.L. ; Cheng, S.C.; Groeneveld, D.C.; Vasic, A.Z.; Pinchon, S.; and Chen, G., "Experimental study of the effect of non-circular flow geometry on the CHF," *Nuclear Engineering and Design*, vol. 187, no. 3, p. 339–362, 1999.
- [43] Qu, W., and Mudawar, I., "Measurement and correlation of critical heat flux in two-phase micro-channel heat sinks," *Int. J. of Heat and Mass Transfer*, vol. 47, p. 2045–2059, 2004.
- [44] Zhang, W. ; Hibiki, T.; Mishima, K.; and Mi, Y. , "Correlation of critical heat flux for flow boiling of water in mini-channels," *International Journal of Heat and Mass Transfer*, vol. 49, no. 5-6, p. 1058–1072, 2006.
- [45] Wojtan, L.; Revellin, R.; and Thome, J.R., "Investigation of saturated critical heat flux in a single, uniformly heated microchannel," *Experimental Thermal and Fluid Science*, vol. 30, no. 8, pp. 765-774, 2006.
- [46] Qi, S.L. ; Zhang, P.; Wang, R.Z.; and Xu, L.X. , "Flow boiling of liquid nitrogen in micro-tubes: Part II - Heat transfer characteristics and critical heat flux," *International Journal of Heat and Mass Transfer*, vol. 50, no. 25-26, pp. 5017-5030, 2007.

- [47] Kosar, A.; Peles, Y.; Bergles, A. E.; and Cole, G. S., "Experimental investigation of critical heat flux in microchannels for flow-field probes," in *Proceedings of the 7th International Conference on Nanochannels, Microchannels, and Minichannels 2009*, Pohang, Korea, Republic of, 2009.
- [48] Basu, S.; Ndao, S.; Michna, G. J.; Peles, Y.; and Jensen, M. K. , "Flow boiling of R134a in circular microtubes part II study of critical heat flux condition," *Journal of Heat Transfer*, vol. 133, no. 5, p. 051503 (9 pp.), 2011.
- [49] Hsieh, S-S.; and Lin, C-Y. , "Correlation of critical heat flux and two-phase friction factor for subcooled convective boiling in structured surface microchannels," *International Journal of Heat and Mass Transfer*, vol. 55, no. 1-3, pp. 32-42, 2012.
- [50] Tibiriçá, C. B. ; Szczukiewicz, S.; Ribatski, G.; and Thome, J. R., "Critical Heat Flux of R134a and R245fa Inside Small-Diameter Tubes," *Heat Transfer Engineering*, vol. 34, no. 5-6, pp. 492-499, 2013.
- [51] Kaya, A. ; O'zdemir, M.R.; Keskinö'z, M.; and Kosar, A., "The effects of inlet restriction and tube size on boiling instabilities and detection of resulting premature critical heat flux in microtubes using data analysis," *Applied Thermal Engineering*, vol. 65, no. 1-2, pp. 575-87, 2014.
- [52] Revellin, R.; and Thome, J.R., "A theoretical model for the prediction of the critical heat flux in heated microchannels," *International Journal of Heat and Mass Transfer*, vol. 51, no. 5-6, pp. 1216-1225, 2008.
- [53] Du, D.X. ; Tian, W.X.; Su, G.H.; Qiu, S.Z.; Huang, Y.P.; and Yan, X. , "Theoretical study on the characteristics of critical heat flux in vertical narrow rectangular channel," *Applied Thermal Engineering* , vol. 36, no. 1, pp. 21-31, 2012.
- [54] Chen, J., "Correlation for Boiling Heat Transfer to Saturated Fluids in Convective Flow," *I & E C Process Design Development*, vol. 5, pp. 322-329, 1966.
- [55] Akers, W.W., Deans, H.A., and Crosser, O.K., "Condensation Heat Transfer within horizontal Tubes," *Chem. Eng. Prog. Symp. Ser.*, pp. 171-176, 1959.
- [56] Rohsenow, W., "A Method of Correlating Heat Transfer Data for Surface Boiling of Liquids," Massachusetts Institute of Technology, Cambridge, Massachusetts, 1951.
- [57] Wu, Z.; Sundén, B.; Li, W.; Wadekar, V.V. , "Evaporative Annular Flow in mini/micro channels A Simple Heat Transfer Model," *Journal of Thermal Science and Engineering Applications*, vol. 5, no. 3, pp. 1-10, 2013.
- [58] Ozawa, M. ; Ami, T.; Ishihara, I.; Umekawa, H.; Matsumoto, R.; Tanaka, Y.; Yamamoto, T.; Ueda, Y., "Flow pattern and boiling heat transfer of CO₂ in horizontal small-bore tubes," *International Journal of Multiphase Flow*, vol. 35, no. 8, pp. 699-709, 2009.
- [59] Li, H.; Wong, T.; Skote, M.; Duan, F., "Non-Newtonian two-phase stratified flow with curved interface through horizontal and inclined pipes," *International Journal of Heat and Mass Transfer*, vol. 74, pp. 113-120, 2014.
- [60] Kandlikar, S. G., "Heat Transfer Mechanisms During Flow Boiling in Microchannels," *J. of Heat Transfer*, vol. 126, no. 1, pp. 08-16, 2004.
- [61] Ducoulombier, M., Colasson, S., Bonjour, J., and Haberschill, P., "Carbon dioxide flow boiling in a single microchannel – Part II: Heat transfer," *Experimental Thermal and Fluid Science*, vol. 35, p. 597–611, 2011.

- [62] Baba, S.; Ohtani, N.; Kawanami, O.; Inoue, K.; Ohta, H. , "Experiments on dominant force regimes in flow boiling using mini-tubes," *Frontiers in Heat and Mass Transfer*, vol. 3, no. 4, pp. 1-8, 2012.
- [63] Bretherton, F. P., "The motion of long bubbles in tubes," *Journal of Fluid Mechanics* , vol. 10, no. 2, pp. 166- 188, 1961.
- [64] Shedd, T. A.; and Newel, T. A.I, "Characteristics of Liquid Film in Horizontal Two Phase Flow," Air Conditioning and Refrigeration Center, University of Illinois, Urbana, IL, 2001.
- [65] Han, Y.; and Shikazono, N., "Thickness of Liquid Film Formed in Micro Channel Slug Flow," in *7th JSME-KSME Thermal and Fluids Engineering Conference. TFEC 2008*, Sapporo, Japan, 2008.
- [66] Harirchian, T., and Garimella, S. V., "A comprehensive flow regime map for microchannel flow boiling with quantitative transition criteria," *Int. J. of Heat and Mass Transfer*, vol. 53, p. 2694–2702, 2010.
- [67] Kew, P. A., and Cornwell, K., "Correlations for the prediction of boiling heat transfer in small-diameter channels," *Applied Thermal Eng.* , vol. 17, pp. 705-715, 1997.
- [68] Suo, M.; and Griffith, P., "Two-phase Flow in capillary tubes," Massachusetts Institute of Technology, Cambridge, Massachusetts, 1963.
- [69] Brauner, N.; and Maron, D.M. , "Stability analysis of stratified liquid-liquid flow," *Int J Multi phase Flow*, vol. 18, no. 1, pp. 103-121, 1992.
- [70] Triplett, K.A., Ghiaasiaan, S.M., Abdel-Khalik, S.I., and Sadowski, D.L., "Gas-liquid two-phase flow in microchannels Part I: two-phase flow patterns," *Int. J. of Multiphase Flow*, vol. 25, pp. 377-394, 1999.
- [71] Mehendale, S.S. ; Jacobi, A.M.; Shah, R.K., "Fluid flow and heat transfer at micro- and meso-scales with application to heat exchanger design," *Appl Mech Rev.*, vol. 53, no. 7, pp. 175-193, 2000.
- [72] Kandlikar, S. G., "Two-Phase Flow Patterns, Pressure Drop, and Heat Transfer during Boiling in Mini-channel Flow Passages of Compact Evaporators," *heat transfer engineering*, vol. 23, no. 1, pp. 5-23, 2002.
- [73] Cheng, P.; and Wu, H.I., "Mesoscale and Microscale Phase Change Heat Transfer," *Advances in Heat Transfer*, vol. 39, p. 461–563, 2006.
- [74] Li, W. ; and Wu, Z., "A general correlation for adiabatic two-phase pressure drop in micro/mini-channels," *Int. J of Heat and Mass Transfer*, vol. 53, no. 13-14, p. 2732–2739, 2010.
- [75] Revellin, R., and Thome, J. R., "A new type of diabatic flow pattern map for boiling heat transfer in microchannels," *J. of Micromech. Microeng.*, vol. 17, p. 788–796, 2007.
- [76] Soliman, H., "The mist-annular transition during condensation and its influence on the heat transfer mechanism," *InL J. Muhiphase Flow*, vol. 12, no. 2, pp. 277-288, 1986.
- [77] Lee, C.H.; and Mudawwar, I., "A mechanistic critical heat flux model for subcooled flow boiling based," *Int. J. Multiphase Flow*, vol. 14, no. 6, pp. 711-728, 1988.
- [78] Shikazono, N.; and Han, Y., "Liquid Film Thickness in Micro-Scale Two-Phase Flow," *Two Phase Flow, phase change and numerical modeling*, pp. 341-364, 2011.
- [79] Garimella, S., Killion, J. D. and Coleman, J. W., "An Experimentally Validated Model for Two-Phase Pressure Drop in the Intermittent Flow Regime for Circular Microchannels,"

- Journal of Fluids Engineering*, vol. 124, p. 205–214, 2002.
- [80] Saisorn, S. and Wongwises, S., "Flow pattern, void fraction and pressure drop of two-phase air–water flow in a horizontal circular micro-channel," *Experimental Thermal and Fluid Science*, vol. 32, p. 748–760, 2008.
- [81] Karayiannis, T.G., Shiferaw, D., Kenning, D.B.R. and Wadekar, V.V., "Flow Patterns and Heat Transfer for Flow Boiling in Small to Micro Diameter Tubes," *Heat Transfer Engineering*, vol. 31, no. 4, p. 257–275, 2010.
- [82] Alexeyev, A.I.; Filippov, Y.P.; and Mamedov, I.S., "Flow patterns of two-phase helium in horizontal channels," *Cryogenics*, vol. 31, pp. 330-337, 1991.
- [83] Kattan, N.; Thome, J.R.; and Favrat, D., "Flow boiling in horizontal tubes. Part I Development of a diabatic two-phase flow pattern map," *J of Heat Transfer*, vol. 120, pp. 140-147, 1998.
- [84] Coleman, J.W.; and Garimella, S., "Characterization of two phase flow patterns in small diameter round and rectangular tubes," *Int. J. of Heat and Mass Transfer*, vol. 42, pp. 1758-1770, 1999.
- [85] Yang, C-Y.; and Shieh C-C., "Flow pattern of air-water and two-phase R-134a in small circular tubes," *Int. J. of Multiphase flow*, vol. 27, no. 7, pp. 1163-1177, 2001.
- [86] Thome, J. R., and El Hajal, J., "Two-Phase Flow Pattern Map for Evaporation in Horizontal Tubes: Latest Version," *Heat Transfer Eng.*, vol. 24, no. 6, pp. 3-10, 2003.
- [87] Rouhani, S.Z.; and Axelsson, E., "Calculation of Void Volume Fraction in the Subcooled and Quality Boiling Regions," *Int. J. Heat Mass Transfer*, vol. 13, no. 2, pp. 383-393, 1970.
- [88] Hassan, I.; Vaillancourt, M. ; and Pehlivan, K., "Two-Phase Flow Regime Transition in Microchannels : A Comprehensive Experimental Study," *Microscale Thermophysical Engineering*, vol. 9, no. 2, p. 165–182, 2005.
- [89] Cheng, L.; Ribatski, G.; Wojtan, L.; Thome, J. R., "New flow boiling heat transfer model and flow pattern map for carbon dioxide evaporating inside horizontal tubes," *Int. J. of Heat and Mass Transfer*, vol. 49, no. 21-22, p. 4082–4094, 2006.
- [90] Revellin, R., "Experimental two-phase fluid flow in microchannels," ÉCOLE POLYTECHNIQUE FÉDÉRALE DE LAUSANNE, Lausanne, 2006.
- [91] Revellin, R., Dupont, V., Ursenbacher, T., Thome, J.R., Zun, I. , "Characterization of diabatic two-phase flows in microchannels: Flow parameter results for R-134a in a 0.5 mm channel," *International Journal of Multiphase Flow*, vol. 32, no. 7, pp. 755-774, 2006.
- [92] Zhang, P.; and Fu, X., "Two-phase flow characteristics of liquid nitrogen in vertically upward 0.5 and 1.0 mm micro-tubes," *Cryogenics* , vol. 49, p. 565–575, 2009.
- [93] Rashid, A.; Björn, P.; and Mohammad, M. H., "A Visualization Study During Flow Boiling of R134a in a Horizontal Microchannel," in *ASME 2010 8th International Conference on Nanochannels, Microchannels, and Minichannels, ICNMM2010 Collocated with 3rd Joint US-European Fluids Engineering Summer Meeting*, Montreal, Canada, 2010.
- [94] Arcanjo, A. A.; Tibiriça, C. B.; and Ribatski, G., "Evaluation of flow patterns and elongated bubble characteristics during the flow boiling of halocarbon refrigerants in a micro-scale channel," *Experimental Thermal and Fluid Science*, vol. 34, no. 6, pp. 766-

- 775, 2010.
- [95] Barnea, D. ; Luninski, Y.; and Taitel, Y., "Flow pattern in horizontal and vertical two phase flow in small diameter pipes," *Canadian Journal of Chemical Engineering*, vol. 61, no. 5, pp. 617-620, 1983.
- [96] Felcar, H.O.M.; Ribatski, G.; and Saiz-Jabardo, J.M., "A gas liquid flow pattern predictive method for macro- and mini scale round channels," in *Proceedings of the 10th UK Heat Transfer Conference*, Edinburgh, Scotland, 2007.
- [97] Ong, C.L., and Thome, J.R., "Flow boiling heat transfer of R134a, R236fa and R245fa in a horizontal 1.030 mm circular channel," *Experimental Thermal and Fluid Science*, vol. 33, p. 651–663, 2009.
- [98] Celata, G.P. ; Cumo, M.; Dossevi, D.; Jilisen, R.T.M.; Saha, S.K.; and Zummo, G., "Flow pattern analysis of flow boiling inside a 0.48 mm microtube," *Int. J. of Thermal Sciences*, vol. 58, pp. 1-8, 2012.
- [99] Mishima, K. ; and Ishii, M., "Flow regime transition criteria for upward two-phase," *Int. J. of Heat and Mass Transfer*, vol. 27, no. 5, pp. 723-737, 1984.
- [100] McQuillan, K.W. ; and Whalley, P.B., "Flow patterns in vertical two-phase flow," *Int. J. of Multiphase Flow*, vol. 11, no. 2, pp. 161-175, 1985.
- [101] Mastrullo, R. ; Mauro, A.W.; Thome, J.R.; Toto, D.; and Vanoli, G.P. , "Flow pattern maps for convective boiling of CO₂ and R410A in a horizontal smooth tube: Experiments and new correlations analyzing the effect of the reduced pressure," *Int. J. of Heat and Mass Transfer*, vol. 55, no. 5-6, pp. 1519-1528, 2012.
- [102] Wojtan, L. ; Ursenbacher, T.; and Thome, J.R., "Investigation of flow boiling in horizontal tubes part I – a new diabatic two-phase flow pattern map," *Int. J. of Heat and Mass Transfer*, vol. 48, no. 14, pp. 2955-2969, 2005.
- [103] Cheng, L., Ribatski, G., Quibén, J.M., and Thome, J.R., "New prediction methods for CO₂ evaporation inside tubes: Part I – A two-phase flow pattern map and a flow pattern based phenomenological model for two-phase flow frictional pressure drops," *Int. J. of Heat and Mass Transfer*, vol. 51, p. 111–124, 2008.
- [104] Barbieri, P. E. L.; Jabardo, J. M. S.; and Bandarra Filho, E. P., "Flow patterns in convective boiling of refrigerant R-134a in smooth tubes of several diameters," in *5th European Thermal-Sciences Conference*, The Netherlands, 2008.
- [105] Canière, H.; Bauwens, B.; T'Joel, C. ; and De Paepe, M., "Mapping of horizontal refrigerant two-phase flow patterns based on clustering of capacitive sensor signals," *Int. J. of Heat and Mass Transfer*, vol. 53, no. 23-24, p. 5298–5307, 2010.
- [106] Ali, R.; Palm, B.; Martin-Callizo, C.; Maqbool, M. H. , "Study of flow boiling characteristics of a micro channel using high speed visualization," *Journal of Heat Transfer*, vol. 135, no. 8, pp. 1-8, 2013.
- [107] Martin-Callizo, C., Palm, B., Owhaib, W., and Ali, R., "Flow Boiling Visualization of R-134a in a Vertical Channel of Small Diameter," *J. of Heat Transfer*, vol. 132, no. 3, p. 031503 (8 pp.), 2010.
- [108] Charnay, R. ; Revellin, R.; Bonjour, J. , "Flow pattern characterization for R-245fa in minichannels: Optical measurement technique and experimental results," *International Journal of Multiphase Flow*, vol. 57, p. 169–181, 2013.

- [109] Tiberiça, C. ; and Ribatski, G., "Flow patterns and bubble departure fundamental characteristics during flow boiling in microscale channels," *Experimental Thermal and Fluid Science*, vol. 59, pp. 152-165, 2014.
- [110] Lazarek, G.M.; and Black, S.H., "Evaporative heat transfer, pressure drop and critical heat flux in a small vertical tube With R-113," *Int. J. of Heat and Mass Transfer*, vol. 25, no. 7, pp. 945-960, 1982.
- [111] Wambsganss, M.W., France, D.M., Jendrzeczyk, J.A., and Tran, T.N., "Boiling Heat Transfer in a Horizontal Small-Diameter Tube," *J. of Heat Transfer*, vol. 115, no. 4, p. 963-972, 1993.
- [112] Yen, T-H., Kasagi, N., and Suzuki, Y., "Forced convective boiling heat transfer in microtubes at low mass and heat fluxes," *Int. J. of Multiphase Flow*, vol. 29, no. 12, pp. 1771-1792, 2003.
- [113] Kandlikar, S.; and Balasubramanian, P., "Extending the applicability of the flow boiling correlation to low Reynolds number flows in microchannels," in *first international conference on microchannels and minichannels*, New York, USA, 2003.
- [114] Jacobi, A. M. and Thome, J. R., "Heat Transfer Model for Evaporation of Elongated Bubble Flows in Micro channels," *J. Heat Transfer*, vol. 124, pp. 1131-1136, 2002.
- [115] Qu, W.; and Mudawar, I., "Flow boiling heat transfer in two-phase micro-channel heat sinks Part I Experimental investigation and assessment of correlation methods," *Int. J. of Heat and Mass Transfer*, vol. 46, no. 15, p. 2755-2771, 2003.
- [116] Thome, J. R., and Consolini, L., "Mechanisms of Boiling in Micro-Channels: Critical Assessment," *Heat Transfer Eng.*, vol. 31, no. 4, p. 288-297, 2010.
- [117] Lee, J.; and Mudawar, I., "Two-phase flow in high-heat-flux micro-channel heat sink PII heat transfer characteristics," *International Journal of Heat and Mass Transfer*, vol. 48, no. 5, pp. 941-955, 2005.
- [118] Lee, P.C., Tseng, F.G., and Pan C., "Bubble dynamics in microchannels. Part I: single microchannel," *International Journal of Heat and Mass Transfer*, vol. 47, no. 25, p. 5575-5589, 2004.
- [119] Fu, X. ; Zhang, P.; Huang, C.J.; Wang, R.Z., "Bubble growth, departure and the following flow pattern evolution during flow boiling in a mini-tube," *International Journal of Heat and Mass Transfer*, vol. 53, no. 21-22, p. 4819-4831, 2010.
- [120] Lie, Y.M.; and Lin, T.F. , "Saturated flow boiling heat transfer and associated bubble characteristics of R-134a in a narrow annular duct," *Int. J. of Heat and Mass Transfer*, vol. 48, no. 25-26, p. 5602-5615, 2005.
- [121] Situ, R. ; Ishii, M.; Hibiki, T.; Tu, J.Y.; Yeoh, G.H.; and Mori, M. , "Bubble departure frequency in forced convective subcooled boiling flow," *Int. J. of Heat and Mass Transfer*, vol. 51, no. 25-26, pp. 6268-6282, 2008.
- [122] Agostini, B. ; Revellin, R.; and Thome, J.R. , "Elongated bubbles in microchannels Part I Experimental study and modeling of elongated bubble velocity," *Int. J. of Multiphase Flow*, vol. 34, no. 6, pp. 590-601, 2008.
- [123] Revellin, R. ; Agostini, B.; and Thome, J.R., "Elongated bubbles in microchannels. Part II Experimental study and modeling of bubble collisions," *Int. J. of Multiphase Flow*, vol. 34, no. 6, pp. 602-613, 2008.

- [124] Situ, R.; Hibiki, T.; Ishii, M.; Mori, M., "Bubble lift-off size in forced convective subcooled boiling flow," *Int. J. of Heat and Mass Transfer*, vol. 48, no. 25-26, pp. 5536-5548, 2005.
- [125] Moriyama, K., Inoue, A., "Thickness of the liquid film formed by a growing bubble in a narrow gap between two horizontal plates," *J. Heat Transfer*, vol. 118, p. 132–139, 1996.
- [126] Hazuku, T. ; Fukamachi, N.; Takamasa, T.; Hibiki, T.; and Ishii, M. , "Measurement of liquid film in microchannels using a laser focus displacement meter," *Experiments in Fluids*, vol. 38, no. 6, pp. 780-788, 2005.
- [127] Steinbrenner, J.E. ; Hidrovo, C.H.; Fu-Min Wang; Vigneron, S.; Eon Soo Lee; Kramer, T.A.; Ching-Hsiang Cheng; Eaton, J.K.; and Goodson, K.E., "Measurement and modeling of liquid film thickness evolution in stratified two-phase microchannel flows," *Applied Thermal Engineering*, vol. 27, no. 10, pp. 1722-1727, 2007.
- [128] Han, Y., and Shikazono, N., "Measurement of the liquid film thickness in micro tube slug flow," *Int. J. of Heat and Fluid Flow*, vol. 30, p. 842–853, 2009.
- [129] Han, Y., and Shikazono, N., "The effect of bubble acceleration on the liquid film thickness in micro tubes," *Int. J. of Heat and Fluid Flow*, vol. 31, p. 630–639, 2010.
- [130] Tibiriçá, C. B.; do Nascimento, F. J.; and Ribatski, G., "Film thickness measurement techniques applied to micro-scale two-phase flow systems," *Experimental Thermal and Fluid Science*, vol. 34, no. 4, pp. 463-473, 2010.
- [131] Kanno, H., Han, Y., Saito, Y., and Shikazono, N., "Measurement of liquid film thickness in micro tube annular flow," in *14th International Heat Transfer Conference IHTC 14*, Washington D.C., USA, 2010.
- [132] Kim, S-M. ; and Mudawar, I., "Universal approach to predicting saturated flow boiling heat transfer in minimicro-channels – Part I Dryout incipience quality," *Int.J. of Heat and Mass Transfer*, vol. 64, p. 1226–1238 , 2013.
- [133] Vandervort, C.L. ; Bergles, A.E.; and Jensen, M.K., "An experimental study of critical heat flux in very high heat flux subcooled boiling," *Int. J. of Heat and Mass Transfer*, vol. 37, no. 1, pp. 161-73, 1994.
- [134] Kandlikar, S., "Critical Heat Flux in Subcooled Flow Boiling – An Assessment of Current Understanding and Future Directions for Research," *Multiphase Science and Technology*, vol. 13, no. 3, pp. 207-232, 2001.
- [135] Hsieh, S-S. ; and Lin, C-Y., "Correlation of critical heat flux and two-phase friction factor for subcooled," *Int. J. of Heat and Mass Transfer*, vol. 55, p. 32–42, 2012.
- [136] Katto, Y., "A physical approach to critical heat flux of subcooled flow boiling in round tubes," *Int. J. of Heat and Mass Transfer*, vol. 33, no. 4, pp. 611-620, 1990.
- [137] Wu, Z.; and Li, W., "A new predictive tool for saturated critical heat flux in micro-mini-channels Effect of the heated length to diameter ratio," *Int. J. of Heat and Mass Transfer*, vol. 54, no. 13-14, pp. 2880-2889, 2011.
- [138] Roday, A.P. ; and Jensen, M.K., "Study of the critical heat flux condition with water and R-123 during flow boiling in microtubes. Part I: Experimental results and discussion of parametric effects," *Int. J. of Heat and Mass Transfer*, vol. 52, no. 13-14, pp. 3235-3249, 2009.
- [139] Ong, C.L.; and Thome, J.R. , "Macro-to-microchannel transition in two-phase flow: Part 2

- Flow boiling heat transfer and critical heat flux," *Experimental Thermal and Fluid Science*, vol. 35, no. 6, pp. 873-886, 2011.
- [140] Del Col, D. ; and Bortolin, S., "Investigation of dryout during flow boiling in a single microchannel under non-uniform axial heat flux," *Int. J. of Thermal Sciences*, vol. 57, pp. 25-36, 2012.
- [141] Kaya, A. ;Ozdemir, M.R.; and Kosar, A., "High mass flux flow boiling and critical heat flux in microscale," *Int. J. of Thermal Sciences*, vol. 65, pp. 70-78, 2013.
- [142] Katto, K. ; and Ohno, H. , "An improved version of the generalized correlation of CHF for the forced convective boiling in uniformly heated vertical tubes," *Int. J. of Heat and Mass Transfer*, vol. 27, no. 9, p. 1641–1648, 1984.
- [143] Shah, M., "Improved general correlation for critical heat flux during upflow in uniformly heated vertical tubes," *Int. J. of Heat and Fluid Flow*, vol. 8, no. 4, p. 326–335, 1987.
- [144] Choi, K., Pamitran, A.S., Oh, C-Y., and Oh, J-T., "Boiling heat transfer of R-22, R-134a, and CO₂ in horizontal smooth minichannels," *Int. J. of Refrigeration*, vol. 30, pp. 1336-1346, 2007.
- [145] Consolini, L. ; and Thome, J.R., "A heat transfer model for evaporation of coalescing bubbles in micro-channel flow," *International Journal of Heat and Fluid Flow*, vol. 31, no. 1, pp. 115-125, 2010.
- [146] Ribatski, G., "A critical overview on the recent literature concerning flow boiling and two-phase flows inside micro-scale channels," *Experimental Heat Transfer*, vol. 26, p. 198–246, 2013.
- [147] Moriyama, K. and Inoue, A., "The thermo hydraulic characteristics of two-phase flow in extremely narrow channels," *J. Heat Transfer-Japanese Research*, vol. 21, no. 8, pp. 838-856, 1992.
- [148] Damianides, C.A.; and Westwater, J.W., "Two-phase flow patterns in a compact heat exchanger and in small tubes," in *Second UK National Conference on Heat Transfer*, Glasgow, United kingdom, 1988.
- [149] Yan, Y-Y., and Lin, T-F., "Evaporation heat transfer and pressure drop of refrigerant R-134a in a small pipe," *Int. J. of Heat and Mass Transfer*, vol. 41, pp. 4183-4194, 1998.
- [150] Plesset, M.S. ; and Zwick, S.A., "The growth of vapor bubbles in superheated liquids," *J. of Applied Physics*, vol. 25, pp. 493-500, 1954.
- [151] Thome, J. R., Dupont, V., and Jacobi, A. M., "Heat transfer model for evaporation in micro channels-Part I: presentation of the mode," *Int. J. of Heat and Mass Transfer*, vol. 47, p. 3375–3385, 2004.
- [152] Dupont, V.; Thome, J.R.; Jacobi, A.M., "Heat transfer model for evaporation in microchannels Part II comparison with the database," *Int. J. of Heat and Mass Transfer*, vol. 47, p. 3387–3401, 2004.
- [153] Ribatski, G.; Zhang, W.; Consolini, L.; Xu, J.; Thome, J.R., "On the Prediction of Heat Transfer in Micro-Scale Flow Boiling," *Heat Transfer Engineering*, vol. 28, no. 10, p. 842–851, 2007.
- [154] Agostini, B., Thome, J. R., Fabbri, M., Michel, B., Calmi, D., and Kloter, U., "High heat flux flow boiling in silicon multi-microchannels Part II: Heat transfer characteristics of refrigerant R245fa," *Int. J. of Heat and Mass Transfer*, vol. 51, p. 5415–5425, 2008.

- [155] Mahmoud, M.M.; Karayiannis, T.G.; and Kenning, D.B.R., "Surface effects in flow boiling of R134a in microtubes," *Int. J. of Heat and Mass Transfer*, vol. 54, pp. 3334-33, 2011.
- [156] Oh, J-T., Pamitran, A.S., Choi, K., and Hrnjak, P., "Experimental investigation on two-phase flow boiling heat transfer of five refrigerants in horizontal small tubes of 0.5, 1.5 and 3.0 mm inner diameters," *Int. J. of Heat and Mass Transfer*, vol. 54, p. 2080–2088, 2011.
- [157] Basu, S., Ndao, S., Michna, G. J., Peles, Y., and Jensen, M. K., "Flow Boiling of R134a in Circular Microtubes—Part I: Study of Heat Transfer Characteristics," *Journal of Heat Transfer*, vol. 133, no. 051502, pp. 1-9, 2011.
- [158] Harirchian, T., and Garimella, S. V., "Flow regime-based modeling of heat transfer and pressure drop in microchannel flow boiling," *Int. J. of Heat and Mass Transfer*, vol. 55, p. 1246–1260, 2012.
- [159] Field, B.S. ;and Hrnjak, P. , "Adiabatic two-phase pressure drop of refrigerants in small channels," *Heat Transfer Engineering*, vol. 28, no. 8-9, p. 704–712, 2007.
- [160] Kim, Y.J., Jang, J., Hrnjak, P-S., and Kim, M.S., "Adiabatic Horizontal and Vertical Pressure Drop of Carbon Dioxide Inside Smooth and Microfin Tubes at Low Temperatures," *J. of Heat Transfer*, vol. 130, pp. 1-10, 2008.
- [161] Hashizume, K., "Flow pattern- void fraction and pressure drop refrigerant two-phase flow in a horizontal pipe — I- Experimental data," *Int. J. of Multiphase Flow*, vol. 9, no. 4, pp. 399-410, 1983.
- [162] Lin, S.; KWOK, C. C. K.; LI, R-Y.; CHEN, Z-H.; and CHEN, Z-Y., "Local frictional pressure drop during vaporization for R-12 through capillary tubes," *Int. J. of Multiphase Flow*, vol. 17, no. 1, pp. 95-102, 1991.
- [163] Hahne, E. ; Spindler, K.; and Skok, H. , "New pressure drop correlation for subcooled flow boiling of refrigerants," *Int. J. of Heat and Mass Transfer*, vol. 37, no. 17, pp. 4267-4274, 1993.
- [164] Tran, T.N, Chyu, M.C., Wambsganss, M.W, and France,D.M, "Two-phase pressure drop of refrigerants during Flow boiling in small channels: an experimental investigation and correlation development," *Int. J. of Multiphase Flow*, vol. 26, p. 1739–1754, 2000.
- [165] Yun, R., and Kim, Y., "Two-Phase Pressure Drop of CO₂ in Mini Tubes and Microchannels," *Microscale Thermophysical Engineering*, vol. 8, p. 259–270, 2004.
- [166] Hwang, Y.W., and Kim, M.S., "The pressure drop in microtubes and the correlation development," *Int. J. of Heat and Mass Transfer*, vol. 49, p. 1804–1812, 2006.
- [167] Park, C.Y, and Hrnjak, P.S., "Carbon Dioxide and R410a Flow Boiling Heat Transfer, Pressure Drop, and Flow Pattern in Horizontal Tubes at Low Temperatures," *ACRC TR-258*, vol. 217, p. 333–3115, 2007.
- [168] Huh, C.; and Kim,M.H., "Pressure Drop, Boiling Heat Transfer and Flow Patterns During flow Boiling in a Single Microchannel," *Heat Transfer Engineering*, vol. 28, no. 8-9, pp. 730-737, 2007.
- [169] Pamitran, A.S.; Choia, K.I.; Oh, J.T; and Oh, H.K., "Two-phase pressure drop during CO₂ vaporization in horizontal smooth minichannels," *Int. J. of refrigeration*, vol. 31, pp. 1375-1383, 2008.
- [170] Orell, A., "Experimental validation of a simple model for gas–liquid slug flow in

- horizontal pipes," *Chemical Engineering Science*, vol. 60, no. 5, pp. 1371-181, 2005.
- [171] Quibén, M.J.; and Thome, J.R., "Flow pattern based two phase frictional pressure drop model for horizontal tubes Part II new phenomenological model," *International Journal of Heat and Fluid Flow*, vol. 28, no. 5, p. 1060–1072, 2007.
- [172] Cioncolini, A., Thome, J.R., and Lombardi, C., "Unified macro-to-microscale method to predict two-phase frictional pressure drops of annular flows," *Int. J. of Multiphase Flow*, vol. 35, p. 1138–1148, 2009.
- [173] Mishima, K.; and Hibiki, T., "Some Characteristics of Air-Water Two-Phase Flow in Small Diameter Vertical Tubes," *Int. J. Multiphase Flow*, vol. 22, no. 4, pp. 703-712, 1996.
- [174] Kandlikar, S., "Fundamental issues related to flow boiling in minichannels and microchannels," *Experimental Thermal and Fluid Science*, vol. 26, no. 2-4, pp. 389-407, 2009.
- [175] Hewitt, G.F.; and Roberts, D.N., "Studies of two-phase flow patterns by simultaneous X-ray and flash photography," Atomic Energy Research Establishment, Harwell (England), Harwell, England, 1969.
- [176] Tibirică, C.B., Diniz da Silva, J., and Ribatski, G., "Experimental Investigation of Flow Boiling Pressure Drop of R134A in a Microscale Horizontal Smooth Tube," *J. of Thermal Science and Engineering Applications*, vol. 3, pp. 1-8, 2011.
- [177] Wu, J., Koettig, T., Franke, C., Helmer, D., Eisel, T., Haug, F., and Bremer, J., "Investigation of heat transfer and pressure drop of CO₂ two-phase flow in a horizontal minichannel," *Int. J. of Heat and Mass Transfer*, vol. 54, p. 2154–2162, 2011.
- [178] Choi, C. ; and Kim, M. , "Flow pattern based correlations of two-phase pressure drop in rectangular microchannels," *Int. J. of Heat and Fluid Flow*, vol. 32, no. 6, pp. 1199-1203, 2011.
- [179] Maqbool, M.H., Palm, B., and Khodabandeh, R., "Flow boiling of ammonia in vertical small diameter tubes: Two phase frictional pressure drop results and assessment of prediction methods," *Int. J. of Thermal Sciences*, vol. 54, pp. 1-12, 2012.
- [180] Lim, T.W.; You, S.S.; Kim, J.S.; Moon, S.B.; Seo, D.H., "Two-phase pressure drop due to friction in micro-channel," *J. of Mechanical Engineering Science*, vol. 228, no. 5, pp. 921-931, 2014.
- [181] Yu, W. ; France, D.M.; Wambsganss, M.W.; Hull, J.R., "Two-phase pressure drop, boiling heat transfer, and critical heat flux to water in a small-diameter horizontal tube," *International Journal of Multiphase Flow*, vol. 28, no. 6, pp. 927-941, 2002.
- [182] Qu, W. ; and Mudawar, I., "Measurement and prediction of pressure drop in two-phase micro-channel heat sinks," *Int. J. of Heat and Mass Transfer*, vol. 46, no. 15, pp. 2737-2753, 2003.
- [183] Lee, J. ; and Mudawar, I., "Two-phase flow in high-heat-flux micro-channel Part I—pressure drop characteristics," *Int. J. of Heat and Mass Transfer*, vol. 48, no. 5, pp. 928-940, 2005.
- [184] Choi, K.I.; Pamitran, A.S.; Oh, C. Y.; Oh, J. T., "Two-phase pressure drop of R-410A in horizontal smooth minichannels," *Int. J. of Refrigeration*, vol. 31, no. 1, pp. 119-129, 2008.
- [185] Lee, P. S.; and Garimella, S. V., "Saturated flow boiling heat transfer and pressure drop in silicon microchannel array," *Int. J. of Heat and Mass Transfer*, vol. 51, no. 3-4, pp. 789-

806, 2008.

- [186] Del Col, D. ; Bortolato, M.; and Bortolin, S. , "Comprehensive experimental investigation of two-phase heat transfer and pressure drop with propane in a minichannel," *Int. J. of Refrigeration*, vol. 47, pp. 66-84, 2014.
- [187] Y. Katto, "A generalized correlation of critical heat flux for the forced convection boiling in vertical uniformly heated round tubes," *Int. J. of Heat and Mass Transfer*, vol. 21, p. 1527–1542, 1978.
- [188] Bergles, A.E, and Kandlikar, S. G., "On the Nature of Critical Heat Flux in Microchannels," *J. of Heat Transfer*, vol. 127, pp. 101-107, 2005.
- [189] Chen, T., and Garimella, S. V., "A Study of Critical Heat Flux During Flow Boiling in Microchannel Heat Sinks," *Int. J. of Heat and Mass Transfer*, vol. 134, p. 01–09, 2012.
- [190] Kosar, A., "A model to predict saturated critical heat flux in minichannels and microchannels," *Int. J. of Thermal Sciences*, vol. 48, no. 2, pp. 261-270, 2009.
- [191] Kandlikar, S., "A Scale analysis based theoretical force balance model for critical heat flux (CHF) during saturated flow boiling in microchannels and minichannels," *J. of Heat Transfer*, vol. 132, no. 8, pp. 1-13, 2010.
- [192] Serizawa, A., Feng, Z., and Kawara, Z., "Two-phase flow in microchannels," *Experimental Thermal and Fluid Science* , vol. 26, p. 703–714, 2002.
- [193] Qu, W., and Mudawar, I., "Transport Phenomena in Two-Phase Micro-Channel Heat Sinks," *Int. J. of Electronic Packaging*, vol. 126, p. 213–224, 2004.
- [194] Kuznetsov, V. V., Shamirzaev, A. S., Kozulin, I. A., and Kozlov, S. P., "Correlation of the Flow Pattern and Flow Boiling Heat Transfer in Microchannel," *Heat Transfer Engineering*, vol. 34, p. 235–245, 2013.
- [195] Jiang, L., Wong, M., and Zohar, Y., "Forced Convection Boiling in a Microchannel Heat Sink," *J. Microelectromech. Syst.*, vol. 10, no. 1, p. 80–87, 2001.
- [196] Zhang, L., Koo, J., Jiang, L., Ashghi, M., Goodson, K. E., Santiago, J. G., and Kenny, T. W., "Measurements and Modeling of Two-Phase Flow in Microchannels With Nearly Constant Heat Flux Boundary Conditions," *Int. J. of Microelectromechanical systems*, vol. 11, no. 1, pp. 12-19, 2002.
- [197] Lee, H. J., Liu, D. Y., and Yao, S., "Flow instability of evaporative micro-channels," *Int. J. of Heat and Mass Transfer*, vol. 53, pp. 1740-1749, 2010.
- [198] Ghiaasiaan, S. M., "Two-phase Flow, Boiling, and Condensation in Convective and Miniature Systems," New York: Cambridge University Press, 32 Avenue of the Americas,, 2008.
- [199] Ishii, M., and Mishima, K., "Two-fluid model and hydrodynamic constitutive relations," *Nuclear Engineering and Design*, vol. 82, pp. 107-126, 1984.
- [200] Wallis, B. G., One-dimensional Two-phase Flow, New York, USA: McGraw-Hill, Inc, 1969.
- [201] Kim, S., and Mudawar, I., "Theoretical model for annular flow condensation in rectangular micro-channels," *Int. J. of Heat and Mass Transfer*, vol. 55, p. 958–970, 2012.
- [202] Aussillous, P., and Quere, D., "Quick deposition of a fluid on the wall of a tube," *Physics of fluids*, vol. 12, no. 10, pp. 2367-2371, 2000.

- [203] Park, J. E.; and Thome, J. R., "Critical heat flux in multi-microchannel copper elements with low pressure refrigerants," *Int. J. of Heat and Mass Transfer*, vol. 53, no. 1-3, p. 110–122, 2009.
- [204] Cavallini, A., Del Col, D., and Rossetto, L., "Pressure Drop During Two-Phase Flow of R134a and R32 in a Single Minichannel," *Journal of Heat transfer*, vol. 131, pp. 01-08, 2009.
- [205] Yun, R., Kim, Y., Kim, M. S., "Flow boiling heat transfer of carbon dioxide in horizontal mini tubes," *International Journal of Heat and Fluid Flow*, vol. 26, p. 801–809, 2005.
- [206] Ali, R., Palm, B., and Maqbool, M.H., "Flow Boiling Heat Transfer of Refrigerants R134a and R245fa in a Horizontal Micro-Channel," *Experimental Heat Transfer*, vol. 25, p. 181–196, 2012.
- [207] Mahmoud, M.M., and Karayiannis, T.G., "Heat transfer correlation for flow boiling in small to micro tubes," *Int. J. of Heat and Mass Transfer*, vol. 66, p. 553–574, 2013.
- [208] LaClair, T. J., and Mudawar, I., "Theoretical model for fast bubble growth in small channels with reference to startup of capillary pumped loops used in spacecraft thermal management systems," *International Journal of Heat and Mass Transfer*, vol. 52, p. 716–723, 2009.
- [209] Na, Y.W.; and Chung, J.N., "Two-phase annular flow and evaporative heat transfer in a microchannel," *Int. J. of Heat and Fluid Flow*, vol. 32, pp. 440-450, 2011.
- [210] Das, A.K., Das, P.K., and Saha, P., "Heat transfer during pool boiling based on evaporation from micro and macrolayer," *International Journal of Heat and Mass Transfer*, vol. 49, p. 3487–3499, 2006.
- [211] Celata, G.P., Mishima, K., Zummo, G., "Critical heat flux prediction for saturated flow boiling of water in vertical tubes," *International Journal of Heat and Mass Transfer*, vol. 44, pp. 4323-4331, 2001.
- [212] Thome, J., "Boiling in microchannels: a review of experiment and theory," *International Journal of Heat and Fluid Flow*, vol. 25, p. 128–139, 2004.
- [213] Cioncolini, A., and Thome, J.R., "Entrained liquid fraction prediction in adiabatic and evaporating annular two-phase flow," *Nuclear Engineering and Design*, vol. 243, p. 200–213, 2012.
- [214] Wu, H.Y., and Cheng, P., "Visualization and measurements of periodic boiling in silicon microchannels 2603–2614," *Int. J. of Heat and Mass Transfer*, vol. 46, p. 2603–2614, 2003.
- [215] Wayner, P.C., Jr.; Kao, Y.K.; and LaCroix, L.V., "The interline heat-transfer coefficient of an evaporating wetting film," *International Journal of Heat and Mass Transfer*, vol. 19, no. 5, pp. 487-492, 1976.
- [216] Carey, V., "Liquid-vapor Phase Change Phenomena," New York: Hemisphere, 1992.
- [217] Schonberg, J.A.; DasGupta, S.; and Wayner Jr., P.C., "Augmented Young-Laplace model of an evaporating meniscus in a microchannel with high heat flux," *Experimental Thermal and Fluid Science*, vol. 10, no. 2, pp. 163-170, 1995.
- [218] Vij, A.K.; and Dunn, W.E., "Modeling of Two-Phase Flows in Horizontal Tubes," Air Conditioning and Refrigeration Center, Urbana, 1996.
- [219] Chisholm, D., "A theoretical basis for the Lockhart-Martinelli correlation for two-phase

- flow," *International Journal of Heat and Mass Transfer*, vol. 10, no. 12, pp. 1767-1778, 1967.
- [220] Henstock, W.; and Hanratty, T., "The Interfacial Drag and the Height of the Wall Layer in Annular Flows," *American Institute of Chemical Engineering*, vol. 22, no. 6, pp. 990-1000, 1976.
- [221] Andritsos, N.; and Hanratty, T. J., "Influence of Interfacial Waves in Stratified Gas-Liquid Flows," *AIChE Journal*, vol. 33, no. 3, pp. 444-454, 1987.
- [222] Hartnett, J.P.; and Minkowycz, W.J., "Interfacial Friction Factor in Vertical Upward," *Int. Comm. Heat Mass Transfer*, vol. 28, no. 3, pp. 323-336, 2001.
- [223] Churchill, S., "Friction-Factor Equation Spans All Fluid-Flow Regimes," *Chemical Engineering*, no. 84, p. 91-92, 1977.
- [224] Laohalertdecha, S., and Wongwises, S., "An experimental study into the evaporation heat transfer and flow characteristics of R-134a refrigerant flowing through corrugated tubes," *Int. J. of Refrigeration*, vol. 34, no. 1, pp. 280-291, 2011.
- [225] Han, Y., and Shikazono, N., "Measurement of liquid film thickness in micro square channel," *Int. J. of Multiphase Flow*, vol. 35, p. 896-903, 2009.
- [226] Saitoh, S., Daiguji, H., and Hihara, E., "Effect of tube diameter on boiling heat transfer of R-134a in horizontal small-diameter tubes," *Int. J. of Heat and Mass transfer*, vol. 48, p. 4973-4984, 2005.
- [227] Ducoulombier, M., Colasson, S., Bonjour, J., and Haberschill, P., "Carbon dioxide flow boiling in a single microchannel – Part I: Pressure drops," *Experimental Thermal and Fluid Science*, vol. 35, p. 581-596, 2011.
- [228] Shedd, T., "Void fraction and pressure drop measurements for refrigerant R410a flows in small diameter tubes," multiphase flow visualization and analysis laboratory, Madison, 2010.
- [229] Qian, D.; and Lawal, A., "Numerical study on gas and liquid slugs for Taylor flow in a T-junction microchannel," *Chemical Engineering Science*, vol. 61, no. 23, p. 7609-7625, 2006.
- [230] He, Q.; and Kasagi, N., "NUMERICAL INVESTIGATION ON FLOW PATTERN AND PRESSURE DROP," in *Proceedings of the Sixth International ASME Conference on Nanochannels, Microchannels and Minichannels*, Darmstadt, Germany, 2008.
- [231] Zhuan, R.; and Wang, W., "Flow pattern of boiling in micro-channel by numerical simulation," *International Journal of Heat and Mass Transfer*, vol. 55, no. 5-6, p. 1741-1753, 2012.
- [232] Magnini, M.; Pulvirenti, B.; and Thome, J.R., "Numerical investigation of hydrodynamics and heat transfer of elongated bubbles during flow boiling in a microchannel," *International Journal of Heat and Mass Transfer*, vol. 59, no. 1, p. 451-471, 2013.
- [233] Abiev, R. S., "Simulation of the Slug Flow of a Gas-Liquid System in Capillaries," *Theoretical Foundations of Chemical Engineering*, vol. 42, no. 2, p. 115-127, 2008.
- [234] Cooper, M., "THE MICROLAYER AND BUBBLE GROWTH IN NUCLEATE POOL BOILING," *Int. J. Heat Mass Transfer*, vol. 12, no. 8, pp. 915-933, 1969.
- [235] Mikic, B.B.; Rohsenow, W.M.; Griffith, P., "On bubble growth rates," *International Journal of Heat and Mass Transfer*, vol. 13, no. 4, pp. 657-66, 1970.

- [236] Mehta, B.; and Khandekar, S., "Measurement of local heat transfer coefficient during gas–liquid Taylor bubble train flow by infra-red thermography," *International Journal of Heat and Fluid Flow*, vol. 45, no. 1, pp. 41-52, 2014.
- [237] Patil, C.M.; and Kandlikar, S.G., "Pool boiling enhancement through microporous coatings selectively electrodeposited on fin tops of open microchannels," *International Journal of Heat and Mass Transfer*, vol. 79, pp. 816-828, 2014.
- [238] Houshmand, F.; and Peles, Y., "Transient wall temperature measurements of two-phase slug flow in a microchannel," in *Thermomechanical Phenomena in Electronic Systems - Proceedings of the Intersociety Conference*, NY, United States, 2014.
- [239] Yan, C.; Yan, C.; Sun, L.; Wang, Y.; and Zhang, X., "Slug behavior and pressure drop of adiabatic slug flow in a narrow rectangular duct under inclined conditions," *Annals of Nuclear Energy*, vol. 64, pp. 21-31, 2014.
- [240] Fukano, T.; Kariyasaki, A.; and Kagawa, M., "Flow Patterns and Pressure Drop in Isothermal Gas-Liquid Concurrent Flow in a Horizontal Capillary Tube," in *ANS Proceedings 1989 National Heat Transfer Conference: August 6-9, 1989*, Philadelphia, 1989.
- [241] Abiev, R., "Method for Calculating the Void Fraction and Relative Length of Bubbles under Slug Flow Conditions in Capillaries," *Theoretical Foundations of Chemical Engineering*, vol. 44, no. 1, p. 86–101, 2010.
- [242] Chen, W.L.; Twu, M.C.; Pan, C., "Gas–liquid two-phase flow in micro-channels," *International Journal of Multiphase Flow*, vol. 28, no. 7, p. 1235–1247, 2002.
- [243] Ishii, M., "One-dimensional drift-flux model and constitutive equations for relative motion between phases in various two-phase flow regimes," Argonne National Lab., Ill. (USA), Argonne, Illinois, United States, 1977.
- [244] Barnea, D.; and Brauner, N., "HOLDUP OF THE LIQUID SLUG IN TWO PHASE INTERMITTENT FLOW," *Int. J. Multiphase Flow*, vol. 11, no. 1, pp. 43--49, 1985.
- [245] Taitel, Y.; Saricab, C.; and Bril,J.P., "Slug Flow modeling for downward inclined pipe Flow: theoretical considerations," *International Journal of Multiphase Flow 26 (2000)* 833±844, vol. 26, no. 5, pp. 833-844, 2000.
- [246] Hetsroni, G.; Mosyak, A.; Pogrebnyak, E.; Segal, Z., "Periodic boiling in parallel micro-channels at low vapor quality," *International Journal of Multiphase Flow*, vol. 32, no. 10, p. 1141–1159, 2006.
- [247] N. S. R. Data, "Thermophysical Properties of Fluid Systems," NIST Standard Reference Data, 2011. [Online]. Available: <http://webbook.nist.gov/chemistry/fluid/>. [Accessed 7 January 2015].
- [248] Cornwell, K.; and Kew, P.A., "Boiling in small parallel channels," *In Energy & ficiency in Process Technology*, pp. 624-638, 1993.
- [249] Shah, M., "Chart correlation for saturated boiling heat transfer equations and further study," *ASHRAE Transactions*, vol. 88, no. 1, pp. 185-196, 1982.
- [250] Gungor, K.E.; and Winterton, R.H.S., "A general correlation for flow boiling in tubes and annuli," *J. of Heat and Mass Transfer*, vol. 29, no. 3, pp. 351-358, 1986.
- [251] Liu, Z.; and Winterton, R.H.S., "A general correlation for saturated and subcooled flow boiling in tubes and annuli, based on a nucleate pool boiling equation," *J. of Heat and*

- Mass transfer*, vol. 34, no. 11, pp. 2759-2766, 1991.
- [252] Tran, T.N.; Wambsganss, M. W.; and France, D. M. , "Boiling heat transfer with three fluids in small circular and rectangular," Argonne National Laboratory, University of Chicago, Argonne, Illinois, 1995.
- [253] Kandlikar, S.; and Balasubramanian, P., "An extension of the flow boiling correlation to transition, laminar and deep laminar flows in mini-channels and micro-channels," *Heat Transfer Engineering*, vol. 25, no. 3, p. 86–93, 2004.
- [254] Choo, K. ; and Kim, S.J., "Heat Transfer and Fluid Flow Characteristics of Nonboiling Two-Phase Flow in Microchannels," *J. of Heat Transfer*, vol. 133, no. 10, p. p 102901 (7 pp.), 2011.
- [255] Kim, S.M. ; and Mudawar, I., "Universal approach to predicting saturated flow boiling heat transfer in mini/micro-channels - Part II. Two-phase heat transfer coefficient," *Int. J. of Heat and Mass Transfer*, vol. 64, p. 1239–1256, 2013.
- [256] Fang, X., "A new correlation of flow boiling heat transfer coefficients for carbon dioxide," *Int. J. of Heat and Mass Transfer*, vol. 64, p. 802–807, 2013.
- [257] Kim, K.W.; Chien, N.B.; Choi, K.I.; and Oh, J.T., "Measurement and correlation of boiling heat transfer coefficient of R-1234yf in horizontal small tubes," *J. of Mechanical Science and Technology*, vol. 28, no. 10, pp. 4301-4308, 2014.
- [258] Wu, Z.; Sunden, B.; Yao, S.C.; Wadekar, V.V.; Li, W. , "Simple flow-pattern based heat transfer correlations for flow boiling in micro/minichannels," in *Proceedings of the ASME 2014 12th International Conference on Nanochannels, Microchannels, and Minichannels*, Chicago, Illinois, USA, 2014.
- [259] Chisholm, D., "Pressure gradients due to friction during the flow of evaporating two-phase mixtures in smooth tubes and channels," *Int. J. of Heat and Mass Transfer*, vol. 16, no. 2, pp. 347-358, 1973.
- [260] Lee,H.J. ; and Lee, S.Y. , "Pressure drop correlations for two-phase flow within horizontal rectangular channels with small heights," *International Journal of Multiphase Flow*, v 27, n 5, p , vol. 27, no. 5, pp. 783-796, 2001.
- [261] Zhang, M., and Webb, R.L., "Correlation of Two-phase friction for Refrigerants in Small-Diameter Tubes," *Experimental and Thermal of Fluid Science*, vol. 25, p. 131–139, 2001.

Appendix A

Table (A-1): Essential dimensionless groups for two-phase flow in horizontal mini/micro-channels.

| Dimensionless Group | Symbol | Definition | Notes |
|--------------------------|-------------|--|--|
| Reynolds No. | Re | $\frac{\rho U D_h}{\mu}$ | It shows the significance of inertial force with respect to viscous force. |
| Two-Phase Reynolds No. | Re_{TP} | $\frac{\rho_f U_{TP} D_h}{\mu_f}$ | Proposed by Chen [54], and expressed in terms of the effective two-phase velocity, U_{TP} . |
| Equivalent Reynolds No. | Re_{eq} | $\frac{GD_h}{\mu_f} \left[(1-x) + x(\rho_f/\rho_g)^{0.5} \right]$ | Suggested by Akers et al. [55], and represented in terms of the two-phase dynamic viscosity. |
| Liquid Film Reynolds No. | Re_δ | $\frac{4G(1-x)}{\mu_f(1-\alpha)}$ | It was presented by Wu et al. [57], and expressed in terms of vapor quality and void fraction. |

| | | | |
|---------------------|--------|--|--|
| Bubble Reynolds No. | Re_b | $\frac{G_b D_b}{\mu_b}$ | Rohsenow [56] studied nucleate boiling on heated surface and identified Reynolds number based on bubble diameter and bubble mass flux. |
| Bond number. | Bo | $\frac{g(\rho_f - \rho_g)L^2}{\sigma}$ | The ratio between the gravitational force and surface tension force. Additionally, Bond number can show the tendency of the phase-stratification, Ozawa et al. [58], and indicates the shape of the interface and the effects of wettability angle, Li et al. [59]. |
| Boiling number. | Bl | $\frac{q_w''}{G h_{fg}}$ | The ratio between the applied heat flux q_w'' and the latent heat of evaporation h_{fg} . Moreover, it has been used in several heat transfer correlations for two phase flow, Kandlikar [60]. Moreover, it has been proposed as transition criterion to distinguish two different heat transfer flow regimes in a single micro-channel as presented by Ducoulombier et al. [61] |
| Vapor quality | x | $\frac{\dot{m}_g}{\dot{m}_t}$ | It is defined as the ratio of vapor mass flow rate \dot{m}_g , to the total mass rate \dot{m}_t . Moreover, it is significantly employed to correlate heat transfer and pressure drop database of flow boiling in mini/micro-channels. |
| Weber No. | We | $\frac{G^2 D_h}{\rho \sigma}$ | It represents the ratio between the inertia and surface tension forces. It has been employed particularly for identifying flow pattern |

| | | | |
|----------------------------|-----------|--|---|
| | | | transition boundaries, Kandlikar [60]. Moreover, various ways have been suggested in the literature for calculating Weber number based on the dominant flow pattern. |
| Froude No. | Fr | $\frac{G}{\sqrt{\rho_m(\rho_f - \rho_g)gD_h}}$ | It represents the ratio between inertial and gravitational forces, Baba et al. [62]. |
| Capillary No. | Ca | $\frac{\mu U}{\sigma}$ | It represents the ratio between the viscous force and surface tension force. Moreover, it has been employed intensively for correlating liquid film thickness in slug flow and annular flow regimes, (e.g. Bretherton [63], Irandoust and Andersson [35], Shedd and Newell [64], Han and Shikazono [65]). |
| Confinement No. | Co | $\frac{[\sigma/g(\rho_l - \rho_g)]^{0.5}}{D}$ | It was introduced by Cornwell and Kew [248, 67], and defined as the ratio between the bubble departure diameter and the channel diameter. |
| Convective Confinement No. | N_{con} | $Bo^{0.5} \times Re$ | It was proposed by Harirchian and Garimella [66] as a new confinement transition criterion to distinguish the transition from macro to micro scale channels. It is defined in terms of Bond number and Reynolds. |

Table (A-2): Common predictive methods for evaluating heat transfer coefficient for two-phase flow in mini/micro-channels in mini/micro-channels

| Author(s) | Working fluid(s), orientation | Geometry: D_h [mm], L_h [mm] | Parameter range: G [kg/m ² .s], q_w'' [kW/m ²], T_{sat} [°C], p_{sat} [kPa] | Proposed correlation |
|------------|--|--|--|--|
| Chen [54] | Water, organic fluids, V | | | $h_{tp} = h_{mic} + h_{mac}$ $h_{mac} = 0.023(Re_l)^{0.8}(Pr_l)^{0.4}(k_l/D_h)F$ $h_{mic} = 0.00122 \left(\frac{k_l^{0.79} C_{pl}^{0.45} \rho_l^{0.49} g_c^{0.25}}{\sigma^{0.5} \mu_l^{0.29} h_{lv}^{0.24} \rho_v^{0.24}} \right) \Delta T_{sat}^{0.24} \Delta p_{sat}^{0.75} S$ |
| Shah [249] | Water R11 R12 R22 R113 Cyclohexane V & H | Tubes: $6 \leq D \leq 41mm$ Annuli: $1.1 \leq \delta \leq 6.2 mm$ | | $h_{tp} = \psi h_l$ $h_l = 0.023 \left(\frac{G(1-x)D}{\mu_l} \right)^{0.8} Pr_l^{0.4} (k_l/D)$ $\psi = \text{MAX}(\psi_{nb}, \psi_{cb})$ $\psi_{cb} = 1.8/N^{0.8}$ $Co = [(1/x) - 1]^{0.8} (\rho_g/\rho_l)^{0.5}$ $N = Co \text{ for } Fr_l \geq 0.04$ $N = 0.38CoFr_l^{-0.3} \text{ for } Fr_l < 0.04$ <p>For $N > 1.0$:</p> $\psi_{nb} = 230Bo^{0.5}; \text{ for } Bo > 0.3 \times 10^{-4}$ $\psi_{nb} = 1 + 46Bo^{0.5}; \text{ for } Bo < 0.3 \times 10^{-4}$ $\psi = \text{MAX}(\psi_{nb}, \psi_{cb})$ <p>For $0.1 < N \leq 1.0$:</p> $\psi_{bs} = FBo^{0.5} \exp(2.74N^{-0.1})$ $\psi = \text{MAX}(\psi_{bs}, \psi_{cb})$ <p>For $N \leq 0.1$:</p> $\psi_{bs} = FBo^{0.5} \exp(2.47N^{-0.15})$ $\psi = \text{MAX}(\psi_{bs}, \psi_{cb})$ |

| | | | | |
|--------------------------|---|--|--|---|
| | | | | $F = 14.7; \text{ for } Bo \geq 11 \times 10^{-4}$ $F = 15.43; \text{ for } Bo < 11 \times 10^{-4}$ |
| Lazarek & Black [110] | R113 728 data points V | $D = 3.15 \text{ mm}$ $L_h = 123, 246 \text{ mm}$ | $140 \leq G \leq 740,$ $130 \leq p_{sat} \leq 410$ $3 \leq \Delta T_{sub} \leq 73$ | $Nu = 30Re^{0.857}Bl^{0.714}$ $Nu = h(D_h/k_l)$ |
| Gungor & Winterton [250] | Seven fluids (Water Refrigerants Ethylene-glycol) 4,300 data points V & H Annuli & Tubes | | | $h_{tp} = Eh_l + Sh_{pool}$ $h_l = 0.023(Re_l)^{0.8}(Pr_l)^{0.4}(k_l/D_h)$ $h_{pool} = 55(Pr_l)^{0.12}(-\log_{10}Pr_l)^{-0.55}M^{-0.5}(q_w'')^{0.67}$ $E = 1 + 24000(Bo)^{1.16} + 1.37(1/X_{tt})^{0.86}$ $S = \frac{1}{1 + 1.15 \times 10^{-6}E^2Re_l^{1.17}}$ $X_{tt} = \left(\frac{1-x}{x}\right)^{0.9} \left(\frac{\rho_v}{\rho_l}\right)^{0.5} \left(\frac{\mu_l}{\mu_v}\right)^{0.1}$ |
| Liu & Winterton [251] | Nine fluids 4,202 sat. Data points 991 sub. Data points V & H Annuli & Tubes | $2.95 \leq D_h \leq 32$ | $12.4 \leq G \leq 8179.3$ $0.35 \leq q_w'' \leq 2,620$ $0.2 \leq \Delta T_{sat} \leq 62.3$ $0.0023 \leq p_r \leq 0.895$ $0.1 \leq \Delta T_{sub} \leq 173.7$ | $h_{tp}^2 = (Fh_l)^2 + (Sh_{pool})^2$ $h_l = 0.023(Re_l)^{0.8}(Pr_l)^{0.4}(k_l/D_h)$ $h_{pool} = 55(Pr_l)^{0.12}(-\log_{10}Pr_l)^{-0.55}M^{-0.5}(q_w'')^{0.67}$ $F = \left[1 + xPr \left(\frac{\rho_l}{\rho_v} - 1\right)\right]^{0.35}$ $S = \frac{1}{1 + 0.055F^{0.1}Re_l^{0.16}}$ |
| Tran et al. [252] | R12 R113 R134a H Circular & Rectangular | $2.4 \leq D_h \leq 2.92$ $L_h = 900 \text{ mm}$ | $58 \leq G \leq 832$ $3.6 \leq q_w'' \leq 129$ $0.2 \leq x \leq 0.94$ | $h_{tp} = 840 \times 10^3(Bo^2We_l)^{0.3} \left(\frac{\rho_l}{\rho_v}\right)^{-0.4}$ |
| Tran et al. [1] | R12 R113 | $2.4 \leq D_h \leq 2.92$ | $58 \leq G \leq 832$ $3.6 \leq q_w'' \leq 129$ | $Nu = 770(BoRe_lN_{conf})^{0.62} \left(\frac{\rho_v}{\rho_l}\right)^{0.297}$ |

| | | | | |
|--------------------------------------|--|-----------------------------|-----------------------|---|
| | R134a H Circular & Rectangular | | $0.2 \leq x \leq 0.8$ | |
| Kattan et al. [83] | R134a R502 R123 R402a R404a H Circular 1,141 data points | $D_h = 10.92$ | | $h_{tp} = \frac{\theta_{dry} h_v + (2\pi - \theta_{dry}) h_{wet}}{2\pi}$ $h_{wet} = (h_{nb}^3 + h_{cb}^3)^{1/3}$ $h_{cb} = C Re_L^m Pr_L^{0.4} \frac{k_L}{\delta}$ $h_{nb} = 55 (Pr_l)^{0.12} (-\log_{10} Pr_l)^{-0.55} M^{-0.5} (q_w)^{0.67}$ $m = 0.69; C = 0.0133$ |
| Yu et al. [181] | Water H | $D_h = 2.98$ $L_h = 910$ | $50 \leq G \leq 200$ | $h_{tp} = 64 \times 10^5 (Bo^2 We_l)^{0.27} \left(\frac{\rho_l}{\rho_v}\right)^{-0.2}$ |
| Zhang et al. [34] | Data collected for Water, R11, R12, R113 | | | $h_{tp} = S \cdot h_{nb} + F \cdot h_{sp}$ $h_{nb} = 0.00122 \left(\frac{k_l^{0.79} C_{pl}^{0.45} \rho_l^{0.49} g_c^{0.25}}{\sigma^{0.5} \mu_l^{0.29} h_{lv}^{0.24} \rho_v^{0.24}} \right) \Delta T_{sat}^{0.24} \Delta p_{sat}^{0.75}$ $S = [1 + 2.53 \times 10^{-6} Re_f^{1.17}]^{-1}$ $F = MAX(F', 1); F' = 0.64 \phi_f; \phi_f^2 = 1 + \frac{C}{X} + \frac{1}{X^2}$ <p>For $Re_f < 1000$ & $Re_g < 1000, X = X_{vv}, C = 5$ For $Re_f > 2000$ & $Re_g < 1000, X = X_{tv}, C = 10$ For $Re_f < 1000$ & $Re_g > 2000, X = X_{vt}, C = 12$ For $Re_f > 2000$ & $Re_g > 2000, X = X_{tt}, C = 20$</p> |
| Kandlikar & Balasubramanian [253] | | | | $h_{tp} = MAX(h_{nb}, h_{cb})$ $h_{nb} = 0.6683 Co^{-0.2} (1-x)^{0.8} h_{lo} + 1055 Bo^{0.7} (1-x)^{0.8} F_{Fl} h_{lo}$ $h_{cb} = 1.136 Co^{-0.9} (1-x)^{0.8} h_{lo} + 667.2 Bo^{0.7} (1-x)^{0.8} F_{Fl} h_{lo}$ $For 10^4 \leq Re_{lo} \leq 5 \times 10^6; h_{lo} = \frac{Re_{lo} Pr_l (f/2) (k_l/D)}{1 + 12.7 (Pr_l^{2/3} - 1) (f/2)^{0.5}}$ |

| | | | | |
|---------------------|--|----------------------------------|---|--|
| | | | | $\text{For } 3000 \leq Re_{lo} \leq 10^4; h_{lo} = \frac{(Re_{lo} - 1000)Pr_l(f/2)(k_l/D)}{1 + 12.7(Pr_l^{2/3} - 1)(f/2)^{0.5}}$ $f = [1.58 \ln(Re_{lo}) - 3.28]^{-2.0}$ |
| Choi et al. [144] | R22, R134a, CO2 | $D_h = 1.5; 3.0$ $L_h = 2000$ | $200 \leq G \leq 600$ $10 \leq q_w'' \leq 40$ $0.0 \leq x \leq 1.0$ | $h_{tp} = S \cdot h_{nb} + F \cdot h_{lo}$ $S = 469.1689(\phi_f^2)^{-0.2093} Bo^{0.7402}$ $F = 0.042\phi_f^2 + 0.958$ $h_{nb} = 55(Pr_l)^{0.12}(-\log_{10} Pr_l)^{-0.55} M^{-0.5} (q_w'')^{0.67}$ $h_l = 0.023(Re_l)^{0.8} (Pr_l)^{0.4} (k_l/D_h)$ $\phi_f^2 = 1 + \frac{C}{X} + \frac{1}{X^2}$ $C(tt) = 20; C(vt) = 12; C(tv) = 10; C(vv) = 5;$ |
| Saitoh et al. [37] | R134a; H; Data points: 2,224 | $0.51 \leq D_h \leq 10.92$ | | $h_{tp} = S \cdot h_{pool} + F \cdot h_{lo}$ $S = [1 + 0.4(Re_{tp} \times 10^{-4})^{1.4}]^{-1}$ $F = 1 + [(1/X)^{1.05} / (1 + We_g^{-0.4})]$ $h_{pool} = 207(k_l/d_b) \left(\frac{q_w'' d_b}{k_l T_l} \right)^{0.745} (\rho_g/\rho_l)^{0.581} Pr_l^{0.533}$ $h_l = 0.023(Re_l)^{0.8} (Pr_l)^{0.4} (k_l/D_h)$ $d_b = 0.51(2\sigma/g(\rho_l - \rho_g))^{0.5}$ |
| Bertsch et al. [25] | Data points: 3,899; 12 working fluids; | $0.16 \leq D_h \leq 2.92$ | $20 \leq G \leq 3000$ $4.0 \leq q_w'' \leq 1150$ $0.0 \leq x \leq 1.0$ $-197 \leq T_{sat} \leq 97$ | $h_{FB} = S \cdot h_{NB} + F \cdot h_{conv,tp}$ $S = (1 - x)$ $F = 1 + 80(x^2 - x^6)e^{-0.6Co}$ $h_{conv,tp} = h_{conv,l} \cdot (1 - x) + h_{conv,v} \cdot x$ $h_{conv,k} = \left[3.66 + \frac{0.0668 Re_k Pr(D_h/L)}{1 + 0.04 [Re_k Pr(D_h/L)]^{2/3}} \right] \cdot \left(\frac{k_l}{D_h} \right); k = l, v$ |
| Choo & Kim [254] | Air-Water | $D_h = 0.14; 0.222; 0.334$ | $340 \leq q_w'' \leq 950$ | $Nu_{tp} = 0.023 Re_l^m Pr_l^{0.4} F$ $F = C \cdot X^{-n}$ $m = 0.8 - 0.8[1 + e^{(d^* - 37)/7}]^{-1}; d^* = d\sqrt{\sigma/\rho g}$ $C = 2.94 + 358 \cdot e^{-(0.1d^*)}$ |

| | | | | |
|---------------------|--|---|---|--|
| | | | | $n = 0.7 - 0.8[1 + e^{(d^* - 41)/2}]^{-1}$ |
| Oh et al. [156] | Data points: 1,588 R22, R134a, R410a, C3H8, CO2 Horizontal | $D_h = 0.5; 1.5; 3.0$ $L_h = 330; 1000;$ 1500; 2000; 3000 | $50 \leq G \leq 600$ $5.0 \leq q_w'' \leq 40$ $0.0 \leq x \leq 1.0$ $0.0 \leq T_{sat} \leq 15$ | $h_{tp} = S \cdot h_{nb} + F \cdot h_f$ $S = 0.279 \cdot (\phi_f^2)^{-0.029} Bo^{-0.098}$ $F = MAX[(0.023\phi_f^{2.2} + 0.76), 1]$ $\phi_f^2 = 1 + \frac{C}{X} + \frac{1}{X^2}$ |
| Kim & Mudawar [255] | Data points: 10,805; Water, R134a, R152a, FC72, R11, R113, R123, R1234yf, R1234ze, R22, R236fa, R245fa, R32, R404a, R407c, R410a, R417a, CO2, | $0.19 \leq D_h \leq 6.5$ | $19 \leq G \leq 1608$ $0.0 \leq x \leq 1.0$ $0.005 \leq p_r \leq 0.69$ | $h_{tp} = (h_{nb}^2 + h_{cb}^2)^{0.5}$ $h_{nb} = \left[2,345 \left(Bo \frac{P_H}{P_F} \right)^{0.7} Pr^{0.38} (1-x)^{-0.51} \right] h_f$ $h_{cb} = \left[5.2 \left(Bo \frac{P_H}{P_F} \right)^{0.8} We_f^{-0.54} + 3.5 \left(\frac{1}{X_{tt}} \right)^{0.94} \left(\frac{\rho_g}{\rho_f} \right)^{0.25} \right] h_f$ $h_f = 0.023 Re_f^{0.8} Pr_f^{0.4} \frac{k_f}{\delta}$ |
| Fang [256] | Data points: 2,956; CO2 Horizontal Single tubes | $0.529 \leq D_h \leq 7.75$ | $97.5 \leq G \leq 1400$ $3.93 \leq q_w'' \leq 40$ $0.004 \leq x \leq 0.99$ $0.14 \leq p_r \leq 0.91$ | $Nu_{tp} = 0.00061(S + F) Re_l Fa^{0.11} Pr_l^{0.4} / [\ln(1.024\mu_{l,f}/\mu_{l,w})]$ $S = 41 \times 10^3 Bo^{1.13} - 0.275$ $F = \left(\frac{x}{1-x} \right)^a \left(\frac{\rho_l}{\rho_g} \right)^{0.4}$ $a = \begin{cases} 0.48 + 524 \times 10^{-3} (Re_l Fa^{0.11})^{0.85} - 5.9 \times 10^{-6} (Re_l Fa^{0.11})^{1.85} & \text{for } (Re_l Fa^{0.11}) < 600 \\ 0.87 & \text{for } 600 \leq (Re_l Fa^{0.11}) \leq 6000 \\ 160.8 / (Re_l Fa^{0.11})^{0.6} & \text{for } (Re_l Fa^{0.11}) > 6000 \end{cases}$ $Fa = (\rho_l - \rho_g)\sigma / (G^2 D_h)$ |

| | | | | |
|-----------------------------|--|--|--|---|
| Mahmoud & Karayiannis [207] | R134a; Data points : 5,152 Horizontal | $0.52 \leq D_h \leq 4.26$ $150 \leq L_h \leq 450$ | $100 \leq G \leq 500$ $2.4 \leq q_w'' \leq 175.4$ $600 \leq p \leq 1000$ | $h_{tp} = S \cdot h_{Cooper} + F \cdot h_l$ $F = [1 + (2.812Co^{-0.408}/X)]^{0.64}$ $S = [1 + 2.56 \times 10^{-6}(Re_l F^{1.25})^{1.17}]^{-1}$ |
| Kim et al. [257] | R1234yf; Horizontal | $D_h = 1.5; 3.0$ $L_h = 1000; 2000$ | $200 \leq G \leq 650$ $5.0 \leq q_w'' \leq 40$ $T_{sat} = 10; 15$ | $h_{tp} = S \cdot h_{Cooper} + F \cdot h_l$ $F = MAX[(0.065\phi_f^{1.6}), 1]$ $S = a(\phi_f^2)^b Bo^c$ For Intermittent flow : $a = 8.91; b = -0.158; c = 0.19$ For Stratified flow: $a = 4.47; b = -0.1; c = 0.1$ For Annular flow: $a = 6.3; b = -0.23; c = 0.13$ |
| Wu et al. [258] | collected data points: 1,619 Water, Propane, ammonia, CO ₂ , R11, R22, R134a, R141b, R236fa, R245fa, R410A, R1234ze, R600a, HFO-1234yf | $0.19 \leq D_h \leq 2.6$ | $23.4 \leq G \leq 2000$ $1.0 \leq q_w'' \leq 1150$ | For elongated bubbly zone : When $Bl < Bl_{transition}$ $hd_h/k_l = 62.37Bl^{0.279} \left[\frac{Gd_h x}{\mu_l(1-x)} \right]^{0.39} Bo^{0.195}$ When $Bl \geq Bl_{transition}$ & $Bo < 0.48$ $hd_h/k_l = 798(1 - 1.81Bo)Bl^{0.714} Re_l^{0.61}$ When $Bl \geq Bl_{transition}$ & $Bo \geq 0.48$ $hd_h/k_l = 42.15(1 + 3.17Bo)Bl^{0.714} Re_l^{0.61}$ For Annular zone : $h/h_{LF} = 0.0399(Bl^{0.3} Re_l)^{0.933}$ Note: only here Bl is Boiling number, Bo is Bond number |
| Lim et al. [7] | Water | $D_h = 0.5$ | $G = 200; 400; 600$ $100 \leq q_w'' \leq 400$ $p_{in} = 110 - 170 \text{ kPa}$ | $h_{tp} = \frac{Re^{0.196}}{Bo^{0.117} C_{Fr}^{0.42}} \cdot \frac{k}{D_h}$ $C_{Fr} = 0.4905 + Fr_L(1 - x^{3.134})$ $Fr_L = \frac{G}{\rho^2 g D_h}$ |

Note : (V) for Vertical, (H) for Horizontal.

Table (A-3): Pressure drop correlations for two-phase flow in mini/micro-channels.

| Author(s) | Working fluid(s), orientation | Geometry: D_h [mm], L_h [mm] | Parameter range: G [kg/m ² .s], q_w'' [kW/m ²], T_{sat} [°C], p_{sat} [kPa], j [m/s] | Proposed correlation |
|--------------------------|------------------------------------|---|--|--|
| Chisholm [259] | Steam/water mixture | conventional Smooth tubes And channels | | $\Delta p_{tp} = \Phi_{lo}^2 \Delta p_{lo}$ $\Phi_{lo}^2 = 1 + (\Gamma^2 - 1) [Bx^{(2-n)/2} (1-x)^{(2-n)/2} + x^{2-n}]$ $\Gamma = \left(\frac{\Delta p_{go}}{\Delta p_{lo}} \right)^{0.5}; \quad B = \frac{C\Gamma - 2^{2-n}}{\Gamma^2 - 1}; \quad C = 1 + \frac{(x/\rho_g)}{(x/\rho_g) + (1-x)/\rho_l}; n = 0.25$ |
| Lin et al. [162] | Data points: 238; R12 | $D_h = 0.66; 1.17$ $L_h = 1500$ | $1440 \leq G \leq 5090$; $0.0 \leq x \leq 0.25$ $4.64 \times 10^3 \leq Re \leq 3.76 \times 10^4$; $630 \leq p_{in} \leq 1320$; $17 \leq T_{in} \leq 53$ | $(dp/dz)_t = \Phi_{lo}^2 (dp/dz)_{lo}$ $\Phi_{lo}^2 = \left[\frac{\ln[(7/Re_t)^{0.9} + 0.27(\varepsilon/D)]}{\ln[(7/Re_{lo})^{0.9} + 0.27(\varepsilon/D)]} \right]^{16} \left[1 + x \left(\frac{\rho_l}{\rho_g} - 1 \right) \right]$ $Re_{lo} = (GD)/\mu_l; \quad Re_t = (GD)/\mu_t$ $\mu_t = \frac{\mu_l \mu_g}{\mu_g + x^{1.4}(\mu_l - \mu_g)}$ |
| Moriyama et al. [8] | R113 Rectangular | With:30 Gap:0.035 – 0.11 $L_h = 265$ | $200 \leq G \leq 1000$; $0.0 \leq x \leq 0.25$ $4 \leq q_w'' \leq 30$; $37 \leq T_{in} \leq 107$; $100 \leq p \leq 200$ | $\Phi_{lv}^2 = 1 + \frac{K}{X_{vv}^2}$ $K = \begin{cases} 0.9 Re_l^{0.3} & \text{for } Re_l > 1.3 \\ 1.0 & \text{for } Re_l \leq 1.3 \end{cases}$ $Re_l = \frac{2\rho_l j_l D_h}{\mu_l}$ |
| Mishima and Hibiki [173] | Air-water Vertical capillary tubes | $1.05 \leq D_h \leq 4.08$ | $0.0896 \leq j_g \leq 79.3$ $0.0116 \leq j_l \leq 1.67$ | $\Phi_{lo}^2 = 1 + \frac{C}{X} + \frac{1}{X^2}$ $C = 21[1 - e^{(-0.319D_h)}]$ |
| Tran et al. [164] | R12; R113; R134a Horizontal | $D_h = 2.46; 2.92$ $L_h = 914$ | $50 \leq G \leq 832$; $0.02 \leq x \leq 0.95$ $2.2 \leq q_w'' \leq 129$; | $\Delta p_{tp} = \Phi_{lo}^2 \Delta p_{lo}$ $\Phi_{lo}^2 = 1 + (4.3\Gamma^2 - 1)[Co^{1.2} x^{0.875} (1-x)^{0.875} + x^{1.75}]$ |

| | | | | |
|-------------------------|--|--|--|--|
| | Circular; Rectangular 610 data points | | $0.04 \leq p_r \leq 0.23$; | $\Gamma^2 = \left(\frac{\Delta p_{go}}{\Delta p_{lo}} \right)$ |
| Lee and Lee [260] | Water-Air; H; Rectangular | $D_h = 0.78$; 1.91; 3.64; 6.67 | $175 \leq Re_{lo} \leq 17,700$ $p_{in} = p_{atm}$; | $\phi_{lo}^2 = 1 + \frac{C}{X} + \frac{1}{X^2}$ $C = A\lambda^q \psi^r Re_{lo}^s$; $\psi = \frac{\mu_l j}{\sigma}$; $\lambda = \frac{\mu_l^2}{\rho_l \sigma D_h}$; $Re_c = 2,000$ For $Re_l \& Re_g < Re_c$: $A = 6.833 \times 10^{-8}$; $q = -1.317$; $r = 0.719$; $s = 0.557$ For $Re_l < Re_c \& Re_g > Re_c$: $A = 6.185 \times 10^{-2}$; $q = 0.0$; $r = 0.0$; $s = 0.726$ For $Re_l > Re_c \& Re_g < Re_c$: $A = 3.627$; $q = 0.0$; $r = 0.0$; $s = 0.174$ For $Re_l \& Re_g > Re_c$: $A = 0.408$; $q = 0.0$; $r = 0.0$; $s = 0.451$ |
| Zhang and Webb [261] | R134a, R22, R404a, Data points: 119 single & multi Circular H | $D_h = 2.13$; 3.25; 6.25; | $200 \leq G \leq 1000$; $0.17 \leq x \leq 0.93$ $20 \leq T_{sat} \leq 65$; $0.2 \leq p_r \leq 0.51$; | $\phi_{lo}^2 = (1-x)^2 + 2.87 \cdot x^2 \cdot p_r^{-1} + 1.68 \cdot x^{0.8} \cdot (1-x)^{0.25} \cdot p_r^{-1.64}$ |
| Yu et al. [181] | Water Circular, H | $D_h = 2.98$; $L_h = 910$; | $50 \leq G \leq 200$; $T_{in} = 80$; $p = 200$; | Modified Chisholm [219, 259] correlation $\phi_{lo}^2 = \left[18.65 \left(\frac{\rho_g}{\rho_l} \right)^{0.5} \left(\frac{1-x}{x} \right) \frac{Re_g^{0.1}}{Re_l^{0.5}} \right]^{-1.9}$ |
| Yun and Kim [165] | CO2 H | Mini-tubes: D_h = 0.98; 2.0 Micro- channels: | $100 \leq G \leq 3570$; $5 \leq q_w'' \leq 48$ | Modified Chisholm parameter: $\phi_{lo}^2 = 1 + \frac{C}{X} + \frac{1}{X^2}$ $C = 21 \cdot [1 - e^{(-1.97 D_h)}]$ |

| | | | | |
|----------------------|--|-----------------------------------|---|---|
| | | $D_h = 1.08; 1.54$ | | |
| Hwang and Kim [166] | R134a | $D_h = 0.244; 0.430; 0.792;$ | $140 \leq G \leq 950 ;$ $0.08 \leq x \leq 0.95$ | $\phi_{lo}^2 = 1 + \frac{C}{X} + \frac{1}{X^2}$ $C = 0.227(Re_{lo})^{0.452} X^{-0.320} Co^{-0.82} ;$ <i>Co: Confinement number</i> |
| Choi and Kim [178] | Water-Nitrogen Rectangular H | $0.141 \leq D_h \leq 0.490$ | $0.075 \leq G_g \leq 80$ $66 \leq G_l \leq 1000$ $0.06 \leq j_g \leq 72$ $0.06 \leq j_l \leq 1.0$ $2 \leq Re_g \leq 2,134$ $32 \leq Re_l \leq 477$ | Based on HFM: bubble regime: $f_{tp} = 6.48Re_{tp}^{-0.85}$ transition regime: $f_{tp} = 5.43Re_{tp}^{-0.85}$ liquid ring regime: $f_{tp} = (AR + 0.46)Re_{tp}^{-0.6}$ Based on SFM: bubble regime: $C = C_m(0.0012G + 1.473)$ transition regime: $C = C_m(0.0008G + 0.95)$ liquid ring regime: $C = C_m(aG + b)$ $C_m = 21(1 - e^{-1.612/Co}) ;$ <i>Co is Confinement No.</i> $a = 0.658AR + 0.13 ; b = 0.0016AR + 0.0003;$ AR: aspect ratio |
| Maqbool et al. [179] | Ammonia, Circular, V | $D_h = 1.224; 1.7$ $L_h = 245$ | $100 \leq G \leq 500 ;$ $0.0 \leq x \leq 1.0$ $15 \leq q_w'' \leq 355;$ $T_{in} = 23; 33; 43$ | $(dp/dz)_t = \phi_{lo}^2(dp/dz)_{lo}$ $\phi_{lo}^2 = 1 + (4.3Y^2 - 1)[0.2Co^{1.2}x^{0.875}(1-x)^{0.875} + x^{1.75}]$ $Y^2 = \left(\frac{\Delta p_{go}}{\Delta p_{lo}}\right)$ |
| Lim et al. [180] | De-ionized water; Rectangular; H | $D_h = 0.50$ | $G = 200; 400; 600; ;$ $100 \leq q_w'' \leq 400$ $0.0 \leq x \leq 0.20$ $110 \leq p_{in} \leq 170;$ | $C = 0.71 (Re_{tp})^{0.91} (We_{tp})^{-0.655}$ $Re_{tp} = \frac{GD_h}{\mu_{tp}} ; We_{tp} = \frac{G^2 D_h}{\rho_{tp} \sigma} ; \mu_{tp} = \left[\frac{x}{\mu_g} + \frac{(1-x)}{\mu_l} \right]^{-1} 2$ |

Note: (V) for vertical, (H) for horizontal